

Molecular Approach toward Gases Absorption by Ionic Liquids

Dissertation

zur

Erlangung des Doktorgrades (Dr. rer. nat.)

der

Mathematisch-Naturwissenschaftlichen Fakultät

der

Rheinischen Friedrich-Wilhelms-Universität Bonn

vorgelegt von

Dzmitry Firaha

aus

Mstizh, Belarus

Bonn 2016

Angefertigt mit Genehmigung der Mathematisch-Naturwissenschaftlichen Fakultät der
Rheinischen Friedrich-Wilhelms-Universität Bonn

Erster Gutachter: Prof. Dr. Barbara Kirchner

Zweiter Gutachter: Prof. Dr. Stefan Grimme

Tag der Promotion: 2. December 2016

Erscheinungsjahr: 2017

Abstract

This thesis reports the theoretical studies of gas absorption in complex systems. These systems, namely ionic liquids, are considered to be promising candidates to substitute conventional gas capture systems which violate principles of Green Chemistry. The primary focus of this work is to understand gas absorption in ionic liquids on the molecular level using first principles methods such as ab initio molecular dynamics simulations and static quantum chemical calculations combined with statistical thermodynamics and predictive thermodynamic models. These methods allow for the derivation of predictive estimates for the knowledge-based design and tuning of ionic liquids for gas capture.

A simple protocol is suggested in the first part of the thesis to distinguish physical from chemical absorption of carbon dioxide (CO_2) in ionic liquids with varying anion basicity. This protocol includes a simple geometric optimization with a continuum solvation model of anion- CO_2 complexes. A value of the O-C-O angle in these optimized structures defines the possible kind of CO_2 absorption in the ionic liquid with the corresponding anion. The anions showing chemical absorption are further narrowed down to those promising for reversible chemical absorption based on the calculated reaction Gibbs free energies. The suggested approaches are easily transferable to other systems if the possible reactions are known. In case of complex reaction mechanisms such as the absorption of CO_2 in amino acid ionic liquids, the application of ab initio molecular dynamics simulations allows for the determination of the possible reactions in the system. The subsequent variation of the structure of the cation and the anion reveals the change of Gibbs free energies and barriers in the reactions. These small structural changes affecting the kinetics and energetics of the CO_2 absorption can be used as recipes for the precise tuning of the absorption rate and the total CO_2 capacity in ionic liquids.

The solvation mechanisms of CO_2 and sulfur dioxide (SO_2) gases in ionic liquids are analyzed in the second part of the thesis. The solvation shells of both gases contain groups

donating weak interactions, e.g., a π -system of the cation or alkyl hydrogen atoms, indicating the high importance of the weak interactions in the CO_2 and SO_2 solvation. The essential difference between the solvation mechanisms of CO_2 and SO_2 is the interaction with an extended cation-anion network of an ionic liquid. CO_2 molecules do not incorporate into the cation-anion network, tending to be solvated by nonpolar groups of an ionic liquid. Instead, SO_2 acts as a linker and incorporates into the cation-anion network, which corresponds to the formation of anion-solute-cation structures. From this qualitative picture, the significantly higher solubility of SO_2 than CO_2 in ionic liquids can be explained.

The last part of the thesis deals with the chemical absorption of CO_2 by carbenes available in some ionic liquids. The ability of the 1-ethyl-3-methylimidazolium acetate ionic liquid to form a carbene varies from gas to bulk phases in presence or absence of CO_2 . While CO_2 suppresses the carbene formation in the gas phase, the opposite effect is observed in the bulk phase. This occurs due to an inverse ionic liquid effect, when an introduction of the neutral molecules in the pure ionic liquid might induce the formation of neutral species like carbenes. The detailed insight into the subsequent reactions of CO_2 with carbene and the transformation of the formed carbene- CO_2 adduct into an isomeric adduct has been performed theoretically in close collaboration with experimentalists. The experimental evidence supported by static quantum chemical calculations and ab initio molecular dynamics simulations allows for the establishment of a possible generalized mechanism of the isomerization of the carbene- CO_2 adduct. The driving force for such isomerization is the high basicity of the system.

The presented theoretical approaches from the combination of first principles methods can be routinely applied to investigate the absorption of other gases in unstudied ionic liquids. The gathered knowledge can be further used for the optimization and precise tuning of the ionic liquids for gas absorption.

Contents

1. Introduction	1
1.1. Types of CO ₂ and SO ₂ Absorption in Ionic Liquids	3
1.2. Theoretical Studies of CO ₂ and SO ₂ Absorption in Ionic Liquids	6
1.2.1. Predictive Thermodynamic Models	6
1.2.2. Force Field Based Methods	7
1.2.3. Static Quantum Chemical Description	8
1.2.4. Improvements of the Static Quantum Chemical Description	9
1.2.5. Ab Initio Molecular Dynamics Approach	9
2. Methodology	11
2.1. Static Quantum Chemical Calculations	11
2.2. Continuum Solvation Model COSMO	13
2.3. Ab Initio Molecular Dynamics Simulations	15
2.4. Statistical Thermodynamics Calculations	16
2.5. Predictive Thermodynamic Model COSMO-RS	18
I. Computer Design and Tuning of Ionic Liquids for CO₂ Absorption	21
3. Computer-Aided Design of Ionic Liquids as CO₂ Absorbents	25
3.1. Introduction	26
3.2. Results and Discussion	27
3.3. Summary	33
3.4. Acknowledgements	34

4. Tuning the Carbon Dioxide Absorption in Amino Acid Ionic Liquids	35
4.1. Introduction	36
4.2. Results and Discussion	39
4.2.1. CO ₂ Absorption Pathways	39
4.2.2. Applied Methodologies and Considered Systems	40
4.2.3. Formation of the Glycinate-CO ₂ Adduct	44
4.2.4. Proton Abstraction from the Glycinate-CO ₂ Adduct	45
4.2.5. Carbamate – Carbamic Acid Equilibrium	46
4.2.6. CO ₂ Absorption in Other AAILs	48
4.3. Conclusion	52
4.4. Acknowledgments	54
II. CO₂ and SO₂ Solvation by Ionic Liquids	55
5. CO₂ Absorption in the Protic Ionic Liquid Ethylammonium Nitrate	59
5.1. Introduction	60
5.2. Results and Discussions	61
5.2.1. Computational Details	61
5.2.2. EAN Liquid Structure	63
5.2.3. CO ₂ Solvation in EAN	67
5.3. Conclusion	70
5.4. Acknowledgements	72
6. SO₂ Solvation in the 1-Ethyl-3-Methylimidazolium Thiocyanate Ionic Liquid	73
6.1. Introduction	75
6.2. Computational Details	77
6.3. Results and Discussion	78
6.3.1. Cation–Anion and Cation–SO ₂ Interactions	78
6.3.2. Anion–SO ₂ Interactions	83
6.4. Conclusion	86
6.5. Acknowledgments	88

III. CO₂ Capture by Carbens in Ionic Liquids	89
7. Carbene Formation in Ionic Liquids: Spontaneous, Induced, or Prohibited?	93
7.1. Introduction	95
7.2. Systems under Study	98
7.3. Computational Methodologies	101
7.4. Results and Discussion	102
7.4.1. Carbene Formation in the Absence of CO ₂	102
7.4.2. Carbene Formation in the Presence of CO ₂ and Electrophilicity of CO ₂ in the Ionic Liquid	105
7.5. Summary and Conclusion	111
7.6. Acknowledgments	114
8. An Abnormal NHC-CO₂ Adduct from Imidazolium Acetate Ionic Liquids	115
8.1. Introduction	117
8.2. Results and Discussion	119
8.3. Conclusion	128
8.4. Experimental Section and Methods	129
8.5. Acknowledgments	130
IV. Summary and Conclusion	131
V. Appendix	137
A. Supporting Information to Chapter 3	139
B. Supporting Information to Chapter 4	153
C. Supporting Information to Chapter 5	158
D. Supporting Information to Chapter 6	164
E. Supporting Information to Chapter 7	169

Contents

F. Supporting Information to Chapter 8	177
Bibliography	181
Acknowledgments	207
Publications	209

List of Figures

1.1. Structure and abbreviations of common cations and anions used as components of ionic liquids.	2
1.2. Possible strategies of ILs modification to assess chemical absorption of CO ₂	4
3.1. Binding energy versus O-C-O angle for the anion-CO ₂ complexes.	28
3.2. Chemical structure of the anion test set with abbreviations.	29
3.3. Correlation of calculated reaction Gibbs free energies and CO ₂ capacities.	32
3.4. List of the anions suitable for the chemical absorption of CO ₂	33
4.1. Simulated boxes, ions, and molecules for modeling the chemical absorption of CO ₂ in the 1-ethyl-3-methylimidazolium glycinate.	40
4.2. The combined distribution function of the N(glycinate)···C(CO ₂) distance versus the N-H bond length in glycinate and an energy diagram representing the formation of the glycinate-CO ₂ adduct.	44
4.3. Combined distribution functions and corresponding energy diagrams describing possible ways of the proton abstraction from the glycinate-CO ₂ adduct.	46
4.4. Combined distribution functions and corresponding energy diagram describing the carbamate-carbamic acid equilibrium.	47
4.5. The time development of the CO ₂ surface coverage.	57
4.6. Combined distribution functions testing the occurrence of the cation-SO ₂ -anion linked structure.	58
5.1. Representative snapshots of the simulation boxes of CO ₂ solvated by ethylammonium nitrate and supercritical CO ₂	62
5.2. Ball-and-stick representation of the ethylammonium cation, the nitrate anion and the CO ₂ molecule.	63

List of Figures

5.3.	The combined distribution function showing the hydrogen bonding between the nitrate anion and the ethylammonium cation.	64
5.4.	The combined distribution function analyzing the proton transfer from the ethylammonium cation to the nitrate anion.	65
5.5.	Radial distribution functions between atoms from ethylammonium cation.	66
5.6.	Probability density distributions of the spherical voids radius for the EAN+4CO ₂ system.	67
5.7.	Radial distribution functions between CO ₂ atoms or selected atoms from the nitrate anion and hydrogen atoms from the ethylammonium cation.	68
5.8.	Time development of the CO ₂ surface covering by polar and nonpolar parts of ethylammonium nitrate and other CO ₂ molecules.	70
5.9.	Combined distribution functions analyzing the mutual orientation of CO ₂ molecules in ethylammonium nitrate and supercritical CO ₂	71
6.1.	A representative snapshot of the simulation box of SO ₂ solvated in 1-ethyl-3-methylimidazolium thiocyanate.	77
6.2.	Ball-and-stick representation of the 1-ethyl-3-methylimidazolium cation, the thiocyanate anion, and the SO ₂ molecule.	79
6.3.	Time development of the SO ₂ surface covering by ions atoms.	80
6.4.	Radial distribution functions between SO ₂ and selected atoms from ions.	82
6.5.	Time development of S''(SO ₂)–S'(anion) and S''(SO ₂)–N'(anion) distances.	84
6.6.	Ball-and-stick representation of the thiocyanate-SO ₂ complex.	85
6.7.	Power spectra of the thiocyanate anion, the SO ₂ molecule, and the thiocyanate-SO ₂ adduct.	87
6.8.	The mechanism for the carbene-CO ₂ adduct formation.	91
6.9.	The suggested mechanism for the transformation between normal and abnormal adducts.	92
7.1.	Formation of carbenes and acetic acid from one ion pair of 1-ethyl-3-methylimidazolium acetate.	96

7.2.	Illustration of possible reaction paths leading to either physical or chemical absorptions of CO ₂ in 1-ethyl-3-methylimidazolium acetate.	98
7.3.	Atom labeling for the 1-ethyl-3-methylimidazolium cation, the acetate anion, and the CO ₂ molecule.	99
7.4.	Representative snapshots of simulated systems.	100
7.5.	Combined distribution functions of the C2–H2 versus the H2–O' distances.	104
7.6.	Optimized structures and gas phase interaction energies of the CO ₂ with the anion, the cation, and the carbene.	106
7.7.	Selected isomers of the 1P _{Me} +CO ₂ system.	108
7.8.	Voronoi cages of CO ₂ in the 1-ethyl-3-methylimidazolium ionic liquid.	110
7.9.	Dependency of the acetate's proton affinity and the acetate → CO ₂ charge transfer on the O'–C'' distances for the acetate–CO ₂ complex.	112
7.10.	The solute–solvent interaction network in general ionic liquid solutions.	114
8.1.	¹³ C spectra of the reaction mixture.	119
8.2.	Formation of normal and abnormal adducts from the 1-ethyl-3-methylimidazolium acetate ion pair and CO ₂	124
8.3.	Formation of the abnormal adduct from the normal adduct via the anionic dicarboxylate.	128
B.1.	Time development of the C''···N3' distance.	156
B.2.	Time development of the N3'–H3' bond length.	156
B.3.	Time development of the O'···H3' intermolecular distance.	157
B.4.	Time development of the O'···H3' intramolecular distance.	157
C.1.	Radial distribution functions between the center of masses of ions.	159
C.2.	Combined distribution functions analyzing mutual orientations of the cation versus anion, cation versus cation, and anion versus anion.	159
C.3.	Calculated power spectra for the whole system, anions, cations, and CO ₂ molecules.	160
C.4.	Dynamics of the surface covering of the anion, cation, and CO ₂ by other ions and CO ₂ molecules.	161

List of Figures

C.5. Combined distribution functions analyzing mutual orientations of the CO ₂ versus anion and cation.	162
C.6. Spatial distribution of cations and anions atoms around CO ₂	163
D.1. Radial distribution functions between the center of masses of cation and anion, cation and cation, anion and anion.	166
D.2. Radial distribution functions between the selected atoms of cation and anion	166
D.3. Radial distribution functions between the center of masses of SO ₂ and anion, SO ₂ and cation.	167
D.4. Radial distribution functions between the sulfur atoms of SO ₂ and anion. .	167
D.5. Angular distribution function between center of masses and atoms of SO ₂ and the closest anion.	168
D.6. Dihedral distribution function for dihedral angle between anion and SO ₂ . .	168
E.1. Radial distribution functions for C2-H2 and O'···H2 distances.	171
E.2. Radial distribution functions for O'···C'' and C2···C'' distances.	172
E.3. Changes in the surfaces of the CO ₂ 's Voronoi cell.	176
F.1. A snapshot of the simulation box of the normal adduct in 1-ethyl-3-methylimidazolium acetate.	177
F.2. A snapshot of the simulation box of the abnormal adduct in 1-ethyl-3-methylimidazolium acetate.	178
F.3. Radial pair distribution functions of the hydrogen bonding between normal or abnormal adducts and acetate anions.	178
F.4. The first peaks of the radial pair distribution functions of the hydrogen bonding between normal or abnormal adduct and acetate anions.	179
F.5. First peaks of the radial pair distribution functions, concerning the hydrogen bonding between normal or abnormal adducts and the imidazolium ring hydrogen atoms	179
F.6. Combined distribution functions showing the mobility of the 1-ethyl-3-methylimidazolium acetate's ring hydrogen atoms in the pure ionic liquid. .	180

List of Tables

3.1. Computed and experimental properties for anion-CO ₂ complexes.	30
3.2. O-C-O angles and related properties for anion-CO ₂ complexes.	31
4.1. Calculated energy barriers of (amino acid anion)-CO ₂ adduct formation in different AAILs.	48
4.2. Calculated Gibbs free reaction energy for the reaction of the trans-carbamic acid formation from CO ₂ and amino acid anion in different AAILs.	50
4.3. Calculated Gibbs free reaction energy for the carbamate-carbamic acid equilibrium in different AAILs.	50
4.4. Calculated Gibbs free reaction energy for the equilibrium between carbamic acid and carbamate.	53
5.1. Simulation parameters for EAN+4CO ₂ and 32CO ₂ systems.	62
6.1. Structural parameters for thiocyanate-SO ₂ adduct.	85
6.2. Vibrational frequencies in cm ⁻¹ for SO ₂ , thiocyanate and thiocyanate-SO ₂ adducts.	86
7.1. Ab initio molecular dynamics parameters for simulated systems.	102
7.2. Computed properties for 1P _{Me} and 1P _{Me} +CO ₂ systems.	103
7.3. Distances between C2 and H2 and O' and H2 pairs in pm.	105
7.4. O'-C'' and C2-C'' distances.	111
8.1. Yield of the different CO ₂ adducts.	120
8.2. Effect of temperature and reaction time on the formation of normal and abnormal adducts.	121

List of Tables

A.1. Computed reaction enthalpies, entropies, and Gibbs free solvation energies for the reaction CO ₂ with anions.	141
A.2. O–C–O angles and reaction Gibbs free energies for the gas-phase and solvated geometries.	142
A.3. Structures, names and abbreviations of anions.	143
B.1. Calculated Gibbs free reaction energy of (amino acid anion)-CO ₂ adduct formation in different AAILs.	155
B.2. Calculated Gibbs free reaction energy of the intramolecular proton transfer in different AAILs.	155

1 Introduction

The substantial emission of carbon dioxide (CO₂) and sulfur dioxide (SO₂) in the atmosphere since the Industrial Revolution^[1-3] is linked nowadays to the global climate change^[4-7] and acid rain,^[8] respectively. The main source of the emission of these gases is the combustion of fossil fuels such as coal, oil, and natural gas.^[9] These fossil fuels are and will continue to be the primary source of the energy for our society in the forthcoming decades since alternative energy sources can nowadays cover only ca. 20 % of the world's energy consumption.^[10] Flue and exhaust gases produced during the combustion of fossil fuels are composed mainly of nitrogen, CO₂, water vapor, excess oxygen as well as small amounts of other gases, including harmful SO₂.^[11,12] Therefore, the capture of CO₂ and SO₂ from the flue and exhaust gases is highly important for preventing undesirable effects on our environment.

Widely applied nowadays technologies for CO₂ and SO₂ capture were developed in the 20th century. They include an application of aqueous solutions of amines, potassium carbonate, chilled ammonia, limestone scrubbing and etc.^[13-18] Unfortunately, these technologies violate the principles of Green Chemistry,^[19] since the components have a high volatility and low stability.^[15] Also, the regeneration of the absorbent requires a lot of energy or is sometimes impossible.^[20,21] All these drawbacks lead to an increase in maintenance costs. Thus, the search for better alternatives for CO₂ and SO₂ absorption is highly required for the sustainable development of our society.

Ionic liquids (ILs)^[22-24] are nowadays considered as a promising class of compounds to substitute the conventional CO₂ and SO₂ capture technologies.^[25-28] ILs usually composed of a large organic cation paired with an organic and inorganic anion (see Figure 1.1). The main advantage of the application of ILs as the absorption media is their negligible low vapor pressure.^[29,30] This property of ILs eliminates solvent loss and, thus, significantly decreases maintenance costs in a long run. Moreover, both CO₂ and SO₂ readily possess

1. Introduction

a high absorption capacity in ILs when compared to other gases.^[31,32] This property allows for the capture of CO₂ and SO₂ from a mixture of gases and a later release for subsequent utilization.^[33,34] Besides, CO₂ and SO₂ absorbed in ILs can be efficiently utilized without their release. For example, chemically absorbed CO₂ can be selectively reduced electrochemically to the formate.^[35,36] The absorbed SO₂ can be reduced via the Claus reaction with hydrogen sulfide (H₂S) at mild conditions.^[37] Alternatively, both gases can be converted to heterocyclic compounds.^[38,39]

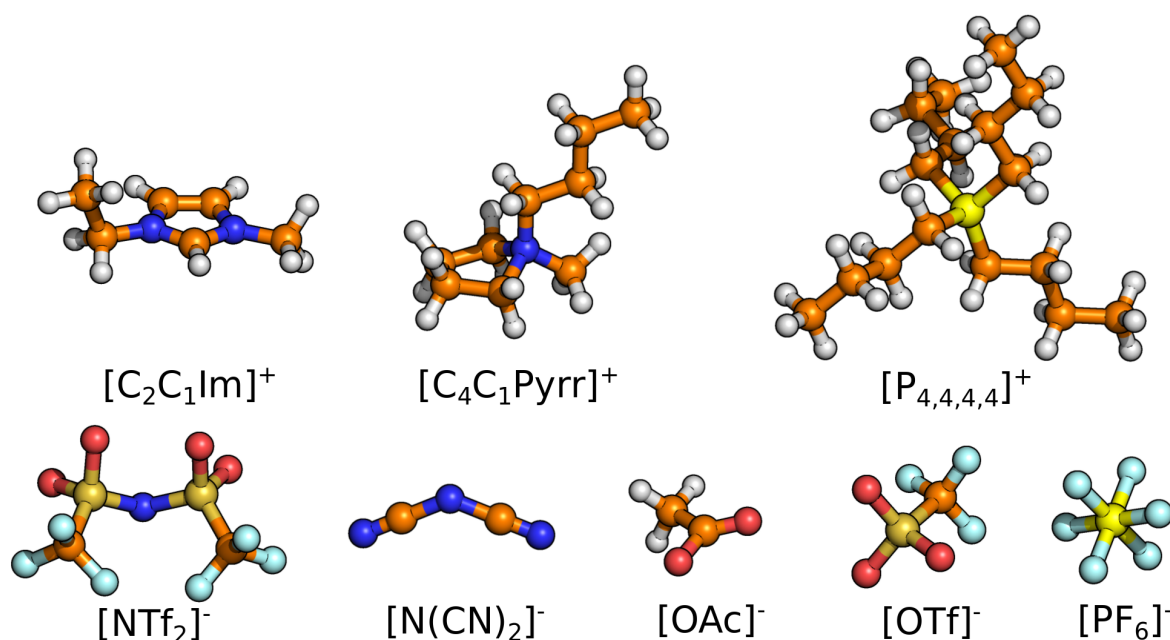


Figure 1.1. Structure and abbreviations of common cations and anions used as components of ionic liquids. White H; brown C; blue N; light blue F; gold S; yellow P.

The properties of ILs for gas absorption can be altered to a great extent via cation and anion exchange, alkyl chain elongation, and ion functionalization.^[40,41] The estimated number of simple cation-anion combinations are around one million (10^6), then there are ca. 10^{12} binary and ca. 10^{18} ternary systems of ILs possible.^[23] The detailed experimental studies of these enormous number of possible ILs and their mixtures might take decades to determine the best candidates for the absorption of CO₂ or SO₂ for a particular case.

To make this search more efficient and systematic, a theoretical insight on the CO₂ and SO₂ absorption is required. To this end, various computational methods^[42] can be applied. However, they allow to consider only specific system characteristics since no universal method providing all system properties has been developed so far. Thus,

the essential challenge for computational methods in application to a real system is to link their results with the experimental data in such a way that the reliable predictive estimates can be established. With validated theoretical protocols, the further studies of the unknown systems can be quickly conducted to generalize their behavior. Subsequently, the optimization and improving the efficiency of the system can be performed.

In the current thesis, computational methods, which explicitly treat the electronic structure, were applied to study gas absorption in ionic liquids. The main emphasis was put on the consideration of the molecular level of CO₂ and SO₂ absorption, establishing the possible reaction mechanisms, and connecting the molecular structure features with macroscopic properties of the absorption process.

1.1 Types of CO₂ and SO₂ Absorption in Ionic Liquids

Two types of absorption processes can be distinguished: physical absorption and chemical absorption. In physical absorption, the solute molecule does not react with the solvent. On the contrary, chemical absorption is characterized by the occurrence of a chemical reaction between the solute and the solvent. On the microscopic level, physical absorption corresponds to a formation of weak dispersion interactions and (if applicable) hydrogen bonding between the solute and solvent molecules, whereas chemical absorption is characterized by the formation of a solute-solvent adduct due to strong localized interaction(s). To achieve a better performance of the solvent, the control of the physio- and chemisorption is highly desirable. In the following, the most important ways of enhancing absorption capacities of CO₂ and SO₂ in ILs are briefly reviewed.

Extensive studies of the physical absorption of CO₂ in ILs have provided a significant amount of the empirical data on solubility.^[43] This data allows to establish general ways to increase CO₂ solubility via introducing groups donating weak interactions or enhancing ionic liquid porosity. The groups donating weak interactions are long alkyl side chains,^[44] their perfluorinated modifications,^[44-46] or linear glymes substituents.^[44,47-49] The porosity of ILs can be controlled by the introduction of cyano-based anions,^[50-52] side chain branching,^[53] or using cyclic polyethers as promising substituents.^[54] The above men-

1. Introduction

tioned methods provide an enhancement of CO₂ solubility on a molar basis ($n_{\text{CO}_2}/n_{\text{solvent}}$). However, the consideration of the CO₂ capacity on a mass basis ($m_{\text{CO}_2}/m_{\text{solvent}}$) is more desirable for a potential industrial application. In this basis, the increase of ILs' porosity has a higher impact than the introduction of the functional groups donating weak interactions.^[55]

Besides the possible ways to enhance the physical absorption, ILs can be modified in such a way that the chemical absorption of CO₂ becomes accessible. This kind of absorption provides a higher CO₂ capacity than physical absorption (at the low partial pressures of CO₂). Therefore, chemical absorption is more desired for a potential industrial application. There are at least four strategies to modify ILs to achieve chemical absorption (Figure 1.2). In the first strategy (A), the cation or/and the anion of the ionic liquid is

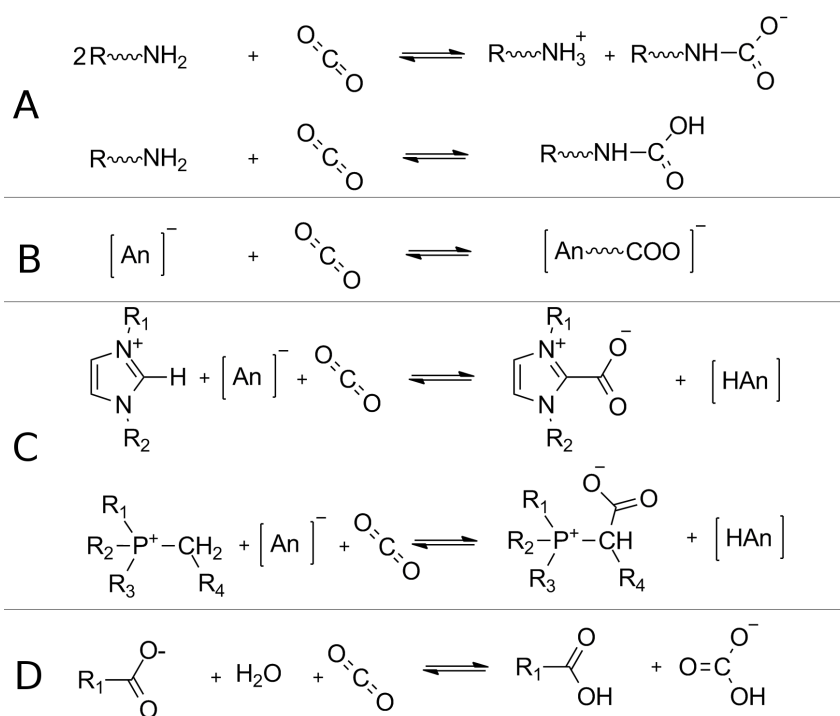


Figure 1.2. Possible strategies of ILs modification to assess chemical absorption of CO₂. A) Introducing the amine group; B) Tuning the anion Lewis basicity; C) Generation of carbenes or ylides; D) Synergistic effect.

functionalized by the introduction of the amine group.^[56–60] This modification of ILs leads to the formation of the complex mixture of the ions containing the amine, the ammonium, the carbamate, and the carbamic acid functional groups attached to the cation or anion. In the second strategy (B), tuning the anion Lewis basicity is the key factor to enhance

1.1. Types of CO₂ and SO₂ Absorption in Ionic Liquids

and control the CO₂ absorption capacity. In this case, the anion reacts with CO₂ directly forming a carboxylate.^[61–67] In the third strategy (C), the particular combination of the cation and anion leads to an occurrence of carbenes^[68,69] or ylides^[70,71] in the ionic liquids. These species are highly reactive and bind CO₂ forming thermodynamically stable products. In the fourth strategy (D), the equimolar mixtures of carboxylate-based ILs with water provide a synergistic effect for the absorption of CO₂. These systems possess chemical CO₂ absorption while pure components show only physical absorption.^[72]

In some ILs, the combination of several absorption mechanisms mentioned above has been detected. For example, imidazolium- and phosphonium-based ionic liquids paired with a highly basic anion show the second and third mechanisms competing (B and C).^[70,71] To achieve the higher CO₂ absorption capacity, the combination of the different strategies (A-C) in one ionic liquid has been suggested.^[73–78] This leads to the multi-site cooperative interactions and provides a complicated mixture of possible products, which is hard to predict from the structure of the cation and the anion.

The physical absorption of SO₂ in ILs is an order magnitude greater than CO₂ under the same external conditions.^[32,79] However, such a high affinity of SO₂ to ILs is still not enough to capture SO₂ from flue and exhaust gases due to its low concentration (ca. 200 ppm, which is ca. 1000 times lower than CO₂ concentration).^[11,12] The successful industrial application of ILs for SO₂ absorption can be revealed only through an improvement of their absorption capacity. The improvement corresponds to the introduction of additional active groups into ILs to increase physical absorption or to provide a chemical reaction with SO₂ molecules. For example, the introduction of ether,^[80,81] halogen,^[82–84] and cyano^[85] functional groups in the cation or the anion increases the SO₂ physisorption. The chemical absorption of SO₂ has been found in ILs with N-heterocyclic anions,^[86–90] a thiocyanate anion,^[91,92] dicarboxylate anions,^[93] and hydroxylammonium cations.^[94] Also, the functionalization of the cation or the anion with an amine group leads to the occurrence of chemical absorption.^[26,27,87]

In most cases, the experimental data on the CO₂ and SO₂ absorption in ILs provides only a macroscopic picture of the process. However, understanding the microscopic level of the absorption process is highly desired for its subsequent improvement. Computational

methods can provide the required tools for such an understanding.

1.2 Theoretical Studies of CO₂ and SO₂ Absorption in Ionic Liquids

There are different theoretical methods available to describe gas absorption in ILs. A brief overview of the most popular and widely applied methods including predictive thermodynamic models, force field-based methods, and static quantum chemical calculations are provided below. At the end of this section, the contribution of this thesis to the theoretical description of gas absorption in ionic liquids is presented via an improvement of the static quantum chemical description and ab initio molecular dynamics simulations.

1.2.1. Predictive Thermodynamic Models

An insight on the gases solubility in ILs can be accessed from the predictive thermodynamic models considered in detail in the recent review of Lei et al.^[43] The predictive thermodynamic models represented by the universal quasichemical functional group activity coefficient (UNIFAC),^[95] the conductor-like screening models (COSMO),^[96,97] regular solution theory,^[98] multiple regression- and neural network-based models,^[99] as well as various equations of state (EOS).^[100–104] These models provide physical properties such as solubility, selectivity, and vapor-liquid equilibria from the known molecular structure or/and physical properties of the compounds. The predictive thermodynamic models allow for a rapid screening among thousands of promising candidates. For example, such a prescreening analysis has been reported^[105–111] for sets of ILs with COSMO for realistic solvation or segment activity coefficient (COSMO-RS^[96] or COSMO-SAC^[97]). This step significantly minimizes the amount of experimental work for the determination of the CO₂ and SO₂ physisorption in ILs. However, these models fail to provide a reliable prediction for ILs showing the chemical absorption since this kind of absorption needs to be explicitly included in the parametrization. Therefore, the results of the predictive thermodynamic models have to be treated carefully for the systems with chemical absorption.

1.2.2. Force Field Based Methods

The force field based methods include classical molecular dynamics and a Monte Carlo approach.^[112,113] In these methods, the energy of the system is represented as the sum of different contributions having an analytical expression with empirical or adjustable parameters, known as a force field. The force field based methods allow to obtain a more detailed picture on gas absorption in ILs despite the fact that fewer systems can be covered when compared to predictive thermodynamic models. The calculation of important macroscopic properties (including gas solubility, density, viscosity, diffusion coefficient, permeability) and revealing a molecular structure around solute molecules are possible with the force field based methods.

A vast amount of classical molecular dynamics^[92,114–130] and Monte Carlo simulations^[131–137] of physisorbed CO₂ and SO₂ in ILs has been conducted aiming to predict the solubility and transport properties of CO₂+IL or SO₂+IL systems as well as to clarify the mechanism of CO₂ or SO₂ solvation. Practical interest, however, represents the consideration of the systems with chemical absorption. Since a high viscosity of ILs is a crucial issue for their potential industrial application, a particular emphasis is devoted to the studies of transport properties of CO₂/SO₂+ILs systems. For example, Maginn et al. studied amine-functionalized ILs to explain the tremendous viscosity increase after CO₂ absorption.^[118] They found that the formation of the extended hydrogen bond network might be the possible explanation of the viscosity increase. Another example studied in the same group is the tetrabutylphosphonium 2-cyanopyrrolid IL.^[124] For this ionic liquid, the viscosity remains independent of the extent of the CO₂ chemisorption due to a lack of the possibility to form the extended hydrogen bond network. On the contrary mentioned above examples, the trihexyl(tetradecyl)phosphonium imidazolate IL exhibits a viscosity decrease after CO₂ absorption.^[64,65] The possible explanation found from classical molecular dynamic simulations is the asymmetry of the newly formed anion-CO₂ adduct, imidazole-1-carboxyate, as opposed to the symmetrical unreacted anion.^[138] To account for both chemical and physical absorption, Zhang et al. developed a reactive force field for CO₂ absorption in the tetrabutylphosphonium glycinate IL.^[139] Besides the consideration of only one possible reaction channel and several possible intermediate species, this

1. Introduction

approach has a huge potential to access the large-scale modeling of the reactive systems.

The transport properties of the SO₂+ILs systems have been recently studied by Balasubramanian et al.^[128] and Zeng et al.^[140]. The results of classical molecular dynamics of the SO₂ absorption in various ionic liquids revealed that SO₂ loading decreases ILs' shear viscosity and enhances the electrical conductivity.

In summary, the force field based methods provide both the micro- and macroscopic view of gas absorption in ionic liquids. The classical molecular dynamic approach allows to capture and explain the transport properties hardly accessible from other computational methods. However, the results from this approach strongly depend on the quality of the force field parametrization.

1.2.3. Static Quantum Chemical Description

Static quantum chemical (QC) calculations allow to distinguish between the interaction sites of the cation or anion and solute molecule as well as quantitatively characterize these interactions.^[141–146] In this approach, the electrons are treated explicitly by finding an approximate solution of the Schrödinger equation (see section 2.1).

In most cases, theoretical results from static QC calculations are helpful to explain the experimental data on the possible and competing products (see Figure 1.2) in some ILs like amine-functionalized ILs^[142,144] or imidazolium and phosphonium-based ILs.^[70,71] Besides, the experimental results on the solubility can be correlated against the interaction energies. For example, Balasubramanian et al.^[141] have suggested correlating the experimental results of CO₂ absorption in the set of imidazolium-based ILs with fluorinated anions against the interaction energies of the anion-CO₂ complexes. Babarao et al.^[122] found a linear dependence between the CO₂ solubility and cation-anion interaction energies. However, these correlations are only applicable to a specific set of ILs and do not represent the generalized behavior of CO₂ in ILs.

The possible reason the results of static QC calculations fail to quantitatively and sometimes qualitatively interpret the experimental results is that interaction energies or other quantities are calculated in the vacuum at 0 K while the experiment is conducted near room temperature in a liquid phase. Whereas thermal corrections for the finite

temperature can be easily calculated from statistical thermodynamics (see section 2.4), the including of the solvation correction in ionic liquids is not a trivial task. Therefore, the attempts to correlate the theoretical results with the experiment do not always work.

1.2.4. Improvements of the Static Quantum Chemical Description

The conventional results of the static QC calculations can be significantly improved making them more valuable for qualitative and quantitative predictions. The first way is the inclusion of a continuum solvation model in the geometry optimization (see Part I). This modification allows for accounting a high polarizable effect of the media which is essential for processes in ionic liquids. The result of this simple modification provides the possibility to distinguish chemical from physical absorption for CO₂ in ionic liquids with a variable basicity of the anion (see Chapter 3).

Another way of the improvement of the QC results is a calculation of the Gibbs free energies. To this end, the energies from static QC calculations need to be combined with the thermal correction energies from statistical thermodynamics calculations and solvation energies from a predictive thermodynamic model.^[147] Such an approach allows for obtaining the relative Gibbs free energies and barriers for the most important reactions occurring during the CO₂ absorption process. These quantities are much better for the comparison with the experimental absorption capacities or absorption rates. Finally, the change in the calculated Gibbs free energies and barriers due to the cation and anion functionalization can be converted into the recipes for precise system tuning (see Chapter 4).

1.2.5. Ab Initio Molecular Dynamics Approach

Ab initio molecular dynamics (AIMD) is a method free from the extensive parameterization in contrast to the predictive thermodynamic models and force field-based methods. In this method, the properties of the system are derived from the electronic structure methods and propagated in time. Such an approach allows for adjusting the system to spontaneous events like specific interactions, chemical reactions, or, at least, their indication. This robustness of the approach and well-established analysis tools available in

1. Introduction

TRAVIS software^[148] allow for a better understanding of different processes occurring in the course of gas absorption in ILs. Moreover, the AIMD method bridges the gap between large-scale classical molecular dynamics simulations and static QC calculations for large molecular systems providing an unbiased dynamic view from the first principles. Therefore, this method has been extensively applied in this thesis.

Establishing the absorption mechanisms of CO₂ and SO₂ in ILs was one of the primary goals of the conducted AIMD simulations. The consideration of gases physisorption in ILs has revealed that gases enter into ILs via small voids forming specific interactions with cations and anions (see Chapter 5). AIMD simulations have shown that weak dispersion interactions with cations dominate in the solvation shell of CO₂ and SO₂ (see Chapters 5-7 and Ref. [149]). Next to the physical absorption, AIMD allows to explore chemical absorption (see Chapters 4, 6-8 and Ref. [150]). In some cases, the direct observation of the solute-solvent adduct formation has been detected as, for example, acetate-CO₂,^[150] glycinate-CO₂ (Chapter 4), and thiocyanate-SO₂ (Chapter 6) adducts. In other cases, the observation of chemical reactions is not possible due to high energy barriers. However, an indication of the chemical process can be easily established from the molecular structure by analyzing the bond elongation or interatomic distance shrinking. Such an establishment of the possible mechanism of carbenes formation, their reaction with CO₂, and subsequent isomerization of the formed carbene-CO₂ adduct have been established for the 1-methyl-3-ethylimidazolium acetate IL (see Chapters 7 and 8).

2 Methodology

In this section, the computational methods applied in the present thesis to study gas absorption in ILs will be briefly described. In the first subsection, the static quantum chemical calculations are introduced. Subsequently, a conductor-like screening model and an ab initio molecular dynamics are considered as examples of the implicit and explicit solvation models. Finally, statistical thermodynamics and a predictive thermodynamic model COSMO-RS (conductor-like screening model for realistic solvation) are outlined.

2.1 Static Quantum Chemical Calculations

The determination of a total energy of a molecule is the primary focus of static quantum chemical (QC) calculations. The total energy of the system (E) is obtained via the approximate solution of the time-independent non-relativistic Schrödinger equation $\hat{H}\Psi = E\Psi$. Within the Born–Oppenheimer approximation, the motion of electrons can be separated from the motion of nuclei.^[151] This approximation allows for considering only an electronic component of the wave function Ψ_e , for a fixed nuclei configuration $\hat{H}_e\Psi_e = E_e\Psi_e$. To access the total energy of the system, the electronic energy (E_e) needs to be summed up with the potential energy for the nuclei configuration. The electronic energy can be found from an approximate solution of the electronic Schrödinger equation with wavefunction or density functional theories (WFT and DFT).

WFT methods are based on the Hartree–Fock self-consistent field procedure.^[152,153] In this approach, the movement of the electron is considered in the mean-field created by other electrons. This allows for representing the wavefunction as a single Slater determinant of one-electron wavefunctions (molecular orbitals). Subsequently, the electronic energy and approximate wavefunction can be obtained iteratively. The Hartree–Fock method underestimates the total energy of the system due to the lack of the correlation

2. Methodology

energy between electrons. The accounting of the electron correlation is possible with different approaches such as the Møller–Plesset (MP) theory, coupled cluster (CC), and configuration interaction (CI) methods. These approaches use wavefunction from the Hartree–Fock method.*

Nowadays a coupled cluster method with single, double, and perturbative triple excitations, CCSD(T), is considered the gold standard in the WFT for the energies of closed shell systems,^[156] which are the primary object of the present thesis. However, the method scales with the number of basis functions (N) as $O(N^7)$, which significantly limits its application in systems with more than 20 atoms. Therefore, a simplification of the CCSD(T) method, which reduces its complexity, needs to be applied to study larger systems. Among the simplification schemes of the CCSD(T) method, the domain-based local pair of natural orbital (DLPNO) scheme^[157,158] can be considered a reasonable alternative to the conventional method. The DLPNO-CCSD(T) method with energy extrapolation to the complete basis set provides similar accuracy as the CCSD(T) method while being cheap on computational resources with $O(N^{2.3})$ scaling.^[159]

DFT is another approach providing an approximate solution for the electronic Schrödinger equation. The central focus of DFT is the electron density (ρ) of the system rather than the wavefunction (Ψ). The exact energy of the system and related electronic properties are determined only by the electron density of the system.

The construction formalism of ρ has been suggested by Kohn and Sham.^[160] They introduced a fictitious reference system of noninteracting particles that generates the same density as a given system of interacting particles. The noninteracting particles are moving in the external potential, which depends on the electron density. The wave function is represented as a single Slater determinant of one-particle wave functions (Kohn–Sham orbitals ϕ), similar to the Hartree–Fock method. The occupied orbitals (Kohn–Sham orbitals) allow for the construction of the electron density.

$$\rho = \sum_{m, \text{occupied}} |\phi_m|^2 \quad (2.1)$$

*See the books by Atilla Szabo and Neil S. Ostlund^[154] or by Ira Levine^[155] for more details.

Finally, the system energy and Kohn-Sham orbitals are obtained iteratively.[†]

Since the exact expression for the external potential is not known, different approximations have been suggested providing various DFT levels of theory. DFT methods classification includes the local density (VWN^[162]), semi-local or generalized density (BLYP,^[163,164] PBE^[165,166]), and meta generalized density (TPSS^[167]) approximations. Subsequently, the mixing of the approaches mentioned above with the results of the WFT give hybrid (B3LYP^[168]), meta-hybrid (PW6B95^[169]), and the double hybrid (B2PLYP^[170]) functionals. The mentioned above sequence of the methods corresponds in general to the increase of their accuracy, however, more computational time is required with formal scaling from $O(N^2)$ to $O(N^5)$ for local density approximation and double hybrid functionals, respectively.

The lack of the proper treatment of the dispersion interaction for some DFT methods requires the introduction of the corresponding correction. There are empirical,^[171,172] non-local,^[173] and many-body^[174] dispersion correction schemes available to improve the results of the conventional DFT methods. In this thesis, the empirical dispersion correction from Grimme^[171,172] was applied in most static DFT calculations and ab initio molecular dynamics simulations. This fast and robust correction scheme provides improved results for various systems^[175–177] including ionic liquids.^[178–181]

2.2 Continuum Solvation Model COSMO

So far the properties calculated from the WFT or DFT methods correspond to the gas phase. However, the impact of solvent on the solute molecules is often crucial, especially, for gas absorption in ionic liquids. The description of molecules possessing chemical reactions in the solvent is a complex problem requiring an explicit treatment of the solvent. Such an approach is considered in the subsection 2.3. Here, the simplified method of an implicit treatment of the solvent via a continuum solvation model is introduced.

In this method, a solute molecule is considered in the media with dielectric constant ϵ . The solute volume is separated from the media by a cavity. This cavity is constructed from

[†]More details on the theory can be found in the book by Reiner M. Gross and Eberhard K. Dreizler.^[161]

2. Methodology

the scaled van der Waals radii of atoms in the solute molecule. The dielectric polarization of the media is represented by a charge distribution on the surface of the solute cavity (q). This charge distribution can be evaluated from the following equation:

$$\hat{A}q + \hat{B}Q = 0 \quad (2.2)$$

where Q is the charge density in the cavity created by nuclei charges and the electron density of the solute. The electron density of the solute can be easily evaluated from a wavefunction of the solute (see the previous subsection). \hat{A} and \hat{B} are linear operators defined by boundary conditions employed.

Since the analytical function of the charge distribution on the surface is only available for simple cases, the partition of the surface of the arbitrary cavity needs to be performed to find a numerical solution. The effective charges on each surface segment can be found by solving a system of linear equations obtained from the equation mentioned above. The surface charges around the solute molecule can be used as external charges within the self-consistent field procedure of WFT or DFT methods. These charges and the wavefunction of the solute are modified iteratively until their mutual self-consistency.

In the dielectric continuum solvation models, the exact dielectric boundary conditions are considered. On the contrary, the scaled conductor boundary conditions are applied in a conductor-like screening model (COSMO).^[96,182,183] In this model, the solute molecule is considered in a perfect conductor with $\varepsilon = \infty$. This leads to the vanishing total potential on the solute cavity providing favorable boundary conditions. For an alternative medium with a finite dielectric constant the charges are scaled by a factor $f(\varepsilon)$:

$$f(\varepsilon) = \frac{\varepsilon - 1}{\varepsilon + 0.5} \quad (2.3)$$

Since the COSMO is a pure electrostatic model, it provides only an electronic energy contribution to the solvation energy. If the specific interactions between the solute molecules and the solvent are necessary to take into account, post-COSMO methods (like COSMO for realistic solvation, see subsection 2.5) need to be applied.

2.3 Ab Initio Molecular Dynamics Simulations

The description of complicated systems with specific interactions or possible chemical reactions in a bulk phase often requires the use of a more advanced approach than the continuum solvation model. Ab initio molecular dynamics is an approach where the solvent can be treated explicitly in an unbiased way from the first principles.

In the molecular dynamics simulations, the atomic coordinates and velocities are propagated in the time according to Newton's second law via a sequence of the finite times steps. The main idea of the ab initio molecular dynamics is to derive the forces on the atoms from the electronic structure methods briefly described in subsection 2.1. There are Car–Parrinello^[184] and Born–Oppenheimer^[185] molecular dynamics approaches to include the electronic structure methods into a molecular dynamics engine. The essential difference between these two approaches is in the way how the electron structure problem is solved. In the Born–Oppenheimer method the time-independent electronic Schrödinger equation is solved on each step of the simulation, whereas in the Car–Parrinello method the electrons are treated as an additional degree of freedom via a fictitious variable.[‡]

In this thesis, all ab initio molecular dynamics (AIMD) simulations were performed with the Born–Oppenheimer approximation in the CP2K program package.^[187] This program package utilizes dual Gaussian and plane wave basis sets.^[188] The Gaussian basis set is used to represent a wave function and Kohn–Sham matrix in a compact way. The plane wave basis with a pseudopotential on the atoms is more suitable to represent the electron density in systems with periodic boundary conditions. This representation allows for a much faster calculation of the Hartree (Coulomb) and exchange–correlation potentials, which transferred back to the Gaussian basis set. The transformation between the basis sets is performed via fast Fourier transforms allowing for faster calculations energies and forces on atoms than in Gaussian or plane wave basis sets.

[‡]For more details on these theories the readers are referred to the book by Marx and Hutter.^[186]

2.4 Statistical Thermodynamics Calculations

The main scope of the statistical thermodynamic calculations is to obtain the macroscopic properties of the system (enthalpies, entropies, Gibbs free energies, etc.) from the microscopic properties (molecular and spectroscopic data).^[189] The connection between microscopic and macroscopic data is made via the partition function Q . The partition function for the canonical ensemble (NVT) has the following expression:

$$Q_{N,V,T} = \sum_i g_i \exp(-\beta E_i) \quad (2.4)$$

The i index runs over all possible energy levels, g is the degeneracy of the i -th energy levels, β is the thermodynamic beta defined as $\beta = (k_B T)^{-1}$, where k_B is the Boltzmann constant, T is the temperature in Kelvin, E_i is the energy of the level with the index i . The enthalpy H , entropy S , and the Gibbs free energy G can be calculated from the partition function:

$$H = k_B T^2 \left(\frac{\partial \ln Q}{\partial T} \right)_{N,V} + PV \quad (2.5)$$

$$S = k_B \ln Q + k_B T \left(\frac{\partial \ln Q}{\partial T} \right)_{N,V} \quad (2.6)$$

$$G = -k_B \ln Q + PV \quad (2.7)$$

However, the explicit expression of Q for the real system is not trivial to obtain. Thus, the application of certain simplifications is required to access an analytical expression for Q . First, the ideal gas of the indistinguishable molecules is considered. This allows for expressing the canonical partition function via the molecular partition function $q_{V,T}$:

$$Q_{N,V,T} = \frac{q_{V,T}^N}{N!} \quad (2.8)$$

Second, the molecular energy is assumed to be separable into different contributions. Thus, the molecular partition function can be represented as a product of the electronic

q_{el} , translational q_{tr} , rotational q_{rot} , and vibrational q_{vib} partition functions. The electronic partition function will not be considered here since it equals unity for the studied closed-shell systems near room temperature. For the other three contributions, the energy levels for the partition functions can be accessed from the solutions of the Schrödinger equation for the particle in the box, the rigid rotor, and the harmonic oscillator. The sum over all energy levels can be substituted by integration providing analytical expressions for the partition functions:

$$q_{\text{tr}}(V, T) = \frac{V}{h^3} (2\pi m k_{\text{B}} T)^{\frac{3}{2}} \quad (2.9)$$

$$q_{\text{rot}}(T) = \frac{\sqrt{\pi I_{\text{A}} I_{\text{B}} I_{\text{C}}}}{s} \left(\frac{8\pi^2 k_{\text{B}} T}{h^2} \right)^{\frac{3}{2}} \quad (2.10)$$

$$q_{\text{vib}}(T) = \prod_{j=1}^{3M-6(5)} \left(\frac{\exp(-\frac{h\nu_j}{2k_{\text{B}}T})}{1 - \exp(-\frac{h\nu_j}{k_{\text{B}}T})} \right) \quad (2.11)$$

where m is mass of the molecule; I_{A} , I_{B} , and I_{C} are principle moments of inertia; s is a symmetry number; h is the Planck constant; M is the number of atoms in the molecule; which gives $3M - 6$ and $3M - 5$ vibrational modes for non-linear and linear molecules, respectively; ν_j is the vibrational frequency. The thermodynamic functions can be easily derived from the analytical expressions mentioned above.[§]

Such treatment in the ideal gas rigid-rotor-harmonic-oscillator (RRHO) approximation has particular problems with the proper treatment of the vibrational frequencies obtained from WFT and DFT methods. Firstly, the vibrational frequencies obtained from these methods need to be scaled in order to achieve better agreement with the experimental values. Secondly, the low-lying frequencies from the harmonic approximation have a significant impact on the vibrational entropy leading to its overestimation. The minimization of such effects for the vibrational modes corresponding to the internal rotation can be done with Pitzer–Gwinn tables.^[190] An extension towards anharmonic frequencies can be done by the direct energy levels evaluation for the known potential energy of a given vibrational mode.^[191] Grimme has suggested another approach^[147] applicable for all low-lying modes below a specified threshold (e.g., 100 cm^{-1}). The final vibrational entropy contribution

[§]More details on the derivations can be found in the book by Donald A. McQuarrie.^[189]

2. Methodology

for a given frequency is interpolated between the entropies from results of the rotational and harmonic vibrational approximations using a Head-Gordon damping function.

2.5 Predictive Thermodynamic Model COSMO-RS

To access the thermodynamics properties of the solute in the solvent, a predictive thermodynamic model needs to be applied. In this thesis, a conductor-like screening model for realistic solvation (COSMO-RS) was used. The main advantage of this method is that any molecule, ion, or even transition state can be considered at an arbitrary solvent composition to obtain the Gibbs free solvation energy.

Within the COSMO-RS model,^[183,192] the reference state corresponds to the ensemble of noninteracting molecules in a perfect conductor. Each molecule is characterized by screening charge density on the surface (σ) calculated from COSMO-DFT/WFT methods (see subsection 2.2). The interaction energy (E_{int}) for the mentioned above state can be expressed via charge densities of the surface segments. To this end, the assumption that all parts of molecular surfaces can form only pairwise contacts (σ, σ') is applied. Thus, the statistical ensemble of the liquid reduces to an evaluation of the statistical ensemble of pairwise interacting segments. For the convenience, a distribution of the charge densities of the surface segments is characterized by a histogram. This histogram is showing the probability distribution to find a segment with a certain charge density. Such a distribution is also known as a σ -profile, $p(\sigma)$. The weighted sum of the σ -profiles of the solvent's components is used to construct the σ -profile of the solvent.

The calculation of the chemical potential of a solute X in a solvent S , μ_S^X , is performed in two steps in COSMO-RS. In the first step, the chemical potential of the surface segment, $\mu_S(\sigma)$, with screening charge density σ in a solvent S is calculated according to:

$$\mu_S(\sigma) = -k_B T \ln \left[\int p_S(\sigma') \exp \left(-\frac{E_{\text{int}}(\sigma, \sigma') - \mu_S(\sigma')}{k_B T} \right) d\sigma' \right] \quad (2.12)$$

Since $\mu_S(\sigma)$ appears on both sides of the equation, the resulted chemical potential can be found iteratively starting with $\mu_S(\sigma) = 0$ on the right hand side. In the second step, the

2.5. Predictive Thermodynamic Model COSMO-RS

integration of the $\mu_S(\sigma)$ over the surface of the solute X is conducted:

$$\mu_S^X = \int p^X(\sigma)\mu_S(\sigma)d\sigma + \mu_{\text{comb}}^X + \mu_{\text{disp}}^X \quad (2.13)$$

where μ_{comb}^X is a combinatorial contribution, which takes into account the difference in the relative size of the solute and the solvent; μ_{disp}^X is the dispersion interaction term, which is proportional to the surface area of the solute atoms. The mentioned above equations contain adjustable parameters requiring fitting to experimental data.

Part I.

Computer Design and Tuning of Ionic Liquids for CO₂ Absorption

Summary of Part I

An enormous number of theoretically possible ILs^[23] makes it challenging to predict the type of gas absorption in arbitrary ILs using widely applied computational methods. In most cases, the attempts to make such predictions rely on the static quantum chemical calculations in the gas-phase.^[141,143,144,193] These calculations are usually performed for a single cation, anion, and ion pair with a gas molecule.^[141,144,146,193] Subsequently, obtained interaction energies or reaction enthalpies are used to provide a qualitative or quantitative explanation of experimental results.^[141,142,144,146] However, the prediction of the gas absorption behavior with such an approach works only for a particular set of ionic liquids.^[141,193] Therefore, the development of simple and more universal theoretical protocols is highly desired to provide an answer to the expected absorption behavior of the gas in ILs.

In this Part, a set of theoretical protocols has been suggested to evaluate the absorption behavior of CO₂ in two classes of ILs. The first class contains an anion with varying basicity. The second class of ILs contains an amino acid anion obtained from natural amino acids.

For the first class of ILs, the basicity of the anion defines the type of the absorption. Thus, the properties of optimized anion-CO₂ complexes can reveal the types of CO₂ absorption. So far, the optimization of the anion-CO₂ complexes has been performed in the gas-phase^[141,143,193] providing some disagreement with the experimentally observed CO₂ absorption behavior. On the contrary, including a continuum solvation model in the geometry optimization significantly improves the results due to taking into account the high polarizability of ionic liquids. This simple improvement makes it possible to distinguish between chemical and physical absorption only from the value of the O-C-O angle. Two distinct types of interactions can be detected: the anions forming weak (the O-C-O angle >170°) and strong (the O-C-O angle <140°) interactions with CO₂. These groups are in good agreement with experimentally observed physical and chemical absorption of CO₂ in ILs with corresponding anions.

The developed protocol allows for a theoretical evaluation of the possible chemical

2. Computer Design and Tuning of Ionic Liquids for CO₂ absorption

absorption for the anion with varying basicity. However, these results are not useful to define the anions with a moderate binding strength desired for reversible chemical absorption. To specify the region of the potential anions, the Gibbs free energies of the reaction of CO₂ with the anion can be calculated. This characteristic includes thermal, entropy, and solvation corrections allowing for the direct comparison with the experiment. Potentially promising anions useful to design ILs for reversible CO₂ absorption have the calculated reaction Gibbs free energies from -30 to 16 kJ mol⁻¹ (see Chapter 3).

The suggested protocols can be extended to any proposed reaction in ILs. However, some ILs possess a complex set of reactions describing the gas absorption process, for example, CO₂ absorption in amino acid ionic liquids. The application of the gas-phase^[142,144] or bulk-phase^[139] static quantum chemical calculations to this class of ILs allows for considering only the pathways suggested from the chemical intuition. On the contrary, the use of the ab initio molecular dynamics (AIMD) allows to capture the possible reactions or their indication being unbiased from the predefined reaction mechanism. The important intermediates and products, as well as the most probable reaction channels, can be quickly established performing a set of AIMD simulations with a different composition (see Chapter 4). The established reaction pathways can be subsequently used to calculate the reaction Gibbs free energies and barriers according to the protocols from Chapter 3. Subsequently, varying a molecular structure of the cation and anion can be used to establish relative changes in the calculated free energies and barriers. These changes provide recipes for the subsequent knowledge-based design of ILs with improved absorption properties.

3 Computer-Aided Design of Ionic Liquids as CO₂ Absorbents

Dzmitry S. Firaha,* Oldamur Hollóczki,* and Barbara Kirchner*

Keywords: Absorption, Carbon Dioxide, Computer Chemistry, Ionic Liquids

Received: March 11, 2015, *Published online:* May 27th, 2015

Reprinted (adapted) with permission from

D. S. Firaha, O. Hollóczki, B. Kirchner *Angew. Chem. Int. Ed.* **2015**, *54*, 7805–7809.

Copyright ©2015 Wiley-VCH Verlag GmbH & Co. KGaA, Weinheim.

DOI 10.1002/anie.201502296

Own manuscript contribution

- Performance of calculations
- Analysis and interpretation of data
- Manuscript preparation

*Mulliken Center for Theoretical Chemistry, Institut für Physikalische und Theoretische Chemie, Rheinische Friedrich-Wilhelms-Universität Bonn, Berlingstraße 4+6, 53115 Bonn, Germany

3. Computer-Aided Design of Ionic Liquids as CO₂ Absorbents

Abstract Ionic liquids (ILs), vary strongly in their interaction with CO₂. We suggest a simple theoretical approach to predict the CO₂ absorption behavior of ILs. Strong interaction of the CO₂ with the IL anions corresponds to chemical absorption whereas weak interaction indicates physical absorption. A predictive estimate with a clear distinction between physical and chemical absorption can be simply obtained according to geometries optimized in the presence of a solvation model instead of optimizing it only in gas phase as has been done to date. The resulting Gibbs free energies were correlated with experimental capacities. Promising anions, for ionic liquids with reversible CO₂ absorption properties can be defined by a reaction Gibbs free energy of absorption in the range of -30 to 16 kJ mol⁻¹.

3.1 Introduction

Ionic liquids (ILs) are promising solvents for CO₂ absorption from various waste gases, and this property has been attracting significant scientific and technological attention in the last decade. To achieve maximal efficiency regarding the energy needs of both the transport and the regeneration of the absorbent, the absorption enthalpy is necessary to be in a relatively narrow range,^[61,67,144] but it can, of course, deviate from this desired value depending on the aims and the circumstances. Owing to the great variety of ILs (the estimated number of potential IL candidates is ca. 10¹⁵), the solubility and absorption enthalpy of CO₂ in them can be altered to a great extent, which allows a great deal of flexibility in optimizing these processes. On the other hand, this great variety makes the heuristic design of such solvents highly ineffective, requiring much material and effort.

A possible and desirable way to treat this issue is to establish a simple computational procedure that allows us to estimate the solubility of the present gas in the IL in question, so that many candidates can be screened at a time, while by the alternation of the IL structure the different properties can be tuned to the desired value, and finally only the best few substances need to be chosen for experimental inspection. Accordingly, many theoretical data have been published in recent years aiming at an in-depth understanding of CO₂-IL interactions, and also to predict the absorption behavior. To this end, gas-

phase binding energies were correlated with solubilities,^[141,193] and with capacities.^[194] Furthermore, gas-phase reaction enthalpies^[144] were determined from electronic structure methods to match or even predict experimental values.^[67]

Ab initio molecular dynamics simulations^[149] revealed that the CO₂ molecule shares weak but numerous dispersion interactions with the IL cation, while with the anion CO₂ often has a single,^[31,114,149] but the stronger interaction that can be described generally as the formation of a Lewis acid (CO₂)/ base (anion) pair. Although the two kinds of interactions are surmised to be equivalent in total strength in the solution,^[149] for the altering of the CO₂'s solubility the anion is more often the target,^[142] since the strong, and directional interactions are related to many of the anion's properties, such as its basicity.^[64,65]

Herein, we present simple methods based on solvated geometries that provide derive Gibbs free energies in very good agreement with experimental and also in excellent correlation with the experimentally observable absorption capacity (mole CO₂ per mole IL), in addition, the characterization of the interaction is rapidly achieved, helping the further tuning of the related IL absorbent candidates. As a result of this study, we also present several novel ILs that will presumably exhibit excellent absorption characteristics.

3.2 Results and Discussion

The calculated binding energies lie in between 0 and -250 kJ mol^{-1} for the gas-phase geometries and between 0 and -160 kJ mol^{-1} for the solvated geometries. Angles of the CO₂ molecule in the complex between 130° and 180° are found in both the gas and solvated geometries (Figure 3.1). From a chemical reaction that binds CO₂, substantial bending of this linear gas molecule can be expected, just as in the extreme example of its interaction with the very basic hydroxide anion, in which case the reaction results in the hydrocarbonate anion with an O-C-O bond angle of approximately 130° . Interestingly, when the CO₂'s bond angle in the complexes is plotted against the corresponding binding energies, two clear areas with two different complexes are obtained (boxes in Figure 3.1). One group of the anions induce less than 10° bending of the CO₂ and exhibit rather low

3. Computer-Aided Design of Ionic Liquids as CO₂ Absorbents

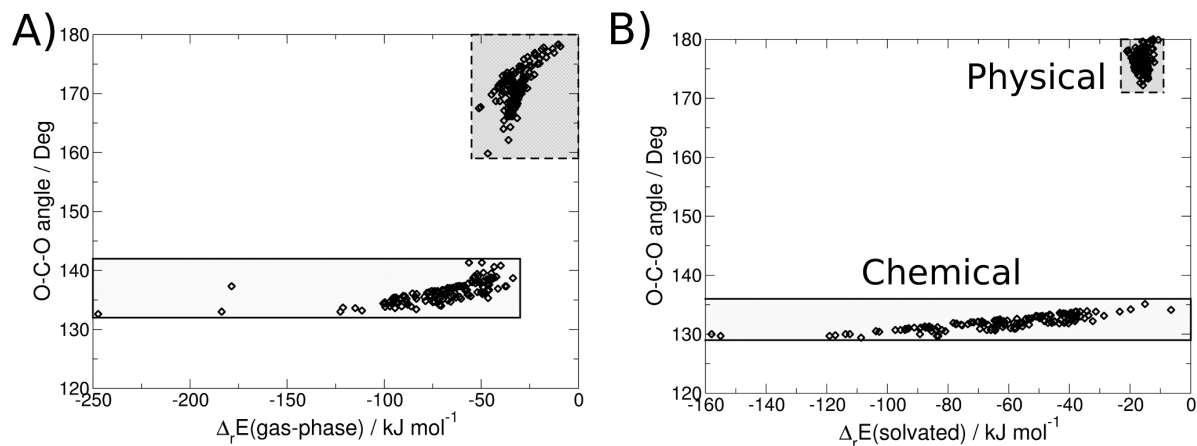
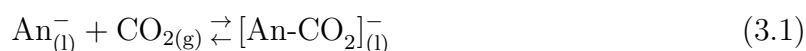


Figure 3.1. Binding energy versus O-C-O angle for the anion–CO₂ complexes. A) The binding energy is derived from standard optimization in the gas phase (isolated molecule); B) The binding energy is derived from optimization accounting for solvation by a continuum model, see Supporting Information A. Comparison of both panels show a much more distinct picture for the solvated geometries.

binding energies while the other group of the investigated structures shows significant bending. These two sorts of complexes can be attributed to physical and chemical absorption, respectively. Therefore, this approach can be considered an exact definition for the term "chemical absorption" in the present process. Below we will show that using the solvated geometries leads to a much better agreement with experimental observations while using gas-phase geometries gives erroneous behavior. From these results, it is also clear that to find a good absorbent candidate, aiming at chemical absorption would be a good choice because due to the larger range of binding energies these anions cover suggests that the tuning of the IL to fit best to the desired process should be more straightforward.

Although the cations (Cat) form many interactions, and thus in total a strong interplay, with the solute gas molecule,^[149] according to previous experimental data^[31,195,196] the absorption can be altered by changing the anion (An), thus, to estimate the effect of the anion on the CO₂'s absorption enthalpy, the enthalpy of the binding reaction [Eq. (3.1)]



serves as a measure. Exception are when the cation is also performing chemical absorption.^[149,197] A value for the equilibrium constant higher than unity indicates a considerable

absorption capacity of ILs at the room temperature and moderate pressure,^[67] which requires a reaction Gibbs free energy ($\Delta_r G_{\text{exp}}$) between -20 and 6 kJ mol^{-1} for the forward reaction. Stronger binding energies will prevent the desorption process. To estimate these values, we employed an approach, which — in contrast to the previous studies^[66,67,144,198] — also takes into account the thermal corrections for the relevant species of Equation (3.1), that is, An^- and $[\text{An-CO}_2]^-$, and the solvation contribution^[147] by accounting for $[\text{Cat}][\text{An}]$ assemblies as ILs (details are given in the Supporting Information A).

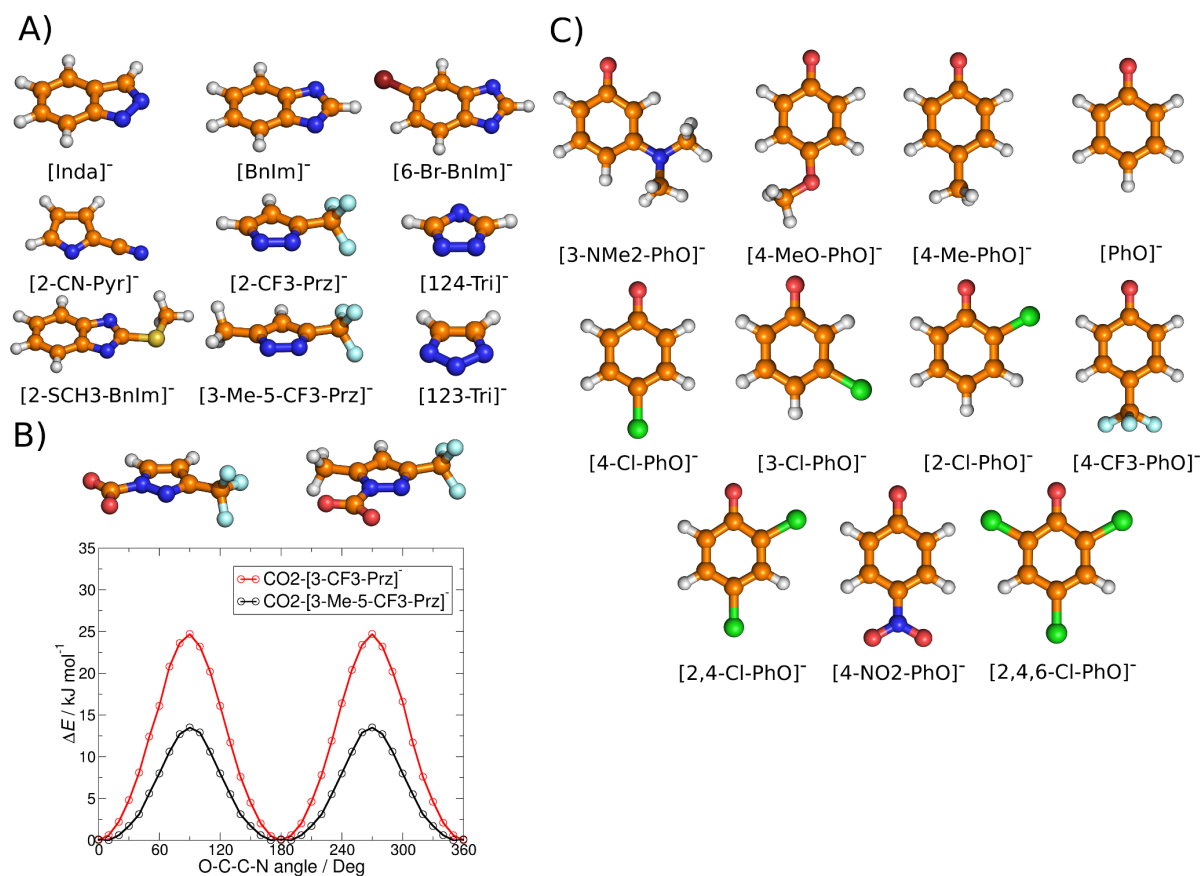


Figure 3.2. Ball-and-stick picture together with abbreviations of the anion test set chosen from A) Ref. [67] left and C) Ref. [66]. White H; brown C; blue N; dark red Br and light blue F; gold S; green Cl. B) Optimized geometries of carboxylates and calculated rotation profile for both of them. Despite the +I effect steric hindrance can decrease the capacity. Note the abbreviations Ph, Pyr etc. are, against the IUPAC recommendations, used to indicate substituted groups, e.g. Ph also indicates C_6H_4 and C_6H_3 .

For a set of anions, for which also $\Delta_r G_{\text{exp}}$ data are available with consistently the same cation trihexyl(tetradecyl)phosphonium; $[\text{P}_{6,6,6,14}]^+$, the calculated and experimental^[67]

3. Computer-Aided Design of Ionic Liquids as CO₂ Absorbents

Table 3.1. Computed and experimental properties.^[a,b]

Anion ^[c]	$\Delta_r H$	$\Delta_r G_{\text{calc}}$	$\Delta_r G_{\text{exp}}$	Abs. cap. ^[d]
[Inda] ⁻	-63	-26	-16	0.92
[BnIm] ⁻	-67	-23	-13	0.91
[6-Br-BnIm] ⁻	-57	-11	-9	0.90
[2-CN-Pyr] ⁻	-47	-7	-6	0.88
[3-CF ₃ -Prz] ⁻	-52	-9	-6	0.87
[124-Tri] ⁻	-60	-9	-4	0.76
[2-SCH ₃ -BnIm] ⁻	-48	1	-3	0.72
[3-Me-5-CF ₃ -Prz] ⁻	-49	3	-2	0.63
[123-Tri] ⁻	-53	-1	2	0.25

[a] Computed reaction gas-phase enthalpies ($\Delta_r H$) and solvated Gibbs free energies ($\Delta_r G_{\text{calc}}$) and derived experimental Gibbs free energies $\Delta_r G_{\text{exp}}$ at 298.15 for the reaction in Equation (3.1) for the anions in Ref. [67]. Ball-and-stick diagrams to the corresponding abbreviations are depicted in Figure 3.2A. All energies in kJ mol⁻¹. [b] The experimental equilibrium constants from Ref. [67] were used to calculate $\Delta_r G_{\text{exp}}$ at 293 K. [c] Definitions for the abbreviations can be found in the Supporting Information A. [d] Absorption capacities in mol CO₂ per mol IL. The data was interpolated to pressure 0.9 bar from the nearest experimental points of Ref. [61, 67].

data are listed in Table 3.1. The two $\Delta_r G$ results show very good agreement, both in absolute values and in the trend, with a largest absolute deviation of 10 kJ mol⁻¹ which means potential candidates to be considered are in the range of -30 to +16 kJ mol⁻¹. This excellent match clearly aids the comparison of experiment and theory, while allowing a more detailed understanding of the IL-CO₂ interactions at the molecular level. Clearly, substitution of the anions with electron-withdrawing (-I and -M effect) or electron-donating (+I and +M effect) groups changes the capacity and $\Delta_r G$ in a logical way. Attaching a bromide substituent to the anion's ring as in [6-Br-BnIm]⁻ compared to [BnIm]⁻ decreases the absorbing abilities, hence the slightly smaller capacity. Adding a SCH₃ group between the two nitrogen atoms which exhibit a high steric demand results in [2-SCH₃-BnIm]⁻ being also a worse absorbent than [6-Br-BnIm]⁻. The +I effect provided by the Me group in [3-Me-5-CF₃-Prz]⁻ compared to [3-CF₃-Prz]⁻ is non-beneficial because of the steric hindrance which is revealed by the additional structures of the two carboxylate complexes and their rotation profile shown in Figure 3.2. Note that for the frequently

applied $\Delta_r H$ values^[66,67,144,198] this agreement is significantly rougher, as these values lack the solvation and entropy contributions.

Table 3.2. O-C-O angles and related properties.^[a]

Anion	O-C-O Angles [°]		$\Delta_r G_{\text{calc}}$ [kJ mol ⁻¹]	Capacity ^[b]
	gas	solv		
[3-NMe ₂ -PhO] ⁻	138	132	-3	0.94
[4-MeO-PhO] ⁻	137	132	-14	0.92
[4-Me-PhO] ⁻	138	132	-9	0.91
[PhO] ⁻	138	132	-7	0.85
[4-Cl-PhO] ⁻	140	132	0	0.82
[3-Cl-PhO] ⁻	141	132	12	0.72
[2-Cl-PhO] ⁻	164	132	11	0.67
[4-CF ₃ -PhO] ⁻	166	133	16	0.61
[2,4-Cl-PhO] ⁻	167	133	19	0.48
[4-NO ₂ -PhO] ⁻	171	134	32	0.30
[2,4,6-Cl-PhO] ⁻	171	134	39	0.07

[a] O-C-O angles, reaction Gibbs free energies ($\Delta_r G_{\text{calc}}$) on solvated geometries, and the experimental CO₂ absorption capacity for trihexyl(tetradecyl)phosphonium ILs. Ball-and-stick pictures of the phenolate anions are provided in Figure 3.2C. [b] The data were taken from Ref. [66]. For [P_{6,6,6,14}][4-NO₂-PhO] ionic liquid the CO₂ capacity was determined at 20° C, whereas for the remaining ILs it was determined at 30° C.

Figure 3.1 shows the distinction between physical and chemical absorption is possible based on the knowledge of very simple reaction energies and calculated O-C-O angles. However, care has to be taken to obtain the right geometries as demonstrated in Table 3.2 in which we list some critical phenolte ionic liquids. Experimental capacities clearly point to chemical absorption^[66] — physical absorption under the same condition does not exceed 0.04 mole CO₂ per mole IL; also, measured FTIR spectra revealed additional peaks at approximately 1600 cm⁻¹;^[66,197] while the ¹³C NMR spectrum provided a new band at $\delta = 161$ ppm during the absorption of CO₂, thereby also indicating the formation of carboxylate salts.^[66] Gas-phase geometries (O-C-O angles in Table 3.2) do not reproduce the given tendency, however interestingly the solvated geometries all behave according to experimental trends in that they show angles around 133°.

3. Computer-Aided Design of Ionic Liquids as CO₂ Absorbents

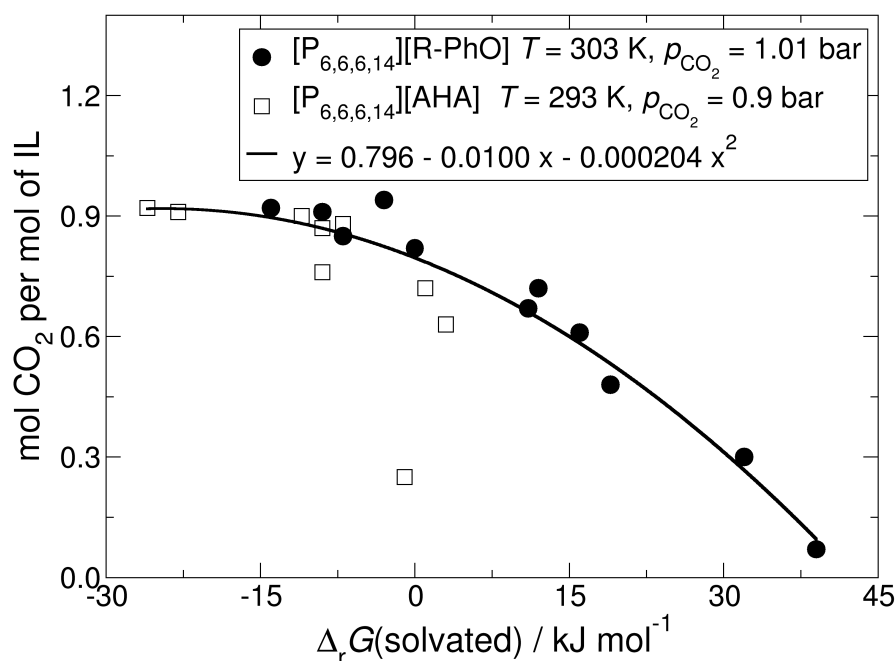


Figure 3.3. Correlation of calculated $\Delta_r G_{\text{calc}}$ and CO₂ capacities. [R-PhO] indicate the phenolate anions in Table 3.2 and Figure 3.2 right; [AHA]=aprotic heterocyclic anions.

Having established a simple procedure to indicate chemical absorption, namely the O-C-O angle of solvated carboxylate geometries, we turn now to the further refinement of predicting suitable CO₂ absorbents. To arrive at a predictive tool we correlated all calculated $\Delta_r G_{\text{calc}}$ values based on solvated geometries with the experimental capacities in Figure 3.3 which demonstrates the applicability. Care has to be taken when dealing with 1,2,3-triazole anions but otherwise the quadratic fit matches the points well enough to provide an estimate and also it confirms the energy range of 16 to -30 kJ mol^{-1} ; note the convergence behavior around -30 kJ mol^{-1} . We used the optimized geometries and the known $\Delta_r G_{\text{calc}}$ range in order to establish possible azalide candidates^[62–65] which are given in Figure 3.4 together with their energies and estimated capacities. Owing to the deviating behavior shown in Figure 3.3, the results for 1,2,3-triazole anions should be treated with special care. While the pyrrole anions show a weak trend with substitution and good capacities in the range of 0.81–0.89 (at the energy range of -2 and -8), the pyrazole anions achieve higher capacities especially when substituted in the α -position with electronegative atoms. While imidazole anions can exhibit superior capacities (0.91

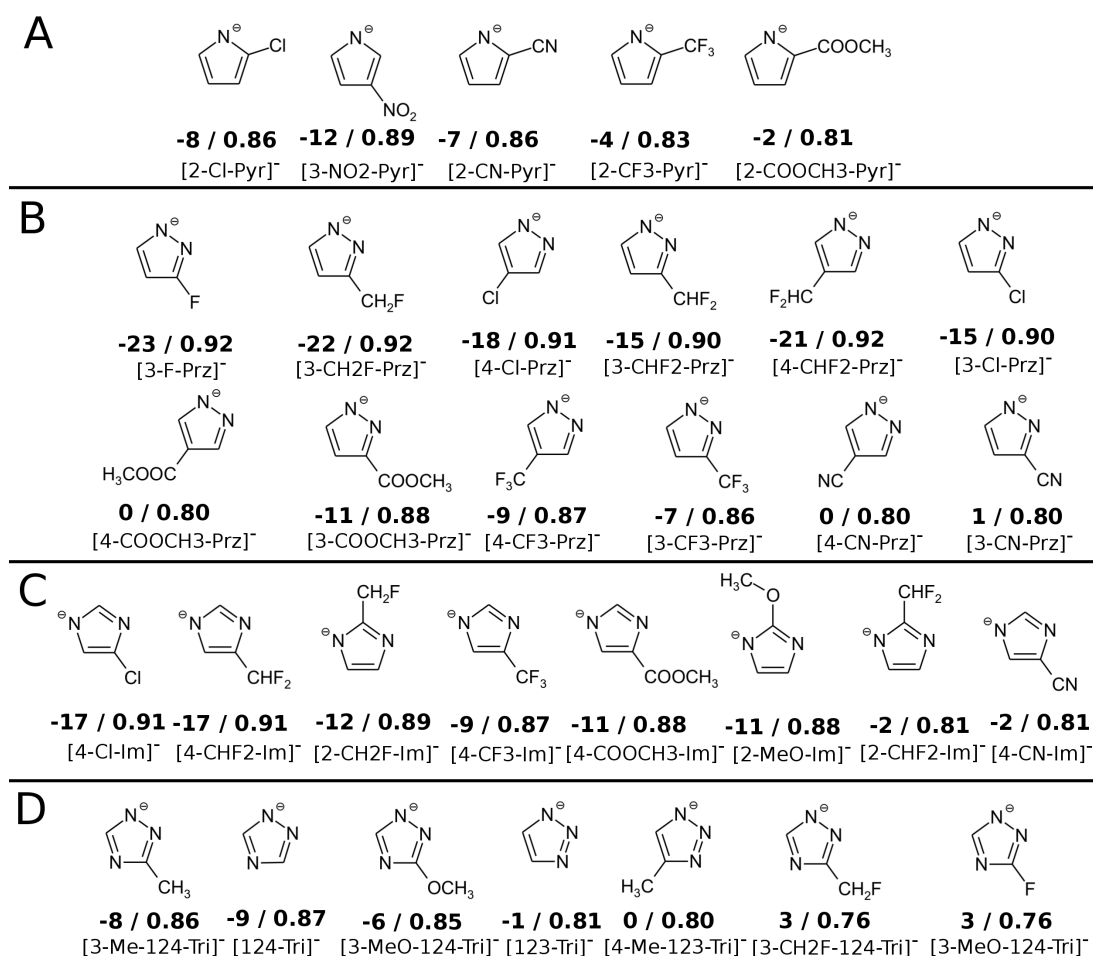


Figure 3.4. List of the anions suitable for the chemical absorption of CO₂. A) contains pyrrolide-based anions, B) pyrazolide-based anions, C) imidazolide-based anions, and D) triazolide-based anions. The values of the $\Delta_r G_{\text{calc}}$ and calculated capacity from the quadratic fit in Figure 3.3 are given under each Lewis structure.

at $\Delta_r G_{\text{calc}} = -17 \text{ kJ mol}^{-1}$ the triazole anions only show moderate (0.76) to good (0.86) capacities.

3.3 Summary

In Conclusion, we can say that when calculated solvated carboxylate geometries exhibit O-C-O-angles smaller than 140° a chemical absorption is very probably. Based on this, calculated $\Delta_r G_{\text{calc}}$ and correlated capacities — if $\Delta_r G_{\text{calc}}$ lies between -30 and 16 kJ mol^{-1} — indicate possible candidates for good to excellent chemical absorption. We provided several examples of possible candidates which might be tested experimentally.

3.4 Acknowledgements

The financial support from DAAD for Dzmitry Firaha, from DFG through project KI-786/12-1, and SPP 1708 is gratefully acknowledged.

4 Tuning the Carbon Dioxide Absorption in Amino Acid Ionic Liquids

Dzmitry S. Firaha* and Barbara Kirchner*

Keywords: Ab Initio Calculations, CO₂ absorption, Amino Acids, Ionic Liquids, Reaction Mechanism

Received: January 29, 2016, *Published online:* May 23th, 2016

Reprinted (adapted) with permission from

D. S. Firaha, B. Kirchner ChemSusChem. **2016**, *13*, 1591–1599.

Copyright ©2016 Wiley-VCH Verlag GmbH & Co. KGaA, Weinheim.

DOI 10.1002/cssc.201600126

Own manuscript contribution

- Performance of the ab initio molecular dynamics simulations
- Performance of the static quantum chemical calculations
- Analysis of the trajectories
- Interpretation of the data
- Manuscript preparation

*Mulliken Center for Theoretical Chemistry, Institut für Physikalische und Theoretische Chemie, Rheinische Friedrich-Wilhelms-Universität Bonn, Berlingstraße 4+6, 53115 Bonn, Germany

4. Tuning the Carbon Dioxide Absorption in Amino Acid Ionic Liquids

Abstract One of the possible solutions to prevent global climate change is the reduction of CO₂ emissions, which is highly desired for the sustainable development of our society. In this work, the chemical absorption of carbon dioxide in amino acid ionic liquids was studied through first-principles methods. The use of readily accessible and biodegradable amino acids as building blocks for ionic liquids makes them highly promising replacements for the widely applied hazardous aqueous solutions of amines. A detailed insight into the reaction mechanism of the CO₂ absorption was obtained through state-of-the-art theoretical methods. This allowed us to determine the reason for the specific CO₂ capacities found experimentally. Moreover, we have also conducted a theoretical design of ionic liquids to provide valuable insights into the precise tuning of the energetic and kinetic parameters of the CO₂ absorption.

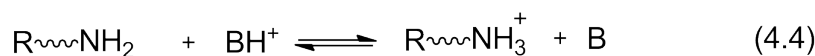
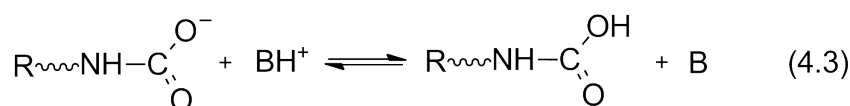
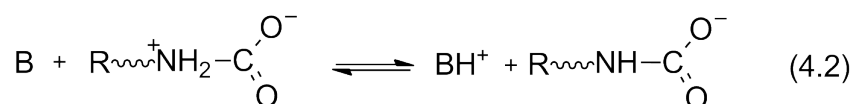
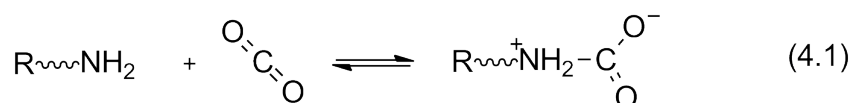
4.1 Introduction

The increasing CO₂ emissions owing to the enormous usage of fossil fuels (coal, oil, and natural gas) as the main source of energy is linked directly to the present global climate changes.^[4-7] Therefore, possible methods to overcome the side effects of CO₂ emission are currently under extensive investigation. One of the starting points is the removal of CO₂ from industrial waste gases. This topic has attracted great interest from scientists in recent decades.^[43,199-201] CO₂ capture in aqueous amine solutions is the most popular and developed method for large-scale applications.^[21,202] However, this technology is far from “green” and sustainable^[203] owing to several serious drawbacks including high regeneration energy, high volatility, instability, and corrosion.^[204-207] All of these drawbacks are responsible for increased maintenance costs; therefore, the development of better alternative for the CO₂ absorption processes is of crucial importance.

Ionic liquids (ILs) occupy a special place^[43,201] among different solid^[199,200] and liquid alternatives (Table 2 in Ref. [208]) for the elimination of the aforementioned problems. These liquids, composed entirely of ions, have shown great potential for the tuning of their physicochemical properties owing to almost infinite possible combinations of different cations and anions. The physical absorption of CO₂ in ILs is higher than that in

conventional organic solvents.^[209] However, the absorption capacities of unmodified ILs are too low to enable their use for CO₂ capture. To increase their CO₂ absorption capacities, ILs need to be modified in such a way that the chemical absorption of CO₂ becomes accessible. The introduction of amine groups in the cation^[56] or anion^[58–60] is one of the easiest and most straightforward methods among the different strategies developed for the enhancement of CO₂ capacity.^[61–65,67–69,71,72]

Amino acid ionic liquids (AAILs) are particular representatives of amine-functionalized ILs.^[210,211] As amino acids are building blocks of proteins and readily available at reasonable prices, the large-scale preparation of high-purity AAILs can be performed readily. Moreover, AAILs possess higher CO₂ absorption rates than those of most ethanolamine derivatives, pure amino acids, amino acid salts, and ILs with aprotic heterocyclic anions (Table 2 in Ref. [208]). Therefore, AAILs are attractive for industrial use. Furthermore, the reaction of CO₂ with the amine group follows the sequence of elementary steps depicted in Equations (4.1)-(4.4);^[212] therefore, AAIL-CO₂ systems are also interesting from an academic point of view.



The CO₂ absorption by amines through the mechanism depicted in Equations (4.1)-(4.4)^[212] is well-established and has been studied extensively for substituted ethanolamines.^[213–218] The formation of the zwitterionic carbamate occurs in the first step of the reaction sequence [Eq. (4.1)]. Subsequently, the zwitterionic carbamate, R-⁺NH₂-COO⁻, undergoes proton abstraction by the Lewis base B [Eq. (4.2)]. Then, the newly formed carbamate or an available amine group can abstract the proton back from BH⁺ [Eqs. (4.3) and (4.4)]. Thus, amine-functionalized solvents with absorbed CO₂ represent

4. Tuning the Carbon Dioxide Absorption in Amino Acid Ionic Liquids

mixtures of carbamates (R-NH-COO^-) ammonium ions (R-NH_3^+), and carbamic acids (R-NH-COOH) at equilibrium. The CO_2 capacity in such equilibrium mixtures varies from 1:2 (1 mole CO_2 per 2 mole of amine or 33 molar %) to 1:1 (or 50 molar %). The existing equilibrium is sensitive to the external conditions and the molecular composition of the solution. For example, lower temperatures or higher CO_2 partial pressures^[60,219,220] shift the equilibrium towards 1:1 capacity.^[59,60,219,220] Similarly, the attachment of the amine group to the anion instead of to the cation provides higher capacities.^[56,58–60] Changing the location of the CO_2 absorption from the bulk to the surface of the IL with an amine functionalized anion also increases the CO_2 capacity to 1:1 at moderate pressure of CO_2 .^[220] Finally, increasing the cation size is responsible for higher CO_2 absorption capacity for some AAILs.^[58,60,221–223]

A vast amount of experimental work has been done on CO_2 absorption in neat AAILs to establish the characteristics of the absorption capacity.^[57–60,222,224] The high viscosities of AAILs before CO_2 absorption and their dramatic increase after CO_2 absorption have led to the investigation of methods to reduce the viscosity, prevent its increase, or both. Mixtures of AAILs with water^[72,225,226] or low-viscosity ILs,^[227,228] the immobilization of AAILs into porous materials,^[208,221,223,229] and AAILs with the possibilities to form intramolecular hydrogen bonds^[230] have been considered. However, the available theoretical work deals with density functional theory calculations of several amine-functionalized anions and cations^[142,144] to explain the 1:2 or 1:1 absorption capacity owing to the stabilization or destabilization effect of the cation or anion on the carbamic acid. This approach and more sophisticated calculations such as G3 and G4 calculations were applied to obtain the enthalpies of the CO_2 absorption.^[58,144] Classical molecular dynamics simulations were applied to explain the dramatic increase of the viscosity by Maginn et al.^[118] The formation of the extended cation-anion network was detected between the carbamate and the ammonium ions. To access large-scale modeling of AAILs+ CO_2 systems, the development of a reactive force field for the tetrabutylphosphonium glycinate was developed by Zhang et al.^[139]

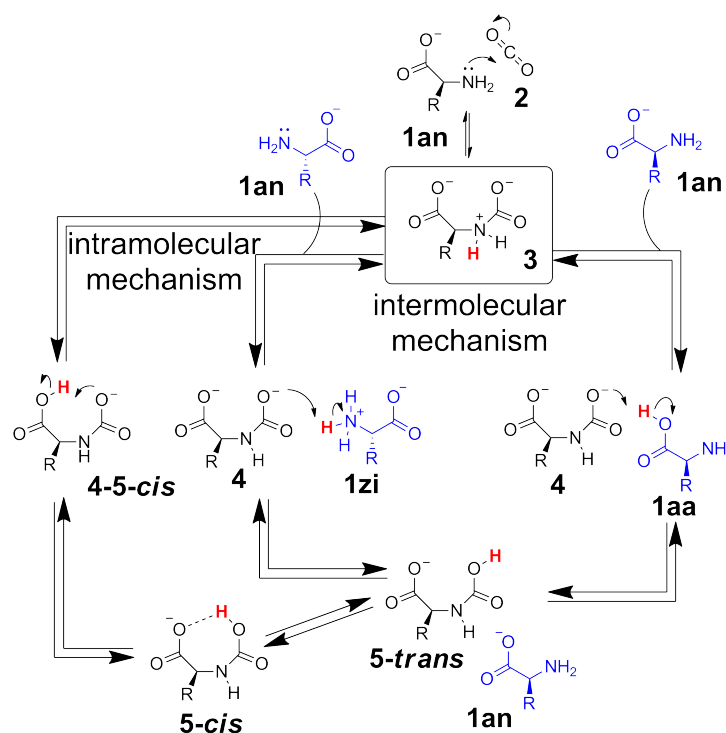
To improve our understanding of systems as sophisticated as AAILs for CO_2 absorption, more extensive and systematic theoretical studies are desirable. Herein, we present

first-principles studies on CO₂ absorption in AAILs to provide valuable recipes for further experimental studies and large-scale modeling. We investigate the possible reactions pathways in the AAIL+CO₂ system through ab initio molecular dynamics. Then, the kinetics and thermodynamic aspects of the CO₂ absorption process are considered for 50 AAILs to derive the structural features responsible for the facilitation of higher absorption rates and the desired 1:1 capacity.

4.2 Results and Discussion

4.2.1. CO₂ Absorption Pathways

We distinguish the inter- and intramolecular mechanism of the CO₂ absorption after the application of the general mechanism from Equations (4.1)-(4.4) to the AAILs (Scheme 4.1).



Scheme 4.1 Possible pathways of CO₂ absorption in AAILs.

The intermolecular mechanism suggested by Caplow^[212] includes an active participation of the media in the abstraction and transfer of the proton from the (amino acid

4. Tuning the Carbon Dioxide Absorption in Amino Acid Ionic Liquids

anion)-CO₂ adduct (**3**). In contrast, the recently suggested intramolecular mechanism^[139] does not require the active participation of the medium. This pathway could be important in systems possessing low hydrogen bond acceptability, low basicity or low mobility of the anion, that is, if AAILs are being used in supported ionic liquids phases.^[231]

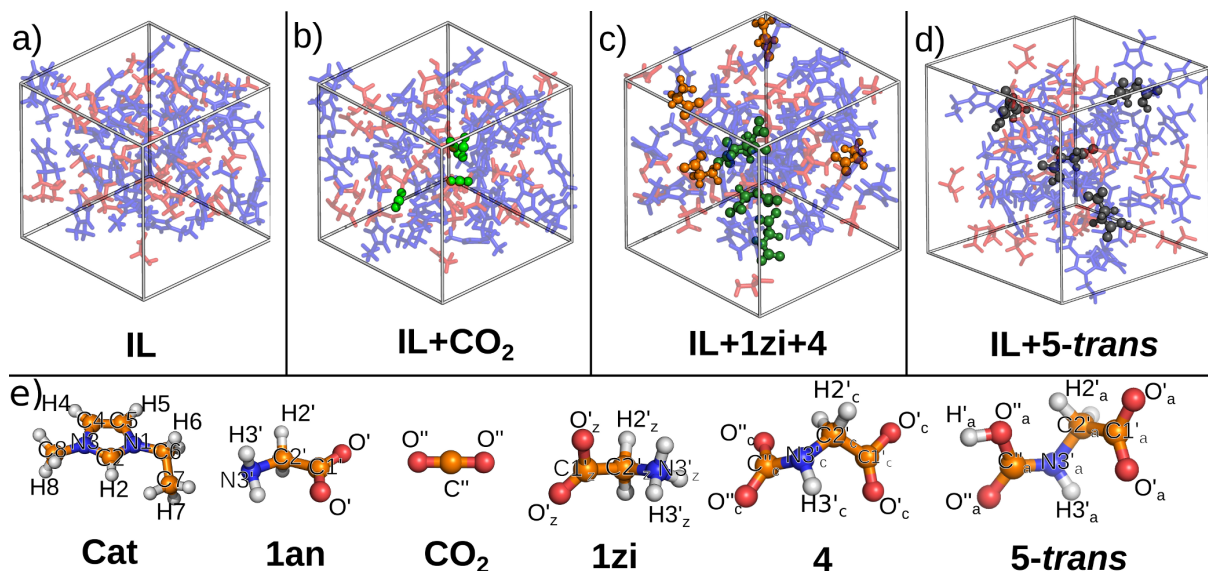


Figure 4.1. Representative snapshots of the simulation boxes: (a) pure IL, (b) IL with CO₂, (c) IL with glycine zwitterion and carbamate (*N*-carboxylate glycinate) and (d) IL with carbamic acid. [C₂C₁Im][Gly] (cations in blue, anions in red) illustrated with sticks and CO₂ (green), glycine zwitterion (orange), carbamate (dark green) and carbamic acid (gray) illustrated with ball-and-stick representation. (e) Ball-and-stick representation of ions and molecule: the [C₂C₁Im]⁺ cation, [Gly]⁻ anion, CO₂, glycine zwitterion, carbamate and carbamic acid in the starting geometries of the simulated boxes. Red: oxygen, blue: nitrogen, orange: carbon, white: hydrogen. Note: atoms from the cation: without primes; atoms from the anion: one prime; atoms from CO₂: two primes; atoms from glycine zwitterion: prime and “z” subscript; atoms from carbamate or carbamic acid: one or two primes and “c” or “a” subscript, respectively.

4.2.2. Applied Methodologies and Considered Systems

The CO₂ absorption in AAILs consists of at least three possible channels or reaction pathways. To determine the most probable and relevant reaction channel, we performed ab initio molecular dynamics (AIMD) simulations. In the AIMD simulations, the forces on the atoms are obtained through electronic-structure methods on-the-fly. Thus, the method does not depend on the quality of the parametrization, which has a large in-

fluence on classical or reactive force fields. The main advantage of AIMD simulations over classical molecular dynamics simulations is that the chemical reactions or at least an indication of their occurrence can be studied. However, the time and size scales of the AIMD simulations are restricted to ca. 100 ps and a few dozen ion pairs. Owing to these obstacles, we only simulated one AAIL, 1-ethyl-3-methylimidazolium glycinate ($[\text{C}_2\text{C}_1\text{Im}][\text{Gly}]$; Figure 4.1, further details can be found in the Supporting Information B). We modeled pure $[\text{C}_2\text{C}_1\text{Im}][\text{Gly}]$ (**IL**) containing 32 ion pairs to be able to compare to the unimpared structure of the pure AAIL. Then, four CO_2 molecules were inserted randomly into the prepared simulation box of pure $[\text{C}_2\text{C}_1\text{Im}][\text{Gly}]$ (**IL+CO₂**) to consider the time evolution and possible indication of chemical absorption. In an additional simulation, 32 $[\text{C}_2\text{C}_1\text{Im}]^+$ cations, 24 $[\text{Gly}]^-$ anions (**1an**), four glycinate zwitterions (**1zi**) and four carbamates (**4**) were treated. This system is coined **IL+1zi+4**. Finally, we simulated the **IL+5-trans** system consisting of 32 $[\text{C}_2\text{C}_1\text{Im}]^+$ cations, 28 $[\text{Gly}]^-$ anions (**1an**) and four carbamic acids (**5-trans**). All trajectories were simulated with the CP2K software^[232] at 350 K (the detailed computational set up is given in the Supporting Information B). The simulated trajectories were subsequently processed with TRAVIS.^[148] The main attention was paid to the analysis of the relevant distances, which are affected most during the course of equilibrium chemical reactions according to Scheme 4.1. We use the "A-B" notation to specify covalently bonded atoms A and B. The "intramolecular A...B" and "intermolecular A...B" notations are related to the non-bonded pair of atoms from the same molecule and different molecules, respectively.

The AIMD simulations provide qualitative results for a particular AAIL and can be extended readily to other AAILs. However, information about the relative stabilities of the intermediates and products as well as the energy barriers of the possible reactions are required to characterize the AAIL+ CO_2 systems quantitatively. To this end, a faster approach delivering the relative free energies and barriers is more desirable than the time-consuming free-energy techniques available from AIMD simulations.^[233] The recent development of first-principles methods allows the evaluation of the accurate and reliable relative Gibbs free energies (ΔG) of the considered intermediates and the products as well as the energy barriers (ΔG^\ddagger) for the chemical reactions.

4. Tuning the Carbon Dioxide Absorption in Amino Acid Ionic Liquids

The evaluation of ΔG and ΔG^\ddagger requires a composite approach. This approach consists of the combinations of DFT and wave-function theories, statistical thermodynamics (StatTD), and a predictive thermodynamic model. In the first step, we performed DFT geometry optimization and frequency calculations of the relevant reactants, transition states, intermediates, and products depicted in Scheme 4.1. We considered different amino acid anions such as glycinate ($[\text{Gly}]^-$), L-alanate ($[\text{Ala}]^-$), L-valinate ($[\text{Val}]^-$), L-leucinate ($[\text{Leu}]^-$), L-isoleucinate ($[\text{Ile}]^-$), L-prolinate ($[\text{Pro}]^-$), L-phenylalanate ($[\text{Phe}]^-$), L-tyrosinate ($[\text{Tyr}]^-$), L-serinate ($[\text{Ser}]^-$) and L-theoninate ($[\text{Thr}]^-$) to test the influence of bulky nonpolar, aromatic, hydroxylic substituents and their combinations with the initial glycinate structure. All calculations were performed with a fixed dielectric constant ($\epsilon = 15$) to obtain stable geometries for the zwitterionic forms of the amino acids. We have also shown previously that the inclusion of the continuum model with a fixed dielectric constant in the optimization procedure allows access to the proper geometries for anion- CO_2 complexes and the subsequent distinction between chemical and physical absorption.^[234,235] In the second step, we performed the calculations of the reliable electronic energies on top of the obtained geometries. These energies are the first contribution required for the calculation of ΔG and ΔG^\ddagger . The coupled-cluster method with single, double, and perturbative triple excitations, CCSD(T), is considered nowadays as a gold standard for closed-shell systems within the wave-function theory.^[156] However, this method scales as $O(N^7)$, in which N is the number of basis functions. Therefore, we used the domain-based local pair natural orbitals approximation of the CCSD(T), DLPNO-CCSD(T),^[158] which scales as $\sim O(N^{2.30})$, that is close to the B3LYP method $\sim O(N^{2.27})$, and provides the energies within error of 1 kJ mol⁻¹ from CCSD(T).^[159] In the third step, we conducted zero point vibrational energies and StatTD calculations of the thermal corrections to the finite temperature ($T = 298.15$ K) from the DFT geometries and frequencies according to the approach described in Ref. [147]. These calculations provide the second contribution to ΔG and ΔG^\ddagger . In the final step, the free solvation energies from the predictive thermodynamic model were calculated. These energies are the final contribution to ΔG and ΔG^\ddagger . The solvation free energy can be obtained from different theoretical approaches such as the universal quasichemical functional-group ac-

tivity coefficient (UNIFAC),^[95] the conductor-like screening model (COSMO),^[96,97,236] and regular solution theory.^[98] Here, we calculated the solvation energies from the COSMO for realistic solvation (COSMO-RS) theory in the COSMOTHERMX14 program.^[237] We used different cations such as 1-ethyl-3-methylimidazolium ($[\text{C}_2\text{C}_1\text{Im}]^+$), 1-decyl-3-methylimidazolium ($[\text{C}_{10}\text{C}_1\text{Im}]^+$), 1-(3,4,5,6,7,8,9,10,11,12-perfluorododecyl)-3-methylimidazolium ($[(\text{C}_F)_{10}\text{C}_2\text{C}_1\text{Im}]^+$), tetraethylphosphonium ($[\text{P}_{2,2,2,2}]^+$) and trihexyl-(tetradecyl)phosphonium ($[\text{P}_{6,6,6,14}]^+$) to test the effects of cation size, the presence of an aromatic system, side-chain elongation, and perfluorination. These cations were combined with the aforementioned anions to model the solvent composition at the beginning of the CO_2 absorption, that is, $[\text{Cat}][1\text{an}]$. This composition was used to characterize the formation of the (amino acid anion)- CO_2 adduct and the intramolecular proton transfer within the adduct. Owing to the change of the solvent composition during the course of the CO_2 absorption, we also consider other solvent compositions such as idealized 1:2, $[\text{Cat}][1\text{zi}]_{0.5}[4]_{0.5}$, and 1:1, $[\text{Cat}][5\text{-trans}]$, for 1-ethyl-3-methylimidazolium glycinate. Finally, to estimate to which extent the equilibrium reactions shifted towards the reactants or products we set the solvent composition between 1:2 and 1:1, that is, $[\text{Cat}][5\text{-trans}]_{0.5}[1\text{zi}]_{0.25}[4]_{0.25}$.

The above-described composite approach provides an estimated error of ΔG and ΔG^\ddagger of approximately 10 kJ mol^{-1} . Such an error prohibits the direct evaluation of the rate and equilibrium constants. However, the relative change of rate and equilibrium constants ($\ln k \sim -\Delta G^\ddagger (RT)^{-1}$ and $\ln K_{\text{eq}} = -\Delta G (RT)^{-1}$) can be easily deduced for a sequence of similar AAILs. This analysis allows the determination of the influence of different functional groups on the considered reaction channels, the absorption rate constants, and the absorption equilibrium constants.

We also postulated that no chemical reactions occur between the cation and anion, owing to the low basicity of the carboxylate and the amine groups. Proton abstraction from the cation by the anion might have caused a carbene^[68,69,238,239] or an ylide^[71] formation, which are responsible for the cation channel of the CO_2 absorption.

4.2.3. Formation of the Glycinate-CO₂ Adduct

An insight into the structural changes that occur in the **IL**+CO₂ system was obtained by considering two important distances involved directly in the reactions [see Eqs. (4.1)-(4.4)]. These are the intermolecular N3'([Gly]⁻)⋯C''(CO₂) distance, which defines the formation of the glycinate-CO₂ adduct (**3**) and the N3'-H3'([Gly]⁻) bond length, which can be used to detect the proton abstraction. The corresponding combined distribution function (CDF) of these distances is presented in Figure 4.2a. Three distinct combina-

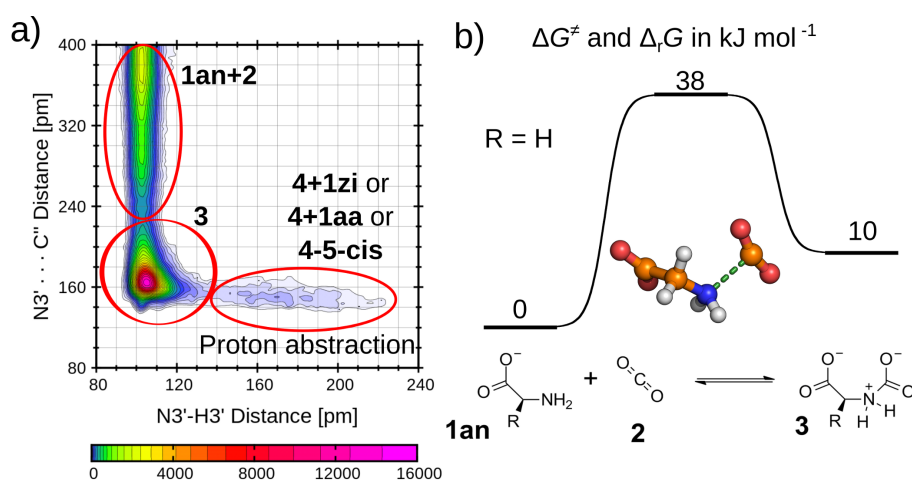


Figure 4.2. (a) CDF analyzing the intermolecular N3'⋯C'' distance versus the N3'-H3' bond length. *Upper left ellipse:* physisorbed CO₂ (**1an+2**), *bottom left ellipse:* glycinate-CO₂ adduct (**3**), *bottom right ellipse:* proton abstraction from the glycinate-CO₂ adduct (**4+1zi** or **4+1aa** or **4-5-cis**). (b) Energy diagram for the formation of the glycinate-CO₂ adduct from CO₂ and glycinate anion. Note: CO₂ is not solvated, whereas the glycinate, the transition state and the glycinate-CO₂ adduct are solvated by the [C₂C₁Im][Gly] IL. The relative energies for the transition state and the product for other AAILs are summarized in Table 4.1 and Table B.1, respectively.

tions of the intermolecular N3'⋯C'' distance and the N3'-H3' bond length are detected clearly in the plot. The long-short combination corresponds to the physisorbed state of CO₂ in AAIL (**1an+2**). The short-short combination represents the formed glycinate-CO₂ adduct (**3**). The short-long combination indicates the proton abstraction (**4+1zi**, **4+1aa**, **4-5-cis**). Our results show that the formation of the glycinate-CO₂ adduct is reversible (Figure B.1). This indicates that the energy barrier for the CO₂ release from the adduct is thermally accessible. To verify this hypothesis, we calculate the relative

Gibbs free energies from the composite approach for the solvated transition state and the solvated adduct with respect to unsolvated CO₂ and the solvated anion (Figure 4.2b). The barrier of the forward reaction is 38 kJ mol⁻¹, whereas that of the reverse reaction is 28 kJ mol⁻¹. The latter value agrees well with values (29-42 kJ mol⁻¹) obtained from metadynamics simulations of the zwitterionic monoethanolamine-CO₂ adduct dissociation in aqueous solutions^[215-217] and with values (34-50 kJ mol⁻¹) from DFT and StatTD calculations augmented Solvation Model based on Density (SMD) for several substituted ethanolamines.^[218]

4.2.4. Proton Abstraction from the Glycinate-CO₂ Adduct

As we highlighted previously, the time evolution of the **IL**+CO₂ system leads to the formation of the glycinate-CO₂ adduct (**3**), which undergoes subsequent proton abstraction by the carboxylate or amine groups. The three most probable reaction channels of the proton abstraction are considered. The first one is the intramolecular mechanism shown in Figure 4.3a and d, which involves carboxylate group of the adduct (**3**). Two important distances were analyzed in the corresponding CDF in Figure 4.3a, that is, the intramolecular O'···H3' distance versus the N3'-H3' bond length. The second and the third pathways are the intermolecular mechanisms presented in Figure 4.3b and e for the amine group and in Figure 4.3c and f for the carboxylate group of [Gly]⁻. The corresponding CDFs include the intermolecular N3'···H3' or O'···H3' distances versus the N3'-H3' bond length. The events related to the proton abstraction exhibit the short intramolecular O'···H3' or intermolecular N3'···H3' or O'···H3' distances and long N3'-H3' bond length, that is, these events occur in the right-bottom region of the corresponding CDF (Figure 4.3a-c). Our simulations display the intermolecular pathway of the proton abstraction. The energy barriers delivered by the composite approach are 17, 16 and 2 kJ mol⁻¹ for the considered reactions (Figure 4.3d-f). The seeming disagreement between the barrier height and the probability to find the product of intra- or intermolecular proton abstraction might be explained by the short simulation time of the **IL**+CO₂ trajectory, larger absolute error for the intermolecular barriers than for intramolecular barrier or lack of the explicit solvation demonstrating the limitation of the implicit model. Another important observation here

4. Tuning the Carbon Dioxide Absorption in Amino Acid Ionic Liquids

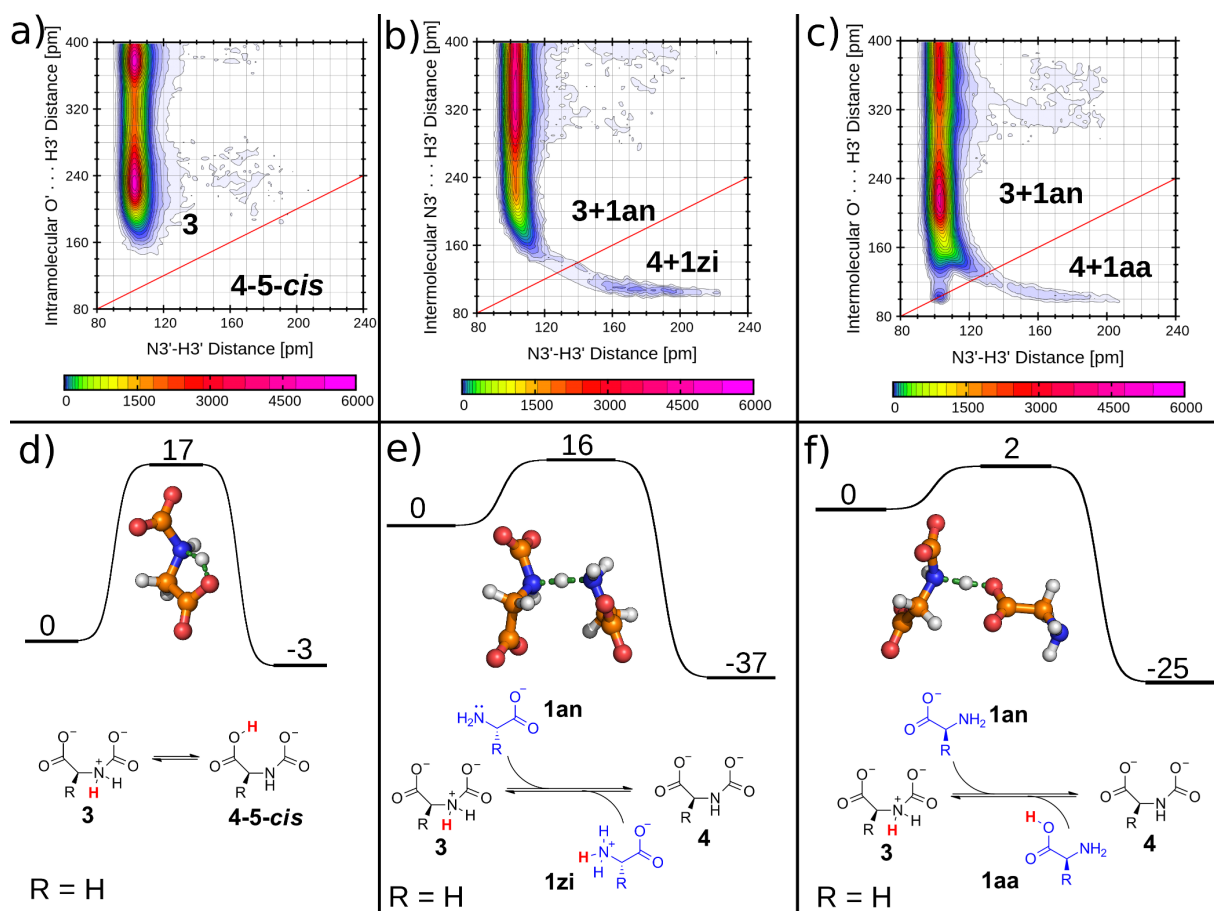


Figure 4.3. Upper panel: CDFs analysing intra- and intermolecular pathways of the proton abstraction for the glycinate-CO₂ adduct (a), from the glycinate-CO₂ adduct by the amine (b) or the carboxylate (c) group of [Gly]⁻ anion. Bottom panel: Potential energies diagrams of the intra- and intermolecular pathways for the proton abstraction in glycinate-CO₂ adduct (d), from glycinate-CO₂ adduct by amine (e) or carboxylate (f) group of [Gly]⁻ anion. Relative energies and barriers are given in kJ mol⁻¹. The energy barriers for the intramolecular pathway for other AAILs are summarized in Table B.2.

is the stability of the zwitterionic form against the neutral form of glycine amino acid. This provides a reasonable starting point to consider an equilibrium between carbamate and carbamic acid, which is discussed subsequently.

4.2.5. Carbamate – Carbamic Acid Equilibrium

The equilibrium between carbamate and carbamic acid is important to shift the CO₂ capacity of the AAILs towards the desired 1:1 absorption. As mentioned in the previous subsection, the zwitterionic form of glycine (1zi) and carbamate (4) solvated

by $[\text{C}_2\text{C}_1\text{Im}][\text{Gly}]$ (**IL+1zi+4** system) is a reasonable starting point for more detailed consideration. Additionally, we simulated the **IL+5-trans** system {four carbamic acid molecules (**5-trans**) in $[\text{C}_2\text{C}_1\text{Im}][\text{Gly}]$ } to explore this equilibrium from another starting composition. The CDF depicted in Figure 4.4a displays the proton transfer from (**1zi**) to (**4**), whereas the CDF in Figure 4.4b shows the back reaction of the proton transfer from (**5-trans**) to (**1an**). The high occurrence of the (**1zi**)+(4) pair against (**1an**)+(5-trans) pair indicates that the equilibrium is shifted towards the former pair or to the 1:2 absorption. The findings from AIMD simulations are completely in agreement with

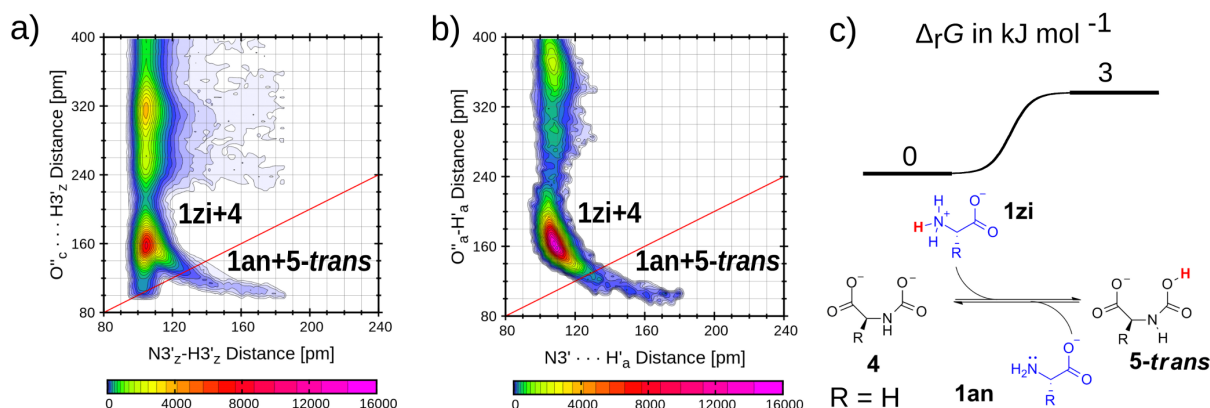


Figure 4.4. CDFs showing the proton abstraction (a) from the glycine zwitterion (**1zi**) by carbamate (**4**) in **IL+1zi+4** system and (b) from carbamic acid (**5-trans**) by glycinate anion (**1an**) in **IL+5-trans** system. (c) Corresponding potential energy diagram.

relative Gibbs free energies from the composite approach. The energy diagram depicted in Figure 4.4c shows a higher ΔG for the carbamic acid (**5-trans**) than for carbamate (**4**). We also checked how this value changes at other solvent compositions due to the conversion of the glycinate anions via the carbamate and ammonium ions to the carbamic acid. The ΔG value increases from 3 kJ mol^{-1} in the $[\text{C}_2\text{C}_1\text{Im}][\text{Gly}]$ to 5 kJ mol^{-1} in the $[\text{C}_2\text{C}_1\text{Im}][\text{1zi}]_{0.5}[\text{4}]_{0.5}$ (1:2 absorption) and returns to the initial value at the complete conversion of $[\text{C}_2\text{C}_1\text{Im}][\text{Gly}]$ into $[\text{C}_2\text{C}_1\text{Im}][\text{5-trans}]$ (1:1 absorption). Thus, we can conclude that both theoretical approaches confirm the higher stability of the carbamate as the dominant product together with the ammonium in the equilibrium mixture. This might be the reason for the shift of the CO_2 capacity to a 1:2 ratio for some AAILs such as $[\text{C}_2\text{C}_1\text{Im}][\text{Gly}]$ ^[223] and tetraethylammonium α - and β -alanate.^[222] Contrarily, tri-

4. Tuning the Carbon Dioxide Absorption in Amino Acid Ionic Liquids

hexyl(tetradecyl)phosphonium glycinate^[58] and most of other AAILs^[59,60] possessing the CO₂ capacity close to 1:1 ratio, which is most likely related to the higher relative stability of the carbamic acid (**5-trans**) against the carbamate (**4**).

4.2.6. CO₂ Absorption in Other AAILs

Insights into the overall mechanistic picture of the reaction pathways of CO₂ absorption in [C₂C₁Im][Gly] were obtained from AIMD simulations and the composite approach. However, the AIMD method is too time-consuming for the exploration of all possible combinations of cations and amino acid anions. In this respect, calculations through the composite approach will serve as a good preliminary prescreening technique before the AIMD simulations. The composite approach allows the investigation of how the variation of the structure of the cation and amino acid anion influences the energetic characteristics of the reactions considered earlier. We explore here 50 AAILs obtained through the combination of the amino acid anions with imidazolium or phosphonium cations.

Table 4.1. Calculated energy barriers of (amino acid anion)-CO₂ adduct formation in different AAILs.^[a]

Cation	Anion									
	[Gly] ⁻	[Ala] ⁻	[Val] ⁻	[Leu] ⁻	[Ile] ⁻	[Pro] ⁻	[Phe] ⁻	[Tyr] ⁻	[Ser] ⁻	[Thr] ⁻
[C ₂ C ₁ Im] ⁺	38	46	50	47	54	33	50	48	46	44
[C ₁₀ C ₁ Im] ⁺	40	47	50	47	54	33	51	48	47	45
[(C _F) ₁₀ C ₂ C ₁ Im] ⁺	44	50	53	49	57	35	53	51	50	47
[P _{2,2,2,2}] ⁺	34	42	47	45	51	30	47	45	43	41
[P _{6,6,6,14}] ⁺	36	43	47	45	51	30	47	45	44	41

[a] The energies are given in kJ mol⁻¹ in the pure AAILs as depicted in Figure 4.2b.

The formation of the (amino acid anion)-CO₂ adduct has the highest energy barrier, ΔG^\ddagger , among all considered reactions. Therefore, we assumed that this step was the rate determining step for the whole CO₂ absorption process. The ΔG^\ddagger value is inversely proportional to the CO₂ absorption rate constant. Thus, the relative change of ΔG^\ddagger for the sequence of AAILs (see Table 4.1) can be used to define the functional group that causes

the increase or decrease of the rate constant. The calculated ΔG^\ddagger changes from 30 to 50 kJ mol⁻¹, which indicates the possibility to adjust the absorption rate constant through the variation of the molecular structure. Notably, that the amino acid anions form the same reaction sequence (with the increase of ΔG^\ddagger) for each considered cation. This allows a comparison of the relative change of the experimental kinetic data for amino acid anions in similar solvents to validate the composite approach. The CO₂ absorption rate estimated from the absorption curves in the (3-aminopropyl)tributylphosphonium AAILs follows the sequence [Gly]⁻ > [Ala]⁻ > [Val]⁻ > [Leu]⁻,^[57] and ΔG^\ddagger decreases as the absorption rate increases. Our calculated ΔG^\ddagger values follow the sequence [Gly]⁻ < [Ala]⁻ ≈ [Leu]⁻ < [Val]⁻. The deviation of the leucinate anion from this sequence is most likely related to the complex mixture of conformers, which we did not account in our model. The results from aqueous solutions of the potassium salts of the amino acids provide the following reactive sequence [Pro]⁻ > [Gly]⁻ > [Ala]⁻ ≈ [Ser]⁻,^[240] which is in good agreement with the results from the composite approach, that is, ΔG^\ddagger increases in the order [Pro]⁻ < [Gly]⁻ < [Ala]⁻ ≈ [Ser]⁻. Thus, the calculated ΔG^\ddagger values can be used to provide an estimated series for the relative change of the absorption rate constants of the amino acid anions, which is expected to be independent of the type of the cation: [Pro]⁻ > [Gly]⁻ > [Ala]⁻ ≈ [Ser]⁻ > [Thr]⁻ > [Tyr]⁻ > [Val]⁻ ≈ [Phe]⁻ > [Ile]⁻. The introduction of the aromatic or bulky nonpolar substituents decreases the absorption rate relative to that of the starting glycinate structure. The influence of the cation on the CO₂ absorption by the anion is less pronounced, and the relative order of the expected rate constant changes as follows: Small cation such as [P_{2,2,2,2}]⁺ is expected to show the higher value of the rate constant. The elongation of the alkyl side chain, the introduction of the imidazolium ring, and the fluorination of the side chain are expected to decrease the absorption rate constant. Surprisingly, according to our prediction, the highest absorption rate among 50 AAILs is expected for the [P_{6,6,6,14}][Pro], which was already found experimentally.^[208]

Apart from the energy barriers for the (amino acid anion)-CO₂ adduct, we also consider the intramolecular barrier of the proton transfer (Table B.1). We found that this barrier for glycinate AAILs is around 17 kJ mol⁻¹ and decreases significantly in other AAILs.

4. Tuning the Carbon Dioxide Absorption in Amino Acid Ionic Liquids

Serinate, proline, phenolate, threoninate AAILs show barriers of approximately 11 kJ mol⁻¹. Alanate, tyrosinate, leucinate, and isoleucinate AAILs possess a barrier of around 7 kJ mol⁻¹, whereas valinate AAILs have a barrier close to 1 kJ mol⁻¹. The barriers found for the intermolecular proton abstraction in [C₂C₁Im][Gly] (2 and 16 kJ mol⁻¹) and in several substituted ethanolamines (5-23 kJ mol⁻¹)^[218] indicates that inter-^[212] and intramolecular^[139] mechanisms are both important. Therefore, we recommend both mechanisms are included in the training set if these systems are studied from a reactive force field.

Table 4.2. Calculated Gibbs free reaction energy for the reaction **1an** + CO₂ ⇌ **5-trans** in different AAILs.^[a]

Cation	Anion									
	[Gly] ⁻	[Ala] ⁻	[Val] ⁻	[Leu] ⁻	[Ile] ⁻	[Pro] ⁻	[Phe] ⁻	[Tyr] ⁻	[Ser] ⁻	[Thr] ⁻
[C ₂ C ₁ Im] ⁺	-15	-13	-11	-12	-10	-20	-9	-3	-8	-8
[C ₁₀ C ₁ Im] ⁺	-13	-11	-10	-11	-11	-19	-8	-2	-6	-7
[(C _F) ₁₀ C ₂ C ₁ Im] ⁺	-9	-7	-7	-8	-8	-17	-5	0	-4	-4
[P _{2,2,2,2}] ⁺	-19	-17	-14	-16	-16	-22	-13	-6	-11	-11
[P _{6,6,6,14}] ⁺	-16	-15	-13	-14	-14	-20	-12	-5	-9	-9

[a] The energies are given in kJ mol⁻¹. The solvent composition used in calculations is between 1:2 and 1:1 absorption capacity, [Cat][5-*trans*]_{0.5}[1zi]_{0.25}[4]_{0.25}.

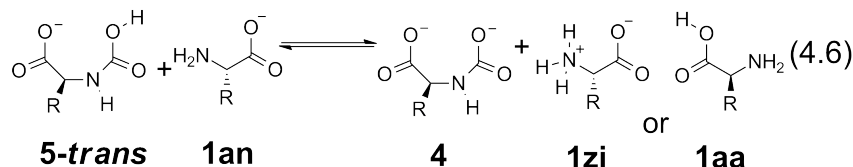
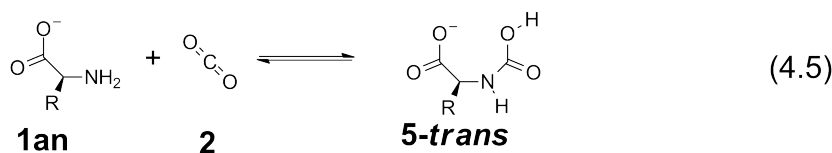
Table 4.3. Calculated Gibbs free reaction energy for the reaction **5-trans** + **1an** ⇌ **4** + **1zi/1aa** in different AAILs.^[a]

Cation	Anion									
	[Gly] ⁻	[Ala] ⁻	[Val] ⁻	[Leu] ⁻	[Ile] ⁻	[Pro] ⁻	[Phe] ⁻	[Tyr] ⁻	[Ser] ⁻	[Thr] ⁻
[C ₂ C ₁ Im] ⁺	-4 ^[b]	2 ^[b]	6	8	6	17	22	17	2	3
[C ₁₀ C ₁ Im] ⁺	-1 ^[b]	5 ^[b]	5	8	6	15	22	17	1	3
[(C _F) ₁₀ C ₂ C ₁ Im] ⁺	1 ^[b]	4	5	8	5	12	21	17	1	2
[P _{2,2,2,2}] ⁺	-2 ^[b]	5 ^[b]	8	10	8	20	23	18	3	4
[P _{6,6,6,14}] ⁺	6 ^[b]	8	8	10	8	19	24	18	3	4

[a] The energies are given in kJ mol⁻¹. The solvent composition used in calculations is between 1:2 and 1:1 absorption capacity, [Cat][5-*trans*]_{0.5}[1zi]_{0.25}[4]_{0.25}. [b] **1zi** is more stable than **1aa**.

Next, we address the influence of the different functional groups on the equilibria of the

reactions in Equations (4.5) and (4.6).



These reactions are important to describe the CO₂ absorption data at different CO₂ pressure via the Two-Reaction Model.^[59,60] The equilibrium constant for the first reaction [Eq. (4.5)] can be obtained by fitting the absorption data^[59,60] and compared with the calculated reaction Gibbs free energies, ΔG (Table 4.2). The evaluated reaction Gibbs free energy at 295 K according to the Two-Reaction Model in [P_{6,6,6,14}][Pro], [P_{6,6,6,14}][Gly] and [P_{6,6,6,14}][Ile] are -16 , -14 and -12 kJ mol⁻¹. These values are in good agreement with the results from composite approach: -20 , -16 and -12 kJ mol⁻¹, respectively. This good agreement allows us to define the influence of the functional groups at this equilibrium in other AAILs. The elongation or branching of the alkyl side chain, the introduction of an aromatic π -system or hydroxyl groups, or the side chain fluorination decrease the ΔG for the equilibrium reaction depicted in Equation (4.5). The decrease of ΔG leads to the reduction in the maximum absorption capacity of the AAILs; on the other hand, the desorption of CO₂ proceeds at lower temperatures and partial pressures of CO₂. Therefore, these tiny changes in the structures of AAILs can be potentially important for a precise and controllable change of the strength of the CO₂ absorption in AAILs.

After the establishing the importance of the molecular features of the reaction Gibbs free energy of the formation of carbamic acid from the amino acid anion and CO₂ [Eq. (4.5)], we considered the carbamic acid – carbamate equilibrium reaction [Eq. (4.6), Table 4.3]. The negative values in Table 4.3 indicate that the carbamate is the dominant product in the equilibrium mixture, that is, the overall equilibrium is shifted towards 1:2 absorption. The positive values indicate that the equilibrium is shifted towards 1:1 absorption and the

4. Tuning the Carbon Dioxide Absorption in Amino Acid Ionic Liquids

dominant product is carbamic acid. As one can see from the Table 4.3, almost all AAILs show 1:1 absorption capacity, as has been found experimentally^[58-60]. For glycinate AAILs with $[P_{2,2,2,2}]^+$, $[C_2C_1Im]^+$, and $[C_{10}C_1Im]^+$ cations the equilibrium is shifted towards 1:2 capacity, similarly to the other glycinate AAILs with small cations;^[222,223] therefore, these AAILs are less valuable for CO₂ absorption. However, the increase of the nonpolar contribution from the cation by the side chain elongation, $[P_{2,2,2,2}]^+ \Rightarrow [P_{6,6,6,14}]^+$, or by the side chain fluorination, $[C_{10}C_1Im]^+ \Rightarrow [(C_F)_{10}C_2C_1Im]^+$, leads to a shift of the equilibrium towards 1:1 absorption. In summary, the nature of the anion is responsible for the domination of the 1:1 or 1:2 absorption, whereas the cation effect occurs due to the presence or absence of an aromatic π -system.

The last important question we address is the relative stability of the *cis* form against the *trans* form of the carbamic acid (Table 4.4). As was recently pointed out by Wang et al.,^[230] the formation of an intramolecular hydrogen bond in the carbamic acid prevents the increase of the viscosity of the AAIL. All previous theoretical results^[142,144] have shown the higher stability of the *cis* form in the gas-phase, which would indicate that the viscosity of the AAILs+CO₂ systems almost do not change during the CO₂ absorption. However, viscosity increases of two orders of magnitude were detected for almost all trihexyl(tetradecyl)phosphonium AAILs studied by Brennecke et al.^[58-60] An exception is the proline AAIL, for which only a twofold increase in the viscosity was detected.^[60] It is clear from our results that the *trans* structure is the dominant structure for most of the AAILs. Moreover, the presence of a hydroxy group in the AAILs prevents the formation of the *cis* form. Only a few AAILs with proline, valinate and isoleucinate tend to form the *cis*-carbamic acid. The lowest reaction Gibbs free energy found for the $[P_{6,6,6,14}][Pro]$ among all trihexyl(tetradecyl)phosphonium AAILs are in the excellent agreement with the observed experimental results.

4.3 Conclusion

A detailed analysis of the chemical absorption of CO₂ in amino acid ionic liquids (AAILs) through first principles calculations has been presented in this work. The most probable

Table 4.4. Calculated Gibbs free reaction energy for the reaction **5-trans** \rightleftharpoons **5-cis** in different AAILs.^[a]

Cation	Anion									
	[Gly] ⁻	[Ala] ⁻	[Val] ⁻	[Leu] ⁻	[Ile] ⁻	[Pro] ⁻	[Phe] ⁻	[Tyr] ⁻	[Ser] ⁻	[Thr] ⁻
[C ₂ C ₁ Im] ⁺	6	5	-1	0	-1	-1	2	4	10	8
[C ₁₀ C ₁ Im] ⁺	6	5	0	1	-1	0	3	4	11	9
[(C _F) ₁₀ C ₂ C ₁ Im] ⁺	7	5	0	1	-1	0	3	4	11	9
[P _{2,2,2,2}] ⁺	5	4	-1	0	-2	-2	1	3	10	8
[P _{6,6,6,14}] ⁺	6	5	-1	1	-1	-2	2	3	11	8

[a] The energies are given in kJ mol⁻¹. The solvent composition used in calculations is between 1:2 and 1:1 absorption capacity, [Cat][5-*trans*]_{0.5}[1zi]_{0.25}[4]_{0.25}.

mechanism of CO₂ absorption in the ionic liquid (IL) 1-ethyl-3-methylimidazolium glycinate ([C₂C₁Im][Gly]) includes the formation of the glycinate-CO₂ adduct and subsequent proton abstraction by the amino or carboxylate group. The composition of the equilibrium mixture of the carbamate, the glycinate zwitterion, and the carbamic acid is shifted towards the carbamate and the glycinate zwitterion. Their dominance in the equilibrium mixture corresponds with the absorption capacity close to 1:2.

The exploration of the energetic characteristics of the most important reactions for a larger set of AAILs showed a certain dependence on the functional groups. The energy barrier for the formation of the (amino acid anion)-CO₂ adduct is the rate-determining step of the CO₂ absorption in AAILs. This barrier can be increased through side chain elongation, the introduction of the aromatic π -system, and perfluorination. The reactivity sequence of the investigated amino acid anions remains the same for different cations.

The Gibbs free energies of the carbamic acid formation from the amino acid anion and CO₂ agree well with the available experimental data. For an AAIL, the introduction of an aromatic π -system, long alkyl chains, a fluorinated substituent, or a hydroxy group leads to an increase in the Gibbs free energies. In other words, these substituents shift the equilibrium towards the reactants.

The equilibrium between carbamic acid and carbamate is shifted towards the carbamic acid or 1:1 absorption in most considered AAILs. For some glycinate AAILs, this equilibrium is shifted towards a 1:2 absorption. The low capacity of glycinate AAILs can be

4. Tuning the Carbon Dioxide Absorption in Amino Acid Ionic Liquids

improved through the introduction of large nonpolar or fluorinated groups.

The equilibrium between *trans* and *cis* form of the carbamic for most AAILs was found to be shifted towards the *trans* form. This form might be responsible for the dramatic viscosity increase after the CO₂ absorption. We found a higher stability of the *cis* form of the carbamic acid for ([P_{6,6,6,14}][Pro]). This might explain the experimentally observed twofold viscosity increase for the trihexyl(tetradecyl)phosphonium L-prolinate ([P_{6,6,6,14}][Pro]).

Thus, the provided detailed insight into the reaction pathways and relative stability of the important participants in CO₂+AAILs systems will serve as a rational design of amine containing ILs for CO₂ absorption.

4.4 Acknowledgments

The financial support from the Deutsche Akademische Austauschdienst (DAAD) for D.S.F. is gratefully acknowledged. B.K. would like to thank the support from the Deutsche Forschungsgemeinschaft under the SPP 1708 project KI768/12-1. We also would like to thank Barbara Intemann for helpful discussions.

Part II.

CO₂ and SO₂ Solvation by Ionic Liquids

Summary of Part II

In the previous part, the set of approaches has been suggested to establish the expected behavior of the CO₂ molecule in various classes of ionic liquids. In this part, the modeling of the explicit solvation of CO₂ and SO₂ in ionic liquids is considered. A detailed insight into the explicit solvation can be easily obtained from the force field-based methods. However, the results from these methods depend strongly on the quality of the force field. An unbiased molecular picture of the explicit solvation can be easily obtained from the ab initio molecular dynamics simulations. With this approach, the electronic structure of the system defines the formation of the specific interactions between the solute and the solvent.

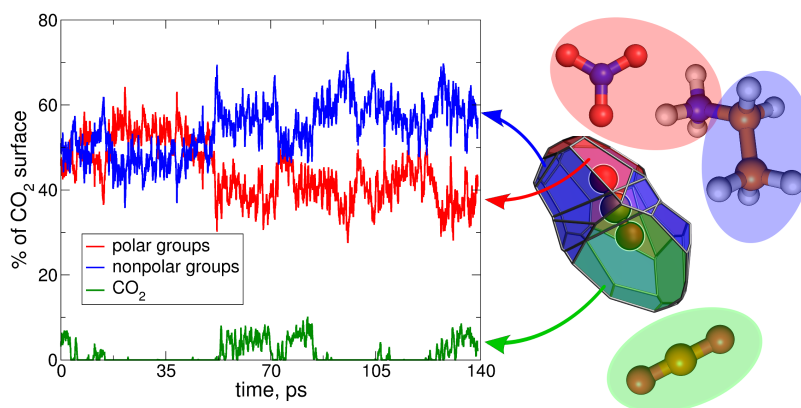


Figure 4.5. The time development of the CO₂ surface coverage by the polar and nonpolar part of ethylammonium nitrate and other CO₂ molecules.

The protic ionic liquid ethylammonium nitrate can serve as an example of a model system to explore gas solvation modes of CO₂. In this ionic liquid the formation of the polar and nonpolar domains, so-called microheterogeneity, can be detected both experimentally and theoretically.^[241–243] The polar domains are represented by a strong hydrogen bonded cation-anion network, whereas weakly interacting ethyl groups form nonpolar domains. Moreover, the available voids in this model ionic liquid are too small making a direct incorporation of CO₂ unfavorable (see Chapter 5). To understand the solvation mechanism, a detailed analysis of the ab initio molecular dynamics simulations of a mixture of ethylammonium nitrate with carbon dioxide has been performed (see Chapter 5). The

4. CO₂ and SO₂ Solvation by Ionic Liquids

structure of the cation-anion network of the ionic liquid remains unperturbed indicating that CO₂ does not incorporate in the polar domains. The essential role in the solvation of CO₂ is devoted to specific weak interactions present in the nonpolar domains (see Figure 4.5). Thus, the energy loss due to CO₂ entering into the ionic liquid via small voids can be fully compensated by the energy gain due to the formation of specific weak interactions.

Due to a significantly greater absorption capacity of SO₂ in ionic liquids than CO₂ under the same conditions,^[32,79] a different solvation mechanism is expected. A particular interest represents the 1-ethyl-3-methylimidazolium thiocyanate ionic liquid, which possesses the highest gravimetric capacity among all pure ionic liquids.^[91] Similar to the solvation of CO₂ in ethylammonium nitrate and 1-ethyl-3-methylimidazolium acetate ILs (Chapters 5 and 7), a significant dominance of groups donating weak interactions can be detected in the solvation shell of SO₂. Despite this similarity in the solvation of CO₂ and SO₂ one essential difference has been found. The SO₂ molecule actively incorporates in the cation-anion network in contrast to the CO₂ molecule (see Figure 4.6). The ab initio molecular dynamics simulations indicates the fabrication of much stronger interactions, such as S(anion)⋯S(SO₂) and O(SO₂)⋯H(cation), instead of weak S(anion)⋯H(cation) interactions. Thus, the formation of the anion-solute-cation network is the dominant mechanism for the solvation of SO₂ in ILs as well as the promising strategy to enhance gas solubility in ILs.

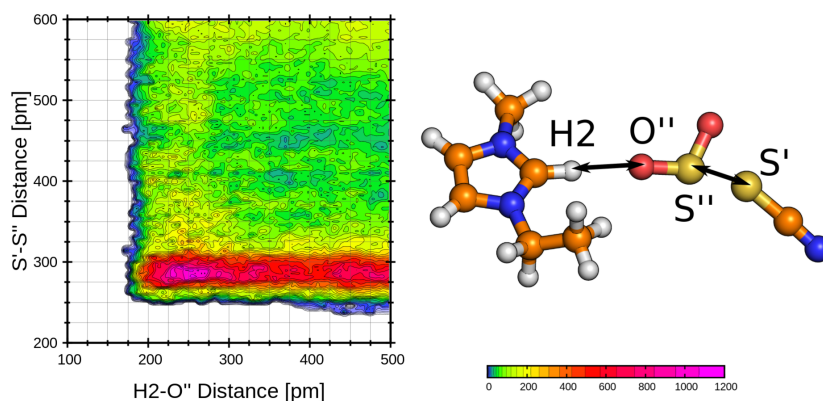


Figure 4.6. The combined distribution function testing the occurrence of the S(anion)⋯S(SO₂)-O(SO₂)⋯H(cation) structure and its ball-and-stick representation.

5 CO₂ Absorption in the Protic Ionic Liquid Ethylammonium Nitrate

Dzmitry S. Firaha* and Barbara Kirchner*

Received: February 18, 2014, Published: June 16, 2014

Reprinted (adapted) with permission from

D. S. Firaha, B. Kirchner *J. Chem. Eng. Data* **2014**, *59*, 3098–3104.

Copyright ©2014 American Chemical Society.

DOI 10.1021/je500166d

Own manuscript contribution

- Performance of the molecular dynamics simulations
- Analysis of the trajectories
- Interpretation of the data
- Manuscript preparation

*Mulliken Center for Theoretical Chemistry, Institut für Physikalische und Theoretische Chemie, Rheinische Friedrich-Wilhelms-Universität Bonn, Berlingstraße 4+6, 53115 Bonn, Germany

Abstract We present a first-principles molecular dynamics study of carbon dioxide solvation by protic ionic liquids using ethylammonium nitrate as an example solvent. Microheterogeneity of the alkyl chains and the extended hydrogen bond network could be observed. Thus, the entire structure of the investigated protic ionic liquid mixed with CO₂ closely resembles the one of the pure liquid. Our data indicates that CO₂ most likely creates an energy loss due to entering the liquid via the too-small voids. But this is fully compensated by specific attractive interactions of CO₂ with the cation and anions of ethylammonium nitrate. This result might serve as an explanation for the question of why the volume of the ionic liquid is not increasing through CO₂ uptake. The CO₂ cluster formation, which shows a structure similar to supercritical CO₂, is guided by the dominance of the nonpolar groups in the CO₂ solvation shell.

5.1 Introduction

Ionic liquids (ILs) caught the interest of scientists in the past few decades due to their unique and tunable physicochemical properties.^[24] Among them are the low vapor pressure and the high gas solubility which promote ILs to be an alternative to the conventional organic solvents used for gas absorption and separation processes.^[43] Carbon dioxide (CO₂) possesses one of the highest solubility in ILs,^[25] whereas ILs are mostly insoluble in supercritical CO₂.^[25,244] The combination of these properties provides different possibilities for applications, e.g. CO₂ absorption from industrial waste gases,^[209] gas separations, extraction processes,^[25,244] and biphasic catalysis.^[245]

Microheterogeneity is another interesting property, which was established for ILs and which must be of importance for gas absorption.^[246,247] It occurs when alkyl chains with two or more carbon atoms are present either in the cation or the anion. Thus, it is dependent on the alkyl chains but also on the nature of the particular anion^[248] leading to the formation of polar and nonpolar domains in IL structure. The existence of microheterogeneity causes the directed orientation or preferable position between the domains for the solute molecules in IL.^[249]

The subset of protic ionic liquids (PILs) received significant interest in recent years.^[250]

PILs can be easily synthesized via neutralization of Brønsted acid and base.^[251] Some of the ions are neutralized because of proton transfer. Moreover, it has been discussed to which extent PILs are molecular liquids or a mixture of ILs and molecular liquids.^[252] The simplicity in the production of PILs and their low cost provide different application fields.^[250] One of the most studied PILs is ethylammonium nitrate (EAN), which was one of the first ILs.^[253] On the one hand, CO₂ is sufficiently soluble in EAN (Henry’s law constant is about 20 MPa, CO₂ in water possesses a constant of 165 MPa for comparison)^[254]. On the other hand, EAN is a nanostructured liquid^[241–243,255] with a hydrogen bond network,^[256] which is similar to monomethylammonium nitrate (MMAN) recently studied in our group^[257] and which is similar to water (see Ref. [258, 259] and quotation therein).

Interestingly, the relationship between the aforementioned properties has not been discussed yet on the molecular level for the EAN+CO₂ system. Thus, there are a lot of open questions. For instance, how does CO₂ in principle dissolve in EAN? Does CO₂ incorporate in the hydrogen bond network, does it stay in the nonpolar domains? Moreover, do CO₂ molecules tend to stay apart or aggregate together? If CO₂ clusters are formed, what is the CO₂ structure in these clusters? The knowledge gathered here will not only give an insight in CO₂ solubility in EAN, but it will also extend our general understanding of influential factors on CO₂ solubility in PILs.

5.2 Results and Discussions

5.2.1. Computational Details

In order to answer the aforementioned questions, the mixture of EAN with CO₂ (8:1 molar ratio) was studied from ab initio molecular dynamics (AIMD). A system containing 32 ion pairs of ethylammonium nitrate and four CO₂ molecules (**EAN+4CO₂**) was simulated in a cubic box with a size of 1733 pm under periodic boundary conditions (Table 5.1 and Figure 5.1). In order to compare the structure of the formed cluster with the liquid structure of supercritical CO₂, 32 molecules CO₂ (**32CO₂**) were simulated in the same manner (size of the cubic box was 1315.45 pm). For details on the preparation of the

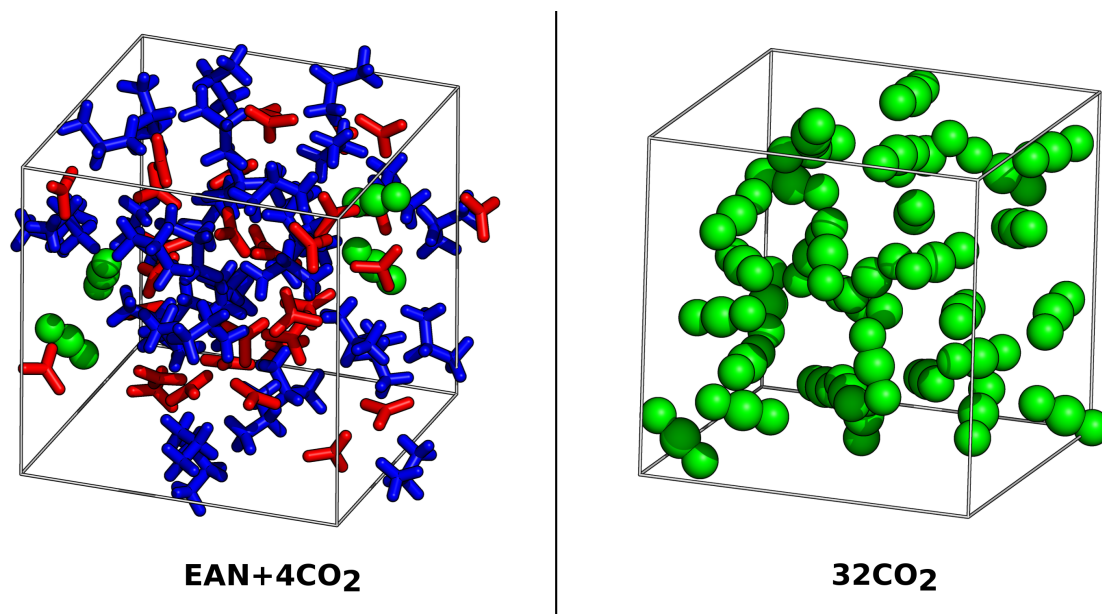


Figure 5.1. Representative snapshots of the simulation boxes. Ethylammonium nitrate in stick (cations in blue, anions in red) and CO₂ (in green) in ball representation.

starting geometry for both systems, see the Supporting Information C.

Table 5.1. Simulation parameters for **EAN+4CO₂** and **32CO₂** systems.

	EAN+4CO₂	32CO₂
Density (g·cm ⁻³)	1.160	1.027
Equilibration time (ps)	17.5 ^[a]	10.0 ^[c]
Physical time (ps)	139 ^[b]	155 ^[c]
Average temperature (K)	350	350

[a] This simulation time includes 10.0 ps with thermostat for individual atoms and 7.5 ps for the complete system with CUTOFF criteria 280 Ry. [b] Higher CUTOFF criteria (350 Ry) was applied for the production simulation, in order to decrease the energy drift for the whole system, see further discussion in this subsection. [c] The default CUTOFF criteria (280 Ry) was applied.

The AIMD simulations were carried out with the CP2K^[187] program package, using the Quickstep module^[188] with the orbital transformation method for faster convergence.^[260] The electronic structure was calculated with the density functional theory utilizing the BLYP-D3 functional with the empirical dispersion correction (D3 with zero damping) from Grimme^[171] since the dispersion-corrected exchange-correlation functional has provided reasonable results for ionic liquids.^[178–181] The molecularly optimized double-zeta basis set (MOLOPT-DZVP-SR-GTH)^[261] with correspondent Goedecker-Teter-Hutter pseudopo-

tentials^[262–264] were applied for all atoms. The density smoothing for the electron density (NN10_SMOOTH) and its derivative (NN10) was used.^[188]

The time step for the simulations was 0.5 fs. The temperature was thermostated to 350 K by Nosé–Hoover chains^[265–267] for individual atoms for 10 ps and the complete system in the main run (see also Table 5.1). For the equilibration (10.0 ps) the CUTOFF criteria for the finest grid level for the DFT calculations was 280 Ry. Since this value provided a high energy drift ($3.2 \cdot 10^{-5}$ a.u./fs) at the beginning of the main run (first 7.5 ps) for **EAN+4CO₂**, we applied a tighter cutoff criteria (350 Ry). This decreased the energy drift by two orders to $2.6 \cdot 10^{-7}$ a.u./fs and excluded the first 7.5 ps of the main run from further consideration. The production simulation was subsequently run for 139 ps for **EAN+4CO₂** and 155 ps for **32CO₂**. Structural analyses of the trajectory were performed using TRAVIS.^[148] Voronoi–Delaunay analysis was carried out with a free available software,^[268] and a home made Python^[269] script to find the probability density distribution of spherical voids radius. Molecule representations were visualized using PyMol^[270] and all graphs were created using Gnuplot 4.6.^[271] The atom labeling used in the following discussion is shown in Figure 5.2.

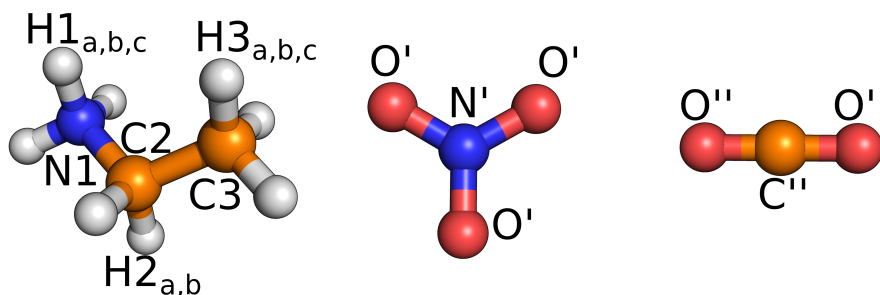


Figure 5.2. Ball-and-stick representation of the cation, the anion and the CO₂ molecule. N: blue; C: orange; O: red and H: white. (Please note that the cation’s atoms are marked without primes, the anion with single primes, and the atoms of the CO₂ with double primes.)

5.2.2. EAN Liquid Structure

The first insight into the structure of ionic liquids can be gained from the radial pair distribution function (RDF), which shows a normalized probability in dependence of the particles distance. Interestingly, the qualitative and quantitative results for RDFs be-

5. CO₂ Absorption in the Protic Ionic Liquid Ethylammonium Nitrate

tween the cations and the anions for the investigated system (see Supporting Information C, Figure C.1) are similar to previous MMAN^[257] and EAN^[256] simulations. This observation indicates that the structure of EAN, which is driven by a strong cation-anion interaction,^[257] remains unperturbed even in the presence of solute molecules such as CO₂ at moderate concentration. The mutual orientation of the ions with respect to each other shows the distinct arrangement in all cases (see corresponding combined distribution functions (CDFs) in the Supporting Information C, Figure C.2). Thus, an in-plane or parallel orientation is most probable for the co-ions, whereas the counterions tend to be perpendicular to their planes between heavy atoms. Obviously, the latter effect appears due to the strong hydrogen bonding between the H1 atoms of the cation and the O' atoms of the anion. On the other hand, the preferable orientation of the cation leads to the aggregation between the ethyl group. An additional insight of the structure of the bulk phase could also be gained from calculated power spectrum (see Supporting Information C, Figure C.3). The data for the whole system, individual ions and molecules are qualitatively and quantitatively in agreement with the experimentally available Raman spectra for pure EAN^[256,258,259,272] and infrared spectrum of physically absorbed CO₂.^[273]

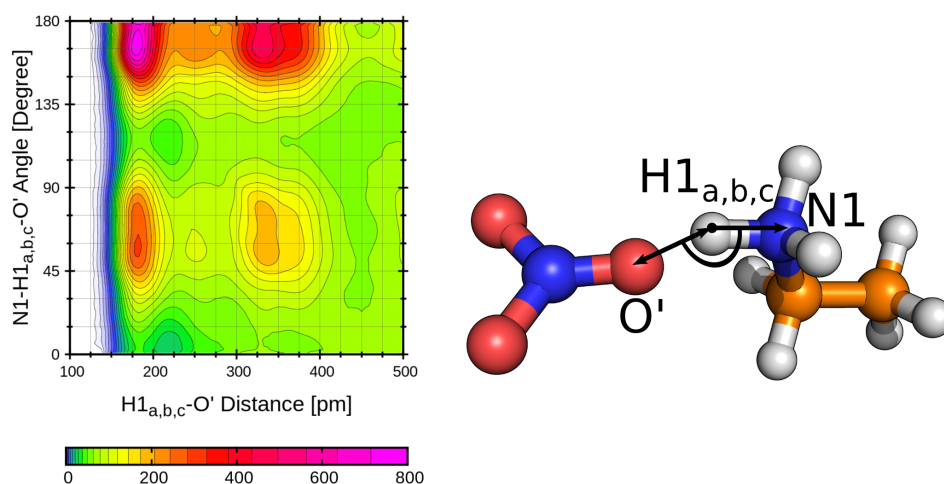


Figure 5.3. The combined distribution function showing the hydrogen bonding between the anion and the cation. $H1_{a,b,c}-O'$ is the distance of the hydrogen bridge and $N1-H1_{a,b,c}-O'$ the angle.

The hydrogen bonding has been discussed in pure MMAN^[257] and EAN.^[256] It is im-

portant to realize, that the hydrogen bond length and directionality for our investigated **EAN+4CO₂** system possess the same values as the aforementioned systems. In the corresponding CDF (Figure 5.3) a distinct peak with the characteristic of the hydrogen bond, about 165° (N-H···O angle) and 180 pm (H···O distance), can be observed, which is in excellent agreement with the experimental crystal structure of MMAN.^[274] It has to be pointed out, that AIMD simulations^[256,257] predict hydrogen bonds more accurately and without any adjustable parameters as opposed to classical molecular dynamics simulations of EAN.^[255,275,276] A more detailed comparison to water will be discussed in the forthcoming article.

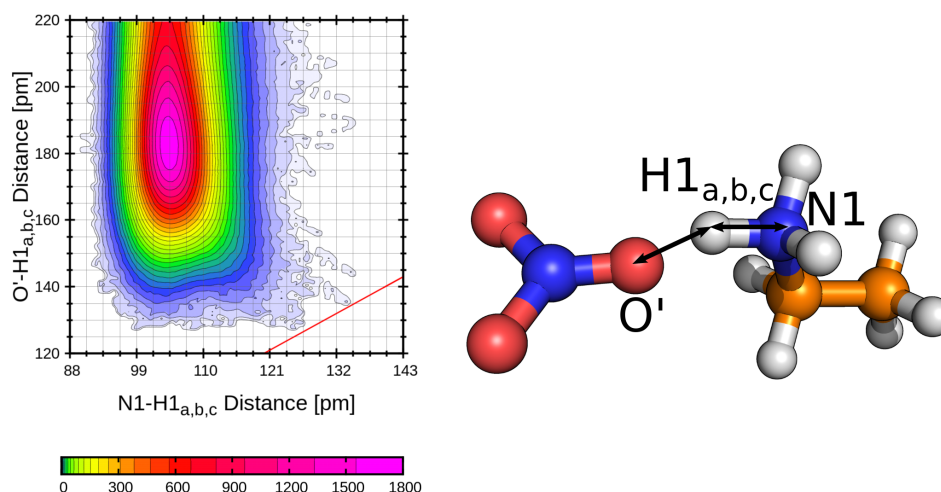


Figure 5.4. The combined distribution function of the O'-H1_{a,b,c} distance versus the N1-H1_{a,b,c} distance. The red line marks those events in which the proton is equally distant to the anion and cation.

Since the hydrogen bond is short and close to linear, the proton transfer, which was determined experimentally,^[277] or at least a certain amount of bond elongation should be observable in our simulations. The corresponding CDF of O'-H1 vs. N1-H1 bonds (Figure 5.4) confirms this idea. A N1-H1 bond elongation mostly occurs when the O' atoms are close to the H1 protons. Nevertheless, rare events without this condition are also possible. Interestingly, the observed bond elongations in the system are less extreme than those detected for the 1-ethyl-3-methylimidazolium acetate mixture with CO₂.^[239] This is obvious with respect to the anion (acetate is more basic than nitrate). However,

5. CO₂ Absorption in the Protic Ionic Liquid Ethylammonium Nitrate

the imidazolium cation is considered far less protic (pKa in range 21-24)^[278] than the ethyl ammonium cation (pKa=10.8).

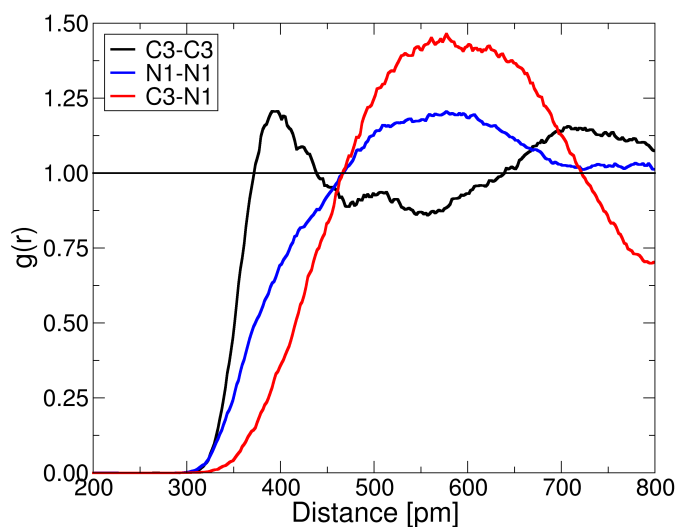


Figure 5.5. RDFs of cation atoms. C3-C3 (black), C3-N1 (red), N1-N1 (blue).

Besides the hydrogen bond network, we studied the microheterogeneity, which was experimentally determined already for EAN with a chain length of only two carbon atoms.^[241,242] Considering the intermolecular RDFs between all heavy atoms of the cation, we obtained distinct peak at short distances for nonpolar ethyl groups (Figure 5.5 about 400 pm). These results suggest an amphiphilicity for the liquid and they are in good agreement with the experimental distance between the ethyl groups in a pure EAN.^[242] The amphiphilicity for the cations can also be drawn from the Voronoi analysis^[279] for the system. The time development of the surface covering of one particle type by another (or even by a certain group of atoms) shows that the anion surface is covered by cations for $\sim 88\%$ and by other anions for $\sim 9\%$, whereas the cation surface is covered only for $\sim 52\%$ by the anion and by other cations for $\sim 43\%$ (see Supporting Information C, Figure C.4). Obviously, since the cation is larger in size than the anion, it has to be in contact with other cations. This changes if we consider the polar (H1 atoms) and nonpolar (H2 and H3 atoms) contributions separately: In this case one could find that $\sim 80\%$ of the cation contribution belongs to its nonpolar part ($\sim 34\%$). Thus, we conclude that microheterogeneity is as persistent in the mixture of EAN with CO₂ as it appears for pure EAN.

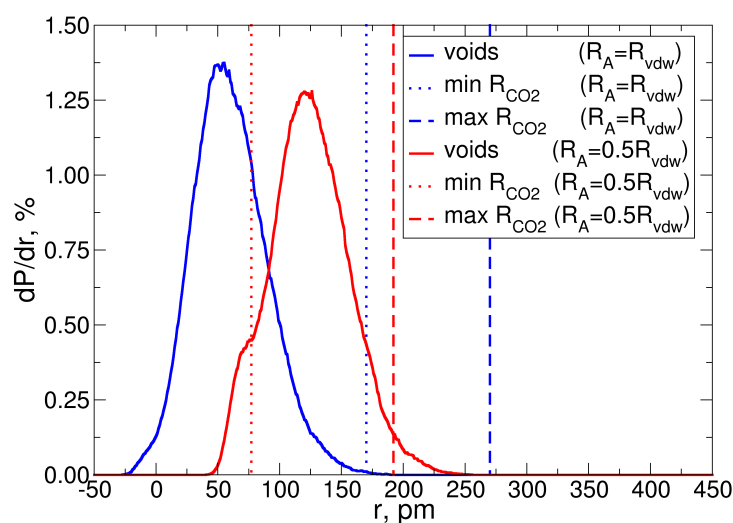
5.2.3. CO₂ Solvation in EAN

Figure 5.6. Probability density distributions of the spherical voids radius (solid lines) for the **EAN+4CO₂** system with van der Waals and half van der Waals radius in red and blue correspondingly. (Please note vertical lines indicates minimal (dotted line) and maximal (dashes line) CO₂ radius with corresponding atomic radii.) In the case of half van der Waals radius, the CO₂ fits into the voids. Thus, inserting CO₂ causes a loss in the energy due to the repulsion, which has to be compensated by specific attractive interactions with the solvent, see further discussion in this section.

In the previous subsection, we showed that the liquid structure of pure EAN and its mixture with CO₂ had a similar hydrogen bond network as well as similar polar domains. Thus, if EAN in mixture with CO₂ possesses the same structural characteristics as the pure liquid, how does it dissolve CO₂? The first insight into this phenomenon could be gained from the Voronoi–Delaunay analysis of spherical voids,^[280] which could give an insight whether the appropriate voids size for CO₂ occurs in the simulations. It is important to realize, that there is only a small or no increase in the molar volume through the CO₂ uptake.^[281,282] Interestingly, the probability density distribution of the spherical voids radius for the investigated system with van der Waals (vdw) radii (Figure 5.6, solid blue line) indicates that there is no appropriate void for the CO₂ molecule (Figure 5.6, vertical dotted and dashes lines). This seeming contradiction, which was also observed for a similar system,^[116] is resolved if the smaller atomic radii are taken into account (Figure 5.6, red lines corresponds to the case with atomic radii of the half of vdw radii,

5. CO₂ Absorption in the Protic Ionic Liquid Ethylammonium Nitrate

as one could see CO₂ fits into the voids). However, this indicates that CO₂ can only be inserted into the IL with repulsive forces when solely the void size is taken into account. This significant loss in the energy due to the repulsion must be compensated by some specific attractive interactions with the surrounding ions. Moreover, for the CO₂ solubility in EAN the specific interactions have to be essential since the smaller nitrogen(II)-oxide molecule — which should fit better to the small voids — is notably less soluble.^[254] The specific interactions will be further discussed in the following.

The analysis of the first solvation shell of the CO₂ molecules shows that there are on average five anions and six cations (cutoff 600 pm). Previously, we observed for CO₂ in 1-ethyl-3-methylimidazolium acetate,^[149,239] that five cations and only one anion are in the first solvation shell. To analyze how CO₂ orients itself with respect to the cation and the anion, we plotted similar CDFs as for the cation-anion mutual orientation (see Supporting Information C, Figure C.5). Interestingly, CO₂ has one distinct orientation with respect to the cation and two with respect to the anion. The solute tends to have a perpendicular orientation to the cation's plane, whereas the anion allows a perpendicular and in-plane or parallel orientation.

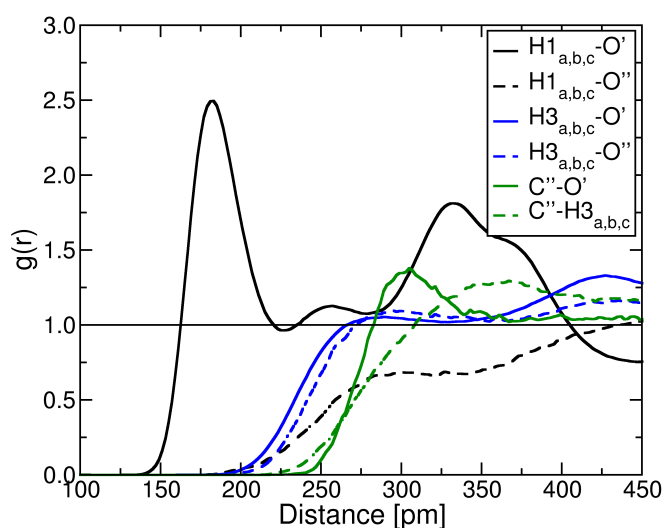


Figure 5.7. Radial distribution functions between the O' atoms of anion (solid lines) and the O'' or C'' atoms of CO₂ (dashes lines) with the H1, H3 atoms of the cation and the C'' atoms of CO₂.

Besides the mutual orientation of CO₂ toward the ions, we studied the interactions

between the solute and the ions in terms of Lewis acidity and basicity for CO₂. Obviously, the O'' atoms (CO₂) interact with the H1, H2, H3 (cation) and the C'' atoms of another CO₂ molecules as a Lewis base. The C'' atoms interact with the O' (anion) atoms as a Lewis acid. Interestingly, for those RDFs, which probe the acid-base interaction in the system (see Figure 5.7), it can be recognized that the O'' atoms are unable to compete with the O' atoms for the most acid proton in the system, because of the smaller basicity. The O'' atoms rather choose the H3 than the H2 and the H1 atoms to form weak interactions. On the other hand, the weak acidity of CO₂ with respect to the low anion's basicity puts the C''-O' interactions in the category of weak interactions. Thus, we could conclude that the CO₂ solubility is not dictated by CO₂ competing with ions for the most acidic and basic centers, but by the weak interactions the solute forms with the ions and by the possibility to use the given voids at least partially. In fact, the number of weak interactions around the CO₂ molecule are considerably high. The corresponding spatial distribution functions (see Supporting Information C, Figure C.6) show the high occurrence of the groups responsible for the weak interactions with a defined (the O' and the N1 atoms) and almost uniform (the C2 and the C3 atoms) distribution around CO₂. In fact, these findings are similar to CO₂ in a 1-ethyl-3-methylimidazolium acetate system^[149,239] where many weak CO₂-cation interactions were also found to contribute considerably to the CO₂ solvation showing that the nonpolar domains are to a large amount responsible for the CO₂ solvation in IL.

The Voronoi analysis is a powerful tool for understanding and monitoring the time development of the particles solvation. Therefore, we employed it to study CO₂ clusters formation and destruction. We obtained the cluster formation of CO₂ molecules, in the beginning, around 70, 105 and 130 ps of simulation time (Figure 5.8). Interestingly, the cluster formation is rather triggered by the nonpolar groups (the H3 and the H2 atoms) and not so much by the polar groups (the N', the O'' and the H1 atoms). Obviously, these conclusions are only valid up to 70 ps. Subsequently, the correlation between the coverage of the CO₂ molecules with the nonpolar groups and the CO₂ aggregations is not detected, whereas the dominance of the nonpolar groups in the solvation shell of CO₂ becomes more pronounced.

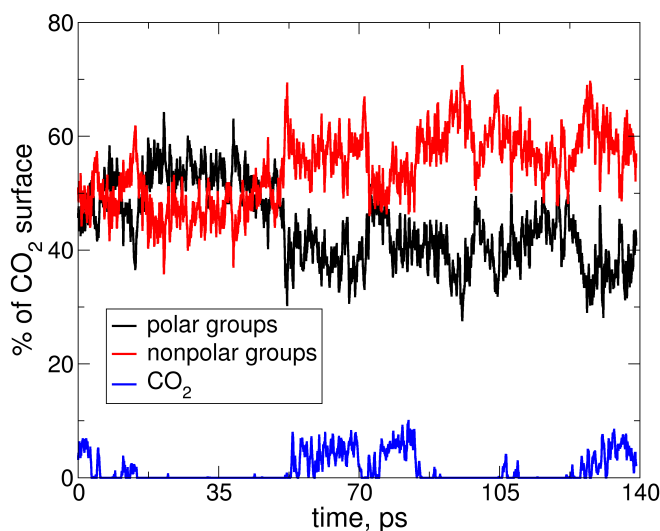


Figure 5.8. Time development of the CO_2 surface covering by polar (the N' , O'' and H1 atoms), nonpolar (the H2 and H3 atoms) groups and other CO_2 molecules. A correlation between the CO_2 cluster formation (blue line) and the dominance of the nonpolar (red line) over polar (black line) surface covering of CO_2 is apparent up to 70 ps. The pronounced dominance of the nonpolar over polar groups in the solvation shell CO_2 was detected after 70 ps.

In order to check, whether CO_2 possesses a similar or rather a different structure than in supercritical state, we studied the mutual orientation of the CO_2 molecules and compared it with the results for supercritical CO_2 simulated at 350 K and 1000 bar (see computational details 5.2.1). The plot of an angular distribution function versus a radial distribution function similar to the hydrogen bond directionality is very suitable for the analysis of a dimer structure (Figure 5.9). It is obvious that both CDFs have similar shapes and the maxima at the same locations. The difference between the two plots might be a consequence of the low sampling in EAN. Further studies are needed. These results indicate that CO_2 forms clusters in the IL, which resemble in their structures those of the supercritical state of CO_2 .

5.3 Conclusion

In this article, we provided detailed insight into the CO_2 solubility in protic ionic liquids from ab initio molecular dynamics simulations. From our simulations, it is obvious, that CO_2 in mixture with ethyl ammonium nitrate neither breaks the strong hydrogen bond

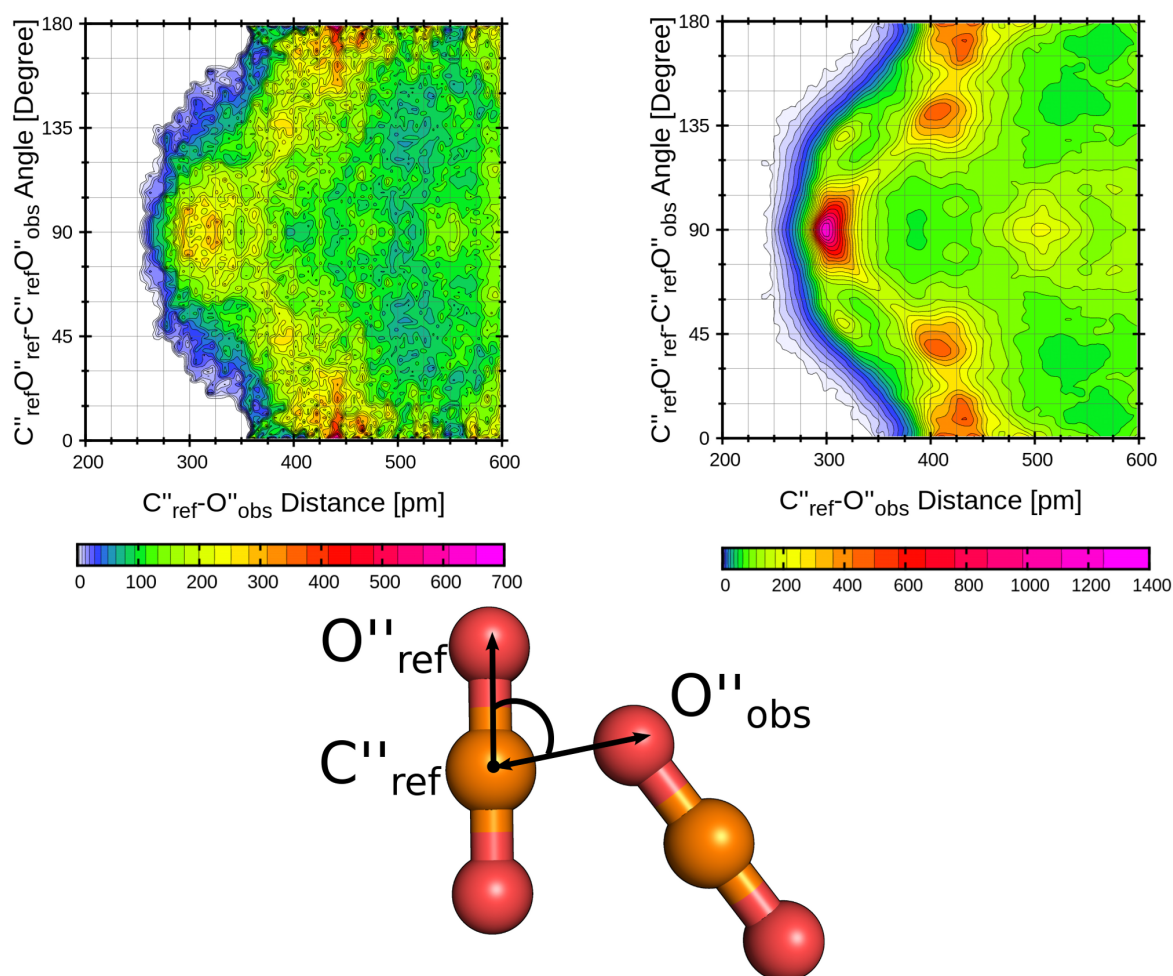


Figure 5.9. Combined distribution functions showing the mutual orientation of CO₂ molecules in EAN (left) and supercritical CO₂ (right). It is visible that both plots exhibit very similar maxima.

network between cation and anion nor disturbs the formation of nonpolar domains, i.e., so-called microheterogeneity. Our data indicates that CO₂ is too large to enter the existing voids. Therefore, CO₂ can only be incorporated via the voids of ethylammonium nitrate by increasing the total energy of the system due to the repulsion. At the same time, CO₂ forms favorable specific interactions with the ions which must compensate this loss. This might explain the seeming contradiction of the too small void sizes observed in previous simulations and the present study and the lack of volume increase when CO₂ is absorbed in the IL, which was observed experimentally.

The dominating specific interaction between the solute and the solvent is mainly defined

5. *CO₂ Absorption in the Protic Ionic Liquid Ethylammonium Nitrate*

by weak interactions between the oxygen atoms (O^{''}) of CO₂ and the H3 atoms (ethyl hydrogen atoms of cation) and the C^{''} (CO₂) and O' atoms (anion) showing that this takes place in between the polar and nonpolar domains, and thus microheterogeneity must be important for the CO₂ absorption. Since these types of interactions are not localized at the particular sites of CO₂, the overall contribution to its solvation is significant.

The formation and breaking of CO₂ clusters were also observed in the simulation. A possible trigger for the clusters formation is the slight dominance of the contribution from nonpolar groups in the CO₂ solvation. The structure of the formed clusters is similar to those in supercritical CO₂. In the forthcoming publication, we will concentrate on the analogy between CO₂ solvation in EAN and water.

5.4 Acknowledgements

The financial support from the Deutsche Akademische Austauschdienst for Dzmitry Firaha is gratefully acknowledged. We would like to thank Dr. Elixabete Rezabal for pointing out to simulate EAN and CO₂, furthermore, we would like to thank Barbara Intemann for carefully reading our article. We also would like to thank the SPP 1708.

6 SO₂ Solvation in the 1-Ethyl-3-Methylimidazolium Thiocyanate Ionic Liquid by Incorporation into the Extended Cation - Anion Network

Dzmitry S. Firaha,* Mikhail Kavalchuk,* and Barbara Kirchner*

Keywords: Linker Effect, Sulfur Dioxide, Ionic Liquids, Gas Absorption, Thiocyanate-SO₂ Adduct, 1-Ethyl-3-methylimidazolium Thiocyanate

Received: October 1, 2014, *Published:* March 31, 2015

Reprinted (adapted) with permission from

D. S. Firaha, M. Kavalchuk, B. Kirchner J. Solution Chem. **2015**, *44*, 838–849.

Copyright ©The Author(s) 2015. This article is published with open access at Springerlink.com

DOI 10.1007/s10953-015-0321-5

*Mulliken Center for Theoretical Chemistry, Institut für Physikalische und Theoretische Chemie, Rheinische Friedrich-Wilhelms-Universität Bonn, Berlingstraße 4+6, 53115 Bonn, Germany

6. *SO₂ Solvation in the 1-Ethyl-3-Methylimidazolium Thiocyanate Ionic Liquid*

Own manuscript contribution

- Performance of the molecular dynamics simulations
- Performance of the static calculations
- Analysis of the trajectories
- Interpretation of the data
- Manuscript preparation

Abstract We have carried out an ab initio molecular dynamics study on the sulfur dioxide (SO₂) solvation in 1-ethyl-3-methylimidazolium thiocyanate for which we have observed that both cations and anions play an essential role in the solvation of SO₂. Whereas the anions tend to form a thiocyanate- and much less often an isothiocyanate-SO₂ adduct, the cations create a "cage" around SO₂ with those groups of atoms that donate weak interactions like the alkyl hydrogen atoms as well as the heavy atoms of the π -system. Despite these similarities between the solvation of SO₂ and CO₂ in ionic liquids, an essential difference could be observed with respect to the acidic protons. Whereas CO₂ avoids accepting hydrogen bonds from the acidic hydrogen atoms of the cations, SO₂ can form O(SO₂)-H(cation) hydrogen bonds and thus together with the strong anion-adduct it actively integrates into the hydrogen bond network of this particular ionic liquid. The fact that SO₂ acts as in this way was termed linker effect by us because the SO₂ can be situated between cation and anion operating as a linker between both. The particular contacts are the H(cation)···O(SO₂) hydrogen bond and a S(anion)-S(SO₂) sulfur bridge. Clearly, this observation provides a possible explanation for the question of why the SO₂ solubility in these ionic liquids is so high.

6.1 Introduction

The capture of sulfur dioxide (SO₂) has drawn significant attention because SO₂ is one of the most harmful air pollutants, mainly originating from the combustion of fossil fuels.^[283] The most traditional and widely used technology for SO₂ capturing from flue gases is limestone scrubbing.^[284] This process has certain disadvantages,^[20] including irreversibility of the reaction and a large amount of waste. Recently, an alternative way of SO₂ absorption in ionic liquids (ILs) was suggested.^[26,27] The high absorption capacity and the good reversibility of the absorption process, as well as unique and tunable properties of ILs, have caused a growing interest for the past decade.^[26,27,32,80,285,286]

SO₂ absorption by ILs can occur in a physical or in a chemical way^[26,27,32,286] from which only in the former case a full and simple recovery is possible. Therefore, the appropriate media for the full or partial recovery of SO₂ depending on the purpose can

6. SO₂ Solvation in the 1-Ethyl-3-Methylimidazolium Thiocyanate Ionic Liquid

be chosen. The physical absorption of SO₂ in ILs is almost independent of the type of the anion and cation,^[286] whereas in a case of the chemical absorption the dependence on the type of IL becomes more pronounced with the nature of the anion playing the crucial role.^[87,92,286] Such a principle difference in the behavior on the microscopic scale might be better understood when the theoretical methods are taken into account.

Static gas-phase calculations of interaction energies and the assignment of principle interaction types based on those values were investigated in several articles.^[82,83,91,92,287] Also, molecular dynamics simulations employing empirical force fields were used for evaluating some physical properties of the systems.^[121,126,135,288] In order to understand the mechanism of SO₂ solvation in more detail, solute-solvent interactions should be taken into account. Thus, the investigation of specific interactions between SO₂ and the IL components, as well as understanding how the interactions influence the instances in the IL, can be provided from a valuable theoretical background which aids in the design of ILs with desired properties.

In this work, we have employed ab initio molecular dynamics (AIMD) simulations in order to obtain insight into the structural and dynamic properties of the SO₂-IL systems. To do so, we have chosen 1-ethyl-3-methylimidazolium thiocyanate ([C₂C₁Im][SCN]) as a model system. This IL is one of the most promising candidate for large-scale application, possessing one of the highest capacity of SO₂ absorption, a rapid absorption rate, and excellent reversibility.^[91] Moreover, the solubility of other gases in this IL is significantly lower than for SO₂ (compare molar fraction of gases in [C₂C₁Im][SCN] at 1 bar and 20° C: SO₂ is 75 %, ^[91] NH₃ – 16.3 %, ^[289] CO₂ – 1.2 % ^[290]), which is a requirement for separation processes.

Recently the structural properties of pure [C₂C₁Im][SCN]^[180,291] and its mixtures with another ionic liquid,^[292] as well as carbon dioxide (CO₂) absorption in imidazolium and ethylammonium ionic liquids^[149,239,293] have been studied from AIMD, providing a solid background for the current investigation. Thus, the knowledge gathered here provides a more thorough understanding of SO₂ solvation in ILs. Moreover, similarities and differences can be identified between SO₂ and CO₂ with respect to their solvation in ILs.

6.2 Computational Details

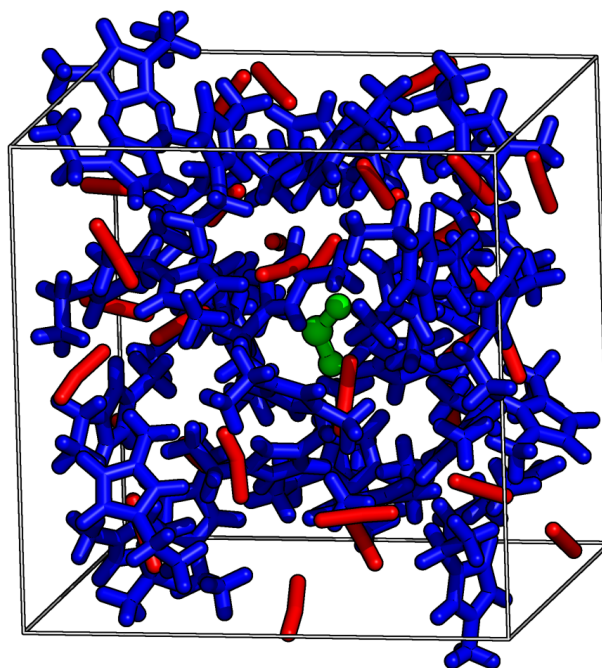


Figure 6.1. A representative snapshot of the simulation box. 1-ethyl-3-methylimidazolium thiocyanate in stick (cations in blue, anions in red) and SO_2 (in green) in ball-and-stick representation.

The mixture of $[\text{C}_2\text{C}_1\text{Im}][\text{SCN}]$ with SO_2 (32:1 molar ratio) was studied from AIMD. A system containing 32 ion pairs of $[\text{C}_2\text{C}_1\text{Im}][\text{SCN}]$ and one SO_2 molecule was simulated in a cubic box with a size of 2031.4 pm (this corresponds to $\rho = 1.086 \text{ g}\cdot\text{cm}^{-3}$) with periodic boundary conditions (Figure 6.1). For details on the preparation of the starting geometry for the system, see the Supporting Information D.

The AIMD simulations were carried out with the CP2K^[187] program package, using the Quickstep module^[188] with the orbital transformation method for faster convergence.^[260] The electronic structure was calculated employing the density functional theory utilizing the BLYP-D3 functional with the empirical dispersion correction (D3 with zero damping) from Grimme^[171] since the dispersion-corrected exchange-correlation functional has provided reasonable results for ionic liquids.^[178–181] The molecularly optimized double- ζ basis set (MOLOPT-DZVP-SR-GTH)^[261] with corresponding Goedecker–Teter–Hutter pseudopotentials^[262–264] was applied for all atoms. The density smoothing for the electron density (NN10_SMOOTH) and its derivative (NN10) was used.^[188] The CUTOFF

6. *SO*₂ Solvation in the 1-Ethyl-3-Methylimidazolium Thiocyanate Ionic Liquid

criterion for the finest grid level for the DFT calculations was 300 Ry.

The temperature was thermostated to 350 K by Nosé–Hoover chain thermostats^[265–267] with a time constant of 100 fs for individual atoms for 5.0 ps and the complete system in the main run. For the equilibration (5.0 ps) the time step 0.5 fs was used. Since this value provided a high energy drift ($2.8 \cdot 10^{-5}$ a.u./fs) at the beginning of the main run (first 22.3 ps), a shorter time step (0.25 fs) was applied. This decreased the energy drift by one order to $3.7 \cdot 10^{-6}$ a.u./fs and excluded the first 25.0 ps (22.3 with 0.5 and 2.7 ps with 0.25 fs time steps) of the main run from further consideration. The production simulation was subsequently run for 58 ps.

Static quantum chemical calculations were performed from the density functional theory (DFT) and wave function theory with the ORCA^[294] program (version 3.0.0^[295]). Geometry optimization was performed on B3LYP-D3(BJ)/def2-TZVPP level, whereas the final energy calculations were done based on DFT geometry applying CCSD(T) level of theory. Extrapolation to the complete basis set limit was carried out according to two-point extrapolation scheme separately for Hartree–Fock energies and CCSD(T) correlation energies. The calculation of *SO*₂ gas frequencies was performed on BLYP-D3(BJ)/def2-TZVPP to be consistent with the exchange-correlation functional, which was applied for bulk simulation. Structural analyses of the trajectory were performed using TRAVIS.^[148,296] Molecule representations were visualized using PyMol,^[270] and all graphs were created using Gnuplot 4.6.^[271] The atom labeling used in the following discussion is shown in Figure 6.2.

6.3 Results and Discussion

6.3.1. Cation–Anion and Cation–*SO*₂ Interactions

To get insight into how *SO*₂ in small concentrations influences the structure of [C₂C₁Im][SCN], we compared corresponding radial distribution functions (RDFs) of the pure IL to the system under study (see Supporting Information D, Figure D.1–D.2, and Ref. [180]). Significant changes in the structure of the IL were not found. This is consistent with MD simulations of systems with a higher concentration of *SO*₂ in ILs^[92,126]

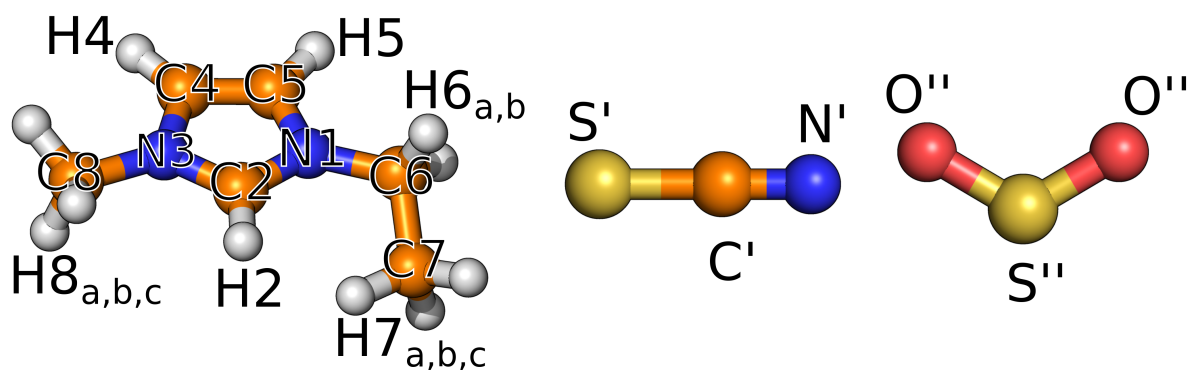


Figure 6.2. Ball-and-stick representation of the cation, the anion, and the SO_2 molecule. N: blue; C: orange; O: red, H: white and S: gold. (Please note that the cation's atoms are marked without primes, the anion with single primes, and the atoms of the SO_2 with double primes.)

as well as with the results obtained previously for CO_2 in ethylammonium nitrate^[293] and in 1-ethyl-3-methylimidazolium acetate.^[149,239] In order to reveal the mode of how SO_2 enters the IL structure and to characterize the solvation shell of the solute molecule, we considered RDFs as well as Voronoi analysis. The latter analysis provides valuable information about the time development or the average of surface covering of a certain particle by other particles or groups of atoms.

Similar to CO_2 in 1-ethyl-3-methylimidazolium acetate^[149,239] SO_2 is surrounded only by one anion and five cations on average in the first solvation shell (the numbers were defined based on the value of integral in the first minimum of the corresponding RDF between centers of mass of solute and ions, see Figure D.3 in the Supporting Information D). From Figure 6.3A it is apparent, that a similar ratio of anions to cations is obtained from the average SO_2 surface covering by anions and cations (18% versus 82%). Both results — RDF as well as Voronoi — indicate the presence of a "cation cage" around SO_2 .

Since a relatively large amount of cations was detected in the first solvent shell of SO_2 , it is worth to figure out in detail which functional groups are important, and how this situation of SO_2 solvation compares to the CO_2 solvation by ILs. To reveal the role of the specific interactions — especially the weak interactions — in the SO_2 solvation, we have separated the SO_2 surface coverage from the cations into three groups: ring hydrogen atoms (H2, H4, H5), heavy ring atoms (N1, C2, N3, C4, C5), and alkyl hydrogen atoms (H6, H7, H8). For these groups we have plotted in Figure 6.3B their fraction to

6. SO_2 Solvation in the 1-Ethyl-3-Methylimidazolium Thiocyanate Ionic Liquid

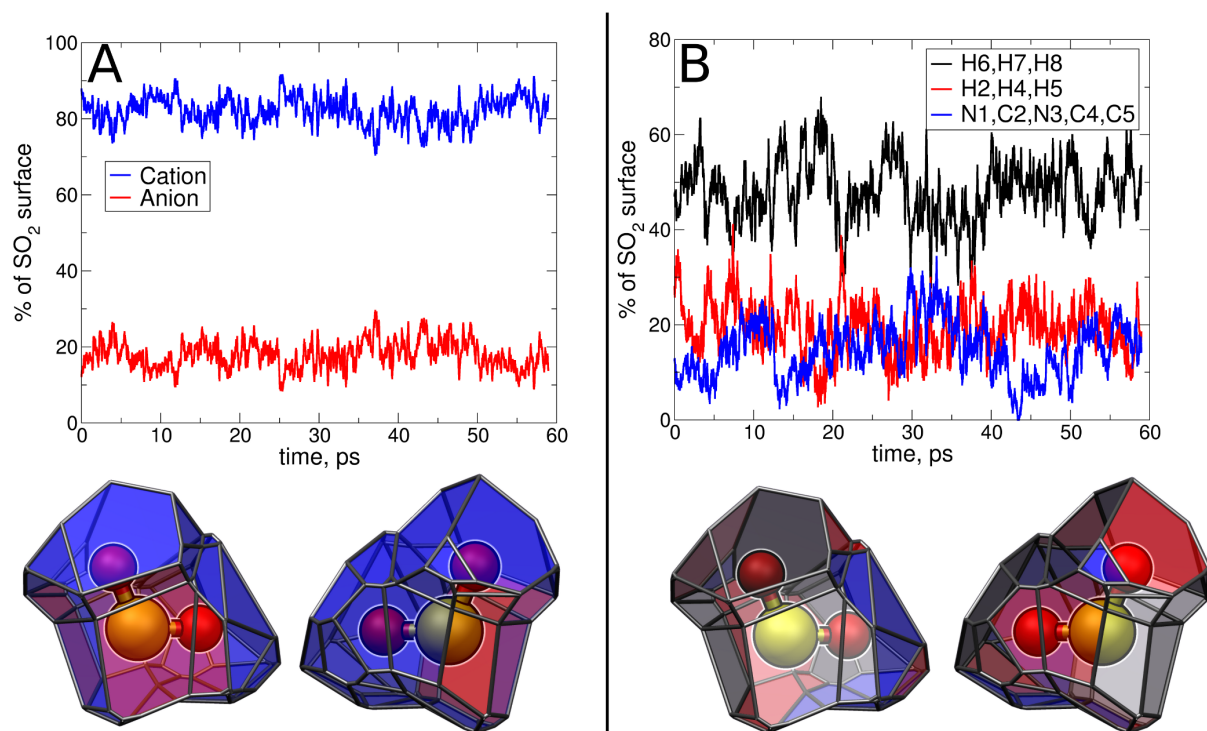


Figure 6.3. Top: Time development of the SO_2 surface covering by ions (panel A, blue lines are cation atoms, and red lines are anion atoms) and cation atoms (panel B, black lines are alkyl hydrogen atoms, red lines are ring hydrogen atoms, and blue lines are ring atoms). Bottom: representative SO_2 Voronoi surfaces, the color code for the surfaces is similar with those for graphs above. (Note gray color was used for the segments belonging to the anion for the bottom right Voronoi surfaces).

the coverage of the Voronoi surface. It is a reasonable first approximation to correspond a dominating coverage (i.e. closest neighbor) to a more important role of the solvating particles for the solute solvation. The ring hydrogen atoms possess a comparable strong interaction with the solute but also with the anion. The strong nature of the latter interaction was shown in several quantum chemical studies.^[297,298] If there are contacts between the SO_2 and the cation ring other than via the ring hydrogen atoms, these are most likely weak solute- π -system interactions. Also, the alkyl hydrogen atoms contacts to the solute represent weak dispersion interaction.^[297,298] Interestingly, the alkyl hydrogen atoms (48%) and heavy ring atoms (15%) coverages — corresponding to the weak interactions — are dominating over the coverage of the ring hydrogen atoms (19%) which correspond to strong interactions. Moreover, these portions are comparable with those from the non-polar part of ethylammonium nitrate to CO_2 solvation.^[293] From these results it is apparent, those weak interactions are important not only for the solvation of

CO₂^[149,239,293] but also for the solvation of SO₂. To support this observation, we compared the experimental SO₂ solubility in different ionic liquids. The increase of the cation's side chain results in the increase of the SO₂ solubility^[32,92,299] which agrees with our findings.

The RDFs — which reflect probabilities of finding two atoms at certain distances normalized by the density — of the cation's hydrogen atoms (H2, H4-H5, H6-H8) with the oxygen atoms of the sulfur dioxide (O'') and the anion tail atoms (N' and S'), are presented in Figure 6.4 on panels A-C. There is a noticeable similarity in the position of the first maximum for the cation-N' and cation-O'' functions albeit with the difference that the O''(SO₂) peaks are less pronounced than the N'([SCN]⁻) peaks. Remarkably, the interplay of CO₂ with a cation in ethylammonium nitrate^[293] or 1-ethyl-3-methylimidazolium acetate^[149,239] shows the opposite behavior, i.e., there are no such peaks between the oxygen atoms of CO₂ and the acidic hydrogen atoms of the cation. Thus, there is no contact of a CO₂ with the cation via the acidic hydrogen atoms. The CO₂ solvation rather takes the form that it competes with dispersion forces in the system such as anion-cation side chain, π - π stacking, and side chain-side chain^[297,298] interactions. These essential differences in the structure of solvated SO₂ and the solvated CO₂ might be one of the reasons for the significantly higher solubility of the former gas in ILs.

Since not only the nature of the anion and the side chain of the cation are important for the SO₂ solvation, but also the role of acidic hydrogen atoms we have examined how the cation exchange in principle influences the SO₂ solubility. For example, the experimental findings on the cation exchange of 1-alkylpyridinium to 1-alkyl-3-methylimidazolium show a slight decrease in the SO₂ solubility in ILs with chloride, bistriflimide, and tetrafluoroborate anions.^[92,287] This changes significantly when ILs with a thiocyanate anion are considered. When the 1-butylpyridinium cation is exchanged for the 1-ethyl-3-methylimidazolium cation at constant thiocyanate anion, the SO₂ solubility increases from 2.6 to 3.0 mol per one mol IL (at 0.1 MPa and 20°C).^[91,92] This opposite behavior detected by experiment might be related to different SO₂ solvation mechanisms which can be explained by microscopic insight given for example by simulations, that is, in the 1-ethyl-3-methylimidazolium thiocyanate ionic liquid we have detected frequent conformations in which the ring hydrogen atoms of the cations are close to the oxygen atoms of

6. SO₂ Solvation in the 1-Ethyl-3-Methylimidazolium Thiocyanate Ionic Liquid

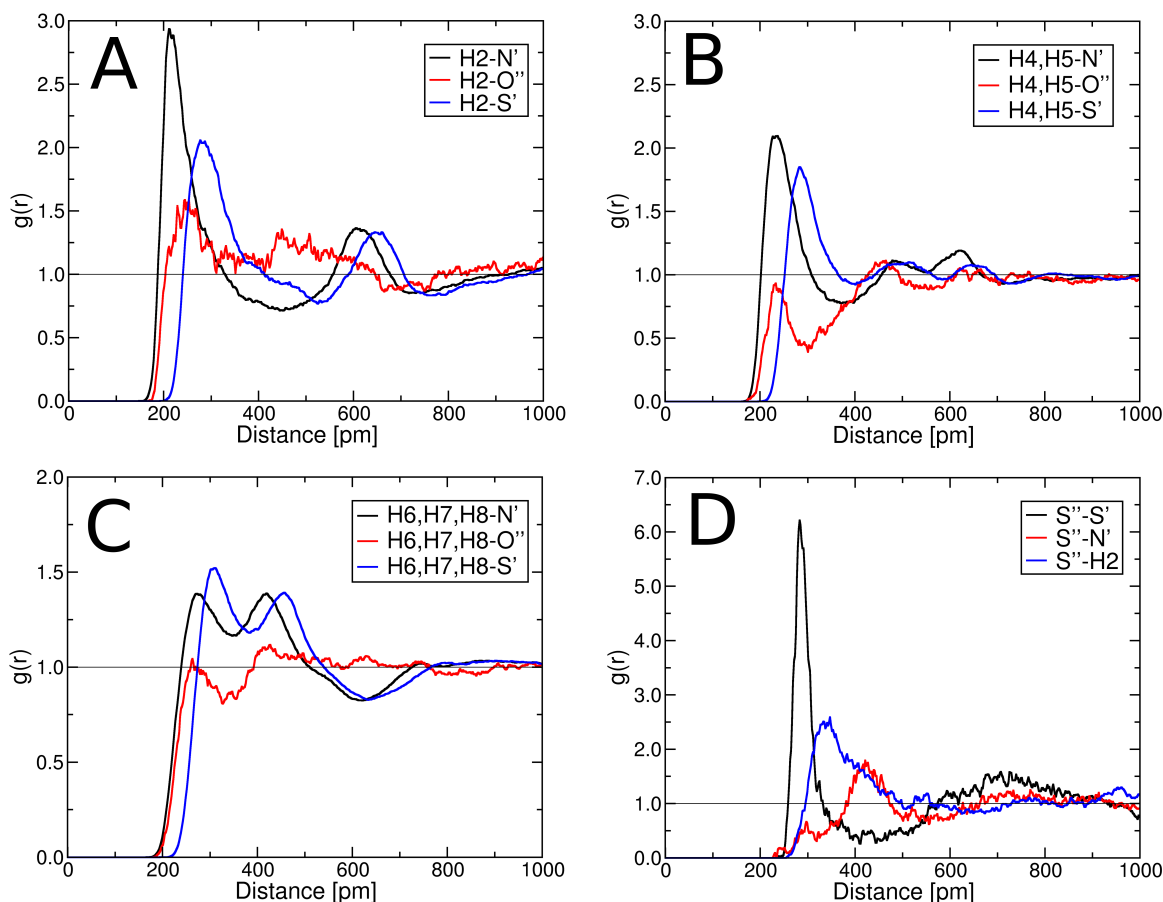


Figure 6.4. Cation-anion and ion-SO₂ interactions. The RDFs between hydrogen atoms and selected atoms from anion and SO₂ are presented on panels A-C, whereas panel D contains the RDFs between S'' (from SO₂) and selected atoms from cation and anion.

the SO₂ and the sulfur atoms of the anions are close to the sulfur atom of the SO₂. It is likely that this newly observed conformation – which we have termed linker conformation or linker effect – is responsible for the good incorporation of SO₂ in this particular ionic liquid by the formation of the following linked structure H2, H4, H5(cation)···O''(SO₂)-S''(SO₂)···S'(anion).

Possible linker bonds between ring hydrogen atoms of the 1-butylpyridinium cation and SO₂ should be weaker due to the lower acidity than those for the 1-ethyl-3-methylimidazolium cation. Thus, the incorporation of SO₂ into the network of hydrogen bonds is limited in the case of ILs consisting of 1-butylpyridinium cations.

6.3.2. Anion–SO₂ Interactions

Only one anion was found in the first solvation shell of SO₂. To understand the nature of the intermolecular forces between the anion and the SO₂, we have carried out static quantum chemical calculations regarding the formation of the anion-SO₂ complex. The results from these calculations showed comparable interaction energies for possible adducts (-68.6 kJ mol⁻¹ for thiocyanate-SO₂ adduct [NCS·SO₂]⁻ and -65.7 kJ mol⁻¹ for isothiocyanate-SO₂ adduct [SCN·SO₂]⁻). Thus, it is likely that the formation of both complexes might occur during the simulation with almost equal probability. Nevertheless, the RDFs for S'-S'' and N'-S'' distances indicate the formation of the thiocyanate adduct is dominating in the system under investigation as depicted in Figure 6.4D. The time development of the distances between the S'' atom and the S' or N' atoms of all anions as shown in Figure 6.5 panels A and B, indicates that SO₂ interacts with one [SCN]⁻ over the majority of the simulation time, see in Figure 6.5 panel A, black line. However, a temporary anion exchange (red, blue and green lines in Figure 6.5 panel A) is observed at around 23 ps and between 45 and 48 ps. The substitution of the S' atom to the N' atom coordination or the change from thiocyanate-SO₂ to isothiocyanate-SO₂ adduct occurs at around 12, 14, and 36 ps (see Figure 6.5 panel B, red, blue and green lines). This transition in the anion coordination at SO₂ is in good agreement with the already known experimental results of the thiocyanate anion complex formation with SO₂ in dilute solutions of acetonitrile.^[300] Thus, the absorption of SO₂ in the ionic liquid under consideration does not take place with a pure thiocyanate-SO₂ complex generation, rather an equilibrium mixture of thiocyanate and isothiocyanate adduct will form.

To understand the structure of the dominant thiocyanate-SO₂ adduct in more detail, we have compared the geometrical parameters from AIMD simulation in bulk and from the static quantum chemical calculation of the isolated adducts with data from crystal structures of the potassium 1,4,7,10,13,16-hexaoxacyclooctadecane thiocyanate-SO₂ adduct [K(18-crown-6)][NCS·SO₂]^[301] and the tetramethylammonium thiocyanate-SO₂ adduct [NMe₄][NCS·SO₂]^[302] (see Figure 6.6 and Table 6.1). Both calculated structures agree well with the crystallographic data for the thiocyanate-SO₂ adducts, see Table 6.1. The differences in distances and angles are explained by the different surroundings for

6. SO_2 Solvation in the 1-Ethyl-3-Methylimidazolium Thiocyanate Ionic Liquid

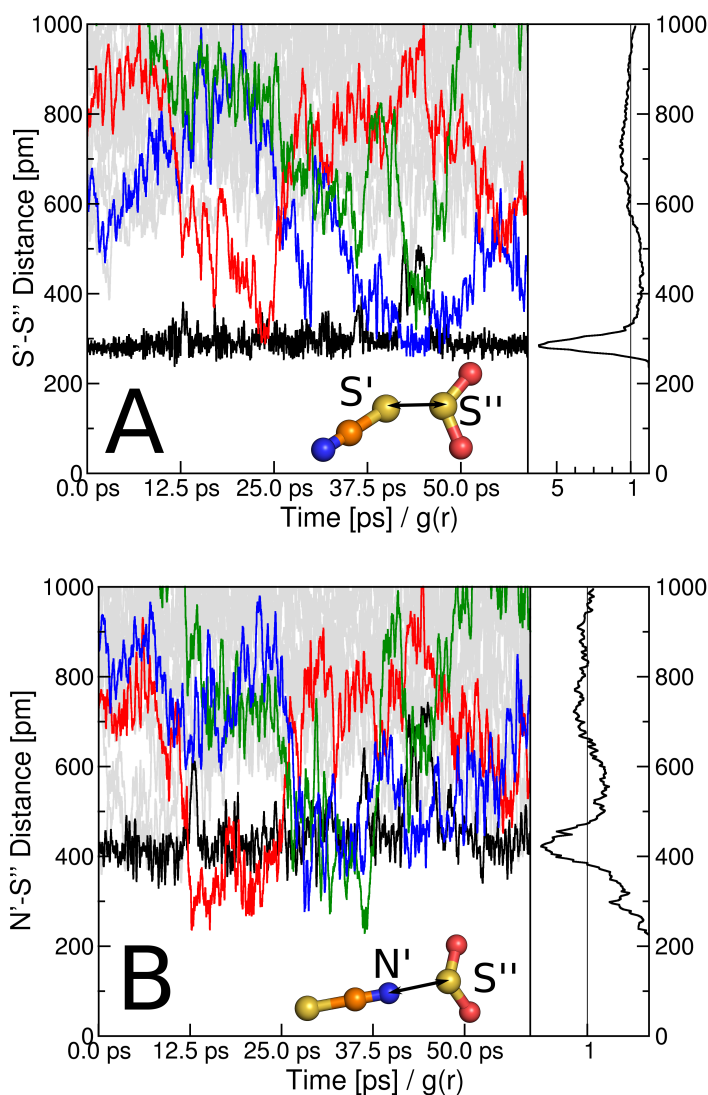


Figure 6.5. Anion- SO_2 interaction. Time development of distances between S'' atom of SO_2 and S' (A) or N' (B) atoms of all 32 anions. Curves corresponding to anions that approach the SO_2 molecule closer than 350 pm during the simulation are coloured black, red, blue and green. Curves corresponding to other anions are colored grey.

$[\text{NCS}\cdot\text{SO}_2]^-$, particularly, the $\text{C}'\text{-S}'\text{-S}''\text{-COM}''$ dihedral angle could be smaller in absolute values due to the stabilization of the selected structure. Considering the most probable distance between S' and S'' atoms (283 pm), we also found good agreement with experimental values of $\text{S}\cdots\text{O}$ distances in complexes of SO_2 with diethyl ester (287 pm) and H_2O (282 pm).^[303]

To clarify how the vibrational frequencies of the SO_2 and the thiocyanate anion change upon thiocyanate- SO_2 adduct formation, power spectra for the adduct have been calcu-

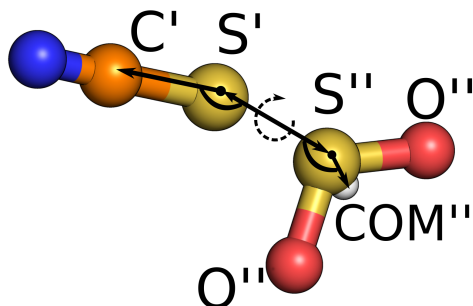


Figure 6.6. Ball-and-stick representation of the $[\text{NCS}\cdot\text{SO}_2]^-$ complex. For structural parameters see Table 6.1.

Table 6.1. Structural parameters for thiocyanate- SO_2 adduct.

	bulk ^[a]	gas ^[b]	[K(18-crown-6)][NCS·SO ₂] ^[c]	[NMe ₄][NCS·SO ₂] ^[c]
S'-S'' (pm)	283	271	274	301
O''-S''-O'' (°)	116	115	119	115
C'-S'-S'' (°)	96	97	99	90
S'-S''-COM'' (°)	109	112	103	107
C'-S'-S''-COM'' (°)	±142	139	-91	74

[a] The maximum of corresponding distribution function from $32\text{P}+\text{SO}_2$ trajectory (see Supporting Information D, Figure D.4-D.6). [b] The structure was optimized in gas-phase on B3LYP-D3(BJ)/def2-TZVPP level of theory. [c] The distance and angles were evaluated from crystallographic structure from Ref. [301] and [302]

lated and compared with the gas-phase vibrational frequencies for SO_2 and the power spectra for the remaining anions (Figure 6.7). Moreover, we summarized the information on the calculated and experimental data for unbound (thiocyanate in bulk and SO_2 in gas-phase) and bound states ($[\text{NCS}\cdot\text{SO}_2]^-$) of the SO_2 and the thiocyanate anion (Table 6.2). It is apparent that the direction of relative shifts for the bands (blue or red shift) are in good agreement with the experimental results, whereas the absolute position of the maximum for the absorption band is reproduced satisfactorily due to the deficiency of the BLYP functional, which has been observed previously.^[296] Interestingly, the experimental infrared spectra for SO_2 dissolved in thiocyanate ILs^[91,92] indicate that the absorption bands of dissolved SO_2 are almost at the same position as fundamental frequencies of SO_2 in the gas-phase.^[304] Care has to be taken in the interpretation of the total spectra since some of the adduct bands might overlap with other bands or have low intensity compared

6. SO₂ Solvation in the 1-Ethyl-3-Methylimidazolium Thiocyanate Ionic Liquid

to the rest of unbound SO₂.

Table 6.2. Vibrational frequencies in cm⁻¹ for SO₂, thiocyanate and thiocyanate-SO₂ adducts.

	Calc.		Expt.	
	SO ₂ (gas), [SCN] ⁻ (bulk)	[NCS·SO ₂] ⁻	SO ₂ (gas), [SCN] ⁻ (bulk)	[NCS·SO ₂] ⁻ or [NC·SO ₂] ⁻
$\nu(\text{CN})$	2019	2044	2052 ^[301]	2090 ^[301]
$\nu_{as}(\text{SO}_2)$	1273	1171	1362 ^[304]	1152 ^{[a] [305]}
$\nu_{sym}(\text{SO}_2)$	1086	1015	1151 ^[304]	1107 ^[301] (1065 ^{[a] [305]})
$\nu(\text{CS})$	739	722	732 ^[301]	725 ^[301]
$\delta(\text{SO}_2)$	485	484	528 ^[304]	-
$\delta(\text{SCN})$	472	454	-	-

[a] The data was taken for cyanide-SO₂ adduct.

6.4 Conclusion

Obtaining a picture, with a microscopic resolution, of the solvation of small gas molecules (like SO₂) is crucial to understand the varying solubilities in different ionic liquids. In this article we have provided a detailed investigation of SO₂ solvation in the [C₂C₁im][SCN] ionic liquid from AIMD. This system is known to be special, because of its high SO₂ solubility. Contacts between the SO₂ and groups that donate weak interactions like the alkyl hydrogen atoms, as well as the π -system of the cation, are numerous in the first solvent shell, whereas only one single thiocyanate anion is found in the first solvent shell forming an anion-SO₂ complex. The dynamics of the anion exchange at the SO₂ was investigated and the formation of different anion-SO₂ adducts were detected. The geometry of the most probable thiocyanate-SO₂ adduct of our bulk simulations resembles those from the static gas-phase calculations and from the available crystal structure, namely we find a pronounced sulfur-sulfur bridge between the anion and the SO₂ which in a few instances is replaced by a N(anion)-S(SO₂) isothiocyanate-adduct. The qualitative and quantitative agreement between calculated and experimental frequencies, as well as potentially important bands for identification of the absorption of SO₂ were detected. More interestingly,

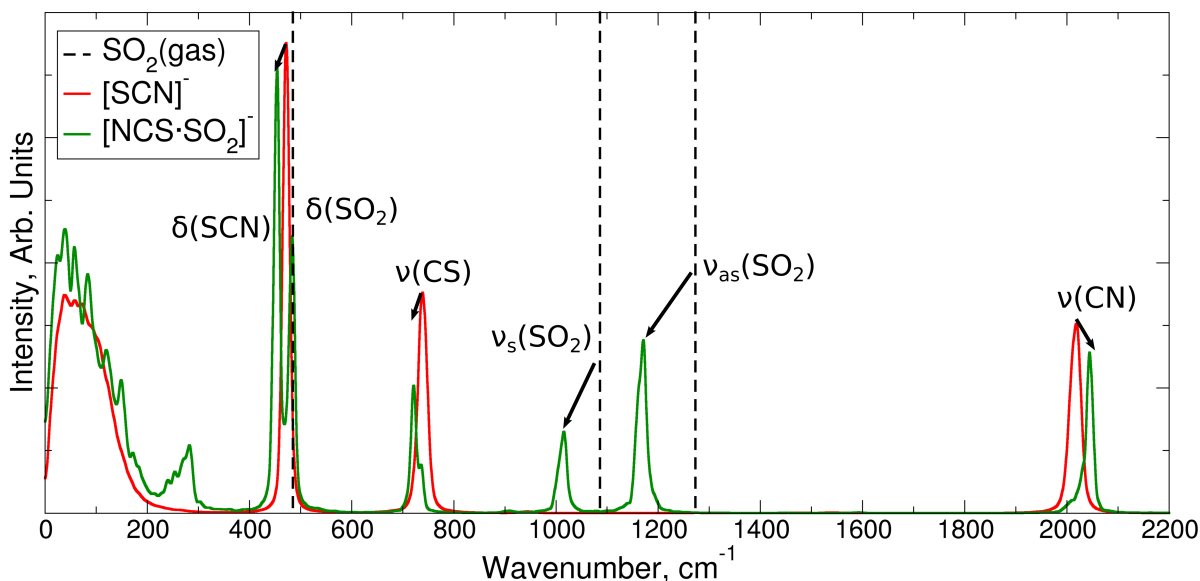


Figure 6.7. Power spectra 31 anions (red) and thiocyanate-SO₂ adduct (green). Vertical dashed black lines marked SO₂ frequencies from gas-phase calculation on BLYP-D3(BJ)/def2-TZVPP level of theory.

and in clear contrast to CO₂, we observed that SO₂ is capable of forming a hydrogen bond with the acidic ring protons of the cation. Thus instead of showing only the usual solvation pattern, we observed that the SO₂ molecule is incorporated into the ionic liquid network, a contact which we called a linker effect, i.e., SO₂ can interact strongly with both the cation and the anion at the same time. Undoubtedly, this linker effect plays a crucial role in the high solubility of SO₂ in the [C₂C₁Im][SCN] IL and does not occur in the solvation of CO₂. It was previously found that while CO₂ interacts with the anions of ILs, it does not form hydrogen bonds by accepting the acidic protons of either the imidazolium or the ammonium cation. Therefore, CO₂ it is not incorporated in the hydrogen bonding network of the ionic liquid. On the contrary, for the solvation of SO₂ in the [C₂C₁im][SCN] ionic liquid, a network of H(cation)⋯O(SO₂)-S(SO₂)⋯S(anion), with SO₂ being a linker molecule, can be fabricated. This means, that given the right combination of cation and anion where the SO₂ can form hydrogen bonds with the cation and a sulfur-sulfur bridge (or a similar bond leading to a strong adduct) with the anion, a good solubility of the SO₂ in the IL should be observed. Thus, the design of potential ionic liquids containing good hydrogen bond donor ability in the cation and sulfur atoms

6. *SO₂ Solvation in the 1-Ethyl-3-Methylimidazolium Thiocyanate Ionic Liquid*

free to from sulfur-sulfur bridges or similar strong adducts in the anion should not only lead to a specific absorption of this particular gas molecule but also to the application of particular purposes of this gas-IL mixture where a more extended hydrogen bond network is needed.

6.5 Acknowledgments

Financial support from Deutsche Akademische Austauschdienst for Dzmitry Firaha is gratefully acknowledged and also support from KI-768/12-1. We would like to thank Barbara Intemann and Oldamur Hollóczki for carefully reading our article.

Part III.

CO₂ Capture by Carbens in Ionic Liquids

Summary of Part III

One of the possible strategies to capture CO₂ is the use of carbenes.^[68,69] These species are formed in some ionic liquid containing, for example, the 1,3-dialkylimidazolium cation and a basic anion like acetate.^[238] Since the carbenes formation is the initial step in the CO₂ absorption process, revealing the mechanism of their formation is of utmost importance.

The static quantum chemical calculations conducted in the gas phase indicate that strong acetate-CO₂ interactions can be detected, while the cation-CO₂ interactions are much weaker (Chapter 7). This might lead to the conclusion that the anion plays a major role in the solvation of CO₂, whereas the cation-CO₂ interactions are not that important. However, the strong anion-CO₂ interaction results in a decrease of the anion's basicity and preventing the carbene formation in the IL, which is in clear contrast to the experiments.^[68,69,306–308] On the contrary to the gas-phase calculations, ab initio molecular dynamics simulations of a bulk mixture of 1-ethyl-3-methylimidazolium acetate with CO₂ reveals a high dominance of the cations in the solvation shell of CO₂. Weak cation-CO₂ interactions disrupt the strong anion-CO₂ interaction. This facilitates the carbene formation making the carbene-CO₂ reaction feasible (see Figure 6.8).

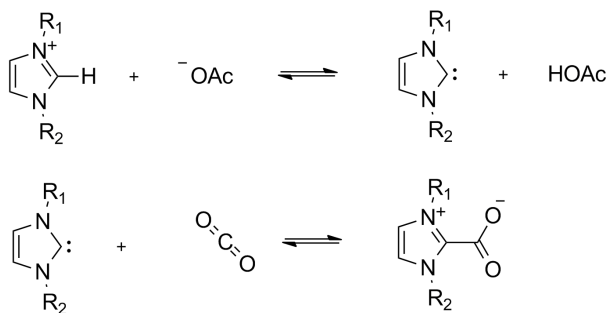


Figure 6.8. The mechanism of carbene-CO₂ adduct formation.

Among the formation of the normal carbene-CO₂ adduct (1,3-dialkylimidazolium-2-carboxylate) the abnormal carbene-CO₂ adduct [1,3-dialkylimidazolium-4(or 5)-carboxylate] has been detected in the products at the excess of CO₂ (see Chapter 8). The experimental evidence contradict the suggestion that the formation of both adducts follows the similar mechanism (see Figure 6.8). In the experiment, the occurrence of the abnormal adduct has been detected at certain conditions like the excess of CO₂ (at the

6. CO₂ Capture by Carbens in Ionic Liquids

high partial pressure of CO₂) or the presence of a potassium carbonate additive (at the low partial pressure of CO₂). Thus, instead of direct formation the abnormal adduct, the isomerization of the initially formed normal adduct into the abnormal adduct can be postulated. The establishing of the probable isomerization mechanism is a challenging task making static quantum chemical calculations and ab initio molecular dynamics simulations useful tools to verify the postulated mechanism (see Figure 6.9). The results of ab initio molecular dynamics simulations are remarkable since the mobility of the proton in the initial cation and the formed normal adduct can be studied. The enhance of the ring's protons mobility in the normal adduct indicates that these protons are the possible target for the proton abstraction by the acetate anions. After the proton abstraction, the formation of the anionic 1,3-dialkylimidazolium-2,4-dicarboxylate as an essential intermediate is assumed. Finally, the decarboxylation and the proton abstraction lead to the formation of the abnormal adduct (see Figure 6.9). A pronounced stability of the abnormal adduct against the normal adduct is explained via the formation of the most favorable hydrogen bonds with the cations found in ab initio molecular dynamics simulations. Thus, the use of the electronic structure methods is the reliable approach for verifying the suggestions for the possible mechanism.

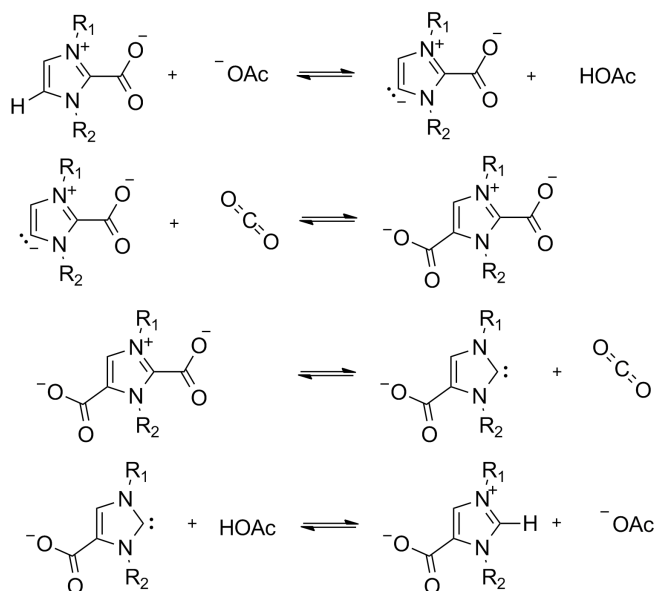


Figure 6.9. The suggested mechanism of the transformation between normal and abnormal adducts.

7 Carbene Formation in Ionic Liquids: Spontaneous, Induced, or Prohibited?

Oldamur Hollóczki,^{*†} Dzmitry S. Firaha,^{*†} Joachim Friedrich,[‡] Martin Brehm,^{*†} Richard Cybik,[†] Martin Wild,[§] Annegret Stark,[§] and Barbara Kirchner^{*†}

Received: January 14, 2013, Published: April 8, 2013

Reprinted (adapted) with permission from

O. Hollóczki, D. S. Firaha, J. Friedrich, M. Brehm, R. Cybik, M. Wild, A. Stark, and B. Kirchner *J. Phys. Chem. B*, **2013**, *117*, 5898–5907

Copyright ©2013 American Chemical Society.

DOI 10.1021/jp4004399

^{*}Mulliken Center for Theoretical Chemistry, Institut für Physikalische und Theoretische Chemie, Rheinische Friedrich-Wilhelms-Universität Bonn, Berlingstraße 4+6, 53115 Bonn, Germany

[†]Wilhelm-Ostwald-Institut für Physikalische und Theoretische Chemie, Universität Leipzig, Linnéstraße 2, 04103 Leipzig, Germany

[‡]Institut für Chemie, Technische Universität Chemnitz, Straße der Nationen 62, 09111 Chemnitz, Germany

[§]Institut für Technische Chemie, Universität Leipzig, Linnéstraße 3-4, 04103 Leipzig, Germany

7. Carbene Formation in Ionic Liquids: Spontaneous, Induced, or Prohibited?

Own manuscript contribution

- Performance of the static calculations
- Analysis of the trajectories
- Discussion of the results
- Co-writing the manuscript

Abstract We present a theoretical study of carbene formation from the 1-ethyl-3-methylimidazolium acetate ionic liquid in the absence and presence of CO₂ in gas and liquid phase. Although CO₂ physisorption constitutes a precursory step of chemisorption (the CO₂'s reaction with carbenes, which forms from cations via proton abstraction by anions), it also enables a very stable CO₂-anion associate. However, this counteracts the chemical absorption by reducing the basicity of the anion and the electrophilicity of the CO₂, which is reflected by charge transfer. Accordingly, the observable carbene formation in the gas phase is hindered in the presence of CO₂. In the neat liquid, the carbene formation is also suppressed by the charge screening compared to the case of the gas phase; nevertheless, indications for carbene incidents appear. Interestingly, in the CO₂-containing liquid we detect more carbene-like incidents than in the neat one, which is caused by the way CO₂ is solvated. Despite the weakness of the CO₂-cation interaction, the CO₂-anion associate is distorted by cations, which can be seen in longer associate distances and reduced "binding" energies. While the single solvating anion is shifted away from CO₂, many more solvating cations approach it compared to the case of the gas phase. This leads to the conclusion that while the ionic liquid effect stabilizes charged species, introducing neutral species such as CO₂ provides an opposite trend, leading to an inverse ionic liquid effect with the facilitation of carbene formation and thus of chemical absorption.

7.1 Introduction

Beyond the mere scientific interest in the unique structure of ionic liquids (ILs),^[178,309–312] their versatility and often advantageous properties (e.g., low vapor pressure, nonflammability, thermal stability, conductivity, high gas solubilities, etc.) induced numerous applications^[313,314] involving their use as potential substitutes for classic organic solvents in chemical syntheses^[24,315] or, perhaps most remarkably, in CO₂ absorption from industrial waste gases.^[316] Due to their diverse and tunable chemistry, imidazolium-based ILs bear several undiscovered possibilities as solvents with functionality beyond the simple addition of the desired chemical effect by the attachment of a functional group.^[313,314] For example, the imidazolium cation can be considered a protonated N-heterocyclic carbene^[317–323] —

7. Carbene Formation in Ionic Liquids: Spontaneous, Induced, or Prohibited?

which also holds great potential as organocatalyst,^[324–328] or as ligand in transition metal complexes^[320,329–336] — that is available via a single deprotonation.

Recently, it has been shown that the deprotonating agent can be the IL's anion itself if it possesses sufficient basicity like the acetate anion [OAc][−] (see Figure 7.1).^[238,337–340] In the vapor of 1-ethyl-3-methylimidazolium acetate ([C₂C₁Im][OAc]) the formation of the carbene could directly be evidenced by spectroscopic and theoretical studies.^[238] Since with less basic anions (e.g., methanesulfonate^[238]) the same spectroscopic methods indicated no carbene in the gas phase rather the isolated ionic isomer **1**, these results show clear correspondence to the basicity of the acetate anion. However, the charge screening (viz. the IL effect^[341,342]) in the chemically more relevant liquid phase stabilizes ionic species in general as compared to that in the vapor phase;^[341,342] thus, the carbene formation is reduced, and no carbenes could yet be detected by any spectroscopic methods in the neat IL. Nevertheless, in pioneering studies by both the Rogers group^[68,69,338] and the Nyulászki group,^[336] the presence of the carbene was observed indirectly in the liquid; the former group detected it via trapping reactions and the latter via catalytic activity in the neat IL.

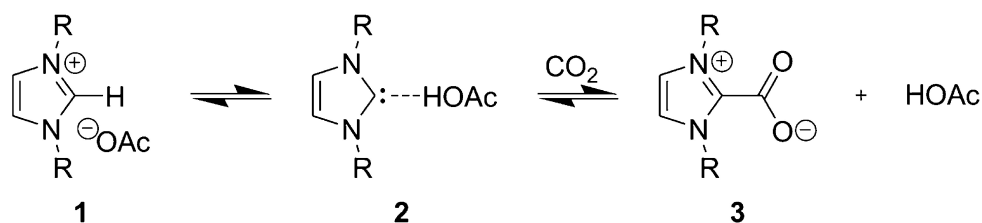


Figure 7.1. Formation of carbenes and acetic acid (**2**) from one ion pair of 1-ethyl-3-methylimidazolium acetate [C₂C₁Im][OAc] (**1**) in the neat IL, and the subsequent chemical absorption of CO₂ to form the carboxylate adduct and the acetic acid (**3**). Such proton transfer processes are expected in ILs possessing basic anions.^[238]

Although these reactions clearly prove the accessibility of the carbene, and ab initio molecular dynamics (AIMD) simulations also indicated extraordinarily elongated C2–H2 bond lengths (see Figure 7.3),^[339] it is not yet clear if the carbene formation is spontaneous or induced by the reactants, and therefore the particular mechanism of each step is far from being understood.

Obviously,^[343] the accessibility of carbenes results in the increased solubility^[344] of CO₂ in [C₂C₁Im][OAc] via the formation of carbene–CO₂ adducts **3** (Figure 7.1),^[68,69]

providing a novel route to design effective solvents for CO₂ capture and processing. However, assuming the reaction occurs via the initial physical absorption of CO₂, it should be kept in mind that physically absorbed CO₂, which possesses significant Lewis acidity, is expected to interact strongly with the anion of the IL.^[31,114,141] The presence of such an anion–CO₂ association has been observed both experimentally^[31,114,273] and theoretically.^[31,114,141,149,150] Clearly, this interaction is significantly stronger if more basic anions are present in the IL,^[141] forming a more stable anion–CO₂ adduct-like structures (Figure 7.2); accordingly, the very basic acetate anion has been shown by gas phase calculations to interact more strongly with physically absorbed CO₂ than chloride, nitrate, trifluoroacetate, or bromide.^[141] In agreement, a recent AIMD study by Shi and colleagues^[150] on the CO₂/[C₂C₁Im][OAc] system (in a 1:1 molar ratio) yielded a very pronounced acetate–CO₂ interaction with a distance between the two species of ca. 150 pm and with a 130° bond angle within the CO₂ moiety. Obviously, the formation of such a stable anion–CO₂ associate reduces the anion’s potential to abstract the proton from the [C₂C₁Im]⁺ cation because the proton has to compete with the CO₂ for the base (Figure 7.2). This is strongly supported by previous AIMD^[339] and experimental studies^[338] showing that even a small amount of hydrogen-bonding solutes (e.g., water) occupy the anions and reduce the carbene formation compared to that in the “dry” system. At the same time, the carbene competes with the anion for the CO₂, which now holds a decreased electrophilicity due to the very same anion–CO₂ association (Figure 7.2).

As the formation of the carboxylate adduct **3** undoubtedly has been evidenced experimentally,^[68,69] both steps in Figure 7.1 have to take place, which is inconsistent with the above-described concepts. These inconsistencies, or even controversies, open the question of how these reactions occur from the mechanistic and structural point of view. Furthermore, it has been shown recently^[149] that (physically absorbed) CO₂ has significant dispersion interactions with the cation as well, which may also have some influence on these reactions via the corresponding structural effects. Thus, for the understanding of the process, a comprehensive in-depth investigation is required, which can only be gained from a microscopic-level point of view. In the present contribution, we investigate the effect of the IL media on carbene formation, and how much the desired release of this

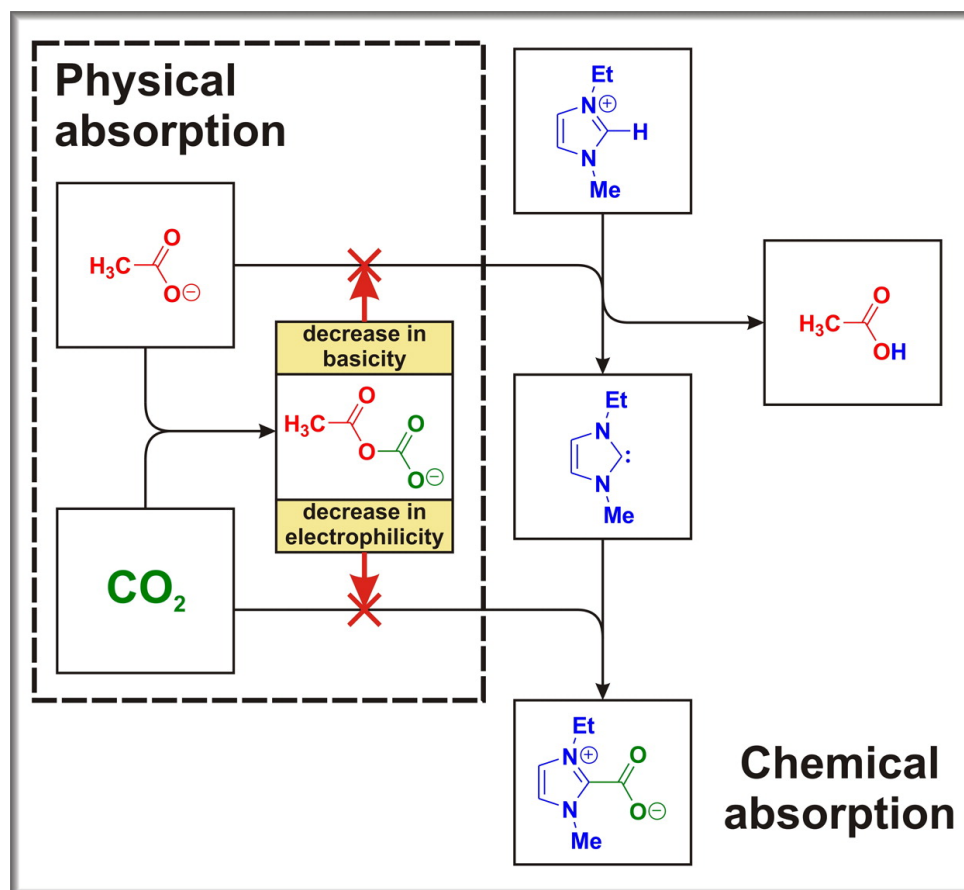


Figure 7.2. Illustration of possible reaction paths leading to either physical or chemical absorptions together with the potential suppressive role due to the CO_2 -anion association, indicated by red arrows.

seemingly transient species is influenced by the presence of CO_2 , in order to understand how chemical absorption may occur. The knowledge gathered here not only will give a conceptual framework for the development of novel ILs being capable of more facile CO_2 absorption and capture but also will extend our general chemical knowledge on reactions in ILs and the corresponding influential factors.

7.2 Systems under Study

For the above-described purposes, we studied four different systems of $[\text{C}_2\text{C}_1\text{Im}][\text{OAc}]$ with different compositions by AIMD simulations. This method has the advantage of modeling the dynamics while adjusting the electronic structure on-the-fly (at each MD step), and it is, therefore, able to monitor polarization and temperature effects as well as

unforeseen spontaneous events, such as reactions. The atom labeling that will be used in this article is presented in Figure 7.3, while a snapshot of each simulation box is shown in Figure 7.4.

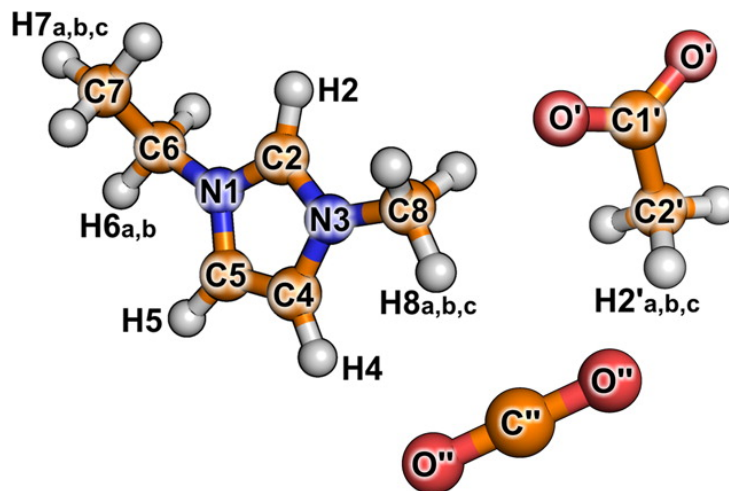


Figure 7.3. Atom labeling as used throughout this article. Key: N, blue; C, orange; O, red; H, white. Atoms denoted with no, single, or double prime belong to cation, anion, and CO_2 molecule, respectively.

We investigated the **1P** system consisting of a single ion pair (Figure 7.4, upper left panel), in order to model the experimentally characterized vapor phase. Please note that the gas phase of aprotic ILs has been proven actually to consist of single isolated ion pairs^[345] (or their carbene–acid hydrogen bonded structural isomer)^[238] instead of larger aggregates, which makes our study of one single ion pair consistent with the experimentally observed vapor behavior. To model the chemically more complex liquid phase, a box which is infinitely replicated by periodic boundary conditions containing 36 ion pairs^[339] (labeled **36P**) has also been studied (Figure 7.4, lower left corner). This provides an observation of the ion–ion interactions’ effect on the carbene formation. By the addition of a single CO_2 molecule to each system, two further computer experiments have been performed, which are labeled **1P+CO₂** and **36P+CO₂** (Figure 7.4, right side). These two systems allow us to describe the relationship between the physical absorption of CO_2 and the proton transfer from the cation to the anion.

In order to characterize the solute–solvent interactions, and the structural effects of CO_2 on the IL particles, static quantum chemical calculations have also been performed on the 1,3-dimethylimidazolium acetate ion pair (**1P_{Me}**) system and on the corresponding

7. Carbene Formation in Ionic Liquids: Spontaneous, Induced, or Prohibited?

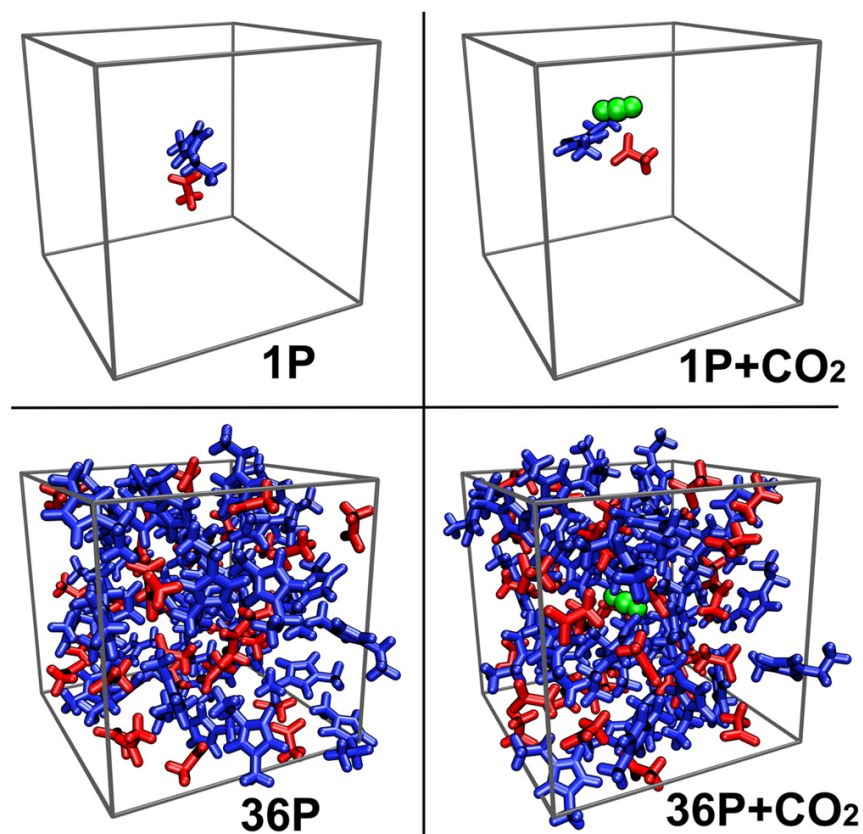


Figure 7.4. Snapshots of each investigated system. Anions are indicated with red, cations with blue, and CO₂ with green. System **1P** (upper left) consists of one ion pair representing the gas phase. The right upper corner shows the **1P+CO₂** system and the lower panels show the boxes of **36P** (left) and **36P+CO₂** (right) systems modeling the liquid by applying periodic boundary conditions (i.e., infinitely replicated boxes). The differences between the upper and lower systems can be defined as the effect of the bulk, while those between the left and right pairs show the CO₂'s structural role.

1P_{Me}+CO₂, which is a system containing both **1P_{Me}** and one CO₂ molecule. In contrast to the AIMD simulations, these calculations provide insight into isolated associates with no dynamical representation but with direct availability of the interaction strength. It should be noted that, in the case of single ion pairs, the alkyl → Me exchange at the nitrogen atoms has been shown^[238,346] to effect the anion–cation interactions and the carbene formation only slightly; therefore, the systems **1P_{Me}** and **1P_{Me}+CO₂** are very comparable to **1P** and **1P+CO₂**, respectively.

Although the existence of “remote” or “abnormal” carbenes has been demonstrated,^[330,347] here we focus only on the abstraction of the most acidic “front” proton at position 2, because the previous trapping reactions (performed by the ionic liq-

uid investigated here) showed clear correspondence to the “normal” carbene, 1-ethyl-3-methylimidazole-2-ylidene.^[68,69,338] The removal of the “rear” protons at positions 4 and 5 of the ring (Figure 7.3) demands 72.7 kJ mol⁻¹ more energy (BP86/TZ2P) for the imidazolium cation.^[331]

As has been discussed above and shown before,^[238] the carbene formation directly corresponds to the basicity of the solution. A more basic anion, however, also forms stronger hydrogen bonds with the cation, resulting in an increase in the C2–H2 bond length and a decrease in the H2–O’ distance; even if the carbene formation would not be observable directly in the above-described bulk phase simulations, the changes in basicity can indirectly be observed via monitoring these expectedly low changes in the bond lengths during the simulations, providing indirect information on the carbene’s accessibility.

7.3 Computational Methodologies

The calculation of system **36P** has been described previously.^[339] These simulations of the pure liquid have been used as the starting point for system **36P+CO₂**. The **1P** and **1P+CO₂** simulations have been started with optimized geometries, which are given in the Supporting Information E. For all the AIMD simulations, the CP2K^[187] program package has been applied using the Quickstep module^[188] with a time step of 0.5 fs, with periodic boundary conditions. The electronic structure has been calculated by density functional theory (DFT) utilizing the BLYP-D functional, which includes the empirical dispersion correction (D3) from Grimme^[171] being necessary for IL systems,^[178,181,348] with the molecularly optimized double- ζ basis set (MOLOPT-DZVP-SR-GTH)^[261] and Goedecker-Teter-Hutter pseudopotentials.^[262–264] The temperature has been thermostated to 350 K by Nose–Hoover chains.^[265–267] More simulation parameters are listed in Table 7.1.

Static quantum chemical calculations have been carried out at the B97-D/6-311+G** level, and the results have been compared with those obtained by different DFT functionals (B97-D, BLYP, BLYP-D, PW91PW91, M05-2X, M06-2X, B3LYP) and ab initio methods (RI-MP2) with different basis sets (6-311+G**, def2-TZVPP, aug-cc-pVTZ).

7. Carbene Formation in Ionic Liquids: Spontaneous, Induced, or Prohibited?

Table 7.1. AIMD parameters.^[a]

	% n/n	ρ	t_{eq}	t	T
1P			15.5	177.6	350
1P+CO₂	50		14.5	160.4	350
36P		1.069	10.0	70.0	350
36P+CO₂	2.7	1.076	5.5	51.8	350

[a] Box size for all systems is 2121.24 pm. Density (ρ) in g cm⁻³; equilibration time (t_{eq}) and physical time (t) in ps; the average temperature (T) in K.

All static quantum chemical results are shown only at the B97-D/6-311+G** level in this article, but a detailed analysis of the data at different levels is given in the Supporting Information E. BLYP, RI-MP2, and BLYP-D calculations have been performed by TURBOMOLE 6.0,^[349,350] while the other calculations with different functionals have been carried out by the Gaussian 09 program package.^[351] The charges are calculated according to the natural bond orbital (NBO) analysis as implemented in Gaussian 09.

The explicitly correlated coupled cluster calculations were performed with the TURBOMOLE program package^[349,352–354] using Version 6.5. We used a Slater-type correlation factor^[355] represented by a linear combination of six Gaussians.^[356] Furthermore, we applied the cc-pVDZ-F12 basis set of Peterson^[357,358] using the corresponding CABS^[359] and the recommended exponent of 0.9 a₀⁻¹ in the correlation factor. The details of the explicitly correlated CCSD(T)(F12)^[352,360] calculations are ansatz 2, approximation B,^[361] and the fixed amplitude approach.^[362]

All analysis of the trajectories were performed by our free software TRAVIS.^[148]

7.4 Results and Discussion

7.4.1. Carbene Formation in the Absence of CO₂

System 1P. As mentioned earlier, several studies have proven that either isolated ion pairs (in the case of nonbasic anions)^[345,363,364] or the isomer carbene–acid complexes (in the case of basic anions)^[238] are present in the vapor of ILs rather than larger aggregates.

Since in AIMD such events as proton transfers are described, the single ion pair of system **1P** provides a direct insight into the carbene formation in the gas phase, induced by the basic acetate anion. According to the previous experimental data,^[238] in **1P** the formation of the carbene is expected. It should be noted here that in accordance with previous results,^[238] the applied density functional methods slightly underestimate the stability of the carbene–acetic acid structure **2** compared to that of the ionic isomer **1** (Figure 7.1 and Table 7.2). Therefore, our study underestimates the degree of carbene formation. Nevertheless, DFT methods are expected to provide the right trends for the changes in this energy difference.^[238] Thus, this discrepancy should not affect any of the present conclusions (for a detailed discussion and comparison to other methods, see the Supporting Information E).

Table 7.2. Computed properties for **1P_{Me}** and **1P_{Me}+CO₂** systems.^[a]

	1P_{Me}		1P_{Me}+CO₂	
	1	2	1	2
ΔE_{rel}	0.0	3.5	0.0	8.8
r(C2–H2)	115.7	163.2	112.1	157.4
r(H2–O')	158.3	107.6	172.9	109.8
$\rho_{\text{BCP}}(\text{C2–H2})$	0.241	0.077	0.263	0.088
$\rho_{\text{BCP}}(\text{H2–O}')$	0.068	0.255	0.048	0.240
ν	2185.1	1943.5	2670.4	1765.9

[a] Relative energies ΔE_{rel} , in kJ mol^{-1} ; bond lengths in pm; electron densities at the bond critical points ρ_{BCP} ;^[365] stretch vibrational frequencies ν (in cm^{-1}) within the C2–H2···O' assembly obtained from static quantum chemical calculations at B97-D/6-311+G** level of theory.

The formation of the carbene can be related to the changes in the C2–H2 and H2–O' distances, as is apparent in Table 7.2. The combined distribution functions (CDFs) of these two distances (when only the closest neighbors are considered) can be seen in Figure 7.5, with an aiding red line at equal bond lengths in each panel. Because in this reaction the increase of the C2–H2 length and the decrease of H2–O' distance are expected, the occurrence of the carbene results in entries in the lower right part of each panel beyond the red line in Figure 7.5. The carbene formation occurs in system **1P**, which has already been indicated from the static quantum chemical calculations shown in Table 7.2 and

7. Carbene Formation in Ionic Liquids: Spontaneous, Induced, or Prohibited?

the published experimental and theoretical data.^[238] In Table 7.3, further numerical data from the AIMD simulations are shown for C2–H2 and O'–H2 distances, including the average values and—to avoid averaging out the rare events—also the smallest and largest values that have been observed. These data also show the occurrence of the carbene in the **1P** trajectories, because a maximum C2–H2 distance of 174.4 pm and minimum H2–O' distance of 99.1 pm have been observed.

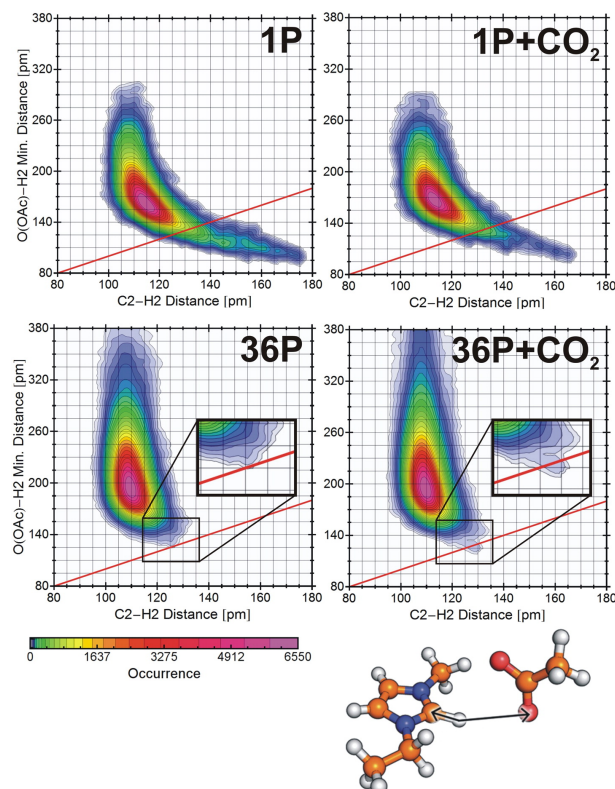


Figure 7.5. Combined distribution functions of the C2–H2 distance versus the H2–O' distance as illustrated by the ball-and-stick image below the graphs from AIMD. The upper panels show the data for the gas phase, and the lower panels show the data for the liquid systems. On the left, the pure system is depicted, and on the right, the system which contains CO₂. The red line marks those events in which the proton is equally distant to anion and cation. Those entries that touch or cross the line are indications for carbene formations.

System 36P. According to the CDFs in Figure 7.5 and the bond length data in Table 7.3, the presence of further ion pairs significantly suppresses the carbene formation compared to the case of the above-described **1P**. Obviously, this is due to the charge screening; thus, there is a real IL effect.^[68,69,342] Still, the graph occasionally touches the red line at equal bond distances in the CDF of the “bulk” of **36P** (Figure 7.5),

Table 7.3. Distances between C2 and H2 and O' and H2 pairs in pm.^[a]

	r(C2–H2)			r(O'–H2)		
	mean	min	max	mean	min	max
1P	114.2	99.6	174.4	174.5	99.1	297.1
1P+CO₂	113.5	98.8	165.5	175.4	104.0	285.5
36P	109.7	97.0	131.4	210.4	134.0	446.2
36P+CO₂	109.6	97.1	131.7	212.3	126.5	448.0

[a] Mean, shortest (min), and longest (max) distances for the nearest neighbors obtained from the AIMD simulations. For the corresponding graphs, see the Supporting Information E.

which, together with the unusually long C2–H2 (130.7 pm) and short O'–H2 (134.0 pm) distances,^[339] clearly indicates significantly basic conditions. Thus, most likely also the accessibility of the carbene in all systems.

7.4.2. Carbene Formation in the Presence of CO₂ and Electrophilicity of CO₂ in the Ionic Liquid

Acetate Anion and CO₂ in the Gas Phase. Since strong anion–CO₂ interactions have been suggested in the literature,^[31,114,141,149,150,273] first the isolated acetate–CO₂ system has been investigated from static quantum chemical calculations. Interestingly, the CO₂ binds stronger to the anion (-47.9 kJ mol⁻¹, B97-D/6-311+G**, see Figure 7.6) than to the carbene in the carbene–CO₂ complex **3** (-37.7 kJ mol⁻¹, see Figure 7.6)! Analyzing the charges of the acetate–CO₂ complex shows that there is a considerable charge transfer from the anion to the “solute” molecule: while the charge of the anion decreases from -1 to -0.88 , the charge of the CO₂ is increased to -0.12 . Such an increase in negative charge at the solute results in the decrease of electrophilicity as discussed in the Introduction 7.1. Moreover, the topological analysis of the electron density reveals that the high interaction energy originates not only from electrostatic interactions but also from a sort of bond formation between the O' and C'' atoms, which makes the acetate–CO₂ and carbene–CO₂ complexes structurally more analogous. Thus, these (gas phase) results all imply that the carbene has to compete for the CO₂ with the anion in the liquid, which has an overwhelmingly higher concentration in addition to the higher interaction

7. Carbene Formation in Ionic Liquids: Spontaneous, Induced, or Prohibited?

energy.

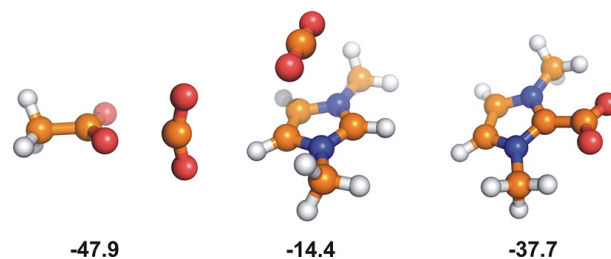


Figure 7.6. Optimized complex structures and gas phase interaction energies (in kJ mol⁻¹) of the CO₂ molecule with the acetate anion (left), the 1,3-dimethylimidazolium cation (center), and the carbene 1,3-dimethylimidazolium-2-ylidene (right) from static quantum chemical calculations. As can be seen according to the interaction energies, the acetate–CO₂ interaction energy by far exceeds that of the other two.

Beyond the effects on the electrophilicity of the CO₂, the aforementioned charge transfer also results in lower proton affinity (EPA) for the acetate–CO₂ structure (1457.6 kJ mol⁻¹, cf. 1483.1 kJ mol⁻¹ for the single anion at the same level). The basicity of the anion in the IL has a large effect on the carbene formation.^[238] Therefore, the difference in proton affinity observed in the gas phase also indicates a reduced concentration of the accessible carbene in the bulk of the IL due to solute–solvent interactions.

System 1P+CO₂. In agreement with the results above, the energy difference between the ionic **1** and carbene-containing **2** is slightly larger in the **1P_{Me}+CO₂** system ($\Delta E_{\text{rel}} = 8.8$ kJ mol⁻¹) than in the **1P_{Me}** ($\Delta E_{\text{rel}} = 3.5$ kJ mol⁻¹, Table 7.2). This decrease in basicity can also be recognized in the structure of the C2–H2...O' hydrogen bond assembly in these two systems. Electron densities at the bond critical points (ρ_{BCP}),^[365] bond lengths, and vibrational frequencies (Table 7.2) of both the ionic **1** and carbene-containing **2** suggest that the C2–H2 bond becomes stronger, while the O'–H2 becomes weaker in the presence of CO₂. This indicates a significant suppression of the proton transfer between the two units.

However, it is interesting to observe that the relative energy of **2** (Table 7.2) is less affected by the presence of CO₂ ($\Delta E_{\text{rel}} = 5.3$ kJ mol⁻¹) than one could assume according to the changes in gas phase proton affinities of the acetate anion induced by the presence of CO₂ ($\Delta E_{\text{PA}} = 25.5$ kJ mol⁻¹, see above).^[238] This indicates that the influential anion–CO₂ interaction may be somewhat reduced by the cation, weakening the CO₂'s suppressive effect on basicity and hence on carbene formation. The differences in the electron densities

at the bond critical points between O' and C'' ($\rho_{\text{BCP}} = 0.035$ in the acetate–CO₂ complex and 0.012 in **1P_{Me}+CO₂**) and in the corresponding O'–C'' distances (231.8 pm in the acetate–CO₂ complex and 277.0 pm in **1P_{Me}+CO₂**) evidence the weakening effect of the cation on the acetate–CO₂ bonding. This also results in lower interaction energies with the CO₂ within system **1P_{Me}+CO₂** (–24.9 kJ mol^{–1}) compared to that in the acetate–CO₂ complex (–47.9 kJ mol^{–1}, see above).

The relative energies of the possible conformations in the **1P_{Me}+CO₂** system (Figure 7.7) allow us to identify the interaction sites between a single ion pair and the CO₂. The most stable isomer **1A** possesses the acetate in front of the [C₂C₁Im]⁺ cation, so that a hydrogen bond can be formed between the anion and cation via the H2, but one of the acetate oxygen atoms is twisted slightly out of the plane of the ring to interact with the CO₂ molecule's C'', which is situated on top of the cation (Figure 7.7). Although by moving the CO₂ to the rear of the ring the acetate regains its in-plane arrangement to also interact additionally with one of the methyl hydrogen atoms, while the CO₂ can still retain its interaction with the cation, the resulting isomeric structure **1B** is less stable by 17.4 kJ mol^{–1}. This energy difference is again lower than the interaction energy between the single acetate anion and the CO₂. On the other hand, the CO₂ can apparently be moved away from the cation with significantly lower energy demand, as indicated by the low relative energy of structure **1C** (1.4 kJ mol^{–1}). This suggests that even if there is an observable interaction between the “solute” and the cation, it is much weaker than the interaction with the anion, as was previously suggested in literature.^[31,114,141]

The AIMD data on the **1P+CO₂** system confirm the suppression of carbene formation, as fewer entries can be observed at long C2–H2 and short H2–O' distances in the upper right panel of Figure 7.5. The numerical data in Table 7.3 also show the shortening of the C2–H2 bond and lengthening of the shortest observed H2–O' (104.0 pm vs 99.1 pm) distances compared to those in the **1P** system. Moreover, the CO₂ molecule is continuously in a narrow distance interval from one of the O' atoms throughout the whole trajectory, whereas its arrangement with respect to the cation is significantly less ordered, as demonstrated by the spatial distribution functions in Figure 7.7, in agreement with the static results on the **1P_{Me}+CO₂** system.

7. Carbene Formation in Ionic Liquids: Spontaneous, Induced, or Prohibited?

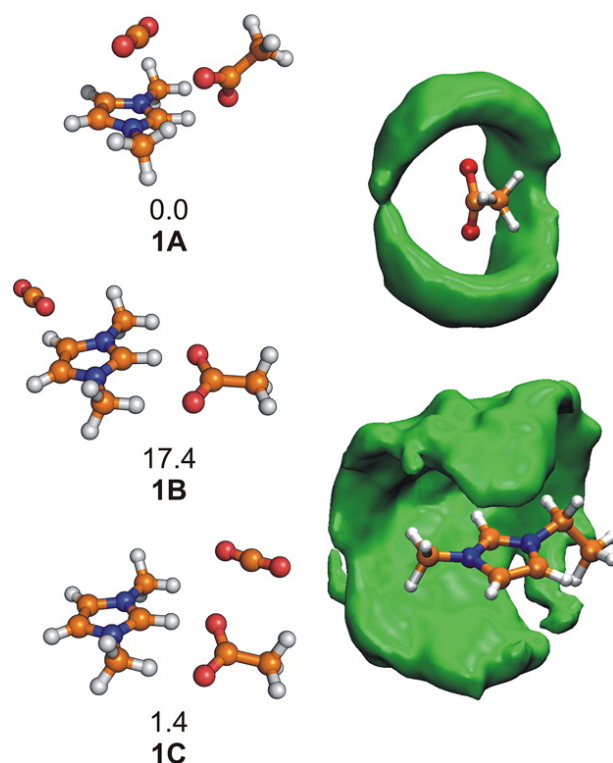


Figure 7.7. Selected isomers of the $1P_{Me}+CO_2$ system (left) together with their relative energies (in kJ mol⁻¹) at the B97-D/6-311/G** level theory from static calculations (for the complete analysis of conformations, see the Supporting Information E). The spatial distribution function of the CO_2 's carbon atom around the acetate anion and around the cation in the $1P+CO_2$ system (right) from the AIMD simulations. Both the relative energies of these isomers and the differences in arrangement around each ion in the AIMD infer the dominance of the anion- CO_2 interaction over the cation- CO_2 .

System $36P+CO_2$. After having seen that the presence of the CO_2 suppresses the basicity of the anion in the isolated acetate- CO_2 and $1P+CO_2$ systems in the gas phase, one could expect similar trends also in the $36P+CO_2$. However, interestingly, the corresponding CDFs in Figure 7.5 indicate that in the liquid phase different changes are induced in the C2-H2...O' assembly by the presence of CO_2 . Although for the neat $36P$ system no entries have been observed under the red line at equal C2-H2 and H2-O' distances, in the $36P+CO_2$ system the plot provides some cases where the H2 is closer to the acetate oxygen than to the C2 of the cation! Furthermore, the numerical data regarding the atomic distances in Table 7.3 also show that the statistical shrinking effect of CO_2 on the C2-H2 bond disappears in the presence of more ion pairs, and in some columns not only similar but also slightly longer C2-H2 bonds can be observed in the

system containing CO₂ compared to that in the neat IL simulation. Because in this data analysis also those ions are involved, which do not interact with the CO₂ directly, one may argue that the lack of the CO₂'s suppressive effect can be explained by the solute affecting the basicity of the anions only locally, and the entries in Table 7.3 correspond to distant ions. Considering such local effects, the mean and longest values could indeed represent ions in the bulk (which is similar to the neat IL), where the formation of the carbene is not or is only slightly disturbed by the presence of the CO₂ molecule. However, any local decrease in basicity, viz. C2–H2 bond shortening, has to be reflected in minimal occurring bond distances close to the CO₂, which should give a visible decrease of the minimum observed distance for the overall system **36P**+CO₂ in Table 7.3. However, this particular extremum distance is also slightly increased, showing clearly that the lack of depression in basicity cannot be explained by the presence of uninfluenced bulk. Thus, the solute–solvent interactions in the bulk phase change in such a manner, compared to that in the gas phase, that the basicity of the acetate anion—thus, the potential of the [C₂C₁Im][OAc] to form carbenes—is recovered, or even increased. This raises the question regarding the solvation modes of (physically absorbed) CO₂ within this IL, which is apparently more complex than has been proposed in literature before.^[31,114,141]

Recently we have shown^[149] that despite the fact that in the literature the dominance of anion–CO₂ interactions is surmised,^[31,114,141] the cation–CO₂ interplay significantly contributes to solvation. While the anion can interact only via the C[−] with the solute, the cation–CO₂ interaction is originated mainly from dispersion interactions via the cationic π -system, which is a less rigid interplay concerning orientation.

Accordingly, although the interaction (see Figure 7.6) in the gas phase with one anion is significantly stronger (-47.9 kJ mol⁻¹) than that with one cation (-14.4 kJ mol⁻¹), five cations and only one single anion can be observed in the first solvate shell of the solute within the system **36P**+CO₂,^[149] resulting in a “cation cage” around CO₂ (see Figure 7.8).

While the anion–CO₂ interplay is enhanced by the bending of the CO₂,^[141,149,150,273] the cation–CO₂ interaction apparently straightens the solute CO₂,^[149] leading to a competition of the two ions for the CO₂.^[149] Therefore, the structures are shown in Figure 7.8

7. Carbene Formation in Ionic Liquids: Spontaneous, Induced, or Prohibited?

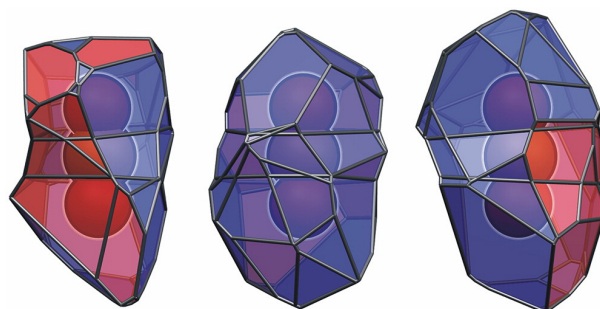


Figure 7.8. Voronoi cages of CO_2 in three selected snapshots of the $36\text{P}+\text{CO}_2$ system showing the contact surfaces of the solute with the anions (red) and with the cations (blue). A complete movie on the changes in solvation modes and more detailed description can be found under the <http://pubs.acs.org/doi/suppl/10.1021/jp4004399> and in the Supporting Information E, respectively.

reflect the weakening or cancellation of the anion– CO_2 interaction. Besides, as has been shown above, the cation–anion interplay also weakens the anion– CO_2 interaction, resulting in larger $\text{O}'\text{--C}''$ distances in the system $1\text{P}_{\text{Me}}+\text{CO}_2$ compared to that in the isolated acetate– CO_2 complex. It is interesting to note that the cation– CO_2 interaction is apparently less affected by the presence of the acetate anion: the interaction energy of -7.4 kJ mol^{-1} with the CO_2 molecule in isomer **1B** is only slightly lower than the $-14.4 \text{ kJ mol}^{-1}$ value between the sole cation and the solute. These effects can be observed clearly by the changes in the anion– CO_2 and cation– CO_2 distances in Table 7.4 while considering only the closest neighboring anions and cations to the solute. Apparently, approaching the liquid ($36\text{P}+\text{CO}_2$) from the gas phase ($1\text{P}+\text{CO}_2$), the anion is situated by an average of ca. 20 pm further away, while the cation comes closer to the CO_2 by an average of ca. 60 pm! Obviously, the anion– CO_2 distance has an effect on the interaction itself. Hence, the basicity of the acetate and the electrophilicity of the CO_2 should change accordingly, as depicted in Figure 7.9.

Therefore, the inconsistencies between the experimental findings that the reaction takes place and the assumptions based on general chemical concepts regarding IL– CO_2 systems (being also in accordance with the gas phase calculations) can be understood by considering that the cation– CO_2 and cation–anion interplays disrupt the anion– CO_2 interactions, and therefore the basicity of the anion, and the electrophilicity of the CO_2 is retained.

Table 7.4. O'–C'' and C2–C'' distances.^[a]

	$r(\text{O}'\text{-C}'')$			$r(\text{C2-C}'')$		
	mean	min	max	mean	min	max
1P+CO₂	300.9	205.2	1006.3	456.4	283.9	742.2
36P+CO₂	320.8	217.1	466.4	397.5	282.5	537.0

[a] The mean, shortest (min), and longest (max) O'–C'' and C2–C'' distances (only the closest neighbor is considered) from AIMD simulations. For the corresponding graphs see the Supporting Information E.

7.5 Summary and Conclusion

In this article, we provide detailed mechanistic insights on the formation of carbenes in the presence and absence of CO₂, as well as on the reaction of this seemingly transient species with the CO₂ from AIMD simulations and static quantum chemical calculations. With these results, we resolved apparent contradictions between the experimental observations and the considerations deduced from basic chemical concepts, such as basicity and electrophilicity. Also, by showing that disregarding the effect of the cation on the solvation of physically absorbed CO₂ in the ionic liquid [C₂C₁Im][OAc] gives a chemically erroneous picture, we put the theory of IL solutions into a novel perspective.

While it has been shown previously that both the initial proton transfer from the cation to the anion that yields carbenes and the reaction of this species with the (physically absorbed) CO₂ giving imidazole-2-carboxylates occur,^[68,69] our static quantum chemical calculations support the formation of a stable Lewis acid–base complex between a single anion and the CO₂. In this structure, the negative charge of the anion is partly transferred to the “solute” molecule, which decreases the electrophilicity of the CO₂ and the proton affinity of the anion. However, a high basicity of the anion and electrophilicity of CO₂ are necessary prerequisites for the formation of the carbene and the carbene–CO₂ adduct, respectively. Moreover, in the gas phase, the stability of the anion–CO₂ complex is somewhat higher than that of the carbene–CO₂ adduct which, considering the overwhelmingly higher concentration of the anion, should prohibit the experimentally observed chemical absorption. In the presence of an additional cation in the system **1P+CO₂**, the anion–CO₂ interaction is somewhat weakened by the anion–cation interplay, but the suppression

7. Carbene Formation in Ionic Liquids: Spontaneous, Induced, or Prohibited?

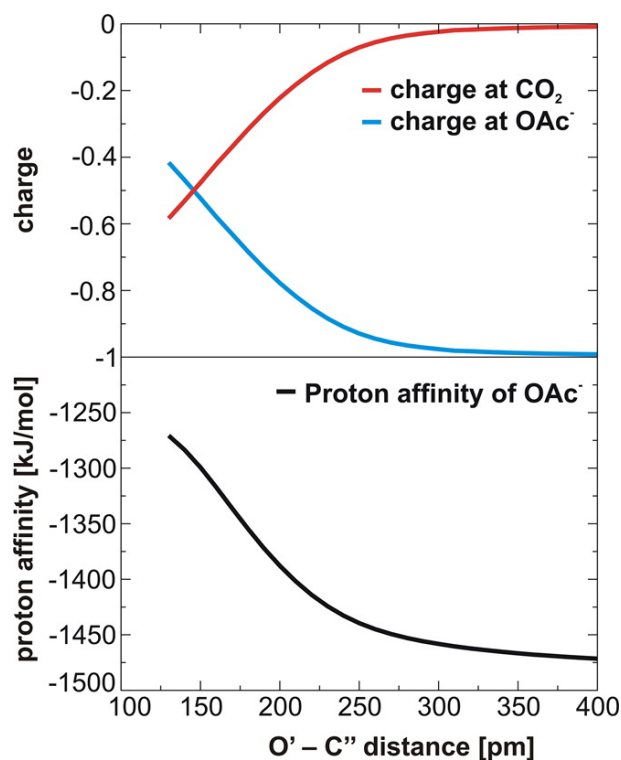


Figure 7.9. Dependency of the acetate's proton affinity and the acetate \rightarrow CO₂ charge transfer on the O'-C'' distances in the acetate-CO₂ system (for details, see the Supporting Information E). The steep curves in the observed O'-C'' range (>200.5 pm, see Table 7.4) show that the disruption of the anion-CO₂ interaction by the cation has a great effect on the carbene formation and the carbene-CO₂ reactions.

of the carbene formation is still indicated via the relative energies of the isomers and the shortening and strengthening of the C2-H2 bonds, as observed by both ab initio quantum chemical calculations and AIMD simulations.

However, surprisingly, in the liquid, the physically absorbed CO₂ apparently does not suppress but rather facilitates the carbene formation, while the anion-solute distance is elongated, indicating further weakening in the acetate-CO₂ interaction. Besides the above-mentioned effect of cation-anion interplay, the lack of suppression can mainly be attributed to the competition^[149] between the anion-CO₂ and cation-CO₂ interactions. Although the former is significantly stronger, the decreasing cation-CO₂ distances in the liquid with respect to the gas phase results show that the lower directionality of the cation-solute interaction prevails in the solvent shell, and a cation cage is formed around the CO₂ molecule. This loosening in the anion-CO₂ interactions results in the recovery of the anion's basicity and the CO₂'s electrophilicity, allowing the chemical absorption of

the CO₂ to occur.

Moreover, regarding the slight facilitation of the neutral carbene and acetic acid formation, one further aspect has to be considered. It has been shown above, in agreement with previous findings in IL research,^[149,345] that charge screening of the ionic liquid media stabilizes the ionic isomer **1** (Figure 7.1) with respect to the nonionic **2** (cf. the CDFs for **1P** and **36P** in Figure 7.5) as a clear ionic liquid effect. Therefore, it is reasonable to assume that by inserting defects into this charge network in the form of neutral molecules (such as CO₂), this charge-stabilizing effect will be canceled out at least partially, and therefore neutral reagents dissolved in ionic liquids might act as slight initiators of carbene formation, resulting thus in an inverse ionic liquid effect. With respect to this line of reasoning, the occurrence of trapping^[68,69,338] and catalytic^[337] reactions in [C₂C₁Im][OAc] that represent carbene reactivity does not necessarily mean that carbenes are present in the neat IL; it only means that they are accessible. Our group is continuously working on this topic, and the results are expected to be published in the upcoming years.

According to the present results, a theoretical framework for the modification of the CO₂'s chemical absorption in ILs has been achieved, defining novel routes for the tuning of the reaction's rate, amount, or reversibility. Beyond the direct conclusion of this particular study, the general message of these results is that, in ionic liquids, the solute-solvent interactions cannot be described by simply considering one of the cation-solute and anion-solute interactions only, even if in the gas phase one of these interactions seems to be significantly stronger than the other. The balance of all interactions between each pair of particles (anion-cation, anion-solute, cation-solute) is influencing the other two interactions as depicted in Figure 7.10, and thus it should be accounted for to obtain chemically relevant results by either experimental or theoretical methods. Because the cation-anion interactions as a result of the charge stabilization are emphasized in the liquid as compared to the gas phase, it is also important to keep in mind that the results of gas phase calculations for describing solute-solvent interactions, even if apparently all interactions are considered, should be handled with special care and criticism because the opposite effects of CO₂ have been shown here for the gas and liquid phase systems.

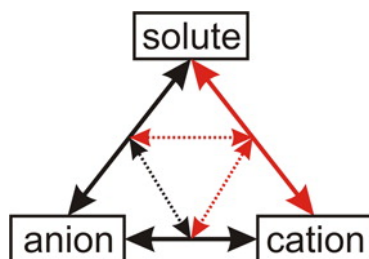


Figure 7.10. The solute–solvent interaction network in general ionic liquid solutions, as deduced from this study. The interactions and cross-interactions that are often neglected when IL solutions are considered are highlighted by the red lines.

7.6 Acknowledgments

The financial support by the Alexander von Humboldt Foundation for the postdoctoral stay of O.H. and by the DFG projects SPP1191, KI768/5-2, and KI768/5-3 are gratefully acknowledged.

8 An Abnormal N-Heterocyclic Carbene-Carbon Dioxide Adduct from Imidazolium Acetate Ionic Liquids: The Importance of Basicity

Zsolt Kelemen,^{*} Barbara Péter-Szabó,[†] Edit Székely,[†] Oldamur Hollóczki,[‡] Dzmitry Firaha,[‡] Barbara Kirchner[‡] József Nagy,[§] László Nyulászi^{*}

Keywords: Basicity, Density Functional Calculations, Ionic Liquids, N-Heterocyclic Carbenes, Supercritical CO₂

Received: April 2, 2014, *Published online:* August 18, 2014

Reprinted (adapted) with permission from

Z. Kelemen, B. Péter-Szabó, E. Székely, O. Hollóczki, D. Firaha, B. Kirchner, J. Nagy, L. Nyulászi *Chem. Eur. J.* 2014, **20**, 13002–13008

Copyright ©2014 Wiley-VCH Verlag GmbH & Co. KGaA, Weinheim.

DOI 10.1002/chem.201402912

^{*}Department of Inorganic and Analytical Chemistry, Budapest University of Technology and Economics, Szt. Gellért tér 4, 1111 Budapest, Hungary

[†]Department of Chemical and Environmental Process Engineering, Budapest University of Technology and Economics, Budafoki út 8, 1111 Budapest, Hungary

[‡]Mulliken Center for Theoretical Chemistry, Institut für Physikalische und Theoretische Chemie, Rheinische Friedrich-Wilhelms-Universität Bonn, Berlingstraße 4+6, 53115 Bonn, Germany

[§]Department of Organic Chemistry and Technology, Budapest University of Technology and Economics, Szt. Gellért tér 4, 1111 Budapest, Hungary

8. *An Abnormal NHC-CO₂ Adduct from Imidazolium Acetate Ionic Liquids*

Own manuscript contribution

- Performance of the preliminary static calculations
- Analysis of the trajectories
- Discussion of the results
- Co-writing the manuscript

Abstract In the reaction of 1-ethyl-3-methylimidazolium acetate $[\text{C}_2\text{C}_1\text{Im}][\text{OAc}]$ ionic liquid with carbon dioxide at 125° C and 10 MPa, not only the known N-heterocyclic carbene (NHC)–CO₂ adduct **I**, but also isomeric aNHC–CO₂ adducts **II** and **III** were obtained. The abnormal NHC–CO₂ adducts are stabilized by the presence of the polarizing basic acetate anion, according to static DFT calculations and ab initio molecular dynamics studies. A further possible reaction pathway is facilitated by the high basicity of the system, deprotonating the initially formed NHC–CO₂ adduct **I**, which can then be converted in the presence of the excess of CO₂ to the more stable 2-deprotonated anionic abnormal NHC–CO₂ adduct via the anionic imidazolium-2,4-dicarboxylate according to DFT calculations on model compounds. This suggests a generalizable pathway to abnormal NHC complex formation.

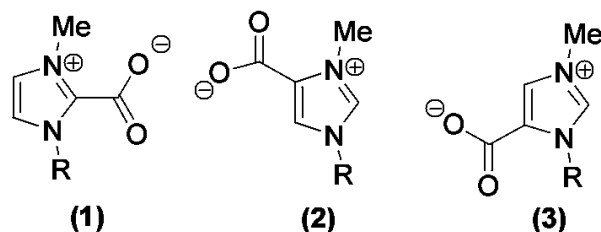
8.1 Introduction

Imidazolium acetate ionic liquids (for example, 1-ethyl-3-methylimidazolium acetate; $[\text{C}_2\text{C}_1\text{Im}][\text{OAc}]$) have unique properties, suggesting applicability for example in cellulose^[366,367] and chitin processing^[368,369] or carbon dioxide absorption.^[245,316,370–373] A key feature of this type of ionic liquids is the high basicity of the acetate anion, which is comparable to that of the N-heterocyclic carbene (NHC) derived from the imidazolium salt by the removal of the proton at the 2-position.

Accordingly, an outstanding nucleophilic acetate reactivity was observed,^[374,375] and the presence of the NHC was concluded experimentally from gas-phase MS and UPS experiments,^[238] from trapping reactions,^[68,69,338,375–377] and also from organocatalytic activity.^[337,378] Among the trapping reactions, the formation of imidazolium-2-carboxylate **1**^[68,69] is of specific importance, having an apparent role in the excellent CO₂ absorption of imidazolium acetate ionic liquids, a property^[149,306–308,378–380] that can be utilized in CO₂ sequestration.^[368,369] Apart from imidazolium-2-carboxylate (**1**), imidazolium-4- (**2**), and imidazolium-5-carboxylates (**3**), which are CO₂ adducts of abnormal carbenes (carbene carbon at the 4- or 5-position; aNHCs),^[330,336,347,381–387] are also known (Scheme 8.1); species **2** with R=Me is a natural product, norzooanemonine.^[388–390] These compounds

8. An Abnormal NHC-CO₂ Adduct from Imidazolium Acetate Ionic Liquids

were obtained by several synthetic pathways.^[391–398] A common motif in these reactions, starting either from imidazole^[393] or from an imidazolium salt,^[394] is that at higher temperatures (above 120° C), the formation of **2** and **3** was reported, suggesting that they are thermodynamically preferred over **1**.



Scheme 8.1 Imidazolium carboxylates.

This is, however, unexpected, because aNHCs are known to be less stable than NHCs,^[330,331,399–404] and likewise their adducts^[330,331,402,403,405–408] are of lower stability, provided that the N-substituents at the imidazolium ring are small.^[401] According to these results, it is reasonable to speculate that at higher temperatures, imidazolium acetate-based ionic liquids also form adducts like **2** or **3**. Interestingly, however, in a variable-temperature study (up to 150° C) of the [C₄C₁Im][OAc]-CO₂ mixture, neither **2** nor **3** was reported at atmospheric pressure,^[378] although by using an anionic dicarbene as starting material at -78° C, the exclusive formation of the aNHC adduct was observed.^[397] As the solubility and, thus, the availability of the CO₂ is also highly dependent on the pressure,^[68,69] apart from the apparent temperature effects the pressure can also be a key to trigger unusual carbene reactivity of imidazolium acetate ionic liquids. Thus, in the light of these contradicting results we decided to investigate the [C₂C₁Im][OAc] and [C₄C₁Im][OAc]-CO₂ mixtures in the 20–130° C temperature range, at pressures up to 10 MPa, to see if and how the formation of the abnormal adducts is possible from such ionic liquids. Considering the aforementioned wide variety of applications of these solvents, the knowledge acquired herein will be of high relevance, providing essential information for the corresponding organocatalytic, or technical chemical uses, and will also contribute to the better understanding of the highly important and potent supercritical CO₂-IL solvent mixtures.^[25,245,316,370–373]

8.2 Results and Discussion

First, $[\text{C}_2\text{C}_1\text{Im}][\text{OAc}]$ was reacted with CO_2 at 130°C and 0.1 MPa, analogously to Besnard and co-workers.^[308]¶ An NMR spectroscopic investigation of the reaction mixture did not reveal any other product than **I** (**1** with $\text{R}=\text{Et}$), in agreement with the previous results.^[308] Similarly, the reaction in an autoclave at 10 MPa pressure and 40°C resulted again in **I** only.

Upon carrying out the reaction at 10 MPa and 125°C , after 1.5 hour treatment, additional lines were observed in the NMR spectrum (Figure 8.1) along with from those of the starting material and the well-known 2-adduct (**I**). In the alkyl region (15-45 ppm) of the ^{13}C NMR spectra, the position of the new peaks is close to those of the $[\text{C}_2\text{C}_1\text{Im}]^+$ cation and the 2-adduct (**I**), showing that the environment of the alkyl chains has only slightly changed in the new product(s).

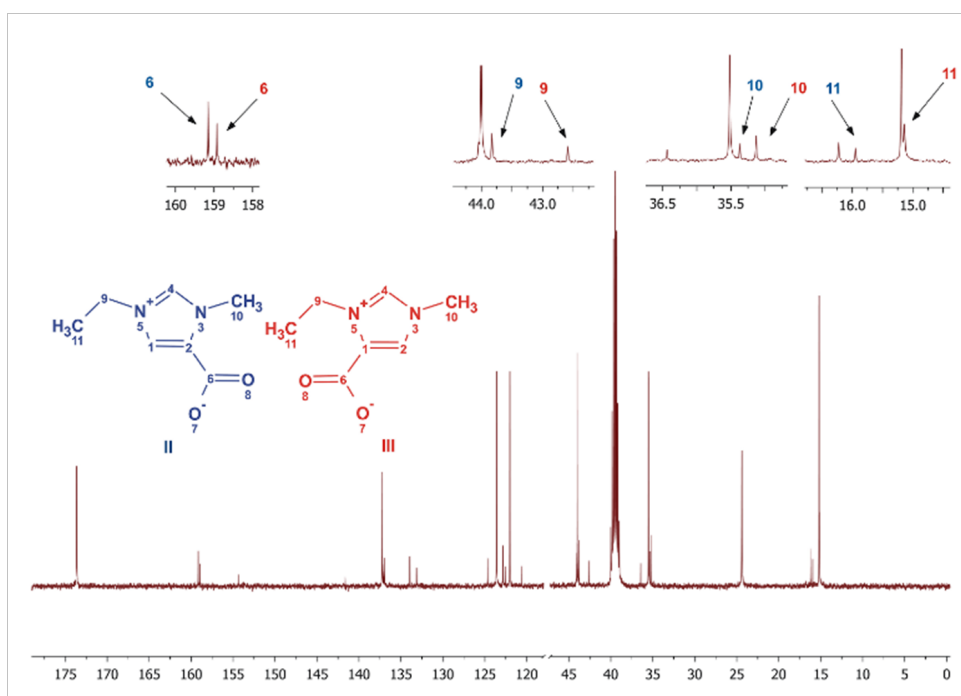


Figure 8.1. ^{13}C spectra of the reaction mixture after 1.5 h at 125°C and 10 MPa. The numbering at the peaks refers to the atom numbering presented on the chemical formulas of **II** and **III**.

New peaks also appear in the 120-165 ppm region. While some of them are close to

¶In Ref. [308], the measurement was carried out at 150°C , but our sample has shown some decomposition at that temperature

8. An Abnormal NHC-CO₂ Adduct from Imidazolium Acetate Ionic Liquids

those of the imidazolium ring carbon atoms, the new peaks at 163 ppm indicate the presence of -COO⁻ groups in the new products. New signals also appear in the 3.5-4.5 ppm (alkyl) region of the ¹H NMR spectra (see the Supporting Information^{||}), again in the close proximity of the original peaks. Further new signals appear near 7.6 and 9.4 ppm in the area of the aromatic protons. All of the new peaks can be clearly identified as aNHC-CO₂ adducts: **II** (**2** with R=Et) and **III** (**3** with R=Et), based on the earlier reported spectra^[337,378] of **2** and **3**, and the 2D NMR spectra (for HSQC, see the Supporting Information). The yields (by NMR spectroscopy) of the products are given in Table 8.1. Using [C₄C₁Im][OAc] instead of [C₂C₁Im][OAc] under identical conditions (125° C, 10 MPa CO₂, 9 h) resulted in similar products (**1**, **2**, and **3** each with R¹=Bu). However, neither NHC-CO₂ nor aNHC-CO₂ adduct formation was observed under the same conditions with [C₂C₁Im][CH₃SO₃] having a non-basic anion.

Table 8.1. Yield of the different CO₂ adducts at 125° C and 10 MPa.^[a]

Time [h]	I	II	III
1.5	18	8	7
4.5	15	10	12
8.5	13	10	13

[a] Yield [%] from NMR spectroscopy.

To further investigate the formation of **II** and **III**, the reaction was also performed at different temperatures and pressures in an autoclave. To determine the ratio of different CO₂ adducts the ¹H NMR relative intensities were used, utilizing the well-separated singlet N-methyl peaks. Although at 125° C the formation of the different adducts is fast, (sampling after 1.5 h **I**: 18 %, **II**: 8 %, **III**: 7 %) at 40° C, only **I** was observed after 7 days (31 %). Increasing the temperature to 60° C, tiny peaks (<1 %) of **II** and **III** appear in the ¹H NMR after 24 h, and the concentration of the abnormal adducts **II** and **III** remains small (ca. 1 %) even at 80° C. Interestingly, at 80° C the concentration of **I** reaches a maximum at the second day (Table 8.2), while the signal intensity of **II** and **III** increases continuously, compensating roughly for the intensity loss of **I**.

^{||}The part of the Supporting Information included in the appendix F. The complete supporting materials are available under <http://dx.doi.org/10.1002/chem.201402912>.

Table 8.2. Effect of temperature and reaction time on the formation of adducts **I-III**.^[a]

Day	40° C			60° C			80° C		
	I	II	III	I	II	III	I	II	III
1	33	0	0	22	<1	<1	29	1	1
2	33	0	0	34	<1	<1	31	2	3
3	_[b]	_[b]	_[b]	32	<1	<1	29	3	3
4	_[b]	_[b]	_[b]	32	<1	<1	25	3	4
5	33	0	0	-	-	-	-	-	-
6	26	0	0	-	-	-	-	-	-
7	31	0	0	-	-	-	-	-	-

[a] Yield [%] from NMR spectroscopy. [b] At 40° C, no samples were taken on days **3** and **4**.

A similar observation can be made at the significantly faster 125° C run (Table 8.1). The ¹H NMR spectrum of the reaction mixture from the 125° C experiment showed that during a two-month storage at ambient temperature, the amount of **I** has decreased significantly (that of **II** and **III** remained virtually unchanged), while in the sample stored at 5° C this was not observed. It would be tempting to explain these observations by the increased thermodynamical stability of **II** or **III** over **I**. However, previous computational results (adducts with small aNHCs are thermodynamically less-stable than their isomers derived from the corresponding NHCs)^[405–408] suggest that this point requires further investigation.

Our B97-D/aug-cc-pVTZ calculations on the isomeric structures revealed that **II** and **III** are less stable than **I** in the gas phase by 10.7 and 10.0 kcal mol⁻¹, respectively. Calculations at other levels, including CAS(8,10)/6-311G** (to check the appropriateness of the single reference description) provided comparable values (see the Supporting Information). While this is somewhat less than the difference between the aNHC and NHC (16.6 and 16.3 kcal mol⁻¹;^[405–408] for comparable results at other levels, see the Supporting Information), but the formation of **I** is still clearly favored. The entropy contribution is also similar for both structures (see the Supporting Information). As the calculated dipole moment of **II** (13.3 D) and of **III** (12.8 D) are larger than that of **I** (8.7 D), we

8. An Abnormal NHC-CO₂ Adduct from Imidazolium Acetate Ionic Liquids

considered the solvent effect by using the PCM approximation,** which indeed reduced somewhat the energy difference depending on the dielectric permittivity (see the Supporting Information). Considering explicit interactions with the possible solvent ions (for optimized structures and interaction energies, see the Supporting Information) reveals that the acetate ion interacting at the imidazolium hydrogen atoms via a proton bridge exhibit the largest binding energy (39.4 kcal mol⁻¹ in case of **III**). Owing to this stabilization, if coordinated by a single acetate ion (at the 2-position of the ring), **II** and **III** are more stable than **I** (coordinated at the 4-position) by 1.1 and 1.8 kcal mol⁻¹, respectively. Modeling solvation effects on the acetate adducts of carboxylates **I–III** by using the PCM model with different dielectric permittivities (see the Supporting Information) resulted in changes of less than 1 kcal mol⁻¹.

To further refine the model, we considered the presence of an additional imidazolium acetate ion pair. Optimization of clusters built from **1** or **2** with R=Me and acetic acid and one further [C₁C₁Im][OAc] ion pair revealed that the relative stability of the two clusters remains similar to that of the normal and abnormal adducts (for the optimized clusters and their relative energies, see the Supporting Information). In these clusters, however, the acetic acid which is necessarily produced during the NHC–CO₂ adduct formation is confined to remain in the vicinity of the adduct, while it was shown by ab initio dynamics calculations^[409] that in case of metal–NHC complex formation from [C₂C₁Im][OAc] it remains well-separated from the otherwise relatively free and available^[410] NHC, which is due to the strong interaction with the bulk acetate ions.^[68,69] The simple model systems described above, containing an adduct and a single acetate anion, does not necessarily account for accurately the adduct–solvent interactions within the bulk of the liquid, where many ions are surrounding the solute. Furthermore, continuum solvation models such as PCM are not accounting for the specific hydrogen bonding interactions between the solvent and the adduct, and therefore they may provide erroneous data.^[411] Accordingly, ab initio molecular dynamics simulations were performed on two periodic simulation boxes, containing either **I** or **II**, one acetic acid, and 35 ion pairs of [C₂C₁Im][OAc] (Support-

**It should be noted that the PCM models have some weakness; furthermore, as finding a suitable relative permittivity (ϵ) of the ionic liquid–CO₂ system is a great challenge, only the effect of the ϵ value was considered.

ing Information F, Figure F.1 and F.2), describing directly the liquid phase. Inspecting the solvation of the two different kinds of adducts in the ionic liquid, the differences in solvation modes and thus the possible thermodynamic driving force for the formation of **II** can be identified. Establishing the radial pair distribution functions between the corresponding atoms in the simulations (for graphs, see the Supporting Information F, Figure F.3–F.5), we found that the oxygen atoms of the nearby acetate anions are significantly closer to the position **2** hydrogen of **II** (1.918 Å), than that at position **4** hydrogen of **I** (2.016 Å). Considering that the strength of the hydrogen bond is regularly clearly indicated by the O–H distances, it is reasonable to rationalize this observation as **II** (in accordance with the DFT calculations above) is gaining extra stabilization compared to **I** by retaining the most acidic hydrogen of the imidazolium ring, which allows a stronger stabilizing interaction with the solvent. It is also worth mentioning that the cationic ring hydrogen atom–carboxylate oxygen atom radial pair distribution functions show a significantly higher peak in case of the abnormal adduct **II** than in the case of **I**, which may also contribute to the stabilization of **II**.

Apart from the relative stability of the CO₂ adduct reaction products (**I–III**), the mechanism of their formation is also of importance. In a recent study,^[239] we suggested the carbene formation to be (at least partly) induced by the presence of the CO₂ molecule, as this small neutral species creates defects in the ion network of the ionic liquids, which disrupts those ion–ion interactions that destabilize the carbene–acetic acid pair with respect to the imidazolium acetate. Accordingly, a slight increase in carbene formation has been observed by ab initio molecular dynamics simulations in a liquid model by the insertion of the CO₂ molecule.^[239] As an extreme case of this effect, it is interesting to consider a mechanism in which the abstraction of H⁺ and the addition of CO₂ occurs spontaneously. Thus, the solute gas molecule actively induces the proton transfer. While an ab initio dynamics study of this process is not feasible owing to the large model system and long simulation required, we have investigated the barrier of the reaction between carbon dioxide and a single [C₂C₁Im][OAc] ion pair with the acetate at the normal and abnormal positions as shown in Figure 8.2.

In the [C₂C₁Im][OAc] ion pair, the most preferred site of the acetate ion is at the 2-

8. An Abnormal NHC-CO₂ Adduct from Imidazolium Acetate Ionic Liquids

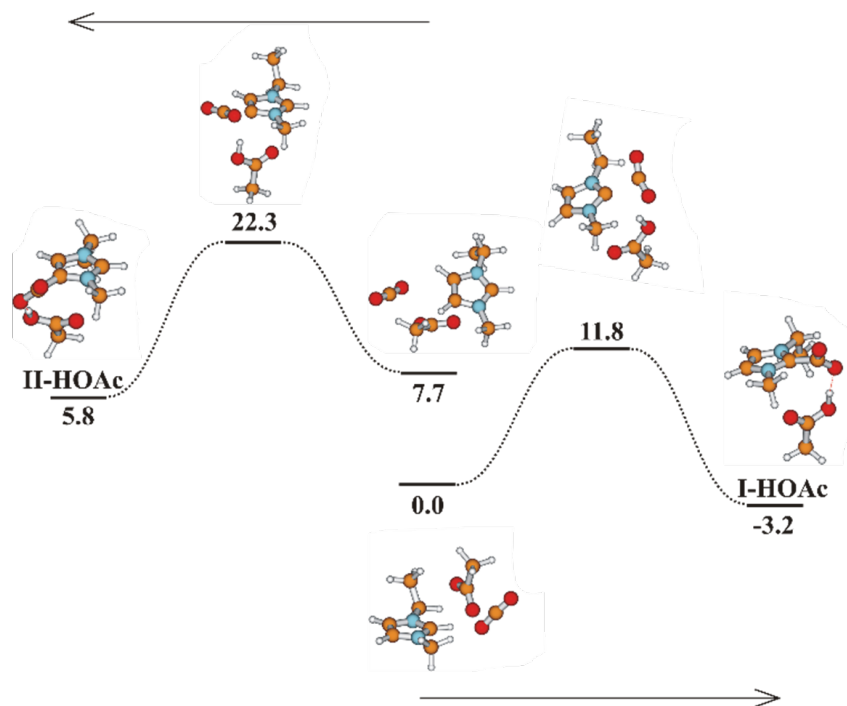


Figure 8.2. Formation of **I** and **II** from the [C₂C₁Im][OAc] ion pair and CO₂.

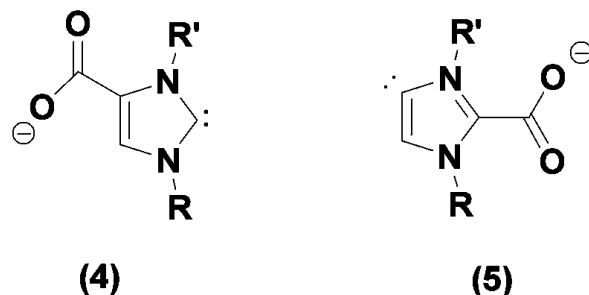
position of the imidazolium ion, the structure with the acetate ion bound at the 4- (or 5)-position is by 11.3 kcal mol⁻¹ higher in energy. The presence of a single CO₂ molecule reduces this difference to 7.7 kcal mol⁻¹ (Figure 8.2). The barriers with respect to their corresponding starting structures are nearly the same (11.8 kcal mol⁻¹ leading to **I** and 14.6 when leading to **II**) in both processes, which means that altogether the formation of the abnormal adduct requires significantly higher activation energy. In agreement, ab initio molecular dynamics simulations on the present ionic liquid showed much lower mobility for the 4- and 5-position hydrogen atoms compared to the 2-position (for the corresponding graphs, see the Supporting Information F, Figure F.6).^[339] These findings are in accordance with the observations that **I** forms at room temperature,^[68,69,149,306–308,378–380] whereas **II** (and **III**) can be obtained at higher temperatures only, although the absolute values of the reaction barrier cannot directly be related to the liquid phase reaction owing to the simplification of the model. Finally, replacement of the acetic acid in the IL by acetate because of the strong acetate–acetic acid interactions^[68,69,409,410] results in structures discussed above with the energetically preferred acetate adduct of **II** (and **III**).

The stability data discussed above indicate that the highly basic acetate counteranion,

which attracts a proton away from the imidazolium ring, has a crucial impact on the stabilization of the abnormal CO₂ adduct. The effect of the CO₂ pressure on the formation of the aNHC adducts **II** and **III** is in accordance with the importance of the above basicity considerations. At high pressure, CO₂ forms a supercritical phase, which extracts acetic acid from the IL phase, reducing the proton concentration. Indeed, a 0.15 mol dm⁻³ acetic acid concentration was observed in the scCO₂ phase from the reaction mixture by a GC analysis. Considering the volume of the scCO₂ phase (ca. 40 mL), 60 mmol acetic acid was extracted from the IL (ca. 100 mmol), reducing significantly its proton content. The importance of basicity was also shown in a separate experiment, when with a K₂CO₃ additive 0.2 equivalent to [C₂C₁Im][OAc] the CO₂ adducts **II** and **III** were already obtained at atmospheric CO₂ pressure (at 125° C). It is also noteworthy in this respect that Tommasi and Sorrentino reported carboxylation of 1,3-dialkylimidazolium chlorides with Na₂CO₃/5 MPa CO₂ through a Kolbe–Schmitt type reaction in anhydrous DMF, resulting in **1** up to 110° C but also with formation of some **2** and **3** at 135° C.^[394]

At an even higher basicity of the environment, full deprotonation of the CO₂ adducts **1–3** might take place, yielding anionic compounds **4** and **5** (Scheme 8.2). Recent DFT calculations showed that the anionic aNHC–CO₂ adduct **4** (R=R'=iPr) was more stable by 10 kcal mol⁻¹ than the isomeric anionic NHC–CO₂ adduct **5** (R=R'=iPr).^[398] This computational result served as explanation for the selective formation of the Li salt of **4** (R=R'=iPr) from the Li salt of the corresponding anionic dicarbene in a reaction with CO₂.^[398] Likewise, **IVa** (**4**, R=Et, R'=Me) and **IVb** (**4**, R=Me, R'=Et) are more stable than **Va** (**5**, R=Et, R'=Me) by 6.9 and 7.0 kcal mol⁻¹, respectively (note that the more bulky iPr substituents at the 1- and 3-positions disfavor the formation of the normal CO₂ adduct).^[412] Reacting with other electrophiles, the (Li salt of the) anionic dicarbene also exhibited similar regioselectivity, the substituents preferring the abnormal position.^[413] As NHC formation has indirectly been observed in [C₂C₁Im][OAc] owing to the presence of the basic acetate anion,^[68,69,238,338,375–377] as was discussed above, it would be tempting to consider that the basicity of the ionic liquid is also sufficient for further deprotonation of the NHC to the anionic dicarbene (at least at high temperature), which should then preferably react at the abnormal position with CO₂, as discussed above.

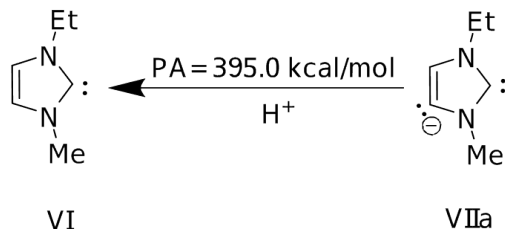
8. An Abnormal NHC-CO₂ Adduct from Imidazolium Acetate Ionic Liquids



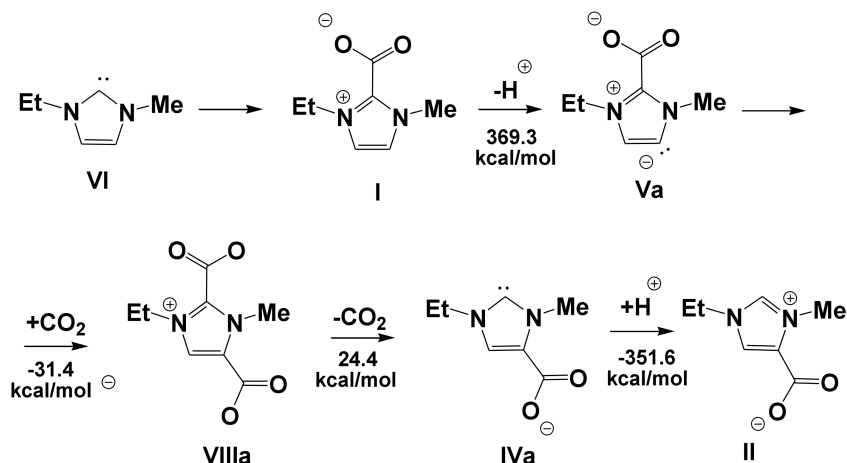
Scheme 8.2 CO₂ adducts of the anionic dicarbenes.

Further support to this surmise might come from the experimental observation of Denk and Rodezno,^[414] who observed a deuterium exchange on the 4- and 5-positions on an imidazole-2-ylidene. To investigate this possibility, we computed the deprotonation energy of NHC **VI** resulting in the anionic dicarbene **VIIa** (Scheme 8.3). However, the deprotonation energy of the NHC is by about 45 kcal mol⁻¹ higher than that of acetic acid (355.3 kcal mol⁻¹ at the same level of theory). Therefore, it is unlikely that the anionic dicarbene itself is involved in the reaction. However, the deprotonation energy of **I**, which is formed readily from [C₂C₁Im][OAc] and high-pressure carbon dioxide,^[68,69,149,306–308,378–380] is only 369.3 kcal mol⁻¹ at the 4-position (Scheme 8.4). As this value is much closer to that of the proton affinity of the acetate ion, the formation of **Va** is reasonable. It is noteworthy that Schmidt and co-workers observed a facile room temperature H/D exchange in **1** (R'=Me).^[396] The CO₂ adduct of **Va** is the anionic dicarboxylate **VIIIa**. This compound forms in a barrierless reaction (no transition structure was obtained and a monotonous stabilization was obtained by a scan), with a binding energy of 31.4 kcal mol⁻¹. The preferred (barrierless) decomposition of **VIIIa** yields **IVa**, releasing carbon dioxide from the 2-position (binding energy 24.4 kcal mol⁻¹), in accordance with the relative stabilities of **IVa** and **Va**, as was discussed above. **II** is obtainable then from **IVa** after protonation (the analogous reaction at the 5-position leading finally to **III** has similar energetics; see the Supporting Information). It is noteworthy that for the explanation of a 2,4-shift of electrophiles under highly basic conditions (in the presence of potassium hexamethyldisilazide) an analogous mechanism has been suggested.^[330] While the above results would indicate the stability of the anionic dicarboxylate **VIIIa** (and **VIIIb**), such species was not observed by Vogt et al.^[398] when they reacted (the Li salt of the) anionic dicar-

bene with CO₂. Apparently, the interaction energy of CO₂ with the (anionic) carbene is less than with Li⁺, which indicates that for a better understanding of the reaction, the presence of the counterion should also be considered.



Scheme 8.3 Proton affinity of the anionic dicarbene VIIa.



Scheme 8.4 Formation of **II** from the CO₂ adduct **I** via the anionic dicarboxylate **VIIIa**.

Calculations on the [C₂C₁Im][OAc] ion pair+2 CO₂ system indeed show a somewhat different picture (Figure 8.3). The aNHC and NHC adducts of CO₂ are about the same energy in the presence of an acetate ion and a further CO₂ molecule, in agreement with our observation that all adducts (**I–III**) could be found in the reaction mixture after a prolonged reaction time. Interestingly, the anionic dicarboxylate in the presence of the acetic acid formed is not stabilized anymore with respect to the acetate complexes. This differs from the behavior of the naked anionic system, where the dicarboxylate anion exhibited the largest stability. Furthermore, the barriers of the dicarboxylate decomposition reactions are similar in both directions, and the barrier of the entire reaction compares favorably with that of the single CO₂ addition to the ion pair (Figure 8.2), leading to the abnormal carbene adduct **II**. As the [C₂C₁Im][OAc] ion pair was used in both model sys-

8. An Abnormal NHC-CO₂ Adduct from Imidazolium Acetate Ionic Liquids

tems, it is reasonable to consider that the similarity of the calculated barriers prevails in the real IL environment as well. It is likely that our observation on the slow conversion of the initially formed **I** to **II** and **III** (at 125° C and 10 MPa CO₂ pressure) proceeds via the dicarboxylate pathway, which is certainly further favored by the large CO₂ concentration.

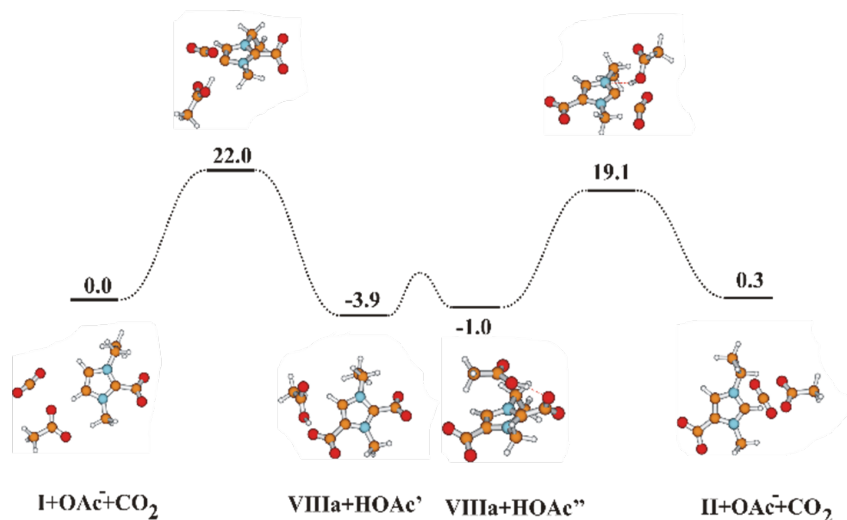


Figure 8.3. Formation of **II** from **I** via **VIIIa**.

8.3 Conclusion

Using both high pressure (10 MPa) CO₂ and high temperature (125° C) in [C₂C₁Im][OAc], not only the known NHC-CO₂ adduct **I**, but also the aNHC-CO₂ adducts **II** and **III** can be detected. A crucial point in the stabilization of the aNHC adduct is the high basicity of the acetate ion containing system, which is further corroborated either by the extraction of the acetic acid by-product into the scCO₂ phase at high CO₂ pressure or by K₂CO₃ additive at low CO₂ pressure. Static DFT calculations in model systems together with AIMD studies indeed show significant stabilizing interactions which are attributable to the basicity of the system.

The present results are generalizable for the formation of aNHC adducts, showing that such products can be obtained from imidazolium ions even without sterically shielded 2-position and anionic dicarbenes provided that sufficiently basic circumstances are applied. Further exploration of this chemistry will be reported in due course.

8.4 Experimental Section and Methods

In the reactions under pressure, freshly distilled carbon dioxide was used (>99.9 %). During the investigation of the effect of the temperature between 40–80° C, a tempered autoclave, designed for reactions in supercritical carbon dioxide,^[415] was used. The IL (ca. 15 mL) was filled in a glassware with a stir bar and it was placed into the reactor. The reaction mixture was stirred continuously. During the sampling, a 2–4 mL liquid sample was collected from the lower section of the reactor while the pressure and temperature in the reactor were kept constant. Owing to the Joule–Thomson effect during the instant pressure drop to atmospheric pressure from 10 MPa in the valve, the samples cooled rapidly (“freezing” the reaction mixture). Precipitation of solids in the cold sample was often observed. In these cases, the mixture was homogenized before the NMR sample was prepared. The experiments at 125° C were carried out in a variable volume view cell of New Ways of Analytics GmBH, also known as Pickel’s cell. The IL (ca. 30 mL) was transferred into the cell, which was then pressurized with CO₂ followed by heating to 125° C. The mixture was continuously stirred by a magnetically coupled immersed stirrer. Besides effective temperature control, the pressure of the reaction mixture was kept constant by decreasing the volume of the cell with the movable piston while ca. 0.5–1 mL samples were collected.

All of the static calculations were carried out with the Gaussian 09 program package^[351] using the B3LYP, B97D, or M06-2X DFT functionals with the conjunction of 6-31+G*, 6-311+G**, aug-cc-pVTZ basis sets. Full geometry optimization was performed, and harmonic vibrational frequencies were calculated at the same level to establish the nature of the stationary points obtained, as characterized by none or a single negative eigenvalue of the Hessian for minima and transition structures, respectively.

Ab initio molecular dynamics on the simulation boxes (for the detailed parameters and a snapshot of each boxes, see the Supporting Information F) with periodic boundary conditions simulations were carried out by using the CP2K program package,^[187] with the BLYP-D3 functional (containing Grimme’s dispersion correction D3),^[171] and the molecularly optimized double- ζ basis set (MOLOPT-DZVP-SR-GTH)^[261] and Goedecker-

8. An Abnormal NHC-CO₂ Adduct from Imidazolium Acetate Ionic Liquids

Teter-Hutter pseudopotentials.^[262–264] The simulations were carried out with a timestep of 0.5 fs in an microcanonical (*NVT*) ensemble, where the N ose–Hoover thermostats were set to 350 K.

8.5 Acknowledgments

Financial support from OTKA K 105417 and COST CM1206 EXIL as well as a scholarship for O.H. from the Alexander von Humboldt Foundation is gratefully acknowledged. E.S. is grateful for a Bolyai fellowship.

Part IV.

Summary and Conclusion

In this thesis, the absorption of two gases, carbon dioxide (CO₂) and sulfur dioxide (SO₂), has been studied in ionic liquids (ILs). Using ab initio molecular dynamics (AIMD) simulations and static quantum chemical (QC) calculations in the gas-phase or with the continuum solvation model allows to study possible solvation mechanisms, specific interactions, and chemical reactions or, at least, their indications. Combining the results of static QC calculations with the results of statistical thermodynamics and predictive thermodynamic models allows for the estimation of the reaction Gibbs free energies and barriers. These quantities are often more representable and comparable with the experimental data than the widely used interaction energies from static QC calculations in the gas-phase.

The generalized molecular level of gas absorption by ionic liquids consists of physical and chemical absorption. The physical absorption of gas takes place before the chemical absorption occurs. The specific interactions between the solute molecule and ions as well as the size of the voids in ionic liquids are the key factors affecting the physisorption of gases in ILs.

The interactions of CO₂ and SO₂ with cations and anions play an important role in the solvation of both gases. Often, the anion forms a single but strong interaction with CO₂ and SO₂ molecules. At the same time, several cations have been found in the solvation shell of these gases. These cations form weak dispersion interactions with gas molecules. As a result, both anion–solute and cations–solute interactions are comparable in strength. Therefore, the presence of groups donating weak interactions like an aromatic π -system and alkyl chains are highly important to control gas physisorption.

The controlling of the voids size in ILs is another crucial issue to improve gas physisorption in ionic liquids. These voids are too small for direct incorporation of the gas molecules. Thus, an energy loss is caused by the gas molecules entering into ILs via small voids. The ability of the anion and cations to form specific interactions with solute molecules compensates this energy loss to some extent defining physical absorption of the gas in ILs.

Apart from physical absorption, chemical absorption can be performed in different ways. The generalized explanation for the occurrence of the chemical absorption is the ability

8. Final Summary and Conclusions

of gas molecules incorporates into the extended cation-anion network of ionic liquids. This behavior has been found for SO₂ absorption in one of the studied ionic liquids. Remarkably, the suggested concept can be further extended to explain the high solubility of other gases such as hydrogen sulfide H₂S, ammonia NH₃, and CO₂. Three cases allowing such incorporation of CO₂ in the structure of ILs have been considered in detail in this thesis. There are reactions with basic anions, with amine groups, and carbenes.

In the first case, the basicity of the anion of ILs plays a major role. To reveal whether an anion is basic enough to react with CO₂, it is sufficient to optimize the anion-CO₂ complex with a continuum solvation model as opposed to the widely applied optimization in the gas-phase. From the geometry of the anion-CO₂ complex, chemical absorption is very probable for the structures exhibiting O-C-O-angles smaller than 140°. The possible candidates among the anions to design the IL for the reversible chemical absorption possess calculated reaction Gibbs free energies between -30 and 16 kJ mol⁻¹. Several examples of potential candidates which can be tested experimentally have been suggested.

In the second case, amine groups in the ILs cause the complex absorption mechanism of CO₂. This mechanism, studied in the amino acid ionic liquids (AAILs), includes the formation of the (amino acid anion)-CO₂ adduct. Then, a proton abstraction takes place by the amino or the carboxylate groups present in the ionic liquid. Finally, the sequence of the proton transfers between this intermediate and the amino acid anion leads to the formation of the equilibrium mixture consisting of the carbamate, the amino acid in neutral or zwitterion form, and the carbamic acid. Controlling the rate of the CO₂ absorption in AAILs is possible via the barrier of the formation of the (amino acid anion)-CO₂ adduct. This barrier increases with the side chain elongation, the introduction of the aromatic π -system, and the perfluorination of the AAIL. Also, amino acid anions form a reactivity sequence, which remains the same for different cations. The overall CO₂ capacity in AAILs can be controlled via the aromatic π -systems, long alkyl chains, fluorinated substituent or hydroxy groups. The presence of the substitutes mentioned above in the structure of AAILs shifts the equilibrium towards the reactants, decreasing the overall CO₂ capacity. Higher absorption capacities of some glycinate AAILs can be achieved via the introduction of large nonpolar/fluorinated groups. Finally, controlling

the equilibrium between intra- and intermolecular hydrogen bonding in the carbamic acid allows for the preventing the viscosity increase in AAILs necessary for the efficient utilization.

In the third case, N-heterocyclic carbenes, available in some ionic liquids, react with CO₂ providing the chemical absorption. The molecular level of carbene formation and the subsequent reactions leading to the formation of the normal and abnormal adduct have been studied at the example of the 1-ethyl-3-methylimidazolium acetate. The conclusion drawn from the gas-phase calculations and simulations suggest that the presence of CO₂ suppresses the formation of the carbenes (1,3-dialkylimidazolium-2-ylidenes) required for the absorption of CO₂. On the contrary, the bulk simulations have explained the formation and stabilization of carbenes. These processes are governed by an inverse ionic liquid effect, which facilitates the stabilization of neutral species such as carbenes by ionic liquids at the presence of other neutral solutes such as CO₂. Subsequently, the stabilized carbenes react with physisorbed CO₂ forming the normal carbene-CO₂ adduct (1,3-dialkylimidazolium-2-carboxylate). The formation of the abnormal carbene-CO₂ adduct [1,3-dialkylimidazolium-4 (or 5)-carboxylate] does not follow a similar mechanism as the formation of the normal adduct. The reason for that is a significantly higher barrier to the formation of the abnormal carbenes [1,3-dialkylimidazolium-4 (or 5)-ylidenes]. Thus, the most probable mechanism for the formation of the abnormal adduct corresponds to the isomerization of the normal adduct. The bulk simulations have revealed an increase of rear protons mobility contrary to the initial imidazolium cation. Therefore, the formation of the anionic dicarboxylate intermediate (1,3-dialkylimidazolium-2,4-dicarboxylate) after the proton abstraction is the most probable mechanism, which links the abnormal and normal carbene-CO₂ adducts.

Considering the SO₂ absorption in ionic liquids, a theoretical explanation of the high absorption capacity of SO₂ in ionic liquids has been found. The driving mechanism is the incorporation of SO₂ molecules in the cation-anion network. Such incorporation was coined as a linker effect since SO₂, opposite to CO₂, can interact strongly with both the cation and the anion at the same time. The solvation of SO₂ in the 1-ethyl-3-methylimidazolium thiocyanate IL leads to the formation of a network of H(cation)···O(SO₂)-S(SO₂)···S(anion),

8. *Final Summary and Conclusions*

where SO_2 plays the role of a linker molecule. Thus, a good solubility of the SO_2 in the IL should be observed providing the right combination of the cation and the anion where SO_2 can form hydrogen bonds with the cation and a stable bond with the anion.

To summarize, the results presented in this thesis show that the design of ionic liquids for gas absorption can be better understood and significantly improved with the help of computational methods. A molecular-level knowledge of gas absorption in ionic liquids hardly accessible from the experiment can be revealed from the computational methods which explicitly treat the electronic structure. The combination of ab initio molecular dynamics simulations and static quantum chemical calculations provide a robust tool for understanding the complex processes in bulk and gas phases. The static quantum chemical calculations can be significantly improved via including the continuum solvation model and also via combining their results with the results of statistical thermodynamics calculations and predictive thermodynamic models to study the processes in the bulk phase. Employing these approaches helps scientists to establish and generalize gas behavior in ionic liquids. This behavior can be further extended to unstudied ionic liquids as well as for other gases. The comprehension of the proposed mechanisms of physi- and chemisorption of gases in ionic liquids can further help in the knowledge-based design and the large-scale modeling.

Part V.

Appendix

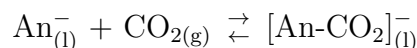
A Supporting Information to Chapter 3

Appendix A contains:

- Computational details
- Structures, names and abbreviations of anions*

Computational Details

Gas-phase and solvated geometries as well as corresponding frequencies were obtained from the density functional theory (DFT) with the ORCA^[294] program (version 3.0.0^[295]). The geometry optimization and frequencies calculations were performed on B3LYP-D3(BJ)/def2-TZVPP level of theory^[168] for the gas-phase geometries. The effect of the solvent on the geometries (solvated geometries) and frequencies was taken into account by conductor-like screening model (COSMO). The dielectric permittivity of media was set $\epsilon=15$, whereas the solvent radius was kept as defaults. Thus, two sets of geometries and frequencies for the CO₂ molecule, an anion and an anion-CO₂ complex were used to calculate the corrections ($\Delta_r G_{\text{RRHO}}^T$ and $\Delta_r \delta G_{\text{solv by [Cat][An]}}^T$) to the pure electronic energy ($\Delta_r E$), in order to obtain the reaction Gibbs free energy ($\Delta_r G$)^[147] for the following reaction:



$$\Delta_r G = \Delta_r E + \Delta_r G_{\text{RRHO}}^T + \Delta_r \delta G_{\text{solv by ([Cat][An])}}^T \quad (\text{A.1})$$

where $\Delta_r G_{\text{RRHO}}^T$ is the change in the sum of corrections between the reactants and product from pure electronic contribution to Gibbs free energy. The sum was calculated

*The corresponding geometries of the anions and the anion-CO₂ complexes are available under <http://dx.doi.org/10.1002/anie.201502296>

A. Supporting Information to Chapter 3

in the rigid-rotor-harmonic-oscillator approximation (RRHO) also including zero-point-vibrational energy for each species.

$$\Delta_r G_{\text{RRHO}}^T = G_{\text{RRHO}}^T([\text{An-CO}_2]^-) - G_{\text{RRHO}}^T([\text{An}]^-) - G_{\text{RRHO}}^T(\text{CO}_2) \quad (\text{A.2})$$

$\Delta_r \delta G_{\text{solv by [Cat][An]}}^T$ is the corresponding change of Gibbs free solvation between the substrate (An^-) and the product ($[\text{An-CO}_2]^-$) in a solvent $[\text{Cat}][\text{An}]$. This correction for each species was calculated from the COSMO-RS continuum solvent model^[183,192,237,416] on the gas-phase and solvated geometries. The solvent $[\text{Cat}][\text{An}]$ was modeled as the 1 by 1 mixture of the cation $[\text{Cat}]^+$ with the anion $[\text{An}]^-$. The data reported here was calculated for the $[\text{P}_{6,6,6,14}][\text{An}]$ solvent for any given anion $[\text{An}]^-$. In principle, the arbitrary cation can be used to calculate this correction.

$$\Delta_r \delta G_{\text{solv by [Cat][An]}}^T = \delta G_{\text{solv by [Cat][An]}}^T([\text{An-CO}_2]^-) - \delta G_{\text{solv by [Cat][An]}}^T([\text{An}]^-) \quad (\text{A.3})$$

$\Delta_r E$ is the change in the total energies between the reactants and product. These energies were calculated on recently proposed the DLPNO-CCSD(T) method,^[157] which can consider as an accurate and affordable alternative to the CCSD(T) method. To obtain reliable data for a basis set incompleteness error (BSIE) has to be taken into account. Thus, two single point calculations on DLPNO-CCSD(T) level with def2-TZVPP and def2-QZVPP^[417,418] basis sets were done. The subsequent two points energy extrapolation to complete basis set (CBS) was performed separately for Hartree—Fock (HF) and correlation parts in according to Ref. [419]. For all calculations the default DLPNO-CCSD(T) parameters were used except of T_{CutPairs} which was set to 10^{-5} Hartree.^[420]

$$\Delta_r E = E([\text{An-CO}_2]^-) - E([\text{An}]^-) - E(\text{CO}_2) \quad (\text{A.4})$$

As one can see from Table A.1 there is no correlation between the absorption capacity and reaction enthalpies. However, if the two additional corrections are taken into account

Table A.1. Computed reaction enthalpies, entropies, and Gibbs free solvation energies at 298.15 K, as well as computed and derived^a Gibbs free energies for the reaction (3.1) of the anions from Ref. [67]. The values without brackets are the results for the gas-phase geometries whereas within brackets are solvated geometries. Abbreviations of different anions are listed below.

Anion	$\Delta_r H/$ (kJ mol ⁻¹)	$\Delta_r S \cdot T/$ (kJ mol ⁻¹)	$\Delta_r \delta G_{\text{solv}}/$ (kJ mol ⁻¹)	$\Delta_r G_{\text{calc}}/$ (kJ mol ⁻¹)	$\Delta_r G_{\text{exp}}/$ (kJ mol ⁻¹) ^[a]	CO ₂ abs. cap. ^[b]
[Inda] ⁻	-63 (-59)	-44 (-44)	-2 (-11)	-21 (-26)	-16	0.92
[BnIm] ⁻	-67 (-67)	-43 (-42)	5 (1)	-20 (-23)	-13	0.91
[6-Br-BnIm] ⁻	-57 (-55)	-44 (-45)	2 (-1)	-10 (-11)	-9	0.90
[2-CN-Pyr] ⁻	-47 (-44)	-45 (-45)	-3 (-9)	-5 (-7)	-6	0.88
[3-CF ₃ -Prz] ⁻	-52 (-50)	-47 (-45)	2 (-4)	-3 (-9)	-6	0.87
[124-Tri] ⁻	-60 (-58)	-43 (-43)	11 (6)	-6 (-9)	-4	0.76
[2-SCH ₃ -BnIm] ⁻	-48 (-45)	-49 (-50)	-1 (-4)	1 (1)	-3	0.72
[3-Me-5-CF ₃ -Prz] ⁻	-49 (-49)	-47 (-55)	2 (-4)	0 (3)	-2	0.63
[123-Tri] ⁻	-53 (-52)	-42 (-42)	14 (9)	3 (-1)	2	0.25

[a] The experimental equilibrium constants from Ref. [67] were used to calculate $\Delta_r G_{\text{exp}}$ at 293 K. [b] The absorption capacity in mol CO₂ per mol IL. The data was interpolated to pressure of 0.9 bar from two nearest experimental points Ref. [67] and [61].

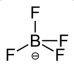

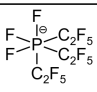
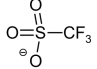
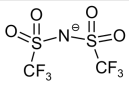
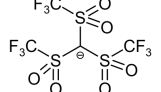
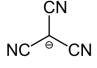
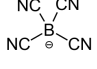
($\Delta_r S \cdot T$ and $\Delta_r \delta G_{\text{solv}}$) the resulting $\Delta_r G_{\text{calc}}$ not only agrees with the experimental sequence, but also close to experimental results. The agreement of the gas-phase $\Delta_r G_{\text{calc}}$ with experiment is better since the COSMO-RS method was originally parameterized on gas-phase geometries. We used the results for solvated geometries since they are better in the description of the experimentally observed results as one can see from the Table A.2.

Table A.2. O–C–O angles and reaction Gibbs free energies ($\Delta_r G_{\text{calc}}$) on the gas-phase and solvated geometries and the experimental CO₂ absorption capacity in corresponding trihexyltetradecylphosphonium IL.^a Abbreviations of different anions are listed provided below.

Anion	O–C–O	$\Delta_r G_{\text{calc}}/$	O–C–O	$\Delta_r G_{\text{calc}}$	CO ₂
	angle	(kJ mol ⁻¹)	angle	(kJ mol ⁻¹)	abs. cap. ^[a]
	gas-phase geometries		solvated geometries		
[3-NMe ₂ -PhO] ⁻	138	-21	132	-3	0.94
[4-MeO-PhO] ⁻	137	-25	132	-14	0.92
[4-Me-PhO] ⁻	138	-4	132	-9	0.91
[PhO] ⁻	138	-2	132	-7	0.85
[4-Cl-PhO] ⁻	140	5	132	0	0.82
[3-Cl-PhO] ⁻	141	13	132	12	0.72
[2-Cl-PhO] ⁻	164	24	132	11	0.67
[4-CF ₃ -PhO] ⁻	166	10	133	16	0.61
[2,4-Cl-PhO] ⁻	167	22	133	19	0.48
[4-NO ₂ -PhO] ⁻	171	20	134	32	0.30
[2,4,6-Cl-PhO] ⁻	171	3	134	39	0.07

[a] The absorption capacity in mol CO₂ per mol IL. The data was taken from Ref. [66]. For the [P₆₆₆₁₄][4-NO₂-PhO] ionic liquid the CO₂ capacity was determined at 20° C, whereas for the remaining ILs it was determined at 30° C.

Table A.3. Structures, names and abbreviations of anions.

Structure	Name	Abbreviation
F^{\ominus}	fluoride	$[F]^{-}$
Cl^{\ominus}	chloride	$[Cl]^{-}$
Br^{\ominus}	bromide	$[Br]^{-}$
I^{\ominus}	iodide	$[I]^{-}$
	tetrafluoroborate	$[BF_4]^{-}$
	hexafluorophosphate	$[PF_6]^{-}$
	tris(pentafluoroethyl)trifluorophosphate	$[PF_3(C_2F_5)_3]^{-}$
	trifluoromethanesulfonate	$[OTf]^{-}$
	bis(trifluoromethylsulfonyl)imide	$[NTf_2]^{-}$
	tris(trifluoromethylsulfonyl)methide	$[CTf_3]^{-}$
$N \equiv C^{\ominus}$	cyanide	$[CN]^{-}$
$^{\ominus}N=N=N^{\ominus}$	azide	$[N_3]^{-}$
$N \equiv O^{\ominus}$	cyanate	$[OCN]^{-}$
$N \equiv S^{\ominus}$	thiocyanate	$[SCN]^{-}$
$NC-N^{\ominus}CN$	dicyanamide	$[N(CN)_2]^{-}$
	tricyanomethide	$[C(CN)_3]^{-}$
	tetracyanoborate	$[B(CN)_4]^{-}$

Continued on next page

Table A.3 – continued from previous page

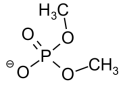
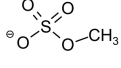
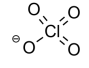
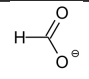
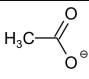
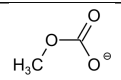
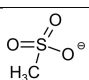
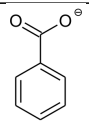
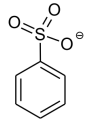
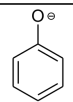
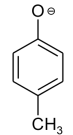
Structure	Name	Abbreviation
	dimethylphosphate	[Me ₂ PO ₄] ⁻
	methylsulfate	[MeSO ₄] ⁻
	perchlorate	[ClO ₄] ⁻
HO [⊖]	hydroxyde	[OH] ⁻
H ₃ C-O [⊖]	methoxide	[MeO] ⁻
	formate	[HCOO] ⁻
	acetate	[MeCOO] ⁻
	methylcarbonate	[MeCO ₃] ⁻
	methanesulfonate	[MeSO ₃] ⁻
	benzoate	[PhCOO] ⁻
	benzenesulfonate	[PhSO ₃] ⁻
	phenolate	[PhO] ⁻
	4-methylphenolate	[4-Me-PhO] ⁻
Continued on next page		

Table A.3 – continued from previous page

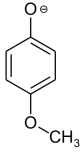
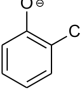
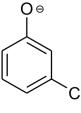
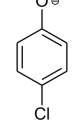
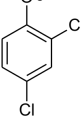
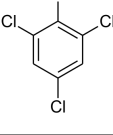
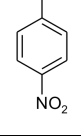
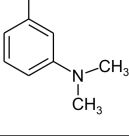
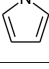
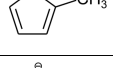
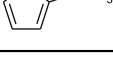
Structure	Name	Abbreviation
	4-methoxyphenolate	[4-MeO-PhO] ⁻
	2-chlorophenolate	[2-Cl-PhO] ⁻
	3-chlorophenolate	[3-Cl-PhO] ⁻
	4-chlorophenolate	[4-Cl-PhO] ⁻
	2,4-dichlorophenolate	[2,4-Cl-PhO] ⁻
	2,4,6-trichlorophenolate	[2,4,6-Cl-PhO] ⁻
	4-nitrophenolate	[4-NO ₂ -PhO] ⁻
	3-(dimethylamino)phenolate	[3-NMe ₂ -PhO] ⁻
	pyrrolide	[Pyr] ⁻
	2-methylpyrrolide	[2-Me-Pyr] ⁻
	2-methoxypyrrolide	[2-MeO-Pyr] ⁻
Continued on next page		

Table A.3 – continued from previous page

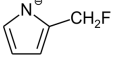
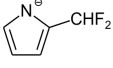
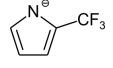
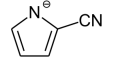
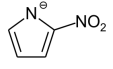
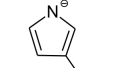
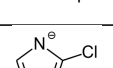
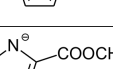
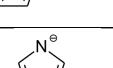
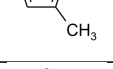
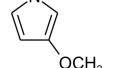
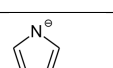
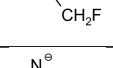
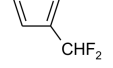
Structure	Name	Abbreviation
	2-(fluoromethyl)pyrrolide	[2-CH ₂ F-Pyr] ⁻
	2-(difluoromethyl)pyrrolide	[2-CHF ₂ -Pyr] ⁻
	2-(trifluoromethyl)pyrrolide	[2-CF ₃ -Pyr] ⁻
	2-cyanopyrrolide	[2-CN-Pyr] ⁻
	2-nitropyrrolide	[2-NO ₂ -Pyr] ⁻
	2-fluoropyrrolide	[2-F-Pyr] ⁻
	2-chloropyrrolide	[2-Cl-Pyr] ⁻
	2-(methoxycarbonyl)pyrrolide	[2-COOCH ₃ -Pyr] ⁻
	3-methylpyrrolide	[3-Me-Pyr] ⁻
	3-methoxypyrrrolide	[3-MeO-Pyr] ⁻
	3-(fluoromethyl)pyrrolide	[3-CH ₂ F-Pyr] ⁻
	3-(difluoromethyl)pyrrolide	[3-CHF ₂ -Pyr] ⁻
	3-(trifluoromethyl)pyrrolide	[3-CF ₃ -Pyr] ⁻
	3-cyanopyrrolide	[3-CN-Pyr] ⁻
Continued on next page		

Table A.3 – continued from previous page

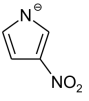
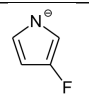
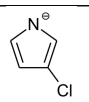
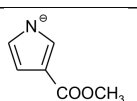
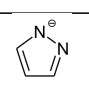
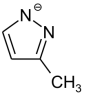
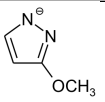
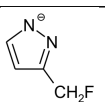
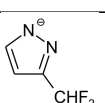
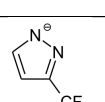
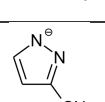
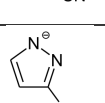
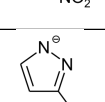
Structure	Name	Abbreviation
	3-nitropyrrolide	[3-NO ₂ -Pyr] ⁻
	3-fluoropyrrolide	[3-F-Pyr] ⁻
	3-chloropyrrolide	[3-Cl-Pyr] ⁻
	3-(methoxycarbonyl)pyrrolide	[3-COOCH ₃ -Pyr] ⁻
	pyrazolide	[Prz] ⁻
	3-methylpyrazolide	[3-Me-Prz] ⁻
	3-methoxypyrazolide	[3-MeO-Prz] ⁻
	3-(fluoromethyl)pyrazolide	[3-CH ₂ F-Prz] ⁻
	3-(difluoromethyl)pyrazolide	[3-CHF ₂ -Prz] ⁻
	3-(trifluoromethyl)pyrazolide	[3-CF ₃ -Prz] ⁻
	3-cyanopyrazolide	[3-CN-Prz] ⁻
	3-nitropyrazolide	[3-NO ₂ -Prz] ⁻
	3-fluoropyrazolide	[3-F-Prz] ⁻
Continued on next page		

Table A.3 – continued from previous page

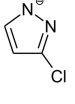







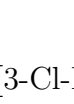
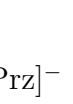

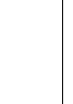

Structure	Name	Abbreviation
	3-chloropyrazolide	[3-Cl-Prz] ⁻
	3-(methoxycarbonyl)pyrazolide	[3-COOCH ₃ -Prz] ⁻
	4-methylpyrazolide	[4-Me-Prz] ⁻
	4-methoxypyrazolide	[4-MeO-Prz] ⁻
	4-(fluoromethyl)pyrazolide	[4-CH ₂ F-Prz] ⁻
	4-(difluoromethyl)pyrazolide	[4-CHF ₂ -Prz] ⁻
	4-(trifluoromethyl)pyrazolide	[4-CF ₃ -Prz] ⁻
	4-cyanopyrazolide	[4-CN-Prz] ⁻
	4-nitropyrazolide	[4-NO ₂ -Prz] ⁻
	4-fluoropyrazolide	[4-F-Prz] ⁻
	4-chloropyrazolide	[4-Cl-Prz] ⁻
	4-(methoxycarbonyl)pyrazolide	[4-COOCH ₃ -Prz] ⁻
	imidazolide	[Im] ⁻
Continued on next page		

Table A.3 – continued from previous page

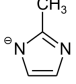
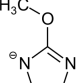
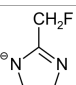
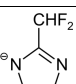
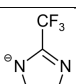
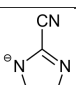
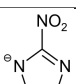
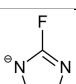
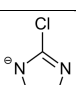
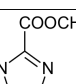
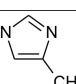
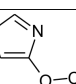
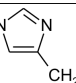
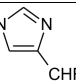
Structure	Name	Abbreviation
	2-methylimidazolidine	[2-Me-Im] ⁻
	2-methoxyimidazolidine	[2-MeO-Im] ⁻
	2-(fluoromethyl)imidazolidine	[2-CH ₂ F-Im] ⁻
	2-(difluoromethyl)imidazolidine	[2-CHF ₂ -Im] ⁻
	2-(trifluoromethyl)imidazolidine	[2-CF ₃ -Im] ⁻
	2-cyanoimidazolidine	[2-CN-Im] ⁻
	2-nitroimidazolidine	[2-NO ₂ -Im] ⁻
	2-fluoroimidazolidine	[2-F-Im] ⁻
	2-chloroimidazolidine	[2-Cl-Im] ⁻
	2-(methoxycarbonyl)imidazolidine	[2-COOCH ₃ -Im] ⁻
	4-methylimidazolidine	[4-Me-Im] ⁻
	4-methoxyimidazolidine	[4-MeO-Im] ⁻
	4-(fluoromethyl)imidazolidine	[4-CH ₂ F-Im] ⁻
	4-(difluoromethyl)imidazolidine	[4-CHF ₂ -Im] ⁻
Continued on next page		

Table A.3 – continued from previous page

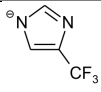
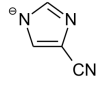
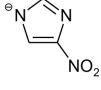
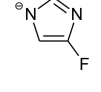
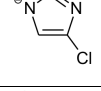
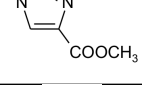
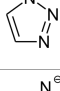
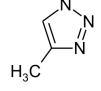
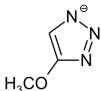
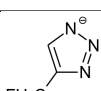
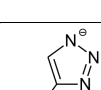
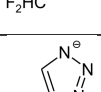
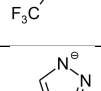
Structure	Name	Abbreviation
	4-(trifluoromethyl)imidazolid	[4-CF ₃ -Im] ⁻
	4-cyanoimidazolid	[4-CN-Im] ⁻
	4-nitroimidazolid	[4-NO ₂ -Im] ⁻
	4-fluoroimidazolid	[4-F-Im] ⁻
	4-chloroimidazolid	[4-Cl-Im] ⁻
	4-(methoxycarbonyl)imidazolid	[4-COOCH ₃ -Im] ⁻
	1,2,3-triazolid	[123-Tri] ⁻
	4-methyl-1,2,3-triazolid	[4-Me-123-Tri] ⁻
	4-methoxy-1,2,3-triazolid	[4-MeO-123-Tri] ⁻
	4-(fluoromethyl)-1,2,3-triazolid	[4-CH ₂ F-123-Tri] ⁻
	4-(difluoromethyl)-1,2,3-triazolid	[4-CHF ₂ -123-Tri] ⁻
	4-(trifluoromethyl)-1,2,3-triazolid	[4-CF ₃ -123-Tri] ⁻
	4-cyano-1,2,3-triazolid	[4-CN-123-Tri] ⁻
Continued on next page		

Table A.3 – continued from previous page

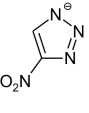
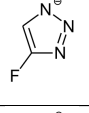
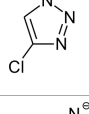
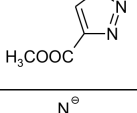
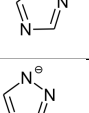
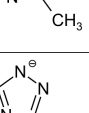
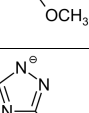
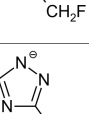
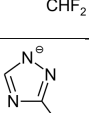
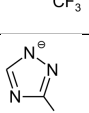
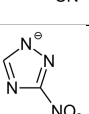
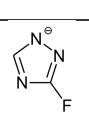

Structure	Name	Abbreviation
	4-nitro-1,2,3-triazolide	[4-NO ₂ -123-Tri] ⁻
	4-fluoro-1,2,3-triazolide	[4-F-123-Tri] ⁻
	4-chloro-1,2,3-triazolide	[4-Cl-123-Tri] ⁻
	4-(methoxycarbonyl)-1,2,3-triazolide	[4-COOCH ₃ -123-Tri] ⁻
	1,2,4-triazolide	[124-Tri] ⁻
	3-methyl-1,2,4-triazolide	[3-Me-124-Tri] ⁻
	3-methoxy-1,2,4-triazolide	[3-MeO-124-Tri] ⁻
	3-(fluoromethyl)-1,2,4-triazolide	[3-CH ₂ F-124-Tri] ⁻
	3-(difluoromethyl)-1,2,4-triazolide	[3-CHF ₂ -124-Tri] ⁻
	3-(trifluoromethyl)-1,2,4-triazolide	[3-CF ₃ -124-Tri] ⁻
	3-cyano-1,2,4-triazolide	[3-CN-124-Tri] ⁻
	3-nitro-1,2,4-triazolide	[3-NO ₂ -124-Tri] ⁻
	3-fluoro-1,2,4-triazolide	[3-F-124-Tri] ⁻
Continued on next page		

Table A.3 – continued from previous page

Structure	Name	Abbreviation
	3-chloro-1,2,4-triazolide	[3-Cl-124-Tri] ⁻
	3-(methoxycarbonyl)-1,2,4-triazolide	[3-COOCH ₃ -124-Tri] ⁻
	tetrazolide	[Ttz] ⁻
	5-methyltetrazolide	[5-Me-Ttz] ⁻
	5-methoxytetrazolide	[5-MeO-Ttz] ⁻
	5-(fluoromethyl)tetrazolide	[5-CH ₂ F-Ttz] ⁻
	5-(difluoromethyl)tetrazolide	[5-CHF ₂ -Ttz] ⁻
	5-(trifluoromethyl)tetrazolide	[5-CF ₃ -Ttz] ⁻
	5-cyanotetrazolide	[5-CN-Ttz] ⁻
	5-nitrotetrazolide	[5-NO ₂ -Ttz] ⁻
	5-fluorotetrazolide	[5-F-Ttz] ⁻
	5-chlorotetrazolide	[5-Cl-Ttz] ⁻
	5-(methoxycarbonyl)tetrazolide	[5-COOCH ₃ -Ttz] ⁻

B Supporting Information to Chapter 4

Appendix B contains:

- Computational details
- Calculated Gibbs free energies
- Time development of selected distances

Computational details*

AIMD simulations. All the ab initio molecular dynamics simulations were carried out with the CP2K^[187] program package, using the QUICKSTEP method.^[188] Such an approach utilizes hybrid Gaussian and plane waves (GPW) basis sets to calculate the energies and forces on atoms. Whereas the Gaussian basis set is used to represent a wave function and Kohn–Sham matrix in a compact way, the plane wave basis is more appropriate for the electron density matrix in the periodic systems. Both matrices become sparse with the increasing the size of the system. Thus, linear-scaling is readily achieved for the evaluation Kohn–Sham kinetic energy and matrix using the screening techniques. Subsequent Fast Fourier Transforms from Gaussian to plane wave basis set save the time to calculate Hartree (or Coulomb) energy.

We utilized standalone BLYP functional^[163,164] with the empirical dispersion correction from Grimme (BLYP-D3-0).^[171] The molecularly optimized double- ζ basis set (MOLOPT-DZVP-SR-GTH)^[261] with corresponding Goedecker–Teter–Hutter pseudopotentials for core electrons^[262–264] was applied for all atoms. A 280 Ry density CUTOFF criterion for the finest grid level for the DFT calculations was used together with multigrid number 5 (NGRID 5 and REL_CUTOFF 30) and with the smoothing for the electron density (NN10_SMOOTH) and its derivative (NN10).^[188]

*The geometries and trajectories we obtained are available from the author upon request.

B. Supporting Information to Chapter 4

A pre-equilibration was performed for the 32 ion pairs employing classical molecular dynamics within periodic boundary conditions, using the LAMMPS program package and the OPLS-AA force field. 1 ns of physical time was simulated, the simulation temperature was set to 350 K. The box size was adjusted to the experimental density extrapolated from Ref. [421], i.e., the length of the cubic box was set to 2062.39 pm for pure $[\text{C}_2\text{C}_1\text{Im}][\text{Gly}]$, **IL** system. The last snapshot of the trajectory was used in further simulations, as well as to prepare the starting geometry for the simulation of ionic liquid CO_2 mixture as follow. Four CO_2 molecules were randomly inserted in the existing structure, **IL+CO₂** system. The box length was adjusted to 2082.61 pm assuming an ideal mixing between solute and solvent. A molar volume of liquid CO_2 was taken at 350 K and 1000 bar from Thermophysical Properties of Fluid Systems on the <http://webbook.nist.gov/chemistry/fluid/>. Since the distinct formation of a glycine zwitterion and carbamate or N-carboxylglycine dianion was found to be more thermodynamically stable, the system of 32 $[\text{C}_2\text{C}_1\text{Im}]^+$ cations 24 glycinate anions, four glycine zwitterions and N-carboxylglycine dianion, **IL+1zi+4** system, was prepared as follow. The step from the trajectory, which contained four glycinate- CO_2 adduct, was modified by transferring the proton from charged $-\text{NH}_2^+$ group in formed glycinate- CO_2 adduct to glycinate anions. The box length was kept the same as for the system of 32 ion pairs and 4 CO_2 molecules. A similar approach was used to set up the **IL+5-trans** system with 4 carbamic acid, 28 glycinate anions, and 32 cations.

CP2K simulations were started on already prepared geometries. The simulation box was equilibrated for 5.0, 5.0, 7.0 and 5.0 ps correspondingly for pure, mixed and two modified systems in a canonical ensemble at constant temperature of 350 K using the Nosé–Hoover thermostats^[265–267] for individual atoms with a time constant of 100 fs and a time step of 0.5 fs. The production trajectory was run for 76, 124, 76 and 36 ps correspondingly for pure, mixed and two modified systems with a thermostat for the whole system with the time constant of 100 fs.

Composite approach. The first step of this process is the geometry optimization and frequency calculations on the B3LYP-D3(BJ)/def2-TZVPP(Grid 5) level of theory^[168,171,172,417,418] with implicit solvation^[96,182] with a fixed dielectric constant ($\epsilon =$

15). The second step is the calculation of reliable electronic energies on DLPNO-CCSD(T)/CBS(X=T,Q) level^[158] for the obtained geometries. The third step is the calculations of the thermal corrections at 298 K according to the method described in Ref. [147]. All static QC mentioned above were performed in ORCA^[294] program (version 3.0.2)^[295]. The final step is the calculation of solvation correction in COSMOTermX14 program.^[183,192,237,416]

Calculated Gibbs free energies

Table B.1. Calculated Gibbs free reaction energy (in kJ mol⁻¹) of (amino acid anion)-CO₂ adduct formation in different AAILs as depicted in Figure 4.3e.

Cation	Anion									
	[Gly] ⁻	[Ala] ⁻	[Val] ⁻	[Leu] ⁻	[Ile] ⁻	[Pro] ⁻	[Phe] ⁻	[Tyr] ⁻	[Ser] ⁻	[Thr] ⁻
[C ₂ C ₁ Im] ⁺	10	23	31	15	32	13	36	37	18	15
[C ₁₀ C ₁ Im] ⁺	14	25	33	16	34	15	38	38	20	17
[(C _F) ₁₀ C ₂ C ₁ Im] ⁺	19	30	37	21	38	16	42	42	23	20
[P _{2,2,2,2}] ⁺	5	18	27	10	28	11	32	33	14	11
[P _{6,6,6,14}] ⁺	9	21	29	12	30	12	34	35	16	13

Table B.2. Calculated Gibbs free reaction energy (in kJ mol⁻¹) of the intramolecular proton transfer in different AAILs.

Cation	Anion									
	[Gly] ⁻	[Ala] ⁻	[Val] ⁻	[Leu] ⁻	[Ile] ⁻	[Pro] ⁻	[Phe] ⁻	[Tyr] ⁻	[Ser] ⁻	[Thr] ⁻
[C ₂ C ₁ Im] ⁺	17	7	1	9	5	11	10	9	12	11
[C ₁₀ C ₁ Im] ⁺	17	7	0	8	5	11	10	9	12	11
[(C _F) ₁₀ C ₂ C ₁ Im] ⁺	16	6	0	8	5	12	10	8	12	11
[P _{2,2,2,2}] ⁺	18	7	1	9	5	11	9	9	12	10
[P _{6,6,6,14}] ⁺	17	7	0	8	5	10	9	8	12	10

Time development for selected distances

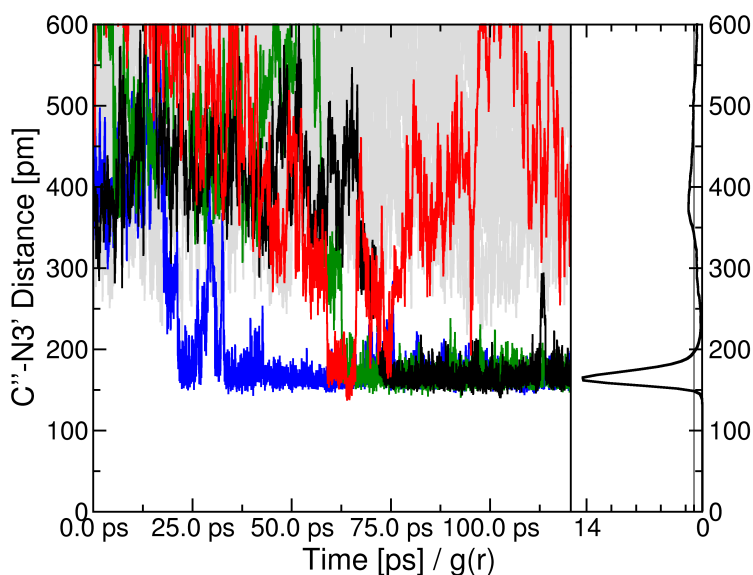


Figure B.1. Time development of the C'' \cdots N3' distance. The corresponding radial distribution function are presented on the right side. Blue, green, red and black lines mark the cases, where the considered distance are below 200 pm at least once during the simulation.

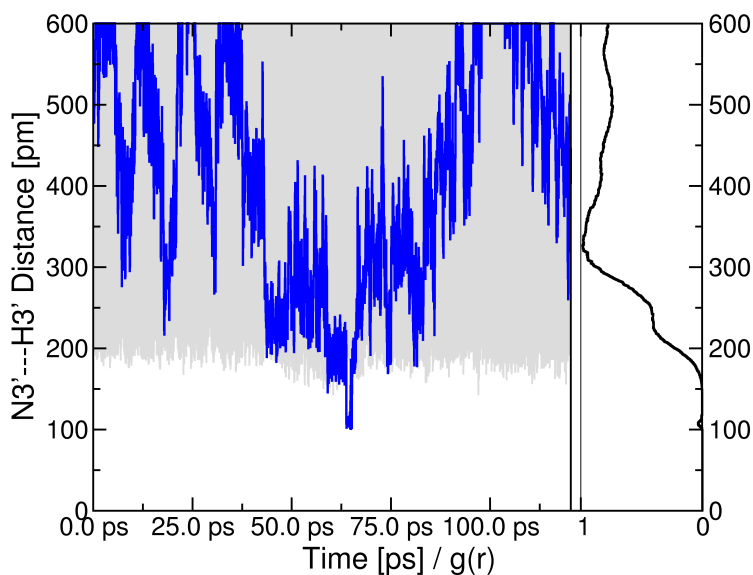


Figure B.2. Time development of the N3'---H3' bond length. The corresponding radial distribution function are presented on the right side. Blue line marks a case where the considered distance approach close to 100 pm. The minimum distance observed was 101.1 pm.

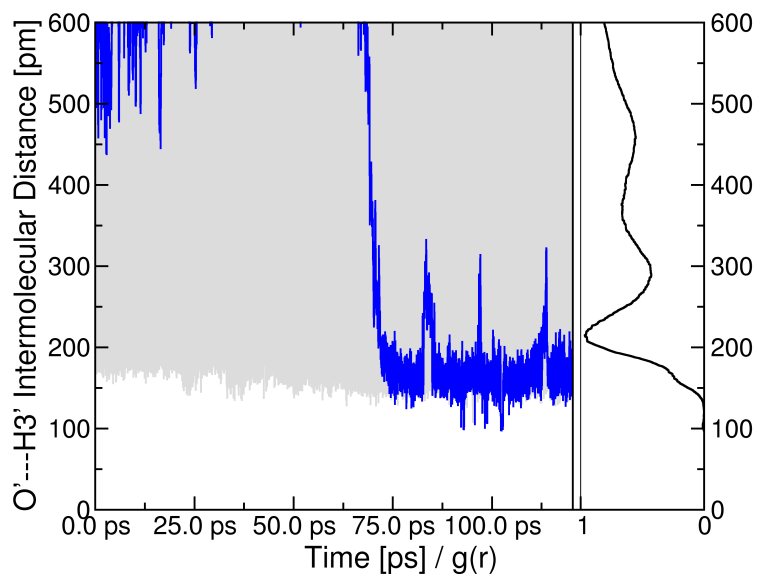


Figure B.3. Time development of the O'...H3' intermolecular distance. The corresponding radial distribution function are presented on the right side. Blue line marks a case where the considered distance approach close to 100 pm. The minimum distance observed was 96.8 pm.

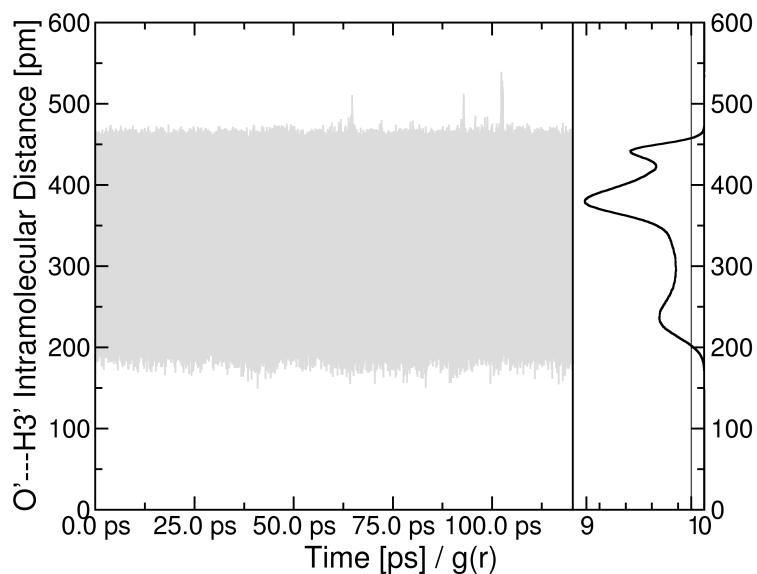


Figure B.4. Time development of the O'...H3' intramolecular distance. The corresponding radial distribution function are presented on the right side. There is no case where the considered distance approach close to 100 pm. The minimum distance observed was 146.9 pm.

C Supporting Information to Chapter 5

Appendix C contains:

- Box construction details
- Plots describing static and dynamic behaviour of EAN+CO₂ system

Box construction details

The size of the boxes for the simulated systems were adjusted to the experimental densities for pure ethylammonium nitrate and CO₂. The density for pure ethylammonium nitrate at 350 K was extrapolated from experimental data between 293 and 318K (J. Solution Chem., **2010**, 39, 1531), whereas the density for supercritical CO₂ (at 350K and 1000 bar) was taken from Thermophysical Properties of Fluid Systems on the <http://webbook.nist.gov/chemistry/fluid/>.

Plots describing static and dynamic behavior of EAN+CO₂ system

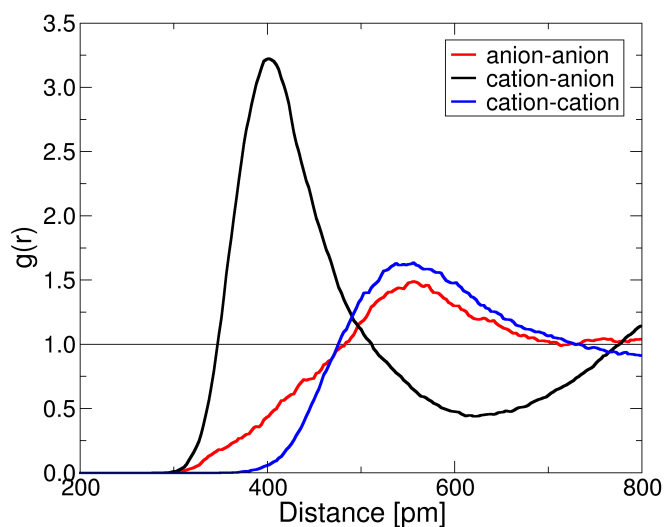


Figure C.1. Radial distribution function between the center of masses of cation-anion (black), anion-anion (red), cation-cation (blue).

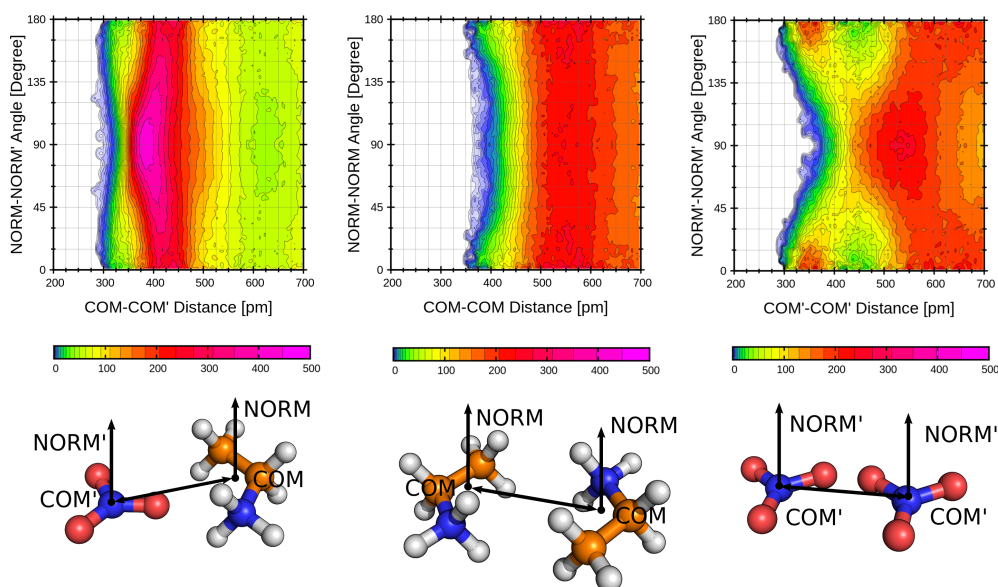


Figure C.2. Combined distribution functions analyzing mutual orientations of the cation versus anion (left), cation versus cation (center), and anion versus anion (right). (Note that COM and COM' stands for center of mass of the cation and anion, while NORM and NORM' stands for the normal vector to the plane of heavy atoms: N1-C2-C3 for the cation and O'-O'-O' for the anion).

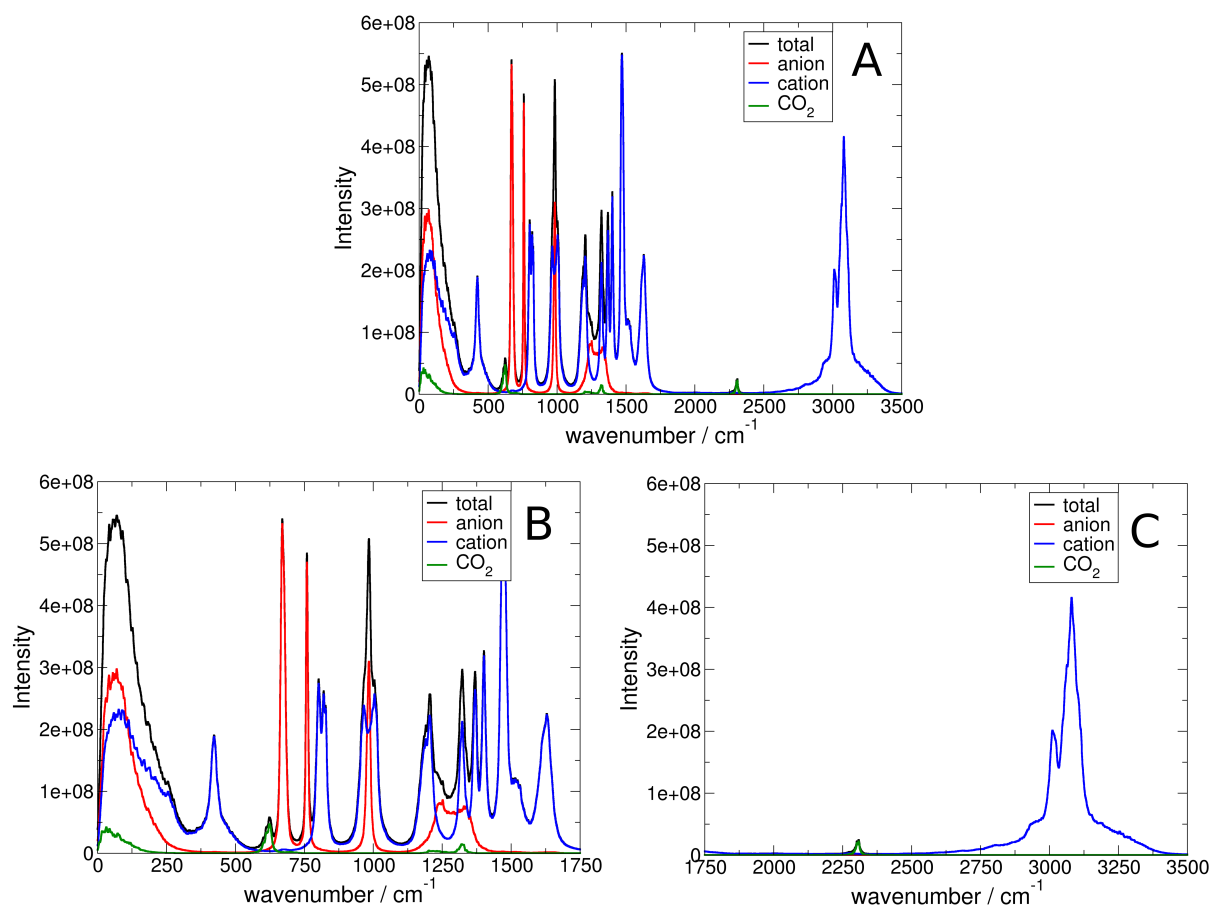


Figure C.3. Calculated power spectra for the whole system (black), anions (red), cations (blue) and CO₂ molecules (green) in the range 0-3500 cm⁻¹ (A), 0-1750 cm⁻¹ (B) and 1750-3500 cm⁻¹ (C).

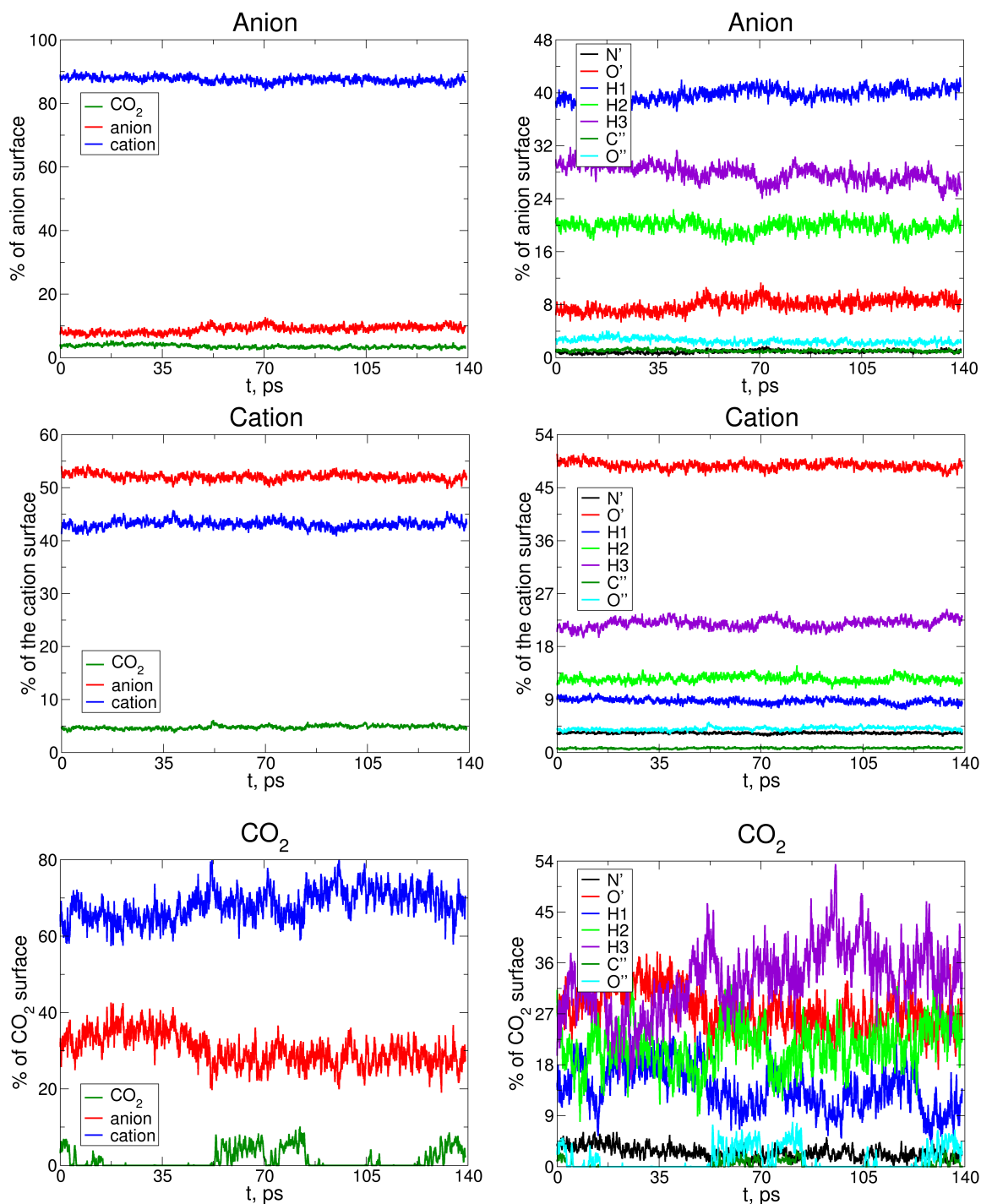


Figure C.4. Dynamics of the surface covering of the anion (upper panel), cation (central panel) and CO₂ (lower panel) by particles (anions: red, cations: blue, CO₂: dark green) on the left side and by atoms (N': black, O': red, H1: blue, H2: green, H3: purple, C'': dark green, O'': cyan) on the right side.

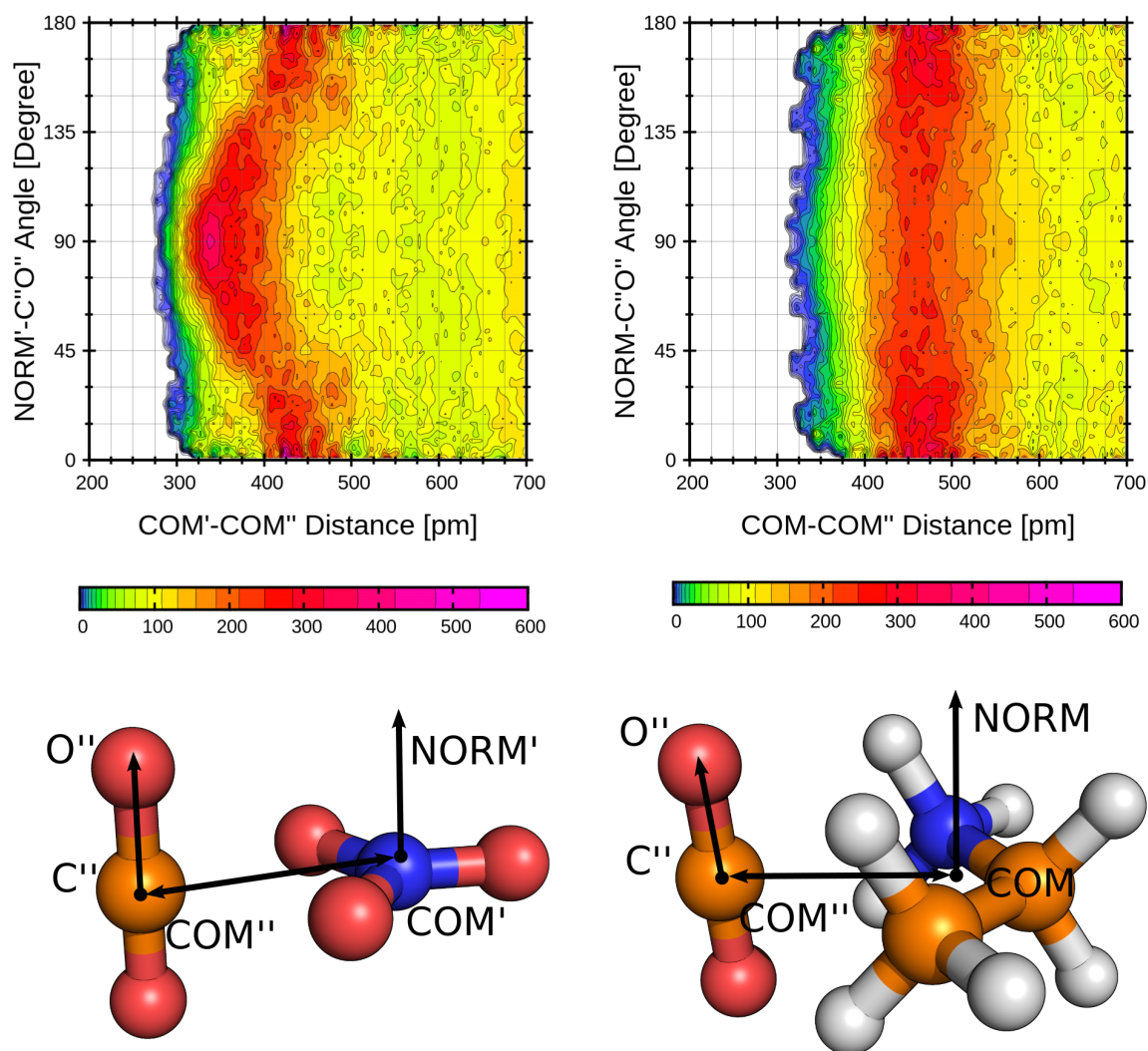


Figure C.5. Combined distribution functions analyzing mutual orientations of the CO₂ versus anion (left) and versus cation (right). (Note that COM, COM' and COM'' stands for the center of mass of the cation, the anion and CO₂, while NORM and NORM' stands for the normal vector to the plane of heavy atoms: N1-C2-C3 for the cation and O'-O'-O' for the anion).

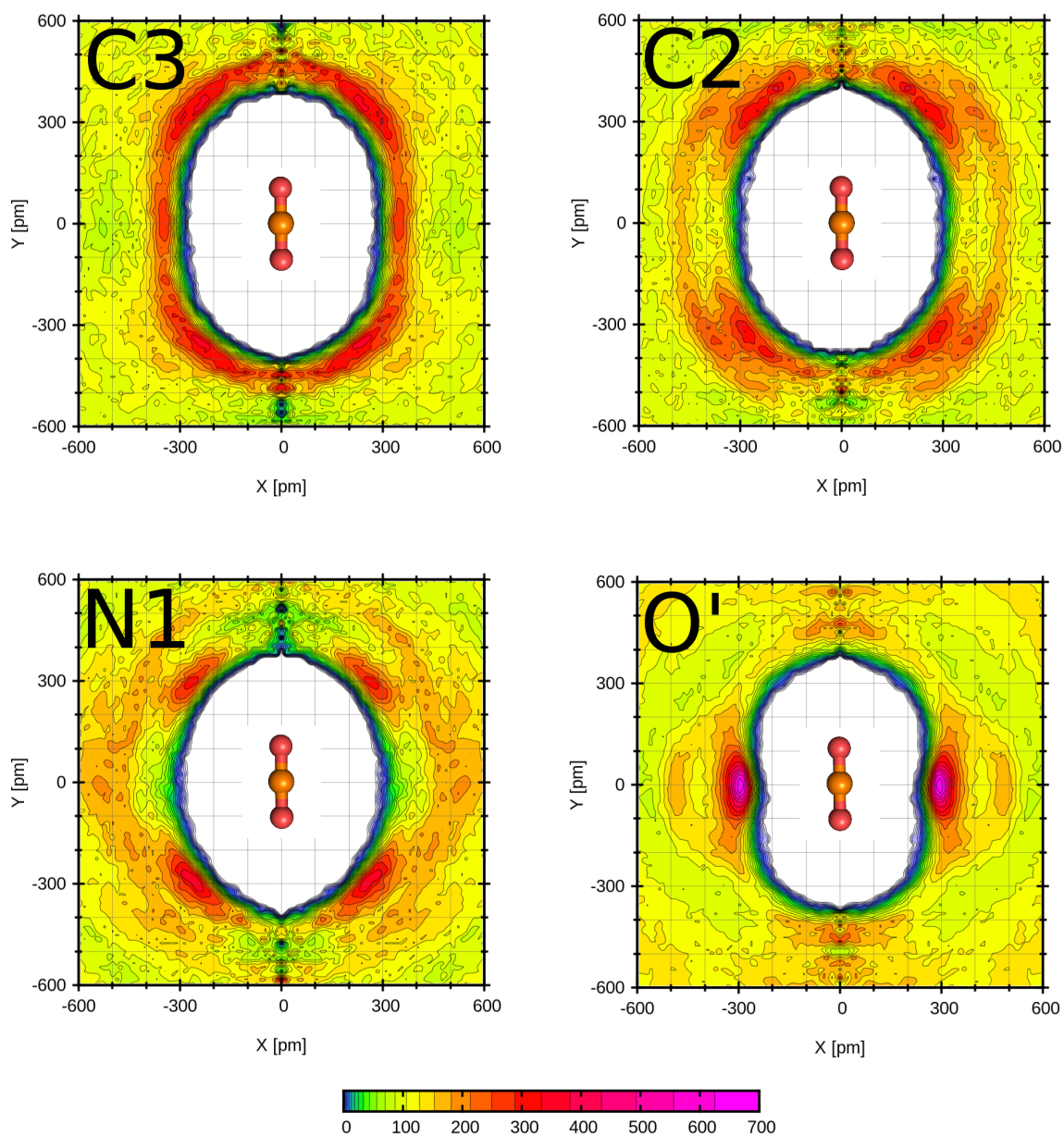


Figure C.6. Spatial distribution of C3 (upper panel, left), C2 (upper panel, right), N1 (lower panel, left) and O' (lower panel, right) atoms around CO₂.

D Supporting Information to Chapter 6

Appendix D contains:

- Box constraction details
- Geometries and energies
- Radial, angular, and dihedral distribution functions

Box constraction details

The box size for the simulated systems was calculated based on the assumption of ideal mixing. The density for pure 1-ethyl-3-methylimidazolium thiocyanate at 350 K was interpolated from experimental data between 278 and 363 K (*J. Chem. Eng. Data*, **2011**, 56, 4813), whereas the density for liquid SO₂ (at 350K and 16.72 bars) was taken from Thermophysical Properties of Fluid Systems on the <http://webbook.nist.gov/chemistry/fluid/>. Since the isothermal compressibility of liquids is approximately 10⁻⁵ bar⁻¹, we neglect the volume expansion for SO₂.

Geometries and energies

Geometries and energies of SO₂ molecule, [SCN]⁻ anion and anion-SO₂ adducts ([NCS·SO₂]⁻ and [SCN·SO₂]⁻):

SO₂

$$E_{\text{tot}}(\text{RI-BLYP-D3(BJ)/def2-TZVPP}) = -548.7119120$$

$$\text{S } 0.000000 \text{ } -0.000000 \text{ } 0.174472$$

$$\text{O } 0.000000 \text{ } -1.259582 \text{ } 0.917671$$

$$\text{O } 0.000000 \text{ } 1.259582 \text{ } 0.917671$$

$$E_{\text{tot}}(\text{B3LYP-D3(BJ)/def2-TZVPP}) = -548.6029282$$

$$E_{\text{tot}}(\text{CCSD(T)/CBS//B3LYP-D3(BJ)/def2-TZVPP}) = -548.0815700$$

S 0.000000 0.000000 0.182191
O 0.000000 -1.238742 0.913811
O 0.000000 1.238742 0.913811

[SCN]⁻

$E_{\text{tot}}(\text{RI-BLYP-D3(BJ)/def2-TZVPP}) = -491.1471375$

S 1.840458 -0.000000 0.000000
C 0.173073 0.000000 -0.000000
N -1.013531 -0.000000 0.000000

$E_{\text{tot}}(\text{B3LYP-D3(BJ)/def2-TZVPP}) = -491.0678994$

$E_{\text{tot}}(\text{CCSD(T)/CBS//B3LYP-D3(BJ)/def2-TZVPP}) = -490.5758235$

S -0.000000 -0.000000 -3.262674
C 0.000000 0.000000 -1.602481
N -0.000000 -0.000000 -0.429976

[NCS·SO₂]⁻

$E_{\text{tot}}(\text{RI-BLYP-D3(BJ)/def2-TZVPP}) = -1039.8969089$

N 0.414423 1.746896 -3.032803
C -0.614095 1.716268 -2.454019
S -2.076509 1.668760 -1.649534
S -1.593892 -0.560155 -0.077801
O -0.765420 -0.046317 1.039443
O -2.990207 -0.915555 0.285280

$E_{\text{tot}}(\text{B3LYP-D3(BJ)/def2-TZVPP}) = -1039.7061239$

$E_{\text{tot}}(\text{CCSD(T)/CBS//B3LYP-D3(BJ)/def2-TZVPP}) = -1038.6835077$

N 0.396362 1.713325 -2.982639
C -0.624209 1.691535 -2.418153
S -2.087389 1.652197 -1.625207
S -1.590080 -0.540016 -0.108497
O -0.761433 -0.026195 0.974980
O -2.958952 -0.880948 0.270082

[SCN·SO₂]⁻

$E_{\text{tot}}(\text{RI-BLYP-D3(BJ)/def2-TZVPP}) = -1039.8935382$

S 0.163613 1.730856 -3.603920
C -0.830348 1.628987 -2.308184
N -1.563223 1.573975 -1.365387
S -1.549605 -0.366801 0.009077
O -1.252951 0.232876 1.328263
O -2.938230 -0.843441 -0.170952

$E_{\text{tot}}(\text{B3LYP-D3(BJ)/def2-TZVPP}) = -1039.7032387$

$E_{\text{tot}}(\text{CCSD(T)/CBS//B3LYP-D3(BJ)/def2-TZVPP}) = -1038.6824159$

S 0.149014 1.775235 -3.585662
C -0.831758 1.607526 -2.296092
N -1.548745 1.499084 -1.363894
S -1.554637 -0.368157 0.007927
O -1.254914 0.252154 1.288456
O -2.929704 -0.809389 -0.161838

Radial, angular, and dihedral distribution functions

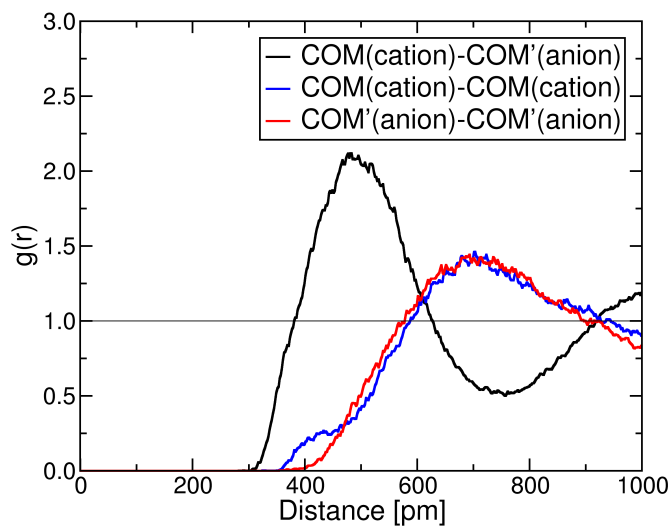


Figure D.1. Radial distribution functions between the center of masses of cation and anion (black), cation and cation (blue), anion and anion (red).

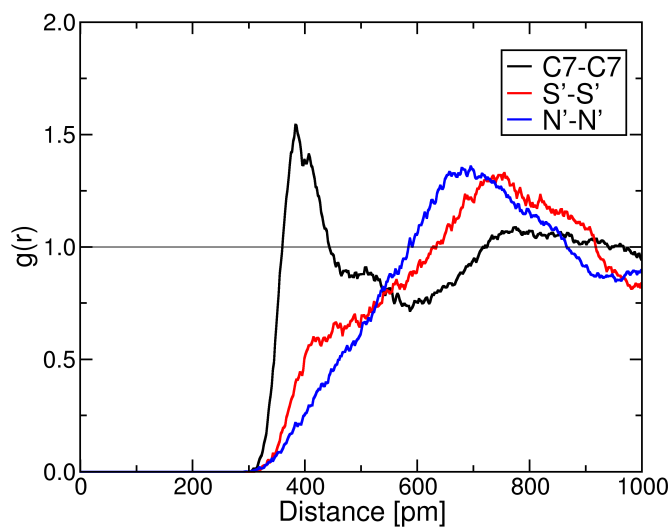


Figure D.2. Radial distribution functions between the selected atoms of cation and anion (see Figure 6.2 in the article for atom labels).

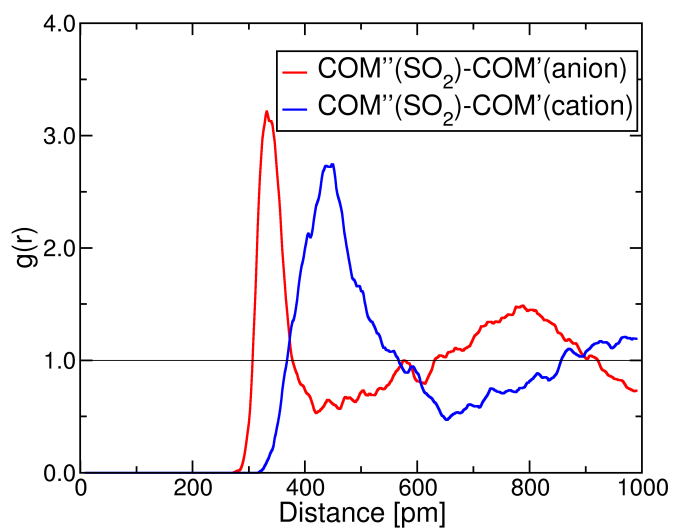


Figure D.3. Radial distribution functions between the center of masses of SO₂ and anion (red), SO₂ and cation (blue). The value of integrals in the first minimum equals one for blue curve and five for red curve.

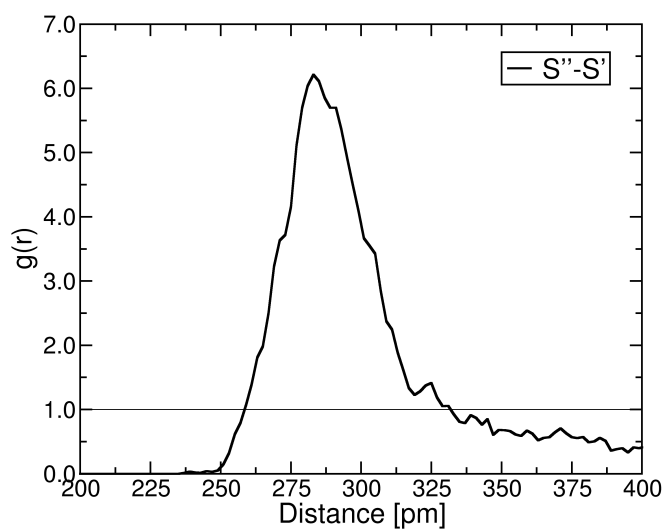


Figure D.4. Radial distribution functions between the sulfur atoms of SO₂ and anion.

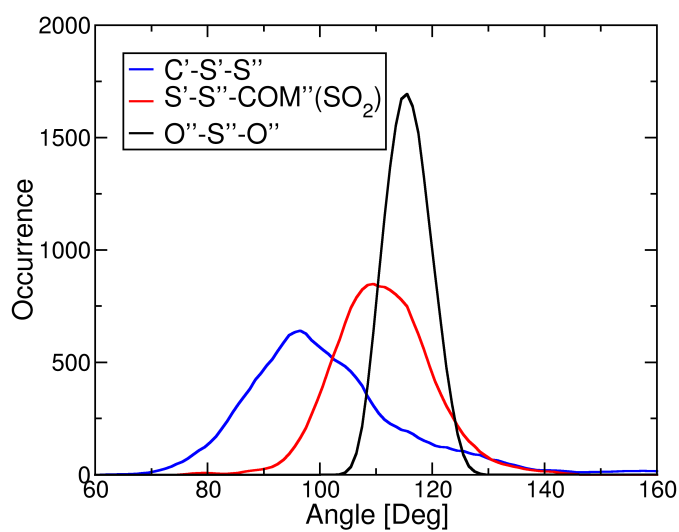


Figure D.5. Angular distribution function between center of masses and atoms of SO₂ and the closest anion.

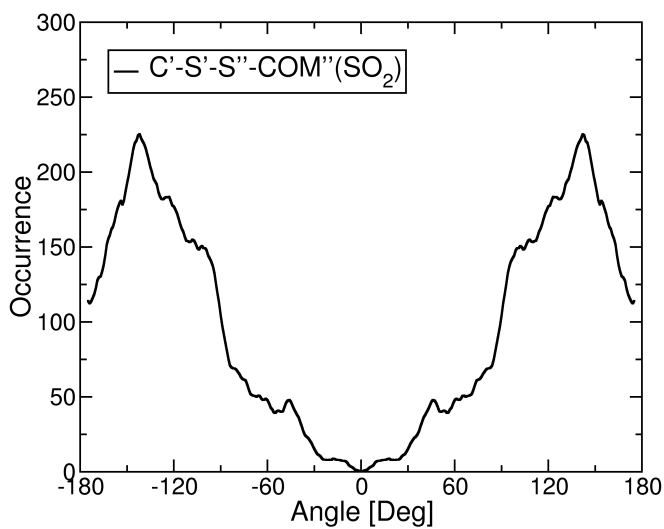


Figure D.6. Dihedral distribution function for dihedral angle between anion and SO₂.

E Supporting Information to Chapter 7

Appendix E contains:

- Starting geometry for AIMD simulations
- RDFs for C2-H2 and O'...H2 distances
- RDFs for O'...C'' and C2...C'' distances
- Relative energies for 1P_{Me} and 1P_{Me+CO₂} systems
- Conformations in the 1P_{Me+CO₂} system
- Time development of the CO₂ surface coverage
- Details of the scans in acetate-CO₂ and acetic acid-CO₂ systems

Starting geometry for AIMD simulations

1P

C 1.31200 -0.01095 -0.34259
C 0.01917 0.13121 0.06931
N 0.04059 0.16851 1.45330
C 1.31084 0.05491 1.87875
N 2.09610 -0.05582 0.79783
C -1.12625 0.33379 2.34740
C 3.55928 -0.20378 0.84738
O 1.79380 0.00074 4.64761
C 3.05807 -0.05153 4.83154
O 3.91975 -0.08959 3.91359
C 3.53259 -0.06932 6.28775
C -1.23248 -0.78319 3.38391
H -1.03335 1.30823 2.83682
H -2.00432 0.36497 1.69591
H 3.85850 -0.18261 1.90424
H 3.83837 -1.15542 0.38651
H 4.01995 0.62282 0.29949
H 1.73526 -0.08520 -1.33264
H -0.89833 0.20811 -0.49385
H 1.62369 0.04456 2.96041
H 4.62393 -0.09185 6.34774
H 3.15232 0.81540 6.81245
H 3.11950 -0.94724 6.79947
H -2.12928 -0.61753 3.99156
H -1.32234 -1.76195 2.89897
H -0.36232 -0.78390 4.04874

1P+CO₂

N 0.91867 0.28089 -0.53918
C -0.09475 -0.50719 0.03723
C 0.18892 -0.60157 1.37800
N 1.36944 0.13075 1.58885
C 1.80034 0.66575 0.41739
C 2.21314 0.16077 2.82483
C 1.23262 0.42817 -1.99150
O 4.44288 0.93856 0.56324
C 4.71005 -0.11366 -0.15672
O 3.97301 -0.57001 -1.11522
C 5.96501 -0.92925 0.22612
C 2.53544 -2.38407 -0.27328
O 1.96993 -2.55179 -1.31233
O 2.95296 -2.36650 0.84963
H 3.21447 0.45647 2.47757
C 1.63227 1.14807 3.85779
H 2.25073 -0.86869 3.20529
H 2.31523 0.21814 -2.05986
H 0.66287 -0.33115 -2.53919
H 0.97272 1.44003 -2.32933
H -0.89041 -0.93640 -0.55128
H -0.32583 -1.11424 2.17574
H 2.85404 1.08085 0.31720
H 6.45826 -1.30627 -0.68141
H 6.64973 -0.32087 0.83112
H 5.62047 -1.79592 0.81734
H 2.27239 1.15910 4.75389
H 1.60195 2.16039 3.42786
H 0.61291 0.85084 4.15173

RDFs for C2-H2 and O'...H2 distances

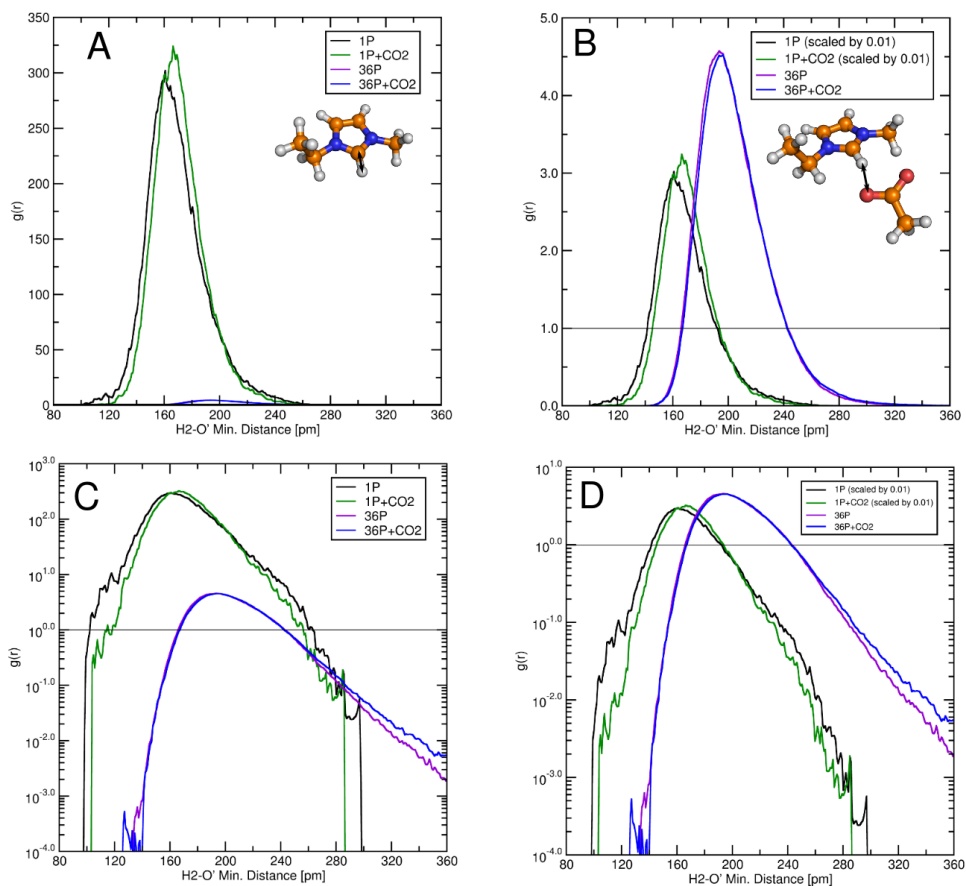


Figure E.1. Scaled radial distribution functions for C2-H2 and O'...H2 distances in linear (A, B) logarithmic (C, D) scales, respectively.

RDFs for O'...C'' and C2...C'' distances

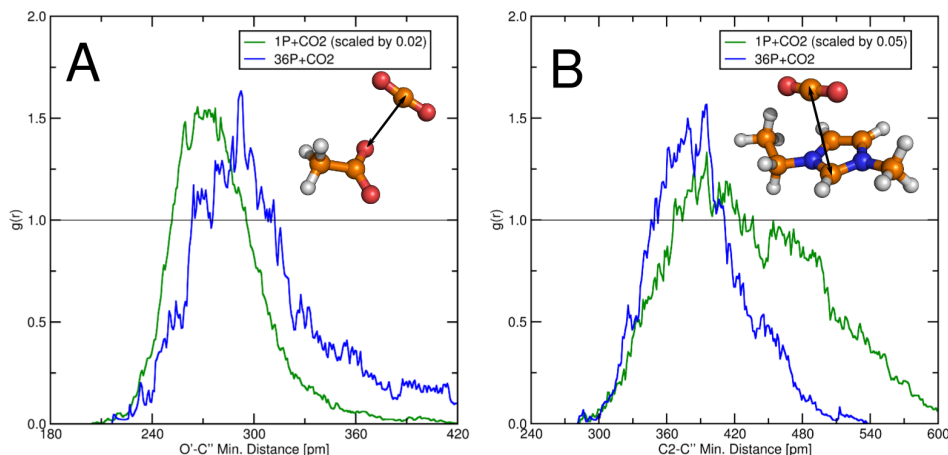


Figure E.2. Scaled radial distribution functions for O'...C'' (A) and C2...C'' (B) distances in linear scale.

Relative energies for 1P_{Me} and 1P_{Me}+CO₂ systems

It has previously been shown that the vapor of 1-ethyl-3-methylimidazolium acetate consists of the carbene – acetic acid complex structure **2** (see *New J. Chem.* **2010**, *34*, 3004). In good agreement, the MP2 and high-level CCSD(T)+ZPVE results support the higher stability of this structure, while many of the DFT functionals – as has also been shown before (see *New J. Chem.* **2010**, *34*, 3004) – predict the ion pair **1** to be more stable. Moreover, by including the dispersion correction to the BLYP functional the relative energy of the neutral **2** rises yet. Nevertheless, by all methods applied, the trend is clearly observable: the presence of the CO₂ molecule destabilizes **2** by ca. 5-10 kJ mol⁻¹, suggesting that even if the order of relative stabilities is different for some methods, to observe trends in carbene formation all may be applied. However, considering the geometry of the optimized structures it can clearly be seen, that the DFT functionals lacking account for dispersion interactions fail to obtain those geometries, which have been the most stable by both MP2 and DFT-D calculations, and significant rearrangements can be observed during optimization. Thus, for the proper description of the liquid (where dispersion in-

teractions are even more important), the BLYP-D functional has been chosen in the ab initio molecular dynamics simulations.

1P_{Me} system

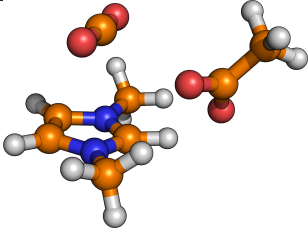
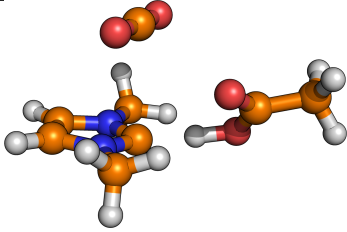
Level of theory	1	2
B97-D/6-311+G**	0.0	3.5
B97-D/6-311+G**+ZPVE ^[b]	0.0	2.5
B97-D/aug-cc-pVTZ	0.0	2.9
B3LYP/6-311+G**	0.0	3.0
PW91PW91/6-311+G**	0.0	3.4
M05-2X/6-311+G**	0.0	3.6
M06-2X/6-311+G**	0.0	-6.5
BLYP/def2-TZVPP ^[a]	0.0	0.7
BLYP-D/def2-TZVPP ^[a]	0.0	4.4
BLYP-D/def2-TZVPP+ZPVE ^[b]	0.0	-0.4
MP2/6-311+G**	0.0	-1.6
RI-MP2/def2-TZVPP ^[a]	0.0	1.7
CCSD(T)(F12)/cc-pVDZ-F12//		
B97-D/6-311+G** ^[a]	0.0	0.3
CCSD(T)(F12)/cc-pVDZ-F12//		
B97-D/6-311+G**+ZPVE ^[b]	0.0	-0.7

[a] The calculations were performed in TURBOMOLE V6.0.

[b] with B97-D/6-311+G** zero point vibrational energies.

E. Supporting Information to Chapter 7

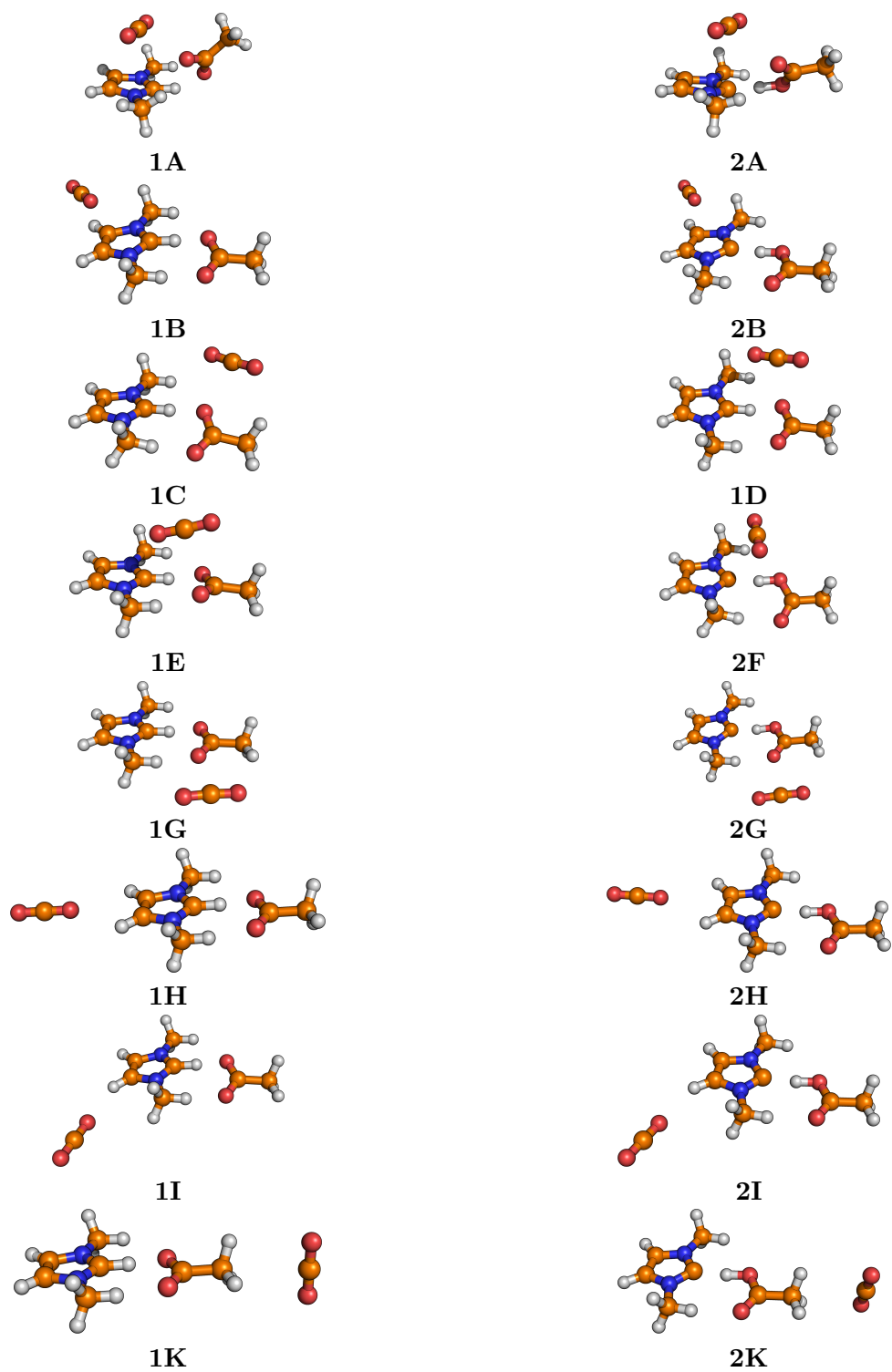
1P_{Me+CO₂} system

Level of theory		
	1A	2A
B97-D/6-311+G**	0.0	8.8
B97-D/6-311+G**+ZPVE ^[b]	0.0	4.5
B97-D/aug-cc-pVTZ	0.0	8.1
B3LYP/6-311+G**	-	-
PW91PW91/6-311+G**	-	-
M05-2X/6-311+G**	0.1	11.9
M06-2X/6-311+G**	0.0	3.6
BLYP/def2-TZVPP ^[a]	-	-
BLYP-D/def2-TZVPP ^[a]	0.0	13.6
BLYP-D/def2-TZVPP+ZPVE ^[b]	0.0	8.9
MP2/6-311+G**	0.0	6.0
RI-MP2/def2-TZVPP ^[a]	0.0	9.8
CCSD(T)(F12)/cc-pVDZ-F12// B97-D/6-311+G** ^[a]	0.0	7.9
CCSD(T)(F12)/cc-pVDZ-F12// B97-D/6-311+G**+ZPVE ^[b]	0.0	3.6

[a] The calculations were performed in TURBOMOLE V6.0.

[b] with B97-D/6-311+G** zero point vibrational energies.

Conformations in the $1P_{\text{Me}+\text{CO}_2}$ system*



*Relative energies and geometries can be found under <http://pubs.acs.org/doi/suppl/10.1021/jp4004399>

Time development of the CO₂ surface coverage

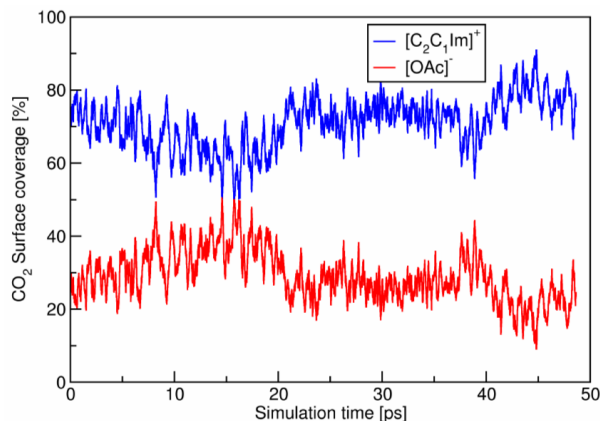
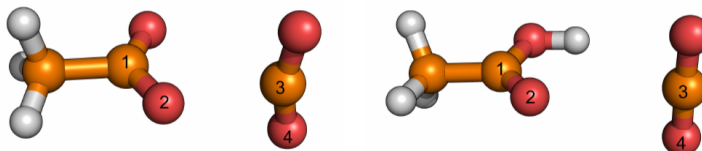


Figure E.3. Changes in the surfaces of the CO₂'s Voronoi cell covered by the anion or the cation during the simulations (in %)

Details of the scans in acetate–CO₂ and acetic acid–CO₂ systems



For both scans the following internal coordinates were kept constant: Angle 1-2-3 was fixed at 120° (in order to prevent the erroneous interaction of CO₂ with the other oxygen atom of the acetate). Dihedral angle 1-2-3-4 was fixed at 90° (in order to prevent the formation of a stabilizing H-bond between the CO₂ and acetic acid). With these restrictions the structure has been optimized with constant 2-3 distance at each ten picometers between 130 and 400 pm. Since the minimum of the obtained interaction energy curve represents almost identical structure to that obtained by a full geometry optimization (shown in Figure 7.6 in the article), the aforementioned restrictions should most likely not result in erroneous conclusions.

F Supporting Information to Chapter 8

Appendix F contains:

- Snapshots of simulated systems
- Selected radial distribution functions
- Selected combined distribution functions

Snapshots of simulated systems

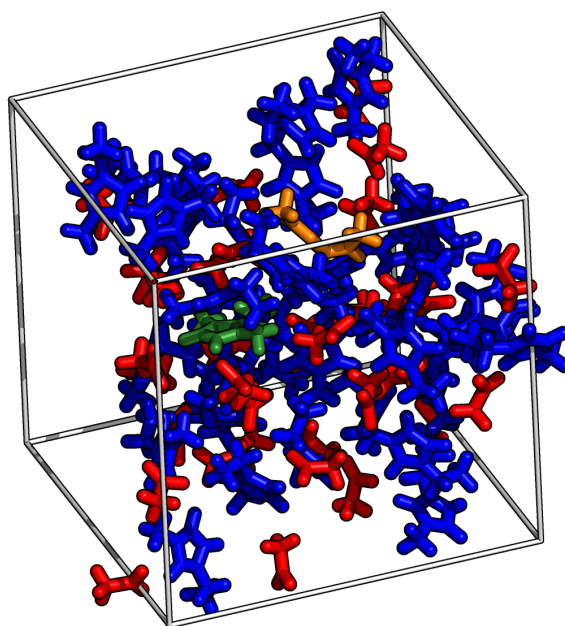


Figure F.1. Simulation box of **I** (dark green), 35 $[\text{C}_2\text{C}_1\text{Im}]^+$ cation (blue), 34 $[\text{OAc}]^-$ (red), one $[\text{H}(\text{OAc})_2]^-$ (orange).

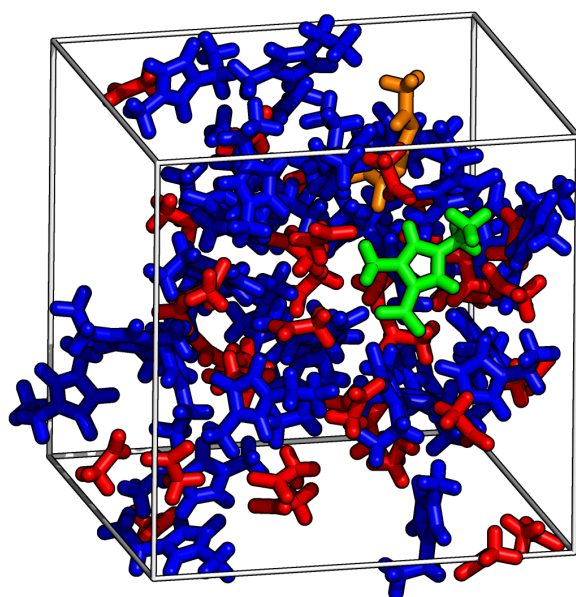


Figure F.2. Simulation box of **II** (light green), 35 $[\text{C}_2\text{C}_1\text{Im}]^+$ cation (blue), 34 $[\text{OAc}]^-$ (red), one $[\text{H}(\text{OAc})_2]^-$ (orange).

Selected radial distribution functions

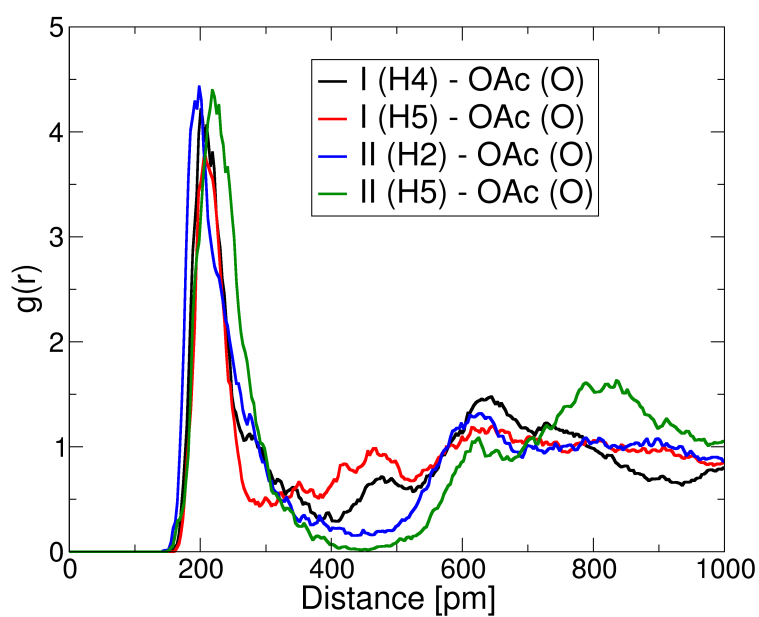


Figure F.3. Radial pair distribution functions concerning the hydrogen bonding between **I** or **II** and the acetate anions.

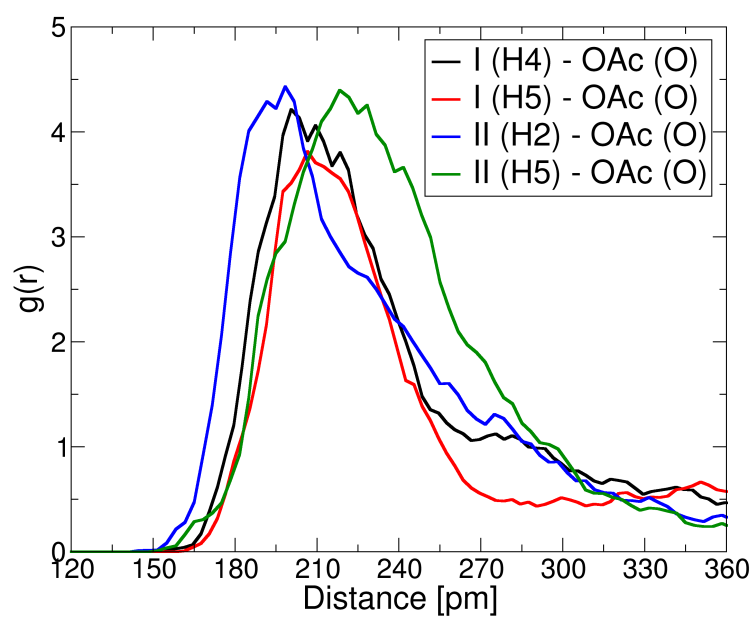


Figure F.4. The first peaks of the radial pair distribution functions, concerning the hydrogen bonding between **I** or **II** and the acetate anions.

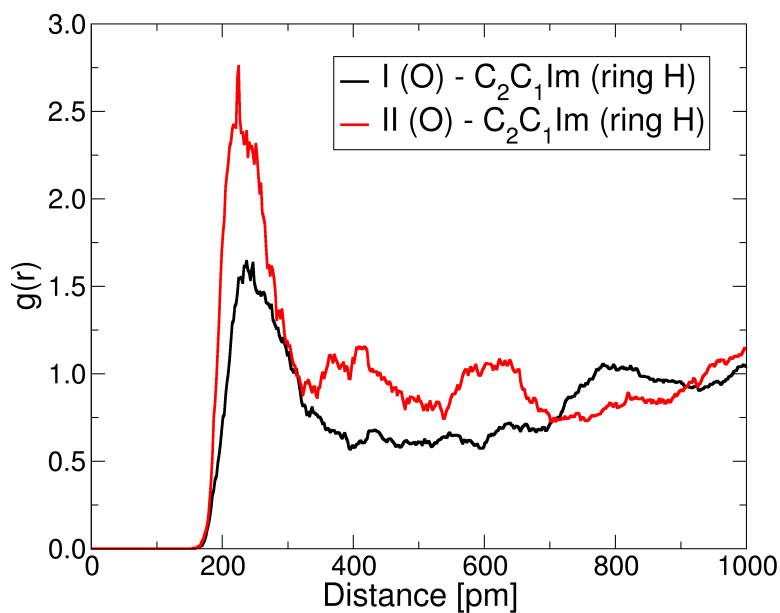


Figure F.5. First peaks of the radial pair distribution functions, concerning the hydrogen bonding between **I** or **II** and the imidazolium cations' ring hydrogen atoms.

Selected combined distribution functions

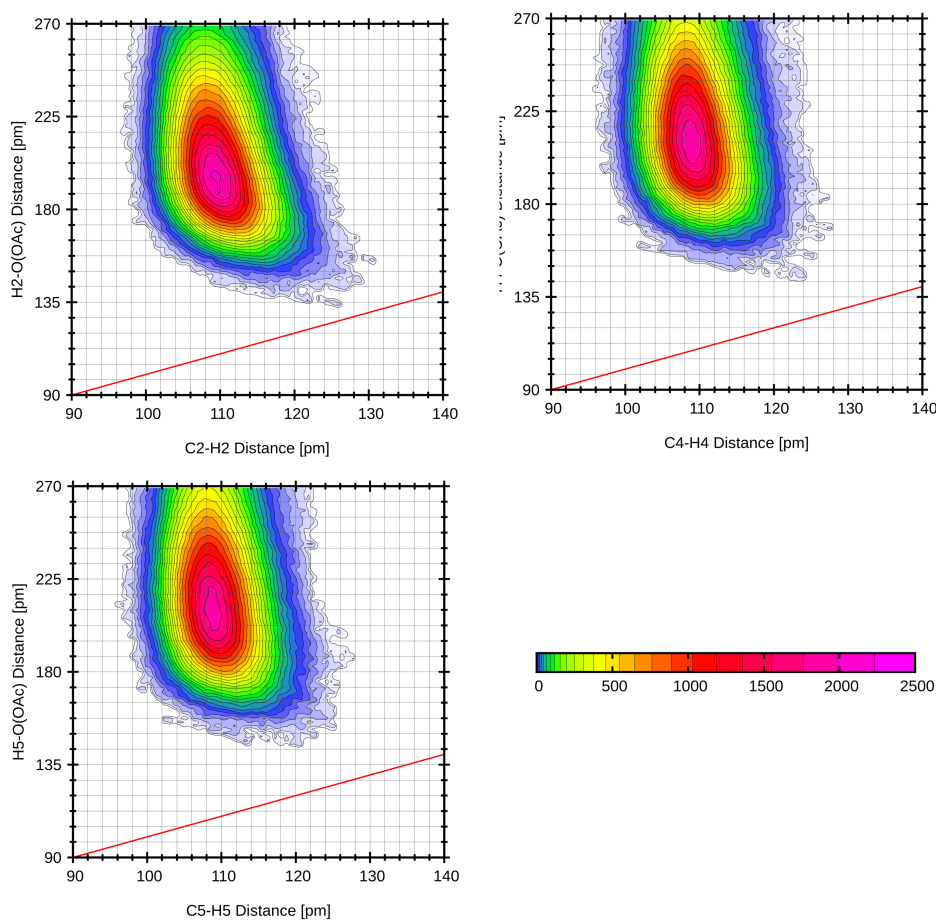


Figure F.6. Combined distribution functions showing the differences in the mobility of the 1-ethyl-3-methylimidazolium acetate's ring hydrogen atoms in the pure 1-ethyl-3-methylimidazolium acetate (see Ref. [339]). While the X axes correspond to the intramolecular C-H bond lengths of the imidazolium cation, the Y-axes show the intermolecular O(anion)-H(cation) distances. At each point of the graph, the occurrence of the corresponding combination of distances in the hydrogen-bonded assemblies is indicated according to the color scale at the right bottom. The proton transfer from the cation to the anion results in long C-H and short O-H distances, thus, in occurrences at the lower right part of the graphs; where the red line corresponds to equal O-H and C-H distances. As expected, the most acidic H2 shows significantly more occurrences close to the red line of equal distances, than the other two ring hydrogen atoms. Thus, the position 4 and 5 protons are less mobile in the solution, and the direct exchange of them to a CO₂ moiety (via an abnormal NHC) is less probable than for the position 2 hydrogen atom (via a normal NHC).

Bibliography

- [1] Lamarque, J.-F. et al. *Atmos. Chem. Phys.* **2010**, *10*, 7017–7039.
- [2] Smith, S. J.; Aardenne, J. v.; Klimont, Z.; Andres, R. J.; Volke, A.; Delgado Arias, S. *Atmos. Chem. Phys.* **2011**, *11*, 1101–1116.
- [3] Meinshausen, M.; Smith, S. J.; Calvin, K.; Daniel, J. S.; Kainuma, M. L. T.; Lamarque, J. F.; Matsumoto, K.; Montzka, S. A.; Raper, S. C. B.; Riahi, K.; Thomson, A.; Velders, G. J. M.; van Vuuren, D. P. P. *Clim. Change* **2011**, *109*, 213–241.
- [4] Stern, N. *Stern Review: The economics of climate change*; HM treasury London: London, 2007.
- [5] Canadell, J. G.; Le Quéré, C.; Raupach, M. R.; Field, C. B.; Buitenhuis, E. T.; Ciais, P.; Conway, T. J.; Gillett, N. P.; Houghton, R.; Marland, G. *Proc. Natl. Acad. Sci. U.S.A.* **2007**, *104*, 18866–18870.
- [6] Figueroa, J. D.; Fout, T.; Plasynski, S.; McIlvried, H.; Srivastava, R. D. *Int. J. Greenh. Gas Control* **2008**, *2*, 9–20.
- [7] Davis, S. J.; Caldeira, K.; Matthews, H. D. *Science* **2010**, *329*, 1330–1333.
- [8] Ellerman, A. D.; Schmalensee, R.; Bailey, E. M.; Joskow, P. L.; Montero, J.-P. *Markets for clean air: The US acid rain program*; Cambridge University Press: Cambridge, 2000.
- [9] Watson, R.; Meira Filho, L.; Sanhueza, E.; Janetos, A. *Clim. Change* **1992**, 25–46.
- [10] Sawin, J. L. et al. *Renewables 2014 Global Status Report*. REN21 Secretariat, Paris, 2014.
- [11] Hu, Y.; Naito, S.; Kobayashi, N.; Hasatani, M. *Fuel* **2000**, *79*, 1925–1932.
- [12] Chamberlain, S. C. Measurement and analysis of gas composition in a staged and unstaged oxy-fired pulverized coal reactor with warm flue gas recycle. Ph.D. thesis, Brigham Young University, 2012; <http://scholarsarchive.byu.edu/etd/3319>.

- [13] Srivastava, R. K. *Controlling SO₂ Emissions – a Review of Technologies*; Nova Science: New York, 2003.
- [14] Srivastava, R. K.; Jozewicz, W.; Singer, C. *Environ. Prog.* **2001**, *20*, 219–228.
- [15] Aaron, D.; Tsouris, C. *Sep. Sci. Technol.* **2005**, *40*, 321–348.
- [16] Yang, H.; Xu, Z.; Fan, M.; Gupta, R.; Slimane, R. B.; Bland, A. E.; Wright, I. *J. Environ. Sci.* **2008**, *20*, 14–27.
- [17] Wang, M.; Lawal, A.; Stephenson, P.; Sidders, J.; Ramshaw, C. *Chem. Eng. Res. Des.* **2011**, *89*, 1609–1624.
- [18] Yu, C.-H.; Huang, C.-H.; Tan, C.-S. *Aerosol Air Qual. Res.* **2012**, *12*, 745–769.
- [19] Anastas, P. T.; Warner, J. C. *Green Chemistry: Theory and Practice*; Oxford University Press: Oxford, 1998.
- [20] Tilly, J. Flue gas desulfurization: cost and functional analysis of large scale proven plants. M.Sc. thesis, Massachusetts Institute of Technology, 1983; <http://hdl.handle.net/1721.1/60646>.
- [21] Rochelle, G. T. *Science* **2009**, *325*, 1652–1654.
- [22] Welton, T. *Chem. Rev.* **1999**, *99*, 2071–2084.
- [23] Plechkova, N. V.; Seddon, K. R. *Chem. Soci. Rev.* **2008**, *37*, 123–150.
- [24] Hallett, J. P.; Welton, T. *Chem. Rev.* **2011**, *111*, 3508–3576.
- [25] Blanchard, L. A.; Hancu, D.; Beckman, E. J.; Brennecke, J. F. *Nature* **1999**, *399*, 28–29.
- [26] Wu, W.; Han, B.; Gao, H.; Liu, Z.; Jiang, T.; Huang, J. *Angew. Chem.* **2004**, *116*, 2469–2471.
- [27] Wu, W.; Han, B.; Gao, H.; Liu, Z.; Jiang, T.; Huang, J. *Angew. Chem. Int. Ed.* **2004**, *43*, 2415–2417.
- [28] Bara, J. E.; Camper, D. E.; Gin, D. L.; Noble, R. D. *Acc. Chem. Res.* **2009**, *43*, 152–159.

- [29] Paulechka, Y. U.; Zaitsau, D. H.; Kabo, G. J.; Strechan, A. A. *Thermochim. Acta* **2005**, *439*, 158–160.
- [30] Zaitsau, D. H.; Kabo, G. J.; Strechan, A. A.; Paulechka, Y. U.; Tschersich, A.; Verevkin, S. P.; Heintz, A. *J. Phys. Chem. A* **2006**, *110*, 7303–7306.
- [31] Anthony, J. L.; Anderson, J. L.; Maginn, E. J.; Brennecke, J. F. *J. Phys. Chem. B* **2005**, *109*, 6366–6374.
- [32] Anderson, J. L.; Dixon, J. K.; Maginn, E. J.; Brennecke, J. F. *J. Phys. Chem. B* **2006**, *110*, 15059–15062.
- [33] Aresta, M. *Carbon dioxide as chemical feedstock*; Wiley-VCH Verlag: Weinheim, 2010.
- [34] Shi, Y. Utilization of sulfur dioxide in organic acids recovery and sulfur trioxide conversion with iron oxide as catalyst. Ph.D. thesis, Iowa State University, 2006; <http://lib.dr.iastate.edu>.
- [35] Hollingsworth, N.; Taylor, S.; Galante, M. T.; Jacquemin, J.; Longo, C.; Holt, K. B.; de Leeuw, N. H.; Hardacre, C. *Angew. Chem.* **2015**, *127*, 14370–14374.
- [36] Hollingsworth, N.; Taylor, S.; Galante, M. T.; Jacquemin, J.; Longo, C.; Holt, K. B.; de Leeuw, N. H.; Hardacre, C. *Angew. Chem. Int. Ed.* **2015**, *54*, 14164–14168.
- [37] Huang, K.; Feng, X.; Zhang, X.-M.; Wu, Y.-T.; Hu, X.-B. *Green Chem.* **2016**, *18*, 1859–1863.
- [38] Yang, Z.-Z.; He, L.-N.; Zhao, Y.-N.; Yu, B. *Environ. Sci. Technol.* **2013**, *47*, 1598–1605.
- [39] Liu, Z. *Chem. Asian J.* **2016**, DOI: 10.1002/asia.201600281.
- [40] Davis, J. H.; Forrester, K. J. *Tetrahedron Lett.* **1999**, *40*, 1621–1622.
- [41] Davis, J. H. *Chem. Lett.* **2004**, *33*, 1072–1077.
- [42] Harrison, P. *Computational methods in physics, chemistry and biology: an introduction*; John Wiley & Sons: New York, 2001.
- [43] Lei, Z.; Dai, C.; Chen, B. *Chem. Rev.* **2013**, *114*, 1289–1326.

- [44] Muldoon, M. J.; Aki, S. N.; Anderson, J. L.; Dixon, J. K.; Brennecke, J. F. *J. Phys. Chem. B* **2007**, *111*, 9001–9009.
- [45] Baltus, R. E.; Culbertson, B. H.; Dai, S.; Luo, H.; DePaoli, D. W. *J. Phys. Chem. B* **2004**, *108*, 721–727.
- [46] Almantariotis, D.; Gefflaut, T.; Pádua, A. A. H.; Coxam, J.-Y.; Costa Gomes, M. F. *J. Phys. Chem. B* **2010**, *114*, 3608–3617.
- [47] Deng, Y.; Morrissey, S.; Gathergood, N.; Delort, A.-M.; Husson, P.; Costa Gomes, M. F. *ChemSusChem* **2010**, *3*, 377–385.
- [48] Jalili, A. H.; Mehdizadeh, A.; Shokouhi, M.; Sakhaeina, H.; Taghikhani, V. *J. Chem. Thermodyn.* **2010**, *42*, 787–791.
- [49] Kanakubo, M.; Makino, T.; Taniguchi, T.; Nokami, T.; Itoh, T. *ACS Sustainable Chem. Eng.* **2016**, *4*, 525–535.
- [50] Mahurin, S. M.; Lee, J. S.; Baker, G. A.; Luo, H.; Dai, S. *J. Membr. Sci.* **2010**, *353*, 177–183.
- [51] Mahurin, S. M.; Hillesheim, P. C.; Yeary, J. S.; Jiang, D.-e.; Dai, S. *RSC Adv.* **2012**, *2*, 11813–11819.
- [52] Makino, T.; Kanakubo, M.; Masuda, Y.; Mukaiyama, H. *J. Solution Chem.* **2014**, *43*, 1601–1613.
- [53] Corvo, M. C.; Sardinha, J.; Casimiro, T.; Marin, G.; Seferin, M.; Einloft, S.; Menezes, S. C.; Dupont, J.; Cabrita, E. J. *ChemSusChem* **2015**, *8*, 1935–1946.
- [54] Giri, N.; Del Pópolo, M. G.; Melaugh, G.; Greenaway, R. L.; Rätzke, K.; Koschine, T.; Pison, L.; Costa Gomes, M. F.; Cooper, A. I.; James, S. L. *Nature* **2015**, *527*, 216–220.
- [55] Carvalho, P.; Kurnia, K.; Coutinho, J. *Phys. Chem. Chem. Phys.* **2016**, DOI: 10.1039/C6CP01896C.
- [56] Bates, E. D.; Mayton, R. D.; Ntai, I.; Davis, J. H. *J. Am. Chem. Soc.* **2002**, *124*, 926–927.
- [57] Zhang, Y.; Zhang, S.; Lu, X.; Zhou, Q.; Fan, W.; Zhang, X. *Chem. Eur. J.* **2009**, *15*, 3003–3011.

- [58] Gurkan, B. E.; de la Fuente, J. C.; Mindrup, E. M.; Ficke, L. E.; Goodrich, B. F.; Price, E. A.; Schneider, W. F.; Brennecke, J. F. *J. Am. Chem. Soc.* **2010**, *132*, 2116–2117.
- [59] Goodrich, B. F.; de la Fuente, J. C.; Gurkan, B. E.; Lopez, Z. K.; Price, E. A.; Huang, Y.; Brennecke, J. F. *J. Phys. Chem. B* **2011**, *115*, 9140–9150.
- [60] Goodrich, B. F.; de la Fuente, J. C.; Gurkan, B. E.; Zadigian, D. J.; Price, E. A.; Huang, Y.; Brennecke, J. F. *Ind. Eng. Chem. Res.* **2011**, *50*, 111–118.
- [61] Gurkan, B.; Goodrich, B. F.; Mindrup, E. M.; Ficke, L. E.; Massel, M.; Seo, S.; Senftle, T. P.; Wu, H.; Glaser, M. F.; Shah, J. K.; Maginn, E. J.; Brennecke, J. F.; Schneider, W. F. *J. Phys. Chem. Lett.* **2010**, *1*, 3494–3499.
- [62] Wang, C.; Luo, H.; Jiang, D.-e.; Li, H.; Dai, S. *Angew. Chem.* **2010**, *122*, 6114–6117.
- [63] Wang, C.; Luo, H.; Jiang, D.-e.; Li, H.; Dai, S. *Angew. Chem. Int. Ed.* **2010**, *49*, 5978–5981.
- [64] Wang, C.; Luo, X.; Luo, H.; Jiang, D.-e.; Li, H.; Dai, S. *Angew. Chem.* **2011**, *123*, 5020–5024.
- [65] Wang, C.; Luo, X.; Luo, H.; Jiang, D.-e.; Li, H.; Dai, S. *Angew. Chem. Int. Ed.* **2011**, *50*, 4918–4922.
- [66] Wang, C.; Luo, H.; Li, H.; Zhu, X.; Yu, B.; Dai, S. *Chem. Eur. J.* **2012**, *18*, 2153–2160.
- [67] Seo, S.; Quiroz-Guzman, M.; DeSilva, M. A.; Lee, T. B.; Huang, Y.; Goodrich, B. F.; Schneider, W. F.; Brennecke, J. F. *J. Phys. Chem. B* **2014**, *118*, 5740–5751.
- [68] Gurau, G.; Rodríguez, H.; Kelley, S. P.; Janiczek, P.; Kalb, R. S.; Rogers, R. D. *Angew. Chem.* **2011**, *123*, 12230–12232.
- [69] Gurau, G.; Rodríguez, H.; Kelley, S. P.; Janiczek, P.; Kalb, R. S.; Rogers, R. D. *Angew. Chem. Int. Ed.* **2011**, *50*, 12024–12026.
- [70] Gohndrone, T. R.; Lee, T. B.; DeSilva, M. A.; Quiroz-Guzman, M.; Schneider, W. F.; Brennecke, J. F. *ChemSusChem* **2014**, *7*, 1970–1975.

- [71] Lee, T. B.; Oh, S.; Gohndrone, T. R.; Morales-Collazo, O.; Seo, S.; Brennecke, J. F.; Schneider, W. F. *J. Phys. Chem. B* **2016**, *120*, 1509–1517.
- [72] Anderson, K.; Atkins, M. P.; Estager, J.; Kuah, Y.; Ng, S.; Oliferenko, A. A.; Plechkova, N. V.; Puga, A. V.; Seddon, K. R.; Wassell, D. F. *Green Chem.* **2015**, *17*, 4340–4354.
- [73] Luo, X.; Guo, Y.; Ding, F.; Zhao, H.; Cui, G.; Li, H.; Wang, C. *Angew. Chem.* **2014**, *126*, 7173–7177.
- [74] Luo, X.; Guo, Y.; Ding, F.; Zhao, H.; Cui, G.; Li, H.; Wang, C. *Angew. Chem. Int. Ed.* **2014**, *53*, 7053–7057.
- [75] Ding, F.; He, X.; Luo, X.; Lin, W.; Chen, K.; Li, H.; Wang, C. *Chem. Commun.* **2014**, *50*, 15041–15044.
- [76] Yang, Q.; Wang, Z.; Bao, Z.; Zhang, Z.; Yang, Y.; Ren, Q.; Xing, H.; Dai, S. *ChemSusChem* **2016**, *9*, 806–812.
- [77] Chen, F.-F.; Huang, K.; Zhou, Y.; Tian, Z.-Q.; Zhu, X.; Tao, D.-J.; Jiang, D.-e.; Dai, S. *Angew. Chem.* **2016**, DOI: 10.1002/ange.201602919.
- [78] Chen, F.-F.; Huang, K.; Zhou, Y.; Tian, Z.-Q.; Zhu, X.; Tao, D.-J.; Jiang, D.-e.; Dai, S. *Angew. Chem. Int. Ed.* **2016**, DOI: 10.1002/anie.201602919.
- [79] Huang, J.; Riisager, A.; Wasserscheid, P.; Fehrmann, R. *Chem. Commun.* **2006**, 4027–4029.
- [80] Hong, S. Y.; Im, J.; Palgunadi, J.; Lee, S. D.; Lee, J. S.; Kim, H. S.; Cheong, M.; Jung, K.-D. *Energy Environ. Sci.* **2011**, *4*, 1802–1806.
- [81] Cui, G.; Wang, C.; Zheng, J.; Guo, Y.; Luo, X.; Li, H. *Chem. Commun.* **2012**, *48*, 2633–2635.
- [82] Cui, G.; Zheng, J.; Luo, X.; Lin, W.; Ding, F.; Li, H.; Wang, C. *Angew. Chem.* **2013**, *125*, 10814–10818.
- [83] Cui, G.; Zheng, J.; Luo, X.; Lin, W.; Ding, F.; Li, H.; Wang, C. *Angew. Chem. Int. Ed.* **2013**, *52*, 10620–10624.

- [84] Cui, G.; Huang, Y.; Zhang, R.; Zhang, F.; Wang, J. *RSC Adv.* **2015**, *5*, 60975–60982.
- [85] Cui, G.; Zhang, F.; Zhou, X.; Li, H.; Wang, J.; Wang, C. *Chem. Eur. J.* **2015**, *21*, 5632–5639.
- [86] Wang, C.; Cui, G.; Luo, X.; Xu, Y.; Li, H.; Dai, S. *J. Am. Chem. Soc.* **2011**, *133*, 11916–11919.
- [87] Yang, D.; Hou, M.; Ning, H.; Ma, J.; Kang, X.; Zhang, J.; Han, B. *ChemSusChem* **2013**, *6*, 1191–1195.
- [88] Cui, G.; Lin, W.; Ding, F.; Luo, X.; He, X.; Li, H.; Wang, C. *Green Chem.* **2014**, *16*, 1211–1216.
- [89] Chen, K.; Lin, W.; Yu, X.; Luo, X.; Ding, F.; He, X.; Li, H.; Wang, C. *AIChE J.* **2015**, *61*, 2028–2034.
- [90] Cui, G.; Zhang, F.; Zhou, X.; Huang, Y.; Xuan, X.; Wang, J. *ACS Sustainable Chem. Eng.* **2015**, *3*, 2264–2270.
- [91] Wang, C.; Zheng, J.; Cui, G.; Luo, X.; Guo, Y.; Li, H. *Chem. Commun.* **2013**, *49*, 1166–1168.
- [92] Zeng, S.; Gao, H.; Zhang, X.; Dong, H.; Zhang, X.; Zhang, S. *Chem. Eng. J.* **2014**, *251*, 248–256.
- [93] Huang, K.; Wang, G.-N.; Dai, Y.; Wu, Y.-T.; Hu, X.-B.; Zhang, Z.-B. *RSC Adv.* **2013**, *3*, 16264–16269.
- [94] Yuan, X. L.; Zhang, S. J.; Lu, X. M. *J. Chem. Eng. Data* **2007**, *52*, 596–599.
- [95] Jakob, A.; Grensemann, H.; Lohmann, J.; Gmehling, J. *Ind. Eng. Chem. Res.* **2006**, *45*, 7924–7933.
- [96] Klamt, A. *J. Phys. Chem.* **1995**, *99*, 2224–2235.
- [97] Lin, S.-T.; Sandler, S. I. *Ind. Eng. Chem. Res.* **2002**, *41*, 899–913.
- [98] Hildebrand, J. H.; Prausnitz, J. M.; Scott, R. L. *Regular and Related Solutions*; Van Nostrand-Reinhold: New York, 1970.

- [99] Oliferenko, A. A.; Oliferenko, P. V.; Seddon, K. R.; Torrecilla, J. S. *Phys. Chem. Chem. Phys.* **2011**, *13*, 17262–17272.
- [100] You, S.-S.; Yoo, K.-P.; Lee, C. S. *Fluid Phase Equilib.* **1994**, *93*, 193–213.
- [101] You, S.-S.; Yoo, K.-P.; Lee, C. S. *Fluid Phase Equilib.* **1994**, *93*, 215–232.
- [102] Skjold-Jørgensen, S. *Fluid Phase Equilib.* **1984**, *16*, 317–351.
- [103] Skjold-Jørgensen, S. *Ind. Eng. Chem. Res.* **1988**, *27*, 110–118.
- [104] Gross, J.; Sadowski, G. *Ind. Eng. Chem. Res.* **2001**, *40*, 1244–1260.
- [105] Zhang, X.; Liu, Z.; Wang, W. *AIChE J.* **2008**, *54*, 2717–2728.
- [106] Maiti, A. *ChemSusChem* **2009**, *2*, 628–631.
- [107] Sumon, K. Z.; Henni, A. *Fluid Phase Equilib.* **2011**, *310*, 39–55.
- [108] Gonzalez-Miquel, M.; Talreja, M.; Ethier, A. L.; Flack, K.; Switzer, J. R.; Biddinger, E. J.; Pollet, P.; Palomar, J.; Rodriguez, F.; Eckert, C. A.; Liotta, C. L. *Ind. Eng. Chem. Res.* **2012**, *51*, 16066–16073.
- [109] Palomar, J.; Gonzalez-Miquel, M.; Polo, A.; Rodriguez, F. *Ind. Eng. Chem. Res.* **2011**, *50*, 3452–3463.
- [110] Lee, B.-S.; Lin, S.-T. *Chem. Eng. Sci.* **2015**, *121*, 157–168.
- [111] García, G.; Atilhan, M.; Aparicio, S. *Phys. Chem. Chem. Phys.* **2015**, *17*, 13559–13574.
- [112] Allen, M. P.; Tildesley, D. J. *Computer Simulation of Liquids*; Oxford University Press: New York, 1989.
- [113] Smit, B. *Mol. Phys.* **1995**, *85*, 153–172.
- [114] Cadena, C.; Anthony, J. L.; Shah, J. K.; Morrow, T. I.; Brennecke, J. F.; Maginn, E. J. *J. Am. Chem. Soc.* **2004**, *126*, 5300–5308.
- [115] Deschamps, J.; Costa Gomes, M. F.; Pádua, A. A. *ChemPhysChem* **2004**, *5*, 1049–1052.
- [116] Huang, X.; Margulis, C. J.; Li, Y.; Berne, B. J. *J. Am. Chem. Soc.* **2005**, *127*, 17842–17851.

- [117] Wang, Y.; Pan, H.; Li, H.; Wang, C. *J. Phys. Chem. B* **2007**, *111*, 10461–10467.
- [118] Gutowski, K. E.; Maginn, E. J. *J. Am. Chem. Soc.* **2008**, *130*, 14690–14704.
- [119] Zhang, X.; Huo, F.; Liu, Z.; Wang, W.; Shi, W.; Maginn, E. J. *J. Phys. Chem. B* **2009**, *113*, 7591–7598.
- [120] Maginn, E. J. *J. Phys. Condens. Matter* **2009**, *21*, 373101.
- [121] Wick, C. D.; Chang, T.-M.; Dang, L. X. *J. Phys. Chem. B* **2010**, *114*, 14965–14971.
- [122] Babarao, R.; Dai, S.; Jiang, D.-e. *J. Phys. Chem. B* **2011**, *115*, 9789–9794.
- [123] Perez-Blanco, M. E.; Maginn, E. J. *J. Phys. Chem. B* **2011**, *115*, 10488–10499.
- [124] Wu, H.; Shah, J. K.; Tenney, C. M.; Rosch, T. W.; Maginn, E. J. *Ind. Eng. Chem. Res.* **2011**, *50*, 8983–8993.
- [125] Aparicio, S.; Atilhan, M. *J. Phys. Chem. B* **2012**, *116*, 9171–9185.
- [126] Mohammadi, M.; Foroutan, M. *J. Mol. Liq.* **2014**, *193*, 60–68.
- [127] Gupta, K. M.; Jiang, J. *J. Phys. Chem. B* **2014**, *118*, 3110–3118.
- [128] Mondal, A.; Balasubramanian, S. *J. Phys. Chem. B* **2016**,
- [129] Gupta, K. M. *Fluid Phase Equilib.* **2016**, *415*, 34–41.
- [130] Tian, Z.; Dai, S.; Jiang, D.-e. *WIREs Comput. Mol. Sci.* **2016**, *6*, 173–197.
- [131] Shah, J. K.; Maginn, E. J. *Fluid Phase Equilib.* **2004**, *222*, 195–203.
- [132] Urukova, I.; Vorholz, J.; Maurer, G. *J. Phys. Chem. B* **2005**, *109*, 12154–12159.
- [133] Shi, W.; Maginn, E. J. *J. Phys. Chem. B* **2008**, *112*, 2045–2055.
- [134] Kerlé, D.; Ludwig, R.; Geiger, A.; Paschek, D. *J. Phys. Chem. B* **2009**, *113*, 12727–12735.
- [135] Ghobadi, A. F.; Taghikhani, V.; Elliott, J. R. *J. Phys. Chem. B* **2011**, *115*, 13599–13607.
- [136] Liu, H.; Dai, S.; Jiang, D.-e. *J. Phys. Chem. B* **2014**, *118*, 2719–2725.

- [137] Ramdin, M.; Balaji, S. P.; Vicent-Luna, J. M.; Gutiérrez-Sevillano, J. J.; Calero, S.; de Loos, T. W.; Vlugt, T. J. *J. Phys. Chem. C* **2014**, *118*, 23599–23604.
- [138] Li, A.; Tian, Z.; Yan, T.; Jiang, D.-e.; Dai, S. *J. Phys. Chem. B* **2014**, *118*, 14880–14887.
- [139] Zhang, B.; van Duin, A. C.; Johnson, J. K. *J. Phys. Chem. B* **2014**, *118*, 12008–12016.
- [140] Zeng, S.; Zhang, X.; Gao, H.; He, H.; Zhang, X.; Zhang, S. *Ind. Eng. Chem. Res.* **2015**, *54*, 10854–10862.
- [141] Bhargava, B.; Balasubramanian, S. *Chem. Phys. Lett.* **2007**, *444*, 242–246.
- [142] Mindrup, E. M.; Schneider, W. F. *ACS Symposium Series 1030 Ionic Liquids: From Knowledge to Application*; (Eds.: N. V. Plechkova, R. D. Rogers, K. R. Seddon), American Chemical Society: Washington, DC, 2009; pp 419–430.
- [143] Teague, C. M.; Dai, S.; Jiang, D.-e. *J. Phys. Chem. A* **2010**, *114*, 11761–11767.
- [144] Wu, C.; Senftle, T. P.; Schneider, W. F. *Phys. Chem. Chem. Phys.* **2012**, *14*, 13163–13170.
- [145] Izgorodina, E. I.; Hodgson, J. L.; Weis, D. C.; Pas, S. J.; MacFarlane, D. R. *J. Phys. Chem. B* **2015**, *119*, 11748–11759.
- [146] García, G.; Atilhan, M.; Aparicio, S. *Phys. Chem. Chem. Phys.* **2015**, *17*, 26875–26891.
- [147] Grimme, S. *Chem. Eur. J.* **2012**, *18*, 9955–9964.
- [148] Brehm, M.; Kirchner, B. *J. Chem. Inf. Model.* **2011**, *51*, 2007–2023.
- [149] Hollóczki, O.; Kelemen, Z.; Könczöl, L.; Szieberth, D.; Nyulászi, L.; Stark, A.; Kirchner, B. *ChemPhysChem* **2013**, *14*, 315–320.
- [150] Shi, W.; Myers, C. R.; Luebke, D. R.; Steckel, J. A.; Sorescu, D. C. *J. Phys. Chem. B* **2012**, *116*, 283–295.
- [151] Born, M.; Oppenheimer, R. *Ann. Phys. (Berlin)* **1927**, *389*, 457–484.
- [152] Hartree, D. R. *Mathematical Proceedings of the Cambridge Philosophical Society*; Cambridge Univ. Press: Cambridge, 1928; Vol. 24; pp 89–110.
- [153] Fock, V. *Z. Phys.* **1930**, *61*, 126–148.

- [154] Szabo, A.; Ostlund, N. S. *Modern quantum chemistry: introduction to advanced electronic structure theory*; Dover Publications: New York, 1989.
- [155] Levine, I. N. *Quantum chemistry*; Prentice Hall: New Jersey, 1991.
- [156] Lee, T. J.; Scuseria, G. E. *Quantum Mechanical Electronic Structure Calculations with Chemical Accuracy*; (Ed.: S. R. Langhoff), Springer Netherlands: Dordrecht, 1995; pp 47–108.
- [157] Riplinger, C.; Neese, F. *J. Chem. Phys.* **2013**, *138*, 034106.
- [158] Liakos, D. G.; Sparta, M.; Kesharwani, M. K.; Martin, J. M. L.; Neese, F. *J. Chem. Theory Comput.* **2015**, *11*, 1525–1539.
- [159] Liakos, D. G.; Neese, F. *J. Chem. Theory Comput.* **2015**, *11*, 4054–4063.
- [160] Kohn, W.; Sham, L. J. *Phys. Rev.* **1965**, *140*, A1133–A1138.
- [161] Gross, E. K. U.; Dreizler, R. M. *Density Functional Theory*; Springer: Berlin, 2013.
- [162] Vosko, S.; Wilk, L.; Nusair, M. *Can. J. Phys.* **1980**, *58*, 1200–1211.
- [163] Becke, A. D. *Phys. Rev. A* **1988**, *38*, 3098–3100.
- [164] Lee, C.; Yang, W.; Parr, R. G. *Phys. Rev. B* **1988**, *37*, 785–789.
- [165] Perdew, J. P.; Burke, K.; Ernzerhof, M. *Phys. Rev. Lett.* **1996**, *77*, 3865–3868.
- [166] Perdew, J. P.; Burke, K.; Ernzerhof, M. *Phys. Rev. Lett.* **1997**, *78*, 1396–1396.
- [167] Tao, J.; Perdew, J. P.; Staroverov, V. N.; Scuseria, G. E. *Phys. Rev. Lett.* **2003**, *91*, 146401.
- [168] Stephens, P. J.; Devlin, F. J.; Chabalowski, C. F.; Frisch, M. J. *J. Phys. Chem.* **1994**, *98*, 11623–11627.
- [169] Zhao, Y.; Truhlar, D. G. *J. Phys. Chem. A* **2005**, *109*, 5656–5667.
- [170] Grimme, S. *J. Chem. Phys.* **2006**, *124*, 034108.
- [171] Grimme, S.; Antony, J.; Ehrlich, S.; Krieg, H. *J. Chem. Phys.* **2010**, *132*, 154104.

- [172] Grimme, S.; Ehrlich, S.; Goerigk, L. *J. Comput. Chem.* **2011**, *32*, 1456–1465.
- [173] Vydrov, O. A.; Van Voorhis, T. *J. Chem. Phys.* **2010**, *133*, 244103.
- [174] Tkatchenko, A.; DiStasio Jr, R. A.; Car, R.; Scheffler, M. *Phys. Rev. Lett.* **2012**, *108*, 236402.
- [175] Goerigk, L.; Grimme, S. *Phys. Chem. Chem. Phys.* **2011**, *13*, 6670–6688.
- [176] Burns, L. A.; Vázquez-Mayagoitia, Á.; Sumpter, B. G.; Sherrill, C. D. *J. Chem. Phys.* **2011**, *134*, 084107.
- [177] Goerigk, L. *J. Chem. Theory Comput.* **2014**, *10*, 968–980.
- [178] Zahn, S.; Kirchner, B. *J. Phys. Chem. A* **2008**, *112*, 8430–8435.
- [179] Izgorodina, E. I.; Bernard, U. L.; MacFarlane, D. R. *J. Phys. Chem. A* **2009**, *113*, 7064–7072.
- [180] Pensado, A. S.; Brehm, M.; Thar, J.; Seitsonen, A. P.; Kirchner, B. *ChemPhysChem* **2012**, *13*, 1845–1853.
- [181] Grimme, S.; Hujó, W.; Kirchner, B. *Phys. Chem. Chem. Phys.* **2012**, *14*, 4875–4883.
- [182] Klamt, A.; Schüürmann, G. *J. Chem. Soc., Perkin Trans. 2* **1993**, 799–805.
- [183] Klamt, A. *WIREs Comput. Mol. Sci.* **2011**, *1*, 699–709.
- [184] Car, R.; Parrinello, M. *Phys. Rev. Lett.* **1985**, *55*, 2471–2474.
- [185] Kresse, G.; Hafner, J. *Phys. Rev. B* **1993**, *47*, 558–561.
- [186] Marx, D.; Hutter, J. *Ab initio molecular dynamics: basic theory and advanced methods*; Cambridge University Press: Cambridge, 2009.
- [187] CP2K Open Source Molecular Dynamics Home Page. Oficial Webpage: <http://www.cp2k.org> (accessed March 01, 2013).
- [188] VandeVondele, J.; Krack, M.; Mohamed, F.; Parrinello, M.; Chassaing, T.; Hutter, J. *Comput. Phys. Commun.* **2005**, *167*, 103–128.

- [189] McQuarrie, D. A. *Statistical Thermodynamics*; HarperCollins Publishers: New York, 1973.
- [190] Pitzer, K. S.; Gwinn, W. D. *J. Chem. Phys.* **1942**, *10*, 428–440.
- [191] Umer, M.; Leonhard, K. *J. Phys. Chem. A* **2013**, *117*, 1569–1582.
- [192] Klamt, A. *COSMO-RS: From Quantum Chemistry to Fluid Phase Thermodynamics and Drug Design*; Elsevier: Amsterdam, 2005.
- [193] Sudha, S. Y.; Khanna, A. *World Acad. Sci., Eng. Technol* **2009**, *57*, 539–542.
- [194] Indarto, A.; Palgunadi, J. *Ionics* **2012**, *18*, 143–150.
- [195] Gonzalez-Miquel, M.; Bedia, J.; Abrusci, C.; Palomar, J.; Rodriguez, F. *J. Phys. Chem. B* **2013**, *117*, 3398–3406.
- [196] Dang, L. X.; Wick, C. D. *J. Phys. Chem. B* **2011**, *115*, 6964–6970.
- [197] Thomas, M.; Brehm, M.; Hollóczki, O.; Kelemen, Z.; Nyulási, L.; Pasinszki, T.; Kirchner, B. *J. Chem. Phys.* **2014**, *141*, 024510.
- [198] Thompson, R. L.; Shi, W.; Albenze, E.; Kusuma, V. A.; Hopkinson, D.; Damodaran, K.; Lee, A. S.; Kitchin, J. R.; Luebke, D. R.; Nulwala, H. *R. Soc. Chem. Adv.* **2014**, *4*, 12748–12755.
- [199] Sumida, K.; Rogow, D. L.; Mason, J. A.; McDonald, T. M.; Bloch, E. D.; Herm, Z. R.; Bae, T.-H.; Long, J. R. *Chem. Rev.* **2011**, *112*, 724–781.
- [200] Pera-Titus, M. *Chem. Rev.* **2014**, *114*, 1413–1492.
- [201] Pan, M.; Wang, C. *Advances in CO₂ Capture, Sequestration, and Conversion*; 2015; Chapter 15, pp 341–369.
- [202] Rackley, S. *Carbon capture and storage*; Elsevier: Oxford, 2009.
- [203] Welton, T. *Proc. R. Soc. A* **2015**, *471*, 20150502.
- [204] Hagewiesche, D. P.; Ashour, S. S.; Al-Ghawas, H. A.; Sandall, O. C. *Chem. Eng. Sci.* **1995**, *50*, 1071–1079.
- [205] Liao, C.-H.; Li, M.-H. *Chem. Eng. Sci.* **2002**, *57*, 4569–4582.

- [206] Ramachandran, N.; Aboudheir, A.; Idem, R.; Tontiwachwuthikul, P. *Ind. Eng. Chem. Res.* **2006**, *45*, 2608–2616.
- [207] Heldebrant, D. J.; Yonker, C. R.; Jessop, P. G.; Phan, L. *Energy Environ. Sci.* **2008**, *1*, 487–493.
- [208] Gurkan, B. E.; Gohndrone, T. R.; McCready, M. J.; Brennecke, J. F. *Phys. Chem. Chem. Phys.* **2013**, *15*, 7796–7811.
- [209] Anderson, J. L.; Dixon, J. K.; Brennecke, J. F. *Acc. Chem. Res.* **2007**, *40*, 1208–1216.
- [210] Fukumoto, K.; Yoshizawa, M.; Ohno, H. *J. Am. Chem. Soc.* **2005**, *127*, 2398–2399.
- [211] Ohno, H.; Fukumoto, K. *Acc. Chem. Res.* **2007**, *40*, 1122–1129.
- [212] Caplow, M. *J. Am. Chem. Soc.* **1968**, *90*, 6795–6803.
- [213] Mindrup, E. M.; Schneider, W. F. *ChemSusChem* **2010**, *3*, 931–938.
- [214] Xie, H.-B.; Johnson, J. K.; Perry, R. J.; Genovese, S.; Wood, B. R. *J. Phys. Chem. A* **2010**, *115*, 342–350.
- [215] Guido, C. A.; Pietrucci, F.; Gallet, G. A.; Andreoni, W. *J. Chem. Theory Comput.* **2012**, *9*, 28–32.
- [216] Ma, C.; Pietrucci, F.; Andreoni, W. *J. Phys. Chem. Lett.* **2014**, *5*, 1672–1677.
- [217] Ma, C.; Pietrucci, F.; Andreoni, W. *J. Chem. Theory Comput.* **2015**, *11*, 3189–3198.
- [218] Gangarapu, S.; Marcelis, A. T. M.; Alhamed, Y. A.; Zuilhof, H. *ChemPhysChem* **2015**, 3000–3006.
- [219] Zhang, Y.; Yu, P.; Luo, Y. *Chem. Eng. J.* **2013**, *214*, 355–363.
- [220] Niedermaier, I.; Bahlmann, M.; Papp, C.; Kolbeck, C.; Wei, W.; Krick Calderón, S.; Grabau, M.; Schulz, P. S.; Wasserscheid, P.; Steinrück, H.-P.; Maier, F. *J. Am. Chem. Soc.* **2014**, *136*, 436–441.
- [221] Zhang, J.; Zhang, S.; Dong, K.; Zhang, Y.; Shen, Y.; Lv, X. *Chem. Eur. J.* **2006**, *12*, 4021–4026.

- [222] Jiang, Y.-Y.; Wang, G.-N.; Zhou, Z.; Wu, Y.-T.; Geng, J.; Zhang, Z.-B. *Chem. Commun.* **2008**, 505–507.
- [223] Wang, X.; Akhmedov, N. G.; Duan, Y.; Luebke, D.; Li, B. *J. Mater. Chem. A* **2013**, *1*, 2978–2982.
- [224] Saravanamurugan, S.; Kunov-Kruse, A. J.; Fehrmann, R.; Riisager, A. *ChemSusChem* **2014**, *7*, 897–902.
- [225] Ma, J.-w.; Zhou, Z.; Zhang, F.; Fang, C.-g.; Wu, Y.-t.; Zhang, Z.-b.; Li, A.-m. *Environ. Sci. Technol.* **2011**, *45*, 10627–10633.
- [226] McDonald, J. L.; Sykora, R. E.; Hixon, P.; Mirjafari, A.; Davis Jr, J. H. *Env. Chem. Lett.* **2014**, *12*, 201–208.
- [227] Gouveia, A. S.; Tomé, L. C.; Marrucho, I. M. *J. Membr. Sci.* **2016**, *510*, 174–181.
- [228] Gouveia, A. S.; Tomé, L. C.; Marrucho, I. M. *J. Chem. Eng. Data* **2016**, *61*, 83–93.
- [229] Wang, X.; Akhmedov, N. G.; Duan, Y.; Luebke, D.; Hopkinson, D.; Li, B. *ACS Appl. Mater. Interfaces* **2013**, *5*, 8670–8677.
- [230] Luo, X. Y.; Fan, X.; Shi, G. L.; Li, H. R.; Wang, C. M. *J. Phys. Chem. B* **2016**, *120*, 2807–2813.
- [231] Kolding, H.; Fehrmann, R.; Riisager, A. *Sci. China Chem.* **2012**, *55*, 1648–1656.
- [232] Hutter, J.; Iannuzzi, M.; Schiffmann, F.; VandeVondele, J. *WIREs Comput. Mol. Sci.* **2014**, *4*, 15–25.
- [233] Laio, A.; Parrinello, M. *Proc. Natl. Acad. Sci. U.S.A.* **2002**, *99*, 12562–12566.
- [234] Firaha, D. S.; Hollóczki, O.; Kirchner, B. *Angew. Chem.* **2015**, *127*, 7916–7920.
- [235] Firaha, D. S.; Hollóczki, O.; Kirchner, B. *Angew. Chem. Int. Ed.* **2015**, *54*, 7805–7809.
- [236] Paulechka, E.; Diky, V.; Kazakov, A.; Kroenlein, K.; Frenkel, M. *J. Chem. Eng. Data* **2015**, *60*, 3554–3561.
- [237] Eckert, F.; Klamt, A. COSMOtherm, Version C3, Release 14.01. COSMOlogic GmbH & Co”, 2013.

- [238] Hollóczki, O.; Gerhard, D.; Massone, K.; Szarvas, L.; Németh, B.; Veszprémi, T.; Nyulászi, L. *New J. Chem.* **2010**, *34*, 3004–3009.
- [239] Hollóczki, O.; Firaha, D. S.; Friedrich, J.; Brehm, M.; Cybik, R.; Wild, M.; Stark, A.; Kirchner, B. *J. Phys. Chem. B* **2013**, *117*, 5898–5907.
- [240] Song, H.-J.; Park, S.; Kim, H.; Gaur, A.; Park, J.-W.; Lee, S.-J. *Int. J. Greenhouse Gas Control* **2012**, *11*, 64–72.
- [241] Atkin, R.; Warr, G. G. *J. Phys. Chem. B* **2008**, *112*, 4164–4166.
- [242] Greaves, T. L.; Kennedy, D. F.; Mudie, S. T.; Drummond, C. J. *J. Phys. Chem. B* **2010**, *114*, 10022–10031.
- [243] Hayes, R.; Imberti, S.; Warr, G. G.; Atkin, R. *Phys. Chem. Chem. Phys.* **2011**, *13*, 3237–3247.
- [244] Scurto, A. M.; Aki, S. N. V. K.; Brennecke, J. F. *J. Am. Chem. Soc.* **2002**, *124*, 10276–10277.
- [245] Jutz, F.; Andanson, J.-M.; Baiker, A. *Chem. Rev.* **2011**, *111*, 322–353.
- [246] Canongia Lopes, J. N. A.; Pádua, A. A. H. *J. Phys. Chem. B* **2006**, *110*, 3330–3335.
- [247] Triolo, A.; Russina, O.; Bleif, H.-J.; Di Cola, E. *J. Phys. Chem. B* **2007**, *111*, 4641–4644.
- [248] Weber, H.; Hollóczki, O.; Pensado, A. S.; Kirchner, B. *J. Chem. Phys.* **2013**, *139*, 084502.
- [249] Canongia Lopes, J. N.; Costa Gomes, M. F.; Pádua, A. A. H. *J. Phys. Chem. B* **2006**, *110*, 16816–16818.
- [250] Greaves, T. L.; Drummond, C. J. *Chem. Rev.* **2008**, *108*, 206–237.
- [251] Yoshizawa, M.; Xu, W.; Angell, C. A. *J. Am. Chem. Soc.* **2003**, *125*, 15411–15419.
- [252] Stoimenovski, J.; Izgorodina, E. I.; MacFarlane, D. R. *Phys. Chem. Chem. Phys.* **2010**, *12*, 10341–10347.
- [253] Walden, P. *Bull. Acad. Imper. Sci. (St. Petersburg.)* **1914**, *8*, 405–422.
- [254] Shiflett, M.; Niehaus, A.; Elliott, B.; Yokozeki, A. *Int. J. Thermophys.* **2012**, *33*, 412–436.

- [255] Song, X.; Hamano, H.; Minofar, B.; Kanzaki, R.; Fujii, K.; Kameda, Y.; Kohara, S.; Watanabe, M.; Ishiguro, S.-i.; Umebayashi, Y. *J. Phys. Chem. B* **2012**, *116*, 2801–2813.
- [256] Bodo, E.; Sferrazza, A.; Caminiti, R.; Mangialardo, S.; Postorino, P. *J. Chem. Phys.* **2013**, *139*, 144309.
- [257] Zahn, S.; Thar, J.; Kirchner, B. *J. Chem. Phys.* **2010**, *132*, 124506.
- [258] Fumino, K.; Wulf, A.; Ludwig, R. *Angew. Chem. Int. Ed.* **2009**, *48*, 3184–3186.
- [259] Fumino, K.; Wulf, A.; Ludwig, R. *Angew. Chem.* **2009**, *121*, 3230–3233.
- [260] VandeVondele, J.; Hutter, J. *J. Chem. Phys.* **2003**, *118*, 4365–4369.
- [261] VandeVondele, J.; Hutter, J. *J. Chem. Phys.* **2007**, *127*, 114105.
- [262] Goedecker, S.; Teter, M.; Hutter, J. *Phys. Rev. B* **1996**, *54*, 1703–1710.
- [263] Hartwigsen, C.; Goedecker, S.; Hutter, J. *Phys. Rev. B* **1998**, *58*, 3641–3662.
- [264] Krack, M. *Theor. Chem. Acc.* **2005**, *114*, 145–152.
- [265] Nosé, S. *J. Chem. Phys.* **1984**, *81*, 511–519.
- [266] Hoover, W. G. *Phys. Rev. A* **1985**, *31*, 1695–1697.
- [267] Martyna, G. J.; Klein, M. L.; Tuckerman, M. *J. Chem. Phys.* **1992**, *97*, 2635–2643.
- [268] Medvedev, N. N.; Voloshin, V. P.; Luchnikov, V. A.; Gavrilova, M. L. Calculation of the Voronoi S-network (Additively weighted Voronoi Diagram). Novosibirsk State University, <http://www.kinetics.nsc.ru/mds/?Software:VNP> (accessed January 15, 2014).
- [269] Python Programming Language. Official Website: <http://www.python.org> (accessed January 15, 2014).
- [270] The PyMOL Molecular Graphics System, Version 1.3, Schrödinger, LLC. Official Website: <http://www.pymol.org> (accessed July 10, 2013).
- [271] Gnuplot. Home Page: <http://www.gnuplot.info> (accessed October 10, 2012).
- [272] Leary, T. J. C.; Levin, I. W. *J. Phys. Chem.* **1984**, *88*, 4074–4078.

- [273] Kazarian, S. G.; Briscoe, B. J.; Welton, T. *Chem. Commun.* **2000**, 2047–2048.
- [274] Bodo, E.; Postorino, P.; Mangialardo, S.; Piacente, G.; Ramondo, F.; Bosi, F.; Ballirano, P.; Caminiti, R. *J. Phys. Chem. B* **2011**, *115*, 13149–13161.
- [275] Hayes, R.; Imberti, S.; Warr, G. G.; Atkin, R. *Angew. Chem. Int. Ed.* **2013**, *52*, 4623–4627.
- [276] Hayes, R.; Imberti, S.; Warr, G. G.; Atkin, R. *Angew. Chem.* **2013**, *125*, 4721–4725.
- [277] Kanzaki, R.; Uchida, K.; Song, X.; Umebayashi, Y.; Ishiguro, S.-i. *Anal. Sci.* **2008**, *24*, 1347–1349.
- [278] Sowmiah, S.; Srinivasadesikan, V.; Tseng, M.-C.; Chu, Y.-H. *Molecules* **2009**, *14*, 3780–3813.
- [279] Voronoi, G. F. *J. Reine Angew. Math.* **1909**, *136*, 67–182.
- [280] Medvedev, N. N.; Voloshin, V. P.; Luchnikov, V. A.; Gavrilova, M. L. *J. Comput. Chem.* **2006**, *27*, 1676–1692.
- [281] Anthony, J. L.; Maginn, E. J.; Brennecke, J. F. *J. Phys. Chem. B* **2002**, *106*, 7315–7320.
- [282] Aki, S. N. V. K.; Mellein, B. R.; Saurer, E. M.; Brennecke, J. F. *J. Phys. Chem. B* **2004**, *108*, 20355–20365.
- [283] United States Environmental Protection Agency. Sulfur Dioxide. Air Emission Sources. Webpage: <http://www.epa.gov/air/emissions/so2.htm> (2011). (Accessed 12 September 2014).
- [284] Ma, X.; Kaneko, T.; Tashimo, T.; Yoshida, T.; Kato, K. *Chem. Eng. Sci.* **2000**, *55*, 4643–4652.
- [285] Luis, P.; Garea, A.; Irabien, A. *J. Membr. Sci.* **2009**, *330*, 80–89.
- [286] Lei, Z.; Dai, C.; Chen, B. *Chem. Rev.* **2014**, *114*, 1289–1326.
- [287] Lee, K. Y.; Kim, C. S.; Kim, H.; Cheong, M.; Mukherjee, D. K.; Jung, K.-D. *Bull. Korean Chem. Soc.* **2010**, *31*, 1937–1940.
- [288] Siqueira, L. J. A.; Ando, R. A.; Bazito, F. F. C.; Torresi, R. M.; Santos, P. S.; Ribeiro, M. C. C. *J. Phys. Chem. B* **2008**, *112*, 6430–6435.

- [289] Yokozeki, A.; Shiflett, M. B. *Appl. Energ.* **2007**, *84*, 1258–1273.
- [290] Kim, J. E.; Kim, H. J.; Lim, J. S. *Fluid Phase Equilib.* **2014**, *367*, 151–158.
- [291] Thar, J.; Brehm, M.; Seitsonen, A. P.; Kirchner, B. *J. Phys. Chem. B* **2009**, *113*, 15129–15132.
- [292] Brüssel, M.; Brehm, M.; Pensado, A. S.; Malberg, F.; Ramzan, M.; Stark, A.; Kirchner, B. *Phys. Chem. Chem. Phys.* **2012**, *14*, 13204–13215.
- [293] Firaha, D. S.; Kirchner, B. *J. Chem. Eng. Data* **2014**, *59*, 3098–3104.
- [294] Neese, F. *WIREs Comput. Mol. Sci.* **2012**, *2*, 73–78.
- [295] Neese, F. ORCA – An Ab Initio, Density Functional and Semiempirical Program Package, V. 3.0. Max-Planck Institut für Chemische Energiekonversion, 2015.
- [296] Thomas, M.; Brehm, M.; Fligg, R.; Vohringer, P.; Kirchner, B. *Phys. Chem. Chem. Phys.* **2013**, *15*, 6608–6622.
- [297] Kirchner, B.; Hollóczki, O.; Lopes, J. N. C.; Pádua, A. A. H. *WIREs Comput. Mol. Sci.* **2015**, 202–214.
- [298] Kossmann, S.; Thar, J.; Kirchner, B.; Hunt, P. A.; Welton, T. *J. Chem. Phys.* **2006**, *124*, 174506.
- [299] Yang, Z.-Z.; He, L.-N.; Song, Q.-W.; Chen, K.-H.; Liu, A.-H.; Liu, X.-M. *Phys. Chem. Chem. Phys.* **2012**, *14*, 15832–15839.
- [300] Wasif, S.; Salama, S. B. *J. Chem. Soc., Dalton Trans.* **1973**, 2148–2150.
- [301] Downs, A. J.; Edwards, A. J.; Martin, R. E.; Parsons, S. *J. Chem. Soc., Dalton Trans.* **1994**, 753–757.
- [302] Kornath, A.; Blecher, O.; Ludwig, R. *Z. Anorg. Allg. Chem.* **2000**, *626*, 731–735.
- [303] Oh, J. J.; Hillig, K. W.; Kuczkowski, R. L. *Inorg. Chem.* **1991**, *30*, 4583–4588.
- [304] Shelton, R. D.; Nielsen, A. H.; Fletcher, W. H. *J. Chem. Phys.* **1953**, *21*, 2178–2183.
- [305] Kornath, A.; Blecher, O.; Ludwig, R. *J. Am. Chem. Soc.* **1999**, *121*, 4019–4022.

- [306] Besnard, M.; Cabaço, M. I.; Chávez, F. V.; Pinaud, N.; Sebastião, P. J.; Coutinho, J. A. P.; Danten, Y. *Chem. Commun.* **2012**, *48*, 1245–1247.
- [307] Cabaço, M. I.; Besnard, M.; Danten, Y.; Coutinho, J. A. P. *J. Phys. Chem. A* **2012**, *116*, 1605–1620.
- [308] Besnard, M.; Cabaço, M. I.; Vaca Chávez, F.; Pinaud, N.; Sebastião, P. J.; Coutinho, J. A. P.; Mascetti, J.; Danten, Y. *J. Phys. Chem. A* **2012**, *116*, 4890–4901.
- [309] Skarmoutsos, I.; Dellis, D.; Matthews, R. P.; Welton, T.; Hunt, P. A. *J. Phys. Chem. B* **2012**, *116*, 4921–4933.
- [310] Hunt, P. A.; Gould, I. R.; Kirchner, B. *Aust. J. Chem.* **2007**, *60*, 9–14.
- [311] Hunt, P. A.; Kirchner, B.; Welton, T. *Chem. Eur. J.* **2006**, *12*, 6762–6775.
- [312] Zahn, S.; Bruns, G.; Thar, J.; Kirchner, B. *Phys. Chem. Chem. Phys.* **2008**, *10*, 6921–6924.
- [313] Wasserscheid, P.; Welton, T. *Ionic Liquids in Synthesis*; Wiley-VCH Verlag: Weinheim, 2008.
- [314] Rogers, R. D.; Seddon, K. R.; Volkov, S. *Green Industrial Applications of Ionic Liquids*; Kluwer Academic Publisher: Dodrecht, 2002.
- [315] Welton, T. *Coord. Chem. Rev.* **2004**, *248*, 2459–2477.
- [316] Brennecke, J. F.; Gurkan, B. E. *J. Phys. Chem. Lett.* **2010**, *1*, 3459–3464.
- [317] Schönherr, H.-J.; Wanzlick, H.-W. *Justus Liebigs Ann. Chem.* **1970**, *731*, 176–179.
- [318] Melaimi, M.; Soleilhavoup, M.; Bertrand, G. *Angew. Chem. Int. Ed.* **2010**, *49*, 8810–8849.
- [319] Melaimi, M.; Soleilhavoup, M.; Bertrand, G. *Angew. Chem.* **2010**, *122*, 8992–9032.
- [320] Díez-González, S. *N-Heterocyclic Carbenes: from Laboratory Curiosities to Efficient Synthetic Tools*; Royal Society of Chemistry: Cambridge, 2011.
- [321] Arduengo, A. J.; Bertrand, G. *Chem. Rev.* **2009**, *109*, 3209–3210.
- [322] Hahn, F. E.; Jahnke, M. C. *Angew. Chem. Int. Ed.* **2008**, *47*, 3122–3172.

- [323] Hahn, F.; Jahnke, M. *Angew. Chem.* **2008**, *120*, 3166–3216.
- [324] Marion, N.; Díez-González, S.; Nolan, S. P. *Angew. Chem. Int. Ed.* **2007**, *46*, 2988–3000.
- [325] Marion, N.; Díez-González, S.; Nolan, S. *Angew. Chem.* **2007**, *119*, 3046–3058.
- [326] Enders, D.; Balensiefer, T. *Acc. Chem. Res.* **2004**, *37*, 534–541.
- [327] Enders, D.; Niemeier, O.; Henseler, A. *Chem. Rev.* **2007**, *107*, 5606–5655.
- [328] Moore, J. L.; Rovis, T. *Asymmetric Organocatalysis*; (Ed.: B. List), Springer: Heidelberg, 2009; pp 118–144.
- [329] Cavallo, L.; Correa, A.; Costabile, C.; Jacobsen, H. *J. Organomet. Chem.* **2005**, *690*, 5407–5413.
- [330] Arnold, P. L.; Pearson, S. *Coord. Chem. Rev.* **2007**, *251*, 596–609.
- [331] Tonner, R.; Heydenrych, G.; Frenking, G. *Chem. Asian J.* **2007**, *2*, 1555–1567.
- [332] Frenking, G.; Solà, M.; Vyboishchikov, S. F. *J. Organomet. Chem.* **2005**, *690*, 6178–6204.
- [333] Díaz-Requejo, M. M.; Pérez, P. J. *J. Organomet. Chem.* **2005**, *690*, 5441–5450.
- [334] Crabtree, R. H. *J. Organomet. Chem.* **2005**, *690*, 5451–5457.
- [335] Díez-González, S.; Marion, N.; Nolan, S. P. *Chem. Rev.* **2009**, *109*, 3612–3676.
- [336] Schuster, O.; Yang, L.; Raubenheimer, H. G.; Albrecht, M. *Chem. Rev.* **2009**, *109*, 3445–3478.
- [337] Kelemen, Z.; Hollóczki, O.; Nagy, J.; Nyulászi, L. *Org. Biomol. Chem.* **2011**, *9*, 5362–5364.
- [338] Rodríguez, H.; Gurau, G.; Holbrey, J. D.; Rogers, R. D. *Chem. Commun.* **2011**, *47*, 3222–3224.
- [339] Brehm, M.; Weber, H.; Pensado, A. S.; Stark, A.; Kirchner, B. *Phys. Chem. Chem. Phys.* **2012**, *14*, 5030–5044.
- [340] Hollóczki, O.; Nyulászi, L. *Electronic Effects in Organic Chemistry*; (Ed.: B. Kirchner), Springer: Heidelberg, 2013; pp 1–24.

- [341] Hallett, J. P.; Liotta, C. L.; Ranieri, G.; Welton, T. *J. Org. Chem.* **2009**, *74*, 1864–1868.
- [342] Lui, M. Y.; Crowhurst, L.; Hallett, J. P.; Hunt, P. A.; Niedermeyer, H.; Welton, T. *Chem. Sci.* **2011**, *2*, 1491–1496.
- [343] Kuhn, N.; Steimann, M.; Weyers, G. *Z. Naturforsch. B* **1999**, *54*, 427–433.
- [344] Shiflett, M. B.; Yokozeki, A. *J. Chem. Eng. Data* **2009**, *54*, 108–114.
- [345] Leal, J. P.; Esperança, J. M.; Minas da Piedade, M. E.; Canongia Lopes, J. N.; Rebelo, L. P.; Seddon, K. R. *J. Phys. Chem. A* **2007**, *111*, 6176–6182.
- [346] Hollóczki, O.; Terleczyk, P.; Szieberth, D.; Mourgas, G.; Gudat, D.; Nyulászi, L. *J. Am. Chem. Soc.* **2011**, *133*, 780–789.
- [347] Aldeco-Perez, E.; Rosenthal, A. J.; Donnadiou, B.; Parameswaran, P.; Frenking, G.; Bertrand, G. *Science* **2009**, *326*, 556–559.
- [348] Malberg, F.; Pensado, A. S.; Kirchner, B. *Phys. Chem. Chem. Phys.* **2012**, *14*, 12079–12082.
- [349] Ahlrichs, R.; Bär, M.; Häser, M.; Horn, H.; Kölmel, C. *Chem. Phys. Lett.* **1989**, *162*, 165–169.
- [350] Eichkorn, K.; Treutler, O.; Oehm, H.; Häser, M.; Ahlrichs, R. *Chem. Phys. Lett.* **1995**, *242*, 652–660.
- [351] Frisch, M. J. et al. Gaussian-09, Revision E.01. Gaussian Inc., Wallingford CT, 2009.
- [352] Tew, D. P.; Klopper, W.; Neiss, C.; Hättig, C. *Phys. Chem. Chem. Phys.* **2007**, *9*, 1921–1930.
- [353] Bachorz, R. A.; Bischoff, F. A.; Glöß, A.; Hättig, C.; Höfener, S.; Klopper, W.; Tew, D. P. *J. Comput. Chem.* **2011**, *32*, 2492–2513.
- [354] Hättig, C.; Tew, D. P.; Köhn, A. *J. Chem. Phys.* **2010**, *132*, 231102.
- [355] Ten-no, S. *Chem. Phys. Lett.* **2004**, *398*, 56–61.
- [356] Tew, D. P.; Klopper, W. *J. Chem. Phys.* **2005**, *123*, 074101–074101.

- [357] Peterson, K. A.; Adler, T. B.; Werner, H.-J. *J. Chem. Phys.* **2008**, *128*, 084102.
- [358] Hill, J. G.; Mazumder, S.; Peterson, K. A. *J. Chem. Phys.* **2010**, *132*, 054108.
- [359] Yousaf, K. E.; Peterson, K. A. *J. Chem. Phys.* **2008**, *129*, 184108.
- [360] Fliegl, H.; Klopper, W.; Hättig, C. *J. Chem. Phys.* **2005**, *122*, 84107–84107.
- [361] Klopper, W.; Samson, C. C. *J. Chem. Phys.* **2002**, *116*, 6397–6410.
- [362] Ten-no, S. *J. Chem. Phys.* **2004**, *121*, 117–129.
- [363] Strasser, D.; Goulay, F.; Kelkar, M. S.; Maginn, E. J.; Leone, S. R. *J. Phys. Chem. A* **2007**, *111*, 3191–3195.
- [364] Armstrong, J. P.; Hurst, C.; Jones, R. G.; Licence, P.; Lovelock, K. R.; Satterley, C. J.; Villar-Garcia, I. J. *Phys. Chem. Chem. Phys.* **2007**, *9*, 982–990.
- [365] Bader, R. *Acc. Chem. Res.* **1985**, *18*, 9–15.
- [366] Sun, N.; Jiang, X.; Maxim, M. L.; Metlen, A.; Rogers, R. D. *ChemSusChem* **2011**, *4*, 65–73.
- [367] Wang, H.; Gurau, G.; Rogers, R. D. *Chem. Soc. Rev.* **2012**, *41*, 1519–1537.
- [368] Barber, P. S.; Griggs, C. S.; Gurau, G.; Liu, Z.; Li, S.; Li, Z.; Lu, X.; Zhang, S.; Rogers, R. D. *Angew. Chem. Int. Ed.* **2013**, *52*, 12350–12353.
- [369] Barber, P. S.; Griggs, C. S.; Gurau, G.; Liu, Z.; Li, S.; Li, Z.; Lu, X.; Zhang, S.; Rogers, R. D. *Angew. Chem.* **2013**, *125*, 12576–12579.
- [370] Zhang, X.; Zhang, X.; Dong, H.; Zhao, Z.; Zhang, S.; Huang, Y. *Energy Environ. Sci.* **2012**, *5*, 6668–6681.
- [371] D'Alessandro, D. M.; Smit, B.; Long, J. R. *Angew. Chem. Int. Ed.* **2010**, *49*, 6058–6082.
- [372] D'Alessandro, D.; Smit, B.; Long, J. *Angew. Chem.* **2010**, *122*, 6194–6219.
- [373] Vogt, M.; Bennett, J. E.; Huang, Y.; Wu, C.; Schneider, W. F.; Brennecke, J. F.; Ashfeld, B. L. *Chem. Eur. J.* **2013**, *19*, 11134–11138.

- [374] Zhao, B.; Greiner, L.; Leitner, W. *Chem. Commun.* **2011**, *47*, 2973–2975.
- [375] Cabaço, M. I.; Besnard, M.; Chávez, F. V.; Pinaud, N.; Sebastião, P. J.; Coutinho, J. A. P.; Mascetti, J.; Danten, Y. *Chem. Commun.* **2013**, *49*, 11083–11085.
- [376] Yoshizawa-Fujita, M.; Johansson, K.; Newman, P.; MacFarlane, D. R.; Forsyth, M. *Tetrahedron Lett.* **2006**, *47*, 2755–2758.
- [377] Jin, C.-M.; Twamley, B.; Shreeve, J. M. *Organometallics* **2005**, *24*, 3020–3023.
- [378] Fèvre, M.; Pinaud, J.; Leteneur, A.; Gnanou, Y.; Vignolle, J.; Taton, D.; Miqueu, K.; Sotiropoulos, J.-M. *J. Am. Chem. Soc.* **2012**, *134*, 6776–6784.
- [379] Shiflett, M. B.; Elliott, B. A.; Lustig, S. R.; Sabesan, S.; Kelkar, M. S.; Yokozeki, A. *ChemPhysChem* **2012**, *13*, 1806–1817.
- [380] Hojniak, S. D.; Khan, A. L.; Hollóczki, O.; Kirchner, B.; Vankelecom, I. F. J.; Dehaen, W.; Binnemans, K. *J. Phys. Chem. B* **2013**, *117*, 15131–15140.
- [381] Mendoza-Espinosa, D.; Donnadiou, B.; Bertrand, G. *J. Am. Chem. Soc.* **2010**, *132*, 7264–7265.
- [382] Guisado-Barrios, G.; Bouffard, J.; Donnadiou, B.; Bertrand, G. *Angew. Chem. Int. Ed.* **2010**, *49*, 4759–4762.
- [383] Guisado-Barrios, G.; Bouffard, J.; Donnadiou, B.; Bertrand, G. *Angew. Chem.* **2010**, *122*, 4869–4872.
- [384] Bouffard, J.; Keitz, B. K.; Tonner, R.; Lavallo, V.; Guisado-Barrios, G.; Frenking, G.; Grubbs, R. H.; Bertrand, G. *Organometallics* **2011**, *30*, 2617–2627.
- [385] Ung, G.; Bertrand, G. *Chem. Eur. J.* **2011**, *17*, 8269–8272.
- [386] Albrecht, M. *Chem. Commun.* **2008**, 3601–3610.
- [387] Crabtree, R. H. *Coord. Chem. Rev.* **2013**, *257*, 755–766.
- [388] Weinheimer, A.; Metzner, E.; Mole, M. *Tetrahedron* **1973**, *29*, 3135–3136.
- [389] Jahn, T.; König, G. M.; Wright, A. D.; Wörheide, G.; Reitner, J. *Tetrahedron Lett.* **1997**, *38*, 3883–3884.

- [390] Tsukamoto, S.; Kato, H.; Hirota, H.; Fusetani, N. *Tetrahedron* **1994**, *50*, 13583–13592.
- [391] Haake, P.; Mantecon, J. *J. Am. Chem. Soc.* **1964**, *86*, 5230–5234.
- [392] Haake, P.; Bausher, L. P.; McNeal, J. P. *J. Am. Chem. Soc.* **1971**, *93*, 7045–7049.
- [393] Holbrey, J. D.; Reichert, W. M.; Tkatchenko, I.; Bouajila, E.; Walter, O.; Tommasi, I.; Rogers, R. D. *Chem. Commun.* **2003**, 28–29.
- [394] Tommasi, I.; Sorrentino, F. *Tetrahedron Lett.* **2006**, *47*, 6453–6456.
- [395] Voutchkova, A. M.; Feliz, M.; Clot, E.; Eisenstein, O.; Crabtree, R. H. *J. Am. Chem. Soc.* **2007**, *129*, 12834–12846.
- [396] Schmidt, A.; Beutler, A.; Albrecht, M.; Snovydyovych, B.; Ramírez, F. J. *Org. Biomol. Chem.* **2008**, *6*, 287–295.
- [397] Tommasi, I.; Sorrentino, F. *Tetrahedron Lett.* **2005**, *46*, 2141–2145.
- [398] Vogt, M.; Wu, C.; Oliver, A. G.; Meyer, C. J.; Schneider, W. F.; Ashfeld, B. L. *Chem. Commun.* **2013**, *49*, 11527–11529.
- [399] Magill, A. M.; Cavell, K. J.; Yates, B. F. *J. Am. Chem. Soc.* **2004**, *126*, 8717–8724.
- [400] Magill, A. M.; Yates, B. F. *Aust. J. Chem.* **2004**, *57*, 1205–1210.
- [401] Day, B. M.; Pugh, T.; Hendriks, D.; Guerra, C. F.; Evans, D. J.; Bickelhaupt, F. M.; Layfield, R. A. *J. Am. Chem. Soc.* **2013**, *135*, 13338–13341.
- [402] Sini, G.; Eisenstein, O.; Crabtree, R. H. *Inorg. Chem.* **2002**, *41*, 602–604.
- [403] Phukan, A. K.; Guha, A. K.; Sarmah, S.; Dewhurst, R. D. *J. Org. Chem.* **2013**, *78*, 11032–11039.
- [404] Guha, A. K.; Sarmah, S.; Phukan, A. K. *Dalton Trans.* **2010**, *39*, 7374–7383.
- [405] Majhi, P. K.; Schnakenburg, G.; Kelemen, Z.; Nyulaszi, L.; Gates, D. P.; Streubel, R. *Angew. Chem. Int. Ed.* **2013**, *52*, 10080–10083.
- [406] Majhi, P. K.; Schnakenburg, G.; Kelemen, Z.; Nyulaszi, L.; Gates, D. P.; Streubel, R. *Angew. Chem.* **2013**, *125*, 10264–10267.

- [407] Gusev, D. G. *Organometallics* **2009**, *28*, 6458–6461.
- [408] Appelhans, L. N.; Zuccaccia, D.; Kovacevic, A.; Chianese, A. R.; Miecznikowski, J. R.; Macchioni, A.; Clot, E.; Eisenstein, O.; Crabtree, R. H. *J. Am. Chem. Soc.* **2005**, *127*, 16299–16311.
- [409] Hollóczki, O. *Inorg. Chem.* **2014**, *53*, 835–846.
- [410] Thomas, M.; Brehm, M.; Hollóczki, O.; Kirchner, B. *Chem. Eur. J.* **2014**, *20*, 1622–1629.
- [411] Terleczyk, P.; Nyulászi, L. *J. Phys. Chem. A* **2009**, *113*, 1096–1104.
- [412] Van Ausdall, B. R.; Glass, J. L.; Wiggins, K. M.; Aarif, A. M.; Louie, J. *J. Org. Chem.* **2009**, *74*, 7935–7942.
- [413] Wang, Y.; Xie, Y.; Abraham, M. Y.; Wei, P.; Schaefer, H. F.; Schleyer, P. v. R.; Robinson, G. H. *J. Am. Chem. Soc.* **2010**, *132*, 14370–14372.
- [414] Denk, M. K.; Rodezno, J. M. *J. Organomet. Chem.* **2001**, *617-618*, 737–740.
- [415] Utczás, M.; Székely, E.; Tasnádi, G.; Monek, É.; Vida, L.; Forró, E.; Fülöp, F.; Simándi, B. *J. Supercrit. Fluids* **2011**, *55*, 1019–1022.
- [416] Klamt, A.; Jonas, V.; Bürger, T.; Lohrenz, J. C. *J. Phys. Chem. A* **1998**, *102*, 5074–5085.
- [417] Schäfer, A.; Horn, H.; Ahlrichs, R. *J. Chem. Phys.* **1992**, *97*, 2571–2577.
- [418] Weigend, F.; Ahlrichs, R. *Phys. Chem. Chem. Phys.* **2005**, *7*, 3297–3305.
- [419] Neese, F.; Valeev, E. F. *J. Chem. Theory Comput.* **2011**, *7*, 33–43.
- [420] Hansen, A.; Bannwarth, C.; Grimme, S.; Petrović, P.; Werlé, C.; Djukic, J.-P. *Chemistry-Open* **2014**, *3*, 177–189.
- [421] Yang, J.-Z.; Zhang, Q.-G.; Wang, B.; Tong, J. *J. Phys. Chem. B* **2006**, *110*, 22521–22524.

Acknowledgments

First of all, I am profoundly grateful to my supervisor Prof. Dr. Barbara Kirchner for the opportunity to join her working group and for giving me the interesting state of the art topic making this thesis possible. I also would like to thank her for the constant support and wise counsels during my PhD. I thank Dr. Oldamur Hollóczy for mentoring me at the beginning of my PhD as well as for the opportunity to be involved in the collaboration project with the experimentalists from the Budapest University of Technology and Economics. In addition, I would like to thank Prof. Dr. Stefan Grimme for accepting to be a reviewer of this thesis.

I also would like to thank the German Academic Exchange service (DAAD) for the financial support during my PhD project. Anzhela Eloeva, Olga Gerschun, Marina Tukalo, and Elena Schmid are gratefully acknowledged for their help during the scholarship.

I am grateful to Prof. Dr. Olav Schiemann and Prof. Dr. Barbara Kirchner for their recommendation letters for the extension of the DAAD scholarship as well as for nominating me for the participation in the 65th Lindau Nobel Laureate Meeting.

Special thanks go to Dr. Werner Reckien, Barbara Intemann, and Nikifor Lazouski for proofreading my thesis.

I would like to express my gratitude to all current and former colleagues in the Kirchner group for the fruitful working atmosphere. Finally, I would like to thank my family. Their constant support made my life during the PhD easier.

Publications

Parts of this thesis have already been published in international, peer-reviewed journals:

1. D. S. Firaha, O. Hollóczki, and B. Kirchner, "Computer-Aided Design of Ionic Liquids as CO₂ Absorbents", *Angew. Chem. Int. Ed.*, **2015**, *54*, 7805–7809.
2. D. S. Firaha and B. Kirchner, "Tuning the Carbon Dioxide Absorption in Amino Acid Ionic Liquids", *ChemSusChem*, **2016**, *13*, 1591–1599.
3. D. S. Firaha and B. Kirchner, "CO₂ Absorption in the Protic Ionic Liquid Ethylammonium Nitrate", *J. Chem. Eng. Data*, **2014**, *59*, 3098–3104.
4. D. S. Firaha, M. Kavalchuk, and B. Kirchner, "SO₂ Solvation in the 1-Ethyl-3-Methylimidazolium Thiocyanate Ionic Liquid by Incorporation into the Extended Cation - Anion Network", *J. Solution Chem.*, **2015**, *44*, 838–849.
5. O. Hollóczki, D. S. Firaha, J. Friedrich, M. Brehm, R. Cybik, M. Wild, A. Stark, and B. Kirchner, "Carbene Formation in Ionic Liquids: Spontaneous, Induced, or Prohibited?", *J. Phys. Chem. B*, **2013**, *117*, 5898–5907
6. Z. Kelemen, B. Péter-Szabó, E. Székely, O. Hollóczki, D. Firaha, B. Kirchner, J. Nagy, L. Nyulászi, "An Abnormal N-Heterocyclic Carbene-Carbon Dioxide Adduct from Imidazolium Acetate Ionic Liquids: The Importance of Basicity", *Chem. Eur. J.*, **2014**, *20*, 13002–13008

Further publications:

1. M. A. Fomich, D. S. Firaha "Microplate as a convenient tool for identification of inorganic compounds by drop reactions", *Chem. Educator*, **2016**, *21*, 3–4.

2. B. Kirchner, F. Malberg, D. S. Firaha, O. Hollóczki "Ion pairing in ionic liquids", *J. Phys.: Condens. Matter*, **2015**, *27*, 463002
3. D. Zaitsau, E. Paulechka, D. S. Firaha, A. V. Blokhin, G. J. Kabo, A. Bazyleva, A. G. Kabo, M. A. Varfolomeev, V. M. Sevruk "Comprehensive study of the thermodynamic properties for 2-methyl-3-buten-2-ol", *J. Chem. Thermodyn.*, **2015**, *91*, 459–473
4. D. S. Firaha, O. Hollóczki, and B. Kirchner, "Computer-gestütztes Design ionischer Flüssigkeiten zur CO₂ -Absorption", *Angew. Chem.*, **2015**, *127*, 7916-7920.
5. D. S. Firaha, Y. U. Paulechka "Kinetics of synthesis of 1-alkyl-3-methylimidazolium ionic liquids in dilute and concentrated solutions", *Int. J. Chem. Kin.*, **2013**, *45*, 771–779.
6. A. P. Gaiduk, D. S. Firaha, V. N. Staroverov "Improved Electronic excitation energies from shape-corrected semilocal Kohn-Sham potentials", *Phys. Rev. Lett.*, **2012**, *108*, 253005.
7. Y. U. Paulechka, G. J. Kabo, A. V. Blokhin, D. S. Firaha "Thermodynamics of ionic liquids precursors: 1-bromobutane and its isomers", *J. Chem. Eng. Data*, **2011**, *56*, 4891–4899.